INAUGURAL DISSERTATION

Zur

Erlangung der Doktorwürde

der

Naturwissenschaftlich-Mathematischen Gesamtfakultät

der

Ruprecht-Karls-Universität Heidelberg

Vorgelegt von

Diplom-Chemikerin Nina Mehrkens

aus Buxtehude

Tag der mündlichen Prüfung: 23.10.2015

Phosphatase Activity of Homo- and Heterodinuclear Transition Metal Complexes of Patellamide Derivatives

Gutachter: Prof. Dr. Peter Comba

Prof. Dr. Dirk-Peter Herten

This thesis has been accomplished at the Institute of Inorganic Chemistry of the Ruprecht-Karls-University in Heidelberg from January 2012 until August 2015 and was supervised by Prof. Dr. Peter Comba.

Experimental work was also performed under supervision of Prof. Dr. Graeme Hanson at the Centre for Advanched Imaging (CAI) and Prof. Dr. Lawrence Gahan at the School of Chemistry and Molecular Biosciences (SCMB) at the University of Queensland, Brisbane, Australia, between September 2013 and March 2014.

Parts or passages of the present thesis have been published or will be submitted in scientific jopurnals:

1.) „Copper Solution Chemistry of Cyclic Pseudo-Octapeptides"; Peter Comba, Nina Dovalil, Gebhard Haberhauer, Klaus Kowski, Nina Mehrkens, *Zeitschrift für anorganische und allgemeine Chemie* 2013, *639* (8-9), 1395-1400

2.) „Dinuclear Zinc(II) and Copper(II)/Zinc(II) complexes of artificial Patellamides as Phosphatase models"; Peter Comba, Annika Eisenschmidt, Lawrence R. Gahan, Graeme R. Hanson, Nina Mehrkens, Michael Westphal, *manuscript in preparation*, 2015

Für Philipp

EINE ENDECKUNG ZU MACHEN BESTEHT DARIN

ETWAS ZU SEHEN, DAS SCHON VIELE GESEHEN HABEN

UND SICH DABEI ETWAS ZU DENKEN, DAS NOCH NIEMAND GEDACHT HAT.

ALBERT V. SZENT-GYÖRGYI NAGYRÁPOLT

DANKSAGUNG

Als erstes möchte ich meinem Betreuer Peter Comba danken; das Thema ist faszinierend und ich könnte mit Spass noch lange weiter daran forschen, außerdem bin ich sehr froh darüber in diese Arbeitsgruppe gekommen zu sein, die auch dank seiner Leitung das ist was sie ist. Nämlich eine Gruppe die sich unterstützt und in der in lustiger, offener und inspirierender Atmosphäre gearbeitet, gelebt und diskutiert wird.

Graeme Hanson, den ich noch kennelernen durfte, möchte ich dafür danken dass ich jetzt ESR messen und simulieren kann, und nebenbei gesagt ist es auch das, was mir am meisten Spass an meiner Arbeit gebracht hat. Your advice has been a great benefit for my work, Thank you.

Lawrence Gahan möchte ich für die Möglichkeit in seinem Labor arbeiten zu können und für den wohl gemeinten Rat danken. Thanks for your advice and for proof reading my thesis.

Bodo Martin möchte ich danken, für seine geduldige Hilfe mit so einigen EDV Problemen, Einstellungen und Zugängen zu Programmen und Servern. Und auch wenn letztendlich ich nicht zu einen der „Rechner“ des Arbeitskreises geworden bin, möchte ich sagen du machts eine gute Vorlesung.

Bei Marion Kerscher möchte ich mich gerne bedanken für die vielen Hilfestellungen mit so einigen Geräten, einer Tür an die man immer anklopfen kann, um seltsame Reaktionsverläufe oder Simulationen zu besprechen und das ein oder andere gemeinsame Feierabendbier. Und natürlich für die Motivation auf der nebligen Piste dieses Jahr, ich hätte ansonsten tatsächlich versucht den Berg zu Fuss herunterzukommen.

Marlies Schilli-Schönbeck und Karin Stelzer möchte ich auch danken, ohne euch wär ich hier so manches Mal in administrativen Papierkram untergegangen.

Bei Maik Jacob möchte ich mich auch bedanken, für die ein oder andere kleine Hilfe im Labor und für Chemikalienbestellungen.

Bei meinen Forschungsstudenten Eric, Clarissa, Wioletta und Jan für die Unterstützung.

Michi, Johannes, Kathi und Simone für die schöne Zeit im Labor 105 ich habe immer gerne dort gearbeitet, Musik gehört, viel gelacht und auch die ein oder andere wissenschaftliche und nichtwissenschaftliche Diskussion geführt.

Den vielen Korrekturlesern, Asha, Annika, Anna, Bianca, Kathi, Johannes, Michi, und Simone bin ich für ihre Korrekturen meines zugegebenermaßen manchmal recht speziellen Englisch-Stils sehr dankbar

Meiner Familie dh. Magret und Dieter Mehrkens sowie Sarah Mehrkens und Johanna Willimek bin ich auch sehr dankbar, ohne euch wär ich zum einen nicht die, die ich jetzt bin und zum anderen nicht dort, wo ich jetzt bin.

Philipp, ich bin dir für die schier unendliche Geduld mit mir und meiner Sturheit, für deine Rolle als Fels in der Brandung, für deine unvorstellbar große Kreativität und deine Liebe dankbar.

TABLE OF CONTENTS

ABSTRACT

Naturally occurring cyclic peptides exist in the ascidians *Lissoclinum Patella* of the Pacific and Indian Oceans. The biological role of these structural interesting marine secondary metabolites is still unclear. The patellamides are able to bind a variety of transition metal ions. Some of the copper(II) complexes of cyclic *pseudo*-peptides are known to form carbonato-bridged complexes when exposed to CO_2. [1] Thus, in previous studies a library of patellamide derivatives has been designed and prepared. The copper(II) coordination properties of these patellamide derivatives is widely understood. Interestingly, the corresponding dinuclear copper(II) complexes are able to very efficiently, catalytically hydrolyze phosphoesters and hydrate CO_2.

The natural peptides are produced by the cyanobacteria *prochloron didemnid,* a photosynthetic symbiont of *L.Patella*. Since the patellamides are extracted from an hydrophilic cytoplasmic environment, together with notably high concentrations of some transition metal ions like copper(II) and zinc(II). It is likely that a natural function of probably existing transition metal complexes in this environment is hydrolase activity. The biologic background as well as the state of the art regarding the copper(II) coordination chemistry is summarized in Chapter 1.

The synthesis of the patellamide derivatives is shortly discussed.

In Chapter 3, the electrochemistry of the copper(II) complexes is discussed. Cyclic voltammetry and square wave voltammetry were used to study the existence of a complexation equilibrium between various species in solution. From the obtained results, it is concluded that the copper(I/II) redox chemistry is probably not a biological relevant metabolic function at neutral pH. Under basic conditions, it is possible that stable copper(I) species exist. It can be proposed that these are carbonate or bicarbonate bridged. Moreover, under basic conditions an oxygenation test reaction was performed, and it was shown that a dinuclear copper(II) complex of an patellamide derivative is involved in an oxygenation reaction under these rather unphysiological conditions. A tentative mechanistic proposal is discussed, which is based on the

observation of a radical coupling product and insights obtained from a low temperature NMR experiment.

In addition, the proposed copper(II) complexation equilibria of the ligand H_4pat^4 is discussed, and the respective EPR spectra with their simulations are in the focus of the last section of Chapter 3. Especially while regarding the formation of heterodinuclear copper(II)/ zinc(II) complexes with H_4pat^4 in Chapter 5 this equilibrium is requested.

Since biological relevant hydrolysis chemistry is often based on zinc enzymes, zinc(II) complexes of the macrocyclic peptides were studied. Chapter 4 presents the formation of zinc(II) complexes, which are explored using isothermal calorimetric titrations in combination with NMR spectroscopy and mass spectrometry. After an overview of the biological relevance of zinc(II) based hydrolases, Chapter 4 presents a proposed zinc(II) complexation equilibrium.

In Chapter 5, the formation of heterodinuclear copper(II)/zinc(II) complexes is described based on spectroscopic results. EPR spectroscopy, paramagnetic NMR and UV/vis spectroscopy in combination with mass spectrometry are used to describe two different heterodinuclear complexes. Furthermore, Chapter 5 descriebes the formation of a copper(II)/zinc(II) complex, due to a distinct cooperative effect, with a ligand that does not form stable spectroscopically characterizable homodinuclear zinc(II) complex.

Phosphoester hydrolysis reactions with a model substrate of all complexes, described in the Chapters 3, 4 and 5, have been investigated in a kinetic assay. The pH dependent results are discussed in Chapter 6. Furthermore the substrate dependency of the initial rate was tested. All complexes disussed exhibit catalytic ativity in a pH range close to neutral. Comparison of all data obtained shows that the zinc(II) complexes are slightly more active than the corresponding homodinuclear copper(II) complexes.

KURZZUSAMMENFASSUNG

Patellamide und Ascidiacyclamid sind natürlich vorkommende zyklische Peptide. Da sie aus Aszidien der Art *Lissoclinum Patella* (vorkommend im Pazifik und im Indischen Ozean) isoliert wurden bezeichnet man sie als marine Metabolite. Sie sind in der Lage verschiedene Übergangsmetallionen zu koordinieren. Einige der dinuklearen Kupfer(II)-Komplexe bilden in Gegenwart von CO_2 carbonatoverbrückte Komplexe. Um die biologische Rolle der Patellamide in Hinblick auf eventuell existierende Kupfer(II)-Komplexe im biologischen Umfeld zu untersuchen, wurde eine kleine Bibliothek synthetisch leichtzugänglicher Derivate der Patellamide erstellt. Die Kupfer(II) Koordinationschemie dieser Derivate ist weitestgehend erforscht. Interessanterweise konnte vor kurzem gezeigt werden, dass die dinuklearen Kupfer(II)-Komplexe der Patellamid-Derivate in der Lage sind sowohl Phosphoester als auch CO_2 katalytisch zu hydrolysieren.

Die natürlich vorkommenden zyklischen Peptide werden von den symbiotisch lebenden cyanobakterien der Art *Prochloron Didemnid* produziert. In Anbetracht der Tatsache, dass die natürlich vorkommenden zyklischen Peptide aus einer hydrophylen zytoplastischen Umgebung extrahiert wurden, zusammen mit bemerkenswerten Konzentrationen an Übergangsmetallionen wie Cu^{2+} und Zn^{2+} isoliert, liegt die Vermutung nahe, dass in der biologischen Umwelt existierende Komplexe als Hydrolasen arbeiten.

Auf die Synthese der Patellamid-Derivate wird in Kapitel 2 kurz eingegangen.

Die Elektrochemie der dinuklearen Kupfer(II)komplexe wird in Kapitel 3 diskutiert. Elektrochemische Ergebnisse wurden mittels cyclovoltammetrischer und square-wave-voltammetrischer Experimente erlangt. Die voltammetrischen Experimente spiegeln die bekannte aber komplexe Gleichgewichtschemie der dinuklearen Kupfer(II)-komplexe in Lösung wieder, was eine exakte Zuordnung der irreversiblen Reduktionen schwierig machte. Die Zuordnung einzelner Potentiale beruht auf publizierten Daten anderer Systeme. So kann man annehmen, dass die irreversiblen und eher positiven Reduktionspotentiale zwischen 350 und 450 mV zur Bildung unstabiler Kupfer(I)/Kupfer(II) Spezies gehören, was in Übereinstimmung

mit den relativ kleinen Stabilitätskonstanten zu erwarten war. Unter basischen Bedingungen und nach Einleitung von CO_2 werden einige zusätzliche negative Reduktionspotentiale gefunden, welche darauf hindeuten, dass die dinuklearen Carbonato-verbrückten Komplexe der Patellamid-Derivate Kupfer(I) stabilisieren.

Dieser Beobachtung folgend, wurde unter basischen Bedingungen der dinukleare Kupfer(II)komplex des Liganden H_4pat^1 einem Oxygenierungstest unterzogen. Der zeigte dass unter diesen recht unphysiologischen Bedingungen Kupfer-vermittelte Sauerstoffchemie möglich ist. Die Oxygenierungsprodukte wurden analysiert und deuten auf eine radikalischen Mechanismus hin. Ein vorläufiger mechanistische Vorschlag wird erläutert, der anhand eines tieftemperatur NMR Experiments an einem ESR-inaktiven dinuklearen Kupfer(II)-Komplex, erstellt wurde.

Desweiteren, wird in Kapitel 3 das Kupfer(II) Lösungsgleichgewicht des Liganden H_4pat^4 erläutert, das mit Hilfe von ESR Spektoskopie, den dazugehörigen Simulationen und Massen spektrommetrischen Ergebnissen aufgestellt wurde. Welches in Hinblick auf die später diskutierte Bildung heterodinuklearer Kupfer(II)/ Zink(II) Komplexe interresant ist.

Da Hydrolyse Chemie in der Natur häufig von Zink(II) Enzymen betrieben wird, und Zink(II) ebenfall sehr konzentriert in den Aszidien gefunden wurde, wird in Kapitel 4 die Zink(II) koordinationschemie der Liganden H_4pat^1, H_4pat^2 und H_4pat^4 diskutiert. Welche mit Hilfe isothermaler kalorimetrischer Titrationen, NMR Spektroskopie und Massenspektrometrie erforscht wurde. Dieses Kapitel, das mit dem biologischen Hintergrund von Zink(II)-hydrolasen eingeleitet wird, endet mit einem vorgeschlagenen Lösungsgleichgewicht der verschiedenen dinuklearen Zink(II)komplexe.

In Kapitel 5 wird die Bildung heterodinuklearer Kupfer(II)/ Zink(II) Komplexe diskutiert, und Anhand von ESR-, UV/vis- und NMR Spektroskopie verdeutlicht. Kapitel 5 liefert außerdem ein Beispiel eines Liganden der durch einen ausgeprägten kooperativen Effekt einen Kupfer(II)/Zink(II) Komplex bildet, obwohl es keinen stabilen spektroskopisch charakterisierbaren homodinuklearen Zink(II)komplex dieses Liganden gibt.

Alle in dieser Dissertation beschrieben Komplexe wurden einem Phosphoesterhydrolyse Assay unterzogen. Die Fähigkeit, einen aktivierten Modell-Phosphoester zu hydrolysieren wurde sowohl in Abhängigkeit von pH Wert untersucht, als auch in einem substratkonzentrationsabhängigen Scan untersucht. Alle Komplexe des Liganden H_4pat^4

zeigten katalytische Aktivität in einem natürlich relevanten pH Bereich. Die Ergebnisse werden ausführlich verglichen und diskutiert. Der Vergleich zeigen deutlich, dass alle dinuklearen Zink(II) Komplexe leicht aktiver sind als die entsprechenden homodinuklearen Kupfer(II) Komplexe.

TABEL OF MOLECULES

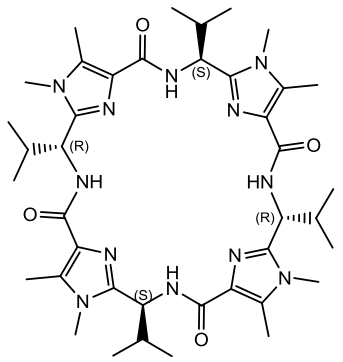

H_4pat^1

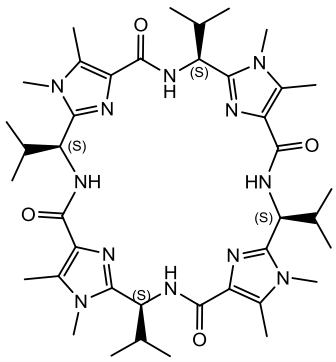

H_4pat^2

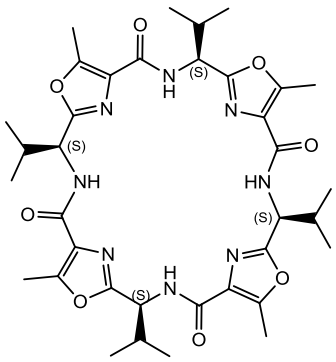

H_4pat^3

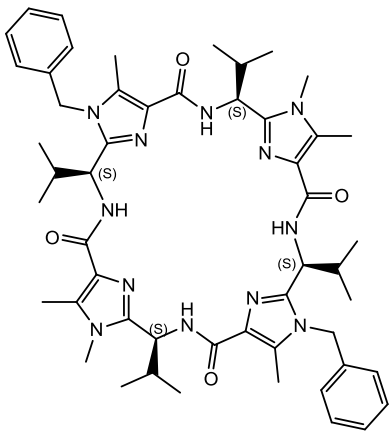

H_4pat^4

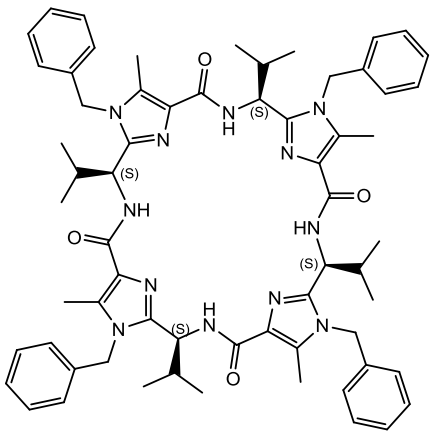

H_4pat^5

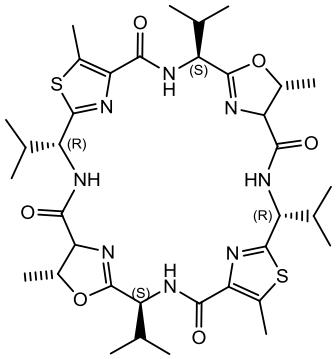

H_4ascA

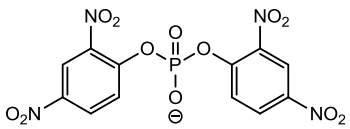

BDNPP

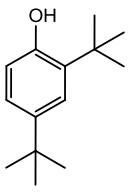

DTBPH

ABREVIATIONS AND ACRONYMS

Å	Ångström
Abs	absorbance
Ala	alanine
AP	alkaline phosphatase
Arg	arginine
Asn	asparagine
Asp	aspartate
ADP	adenosine diphosphate
AP	alkaline phosphatase
ATP	adenosine triphosphate
B	magnetic field
BDTBPH	bis-(2,2´,4,4´-di*tert*butylphenole)
BDNPP	bis-(2,4-dinitrophenyl)phosphate
Bn	benzyl
Brine	saturated aqueous $NaHCO_3$ solution
Bu	butyl
Boc	*tert*butylcarboxycarbonyl
Calc.	calculated
CAPS	3-(cyclohexylamino)-1-propanesulfonic acid
Cbz	carboxybenzyl
CHES	2-(cyclohexylamino)ethanesulfonic acid
CW	continuous wave
CT	charge transfer
CD	circular dichroism
COMU®	(1-cyano-2-ethoxy-2-oxoethylidenaminooxo)dimethylamino-morpholino-carbenium hexafluorophosphate
CV	cyclovoltammetry
Cys	Cysteine

COSY	correlation spectroscopy
conc.	concentrated
d	day(s)
D	deuterium
DART	direct analysis in real time
DFT	density functional theory
DMF	dimethyl formamide
DNA	deoxyribonucleic acid
DTPPH	2,4-di*tert*butylphenole
DTBQ	3,5-di*tert*butylquinone
DCM	dichloromethane
DMSO	dimethylsulfoxide
EDIPA	*N,N*-diisopropylethylamine
EtOAc	ethylacetate
EtOH	ethanol
ESI	electron spray ionization
EPR	electron paramagnetic resonance
et al.	*et alii*
eq.	equivalent(S)
E.coli	escheria coli
Et_2O	diethylether
EPR	electron paramagnetic resonance
FAB	fast atom bombardment
Fc/Fc^+	Ferrocene/ Ferrocenium
FDPP	pentafluorophenyl diphenylphosphinate
g	Landéfactor
G	gauss
Glu	glutamin acid
Gln	glutamine
Gly	glycin
h	hour(s)
His	histidine

Hz	hertz
HCA II	human carbonic anhydrase II
HEPES	4-(2-hydroxyethyl)piperazin-1-ethanesulfonic acid
HMBC	heteronuclear multiple bond correlation
HSQC	heteronuclear single quantum correlation
HR	high resolution
ITC	isothermal titration calorimetry
Ile	Ileucine
K	Kelvin
Leu	leucine
LSE	least square error
Met	methionine
m	meta
mV	milli volt
M	mol/l
MALDI	matrix assisted laser desorption/ionisation
MES	2-(*N*-morpholino)ethanolicsulfonic acid
Me	methyl
MM	molecular mechanics
MeOH	methanol
MeCN	acetonitrile
MS	mass spectrometry
Min	min
ml	milliliters
mM	millimol/l
NMR	nuclear magnetic reosance
NOESY	nuclear overhauser effect spectroscopy
NMM	*n*-methylmorpholine
NIR	near infra red
o	ortho
OTf	triflate
OAc	acetate

p	para
PE	petroleum ether
ppm	parts per million
Phe	phenylalanine
p.a.	pro analysi
pdb	protein data bank
PAP	purple acid phosphatase
Ph	phenyl
rt	room temperature, 25°C
RNA	ribonucleic acid
ROS	reactive oxygen species
Ser	serine
SQW	square-wave-voltammetry
tert	tertiäry
TLC	thin layer chromatography
TFA	trifluoroacetic acid
THF	tetrahydrofuran
Thr	threonine
TON	turnover number
TOF	turnover frequency
UV/vis-NIR	ultraviolet/ visible near infrared
Val	valine
vs.	versus
$\%_{vol}$	volume percent
$\%_{w}$	weigth percent
$ß_{e}$	bohr magneton
δ	chemical shift (NMR)
ν	frequency
ε	extinction coefficient
γ	wavelength

1 Patellamides – Biology and Transition Metal Chemistry

1.1 Cyclic Peptides from Ascidians - Marine Metabolites

The ocean is inspiring and authoritative at the same time. For centuries it has lead humanity to great achievements and it is able to show us the limits of ambition. The ocean covers more than two thirds of the earth's surface and, considering its depth, it represents the largest natural habitat on earth. Nevertheless, we are still at the beginning of understanding its ecosystems and its richness of species. The ocean has inspired humankind in various ways since the beginning of time. There are puzzling pictures from the early Bronze Age, in which the mysteries and features of the ocean are described. Artifacts like these are found at nearly all places where humans have ever been. The ocean is also an inspiration for science, as it harbors a vast amount of unknown and fascinating strategies of life; in addition, new and potentially useful molecules remain to be discovered in the oceanic ecosystems.

Due to their huge differences compared to terrestrial life, organisms from the ocean were often assigned as sources of foreign or strange life- strategies. The biodiversity of the ocean is still to be estimated. From 2000 to 2010 more than 6000 potential new species were discovered, from these 1200 have been proved to be unique species. A global research network "the *census of marine life"* has attempted to count, map, monitor and to track all species.[2] Each of these species has its own life strategy and a unique role in a specific ecosystem, which leads to the conclusion that each single species (from a bacteria to a shark) needs to produce and metabolize a diverse range of highly specialized substances. This is especially true for coral reefs

in tropic and subtropic regions, which bear a high biodiversity and thus an even higher range of promising molecules.

For various reasons, Science is interested in finding new substances and understanding their biological function. They may help us to understand foreign ecosystems and could thus be directly and indirectly useful in dealing with ecologic challenges. Furthermore, the pharmaceutical potential of marine products is generally promising. Also, industrial use of marine products is conceivable, as there are substances, which may be used as efficient and sustainable catalysts.

A classical pharmaceutical drug discovery process is based on high-throughput screenings of rationally designed compounds or of chemical libraries. Reviewing the number of hits by marine natural products in such screenings suggests that it is obvious that this number competes advantageously with the success of notionally realized combinatorial screenings. [3] Isolated marine natural compounds not directly necessary for the growth and development of their producer are defined as secondary metabolites.[4] Most of them are involved, or assumed to be involved, in survival or interspecies communication strategies of their producing organisms. In 1970 though, the Interest in secondary marine natural products was enhanced with the first reports of their antitumor activities.[5,6] In 1980 the two first peptidic secondary metabolites (ulicyclamide and ulithiacyclamide) were discovered and isolated from marine organisms (in *Lissoclinum Patella*) (Figure 1.1).[7]

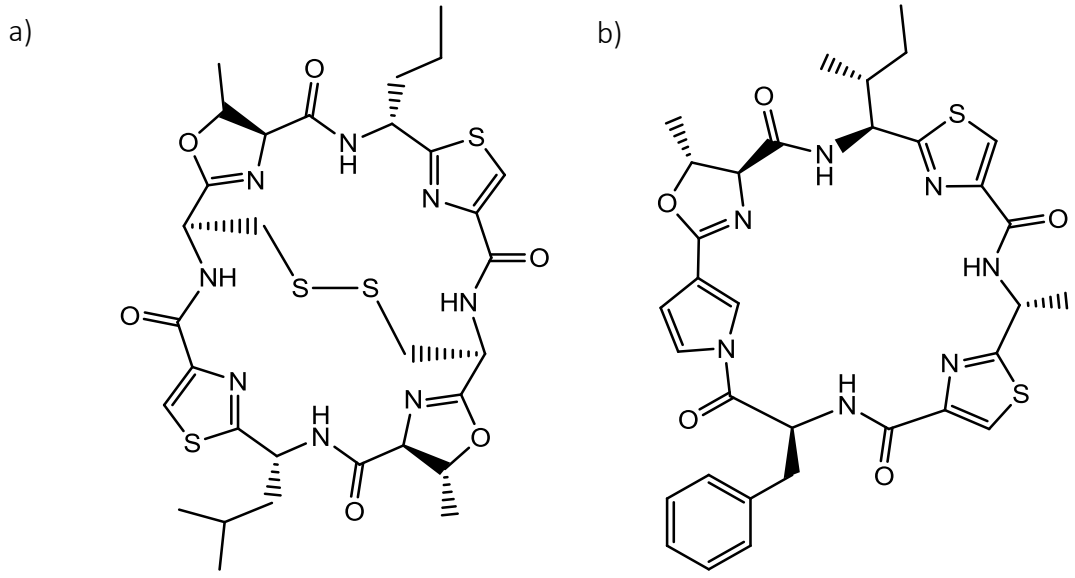

Figure 1.1: Structures of Ulithiacyclamide (a) and Ulicyclamide (b).[7]

These peptidic marine natural products are formed in three ways:- (i) *RIPP*: ribosomal production and post- translational modification; (ii) the production on a non-ribosomal pathway (NRP), which is performed by NRP-enzymes in cytoplasm; or (iii) a mixed process, in which polyketide synthases (PKS) and NRP intervene. Thus, a large structural diversity is posisble, which gives the hosting organism the possibility to be highly accommodative to its environment.[4]

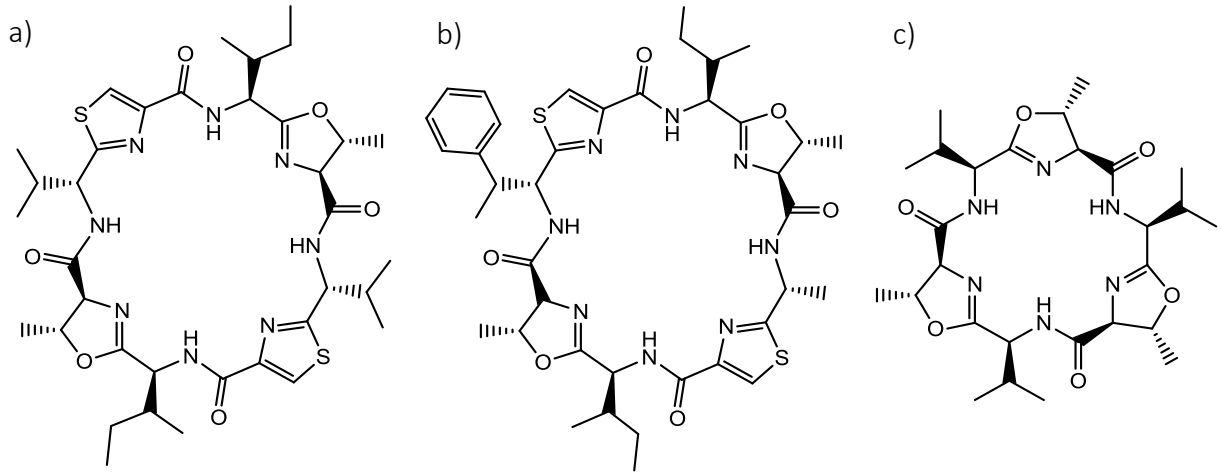

Figure 1.2: Structures: Ascidiacyclamide (a), Patellamide D (b) and Westiellamide (c).[8-10]

During the 1980s Ireland and Scheuer,[11] and others,[12 13-15] discovered further examples of cyclic peptides with a similar molecular scaffold (Figure 1.2). These were the patellamides A-G and ascidiacyclamide, which could be isolated from the same organism, *Lissoclinum Patella*. Since it is more common in nature that cyclic peptides and/or peptides with D-amino acids (e.g. and other unusual substances, like *ß*-aminoacids, γ-amino acids or hydroxo acids) are produced from a non-ribosomal pathway (NRP), the fact that the patellamides and ascidiacyclamide (Figure 1.2a) are produced ribosomally (RIPP) indicates them to have an essential biological role. [16-18]

1.2 The *Prochloron* - *Lissoclinum patella* Symbiotic Association

Cyclic peptides like the patellamides (Figure 1.2a), wetsiellamide (Figure 1.2c) and ulithiacyclamide (Figure 1.1a) are found in the ascidia *Lissoclinum Patella* (Figure 1.3a), one type of a family of sessile filter animals, commonly called sea squirts, that live in coral reefs in

the Pacific and Indian Oceans. The peptides could be isolated in large quantities, up to several gram per dry weight.[16,17] Like most ascidians *L. Patella* lives in a symbiotic relationship with the cyanobacteria *Prochloron didemnid* (Figure 1.5).

Figure 1.3: A colony of the didemnid Ascidiacea *Lissoclinum Patella* covering corals (a), a photograph of a cut through a colony (b).[both reproduced with permission from 19]

Since the biological function of these natural occurring cyclic peptides is still unclear, and considering that the unusual cyclic peptides are produced at the ribosome of Prochloron (RIPP), [16,17,20,21] it is important to understand this symbiosis.

The sea squirt *Lissoclinum Patella* belongs to the phylum *Chordata*, subphylum *Urochordata* (tunicates), class *Ascidiacea*, order *Aplousobranchia* and the family *Didemnidea*. *Lissoclinum Patella* can be found either as solitary organisms but mostly in colonies. Colonies of *L. Patella* are green to green-blue and can reach 10 - 25 cm in diameter, 1 - 2 cm in thickness and weigh up to 200g.[22,23] The larvae of *L. Patella* resemble amphibian tadpoles and have nerve cords which they lose during their development.[24] Ascidians are tunicates because adults (single zooids) of this class live in colonies (usually a few thousand per colony), which are entirely embedded in a tunic. The tunic is a matrix of proteins and cellulose-like carbohydrates containing calcareous spicules, which display for the single exemplars of the invertebrate *L. Patella* a kind of exoskeleton, which maintains their body shape as well as playing a role in digestion and storage of metabolism products. It is possible for a colony to fuse and divide within a day; in addition, a single zooid has the ability to perform a coordinated movement within its tunic.[23,25] Bladder cells, which contain mycosporine-like amino acids (MAA) like shinorine,[26] are embedded in the tunic. MAAs from L. Patella have a strong absorption in UVa (320 - 400 nm) and UVb (280 - 300 nm) but they are transparent to visible light,[26,27] and as a

result they act as ideal sunscreens for *L. Patella*, allowing their producing organism, e.g. its symbiont, to photosynthesize efficiently. Zooids of *L. Patella* are connected to cloacal cavities in the tunic (Figure 1.4), which they use to excrete filtered water and waste products, but also for uptake of photosynthesis products and presumably N_2-fixation products. A colony of *L. Patella* adheres usually to corals, sea grass or stone substrates through a reddish biofilm, which contains further different cyanobacteria, optimizing the utilization of all radiated light. The consideration that *didemnid* ascidians as *L. Patella* are playing a major role in the ecosystem reef has been demonstrated from observations of ascidians smothering scleratinian corals.[28]

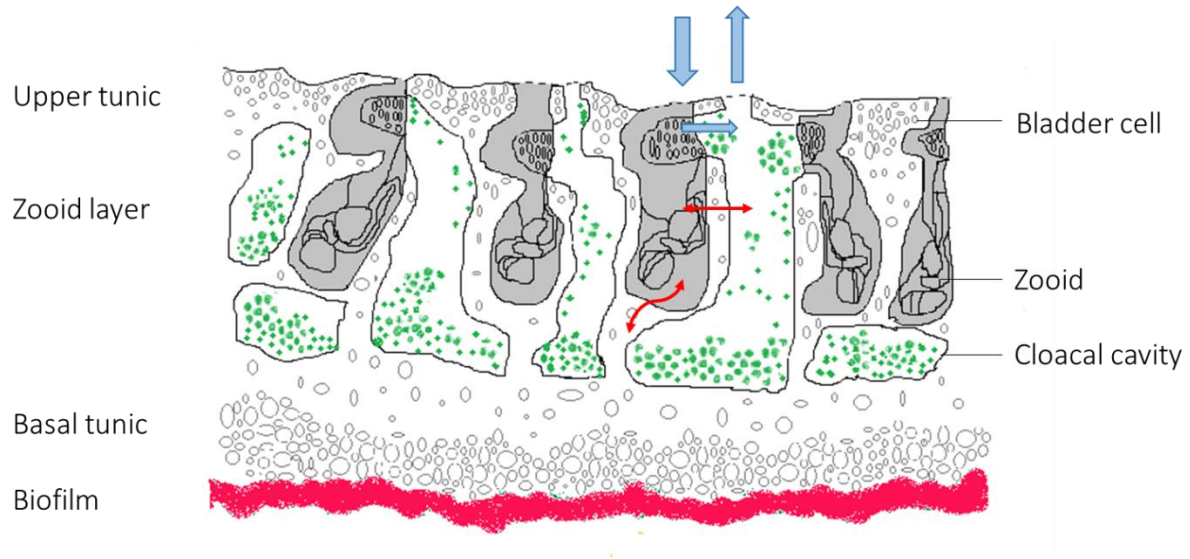

Figure 1.4: *Lissoclinum patella* colonie: schematic cut:. Drawing of a cross-section illustrating the organization of zooids and symbionts in the tunic. The zooids are embedded in the tunic, where they suck in and filter particles out of the seawater. Waste products and filtered water are excreted into the surrounding peribranchial space and in the cloacal cavities. Was redrawn and modified from ref.:26

L. Patella harbors the endosymbiotic living cyanobacterium *Prochloron didemid* (Figure 1.5) in the cloacal cavities, the cyanobacterium involved with photosynthesis and probably N_2- fixation for its host. *Prochloron didemnid* is a unicellular oxygenic photosynthetic prokaryote that possesses besides chlorophyll A and chlorophyll B plant-like thylakoids, and it lacks cyanobacteria-typical phycobilins,[25,29] making *Prochloron* resembling plants chloroplasts. However, molecular biology has shown that *Prochloron* is not an ancestor of green-plant chloroplasts, it is now considered that both have the same ancestors.[30] Despite the fact that the *Prochloron* can be obtained by simply manually pressing a colony, it has eluded cultivation and is thus considered to be an obligate symbiont. Larvae of *L. Patella* were released together with *Prochloron*-cells, and it could be shown that their settling on new substrates is controlled

by light conditions, providing the best photosynthesis conditions for the symbiont *Prochloron*.[18,30]

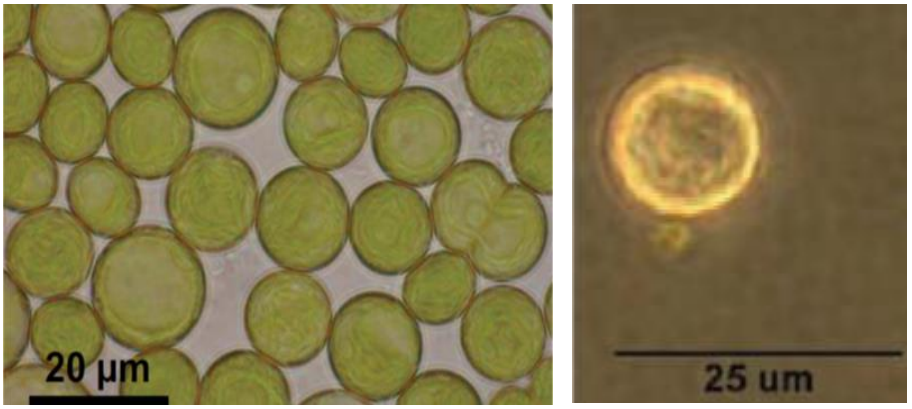

Figure 1.5: Green *Prochloron* cells (left), Reproduced with permission from ref.31 individual *Prochloron* cells (right). Reproduced with permission from ref.16

Prochloron didemnid is an excellent example for chemical diversity in marine cyanobacteria, because so far it has produced the widest range of secondary marine metabolites that have been reported. Therefore, *Prochloron* uses all three of the previously described ways for the formation of marine natural products (RIPP, NRP and PKS).[4] Thus, it may be that the symbiont provides a chemical defense for its host.

Understanding the lifestyle of symbiont and host is important for natural product discovery and chemical ecology, and indeed, also for determining the natural role of the patellamides. As they are produced by the cyanobacteria *Prochloron*, the patellamides are classified as marine cyanobactins. There are also some peptidic terrestrial cyanobactins known, most of them are, in contrast to the patellamides, non-ribosomal products (NRP).[4] Patellamides are known for their versatility, their resistance to proteolysis and their ability to traverse membranes[30] Hence, the patellamides from *L. Patella* display antibacterial-, antiviral- and cytotoxic-activity as well as they are able to reverse multiple-drug resistance in human leukemia cells.[13,32-41] Recently published phylogenetical approaches confirm the suggestion that patellamides and some other secondary metabolites (e.g. trunkamide), are produced from a linear prepeptide, the production of which is dependent on a gene cluster of seven genes called PatA-PatF.[16,17] Five of these seven genes are necessary to build a patellamide.[21] Additionally, it is known that only small changes such as single- point- mutations lead to a different cyclic peptide. Studies have shown that it is possible to influence the DNA of *prochloron* cells by a single point mutation, so that (in an *E.coli* culture) a new artificial cyclic peptide is produced.[16] It was assumed that, in

this way, the ascidians may use different secondary metabolites as a kind of immune- system or they may be used as signal substances against predators or to entice attractors, which may slightly differ from reef to reef. Additionally, the research confirmed that the amount and the kind of patellamide produced varies from ascidian to ascidian, which indicates that the patellamides are needed under the different environmental conditions present.[28] However, it is still unclear on which exact conditions the patellamide production is dependent: water conditions as salinity, temperature or pH could play a role, but also it is possible that nutrients, predators or attractors in different regions may play a role. Parallel to these studies (the methods of which could be described as"reversive genetics") Jaspars et al were able to achieve the same result by using a method called "shotgun cloning".[17] In shotgun cloning, all DNA fragments are transferred solely to an *E. coli* culture, then produces secondary metabolites that are finally analyzed by a high through-put method (e.g. LC-MS). In reversive genetics, in contrast, one first looks for a logically required amino acid sequence, transfers this particular DNA fragment to an *E. coli* culture and lets this produce secondary metabolites, followed by analysis of the final products. [18]

Between 30 and 50% of the carbon required by *L. Patella* is produced by *Prochloron* and mainly delivered as glycolate, which is an inhibitor of photosynthesis.[18,42] Studies with radio labelled $^{14}CO_2$ have shown that most of the carbon transferred (from *Prochloron* to *L. Patella*) was found in the lipids, the nucleic acids and the proteins of the host.[42] In addition to *Prochloron* providing nearly all of the necessary carbon, it is presumed that all nitrogen required for animal survival and nitrogen recycling comes from the same source, and this is indicated from the unusual N^{15}/N^{14} abundance in Prochloron cells. [42-46] Contrary to these findings, it could be shown that *Prochloron didemnid* has no *nif*-genes, which are the known genes for N_2-fixing enzymes.[47]

There are numerous symbiotic cyanobacteria known, which fulfill in addition to photosynthesis, a second small molecule activation for their own metabolism or for that of their host. For example, in a lake at Yellowstone National park (which, is regarding its high salinity, is a biotope with extreme highly adjusted organisms) a cyanobacterium was discovered that is undergoing photosynthesis during the day and nitrogen-fixation at night.[48] *Prochloron* in ascidians can vary the amount of patellamides and the sequences by only small changes in the prepeptide, [21,38] In this way it may be, that *prochloron* has a similar way of dealing with different processes with changing environment or nutrients. The aim to understand the natural biological function of

these cyclic peptides may thus lead to a better understanding of reef ecology. In addition, it may help indirectly to discover and investigate new pharmaceutically interesting peptides.

1.3 Patellamides: Biosynthesis, Conformation and Chemical Features

The chemical diversity of *L. Patella* is displayed by the fact that there are several families of azole and azoline based cyclic peptides isolated from this single species.[24] There are the 21-atom macrocyclic Lissoclinamides (Figure 1.6b), the 18-atom macrocyclic Westiellamide (Figure 1.2c) (which could also be isolated from the terrestrial cyanobacteria *Westiellopsis prolifica*)[10,49] and the patellins (Figure 1.6a). Another interesting peptide from *L. Patella* is tawicyclamide (Figure 1.6c) which has a proline and a thiazoline instead of two oxazolines. Furthermore Prepatellamide A and B (Figure 1.7) could be isolated from *L. Patella*. In both peptides one of the oxazolines is hydrolysed which suggests that they may be precursor molecules for the respective Patellamides.[4,18] All native cyclic peptides are 18- to 24-atom macrocylic azacrowns, with a scaffold composed of altering N-heterocycles combined with amides.

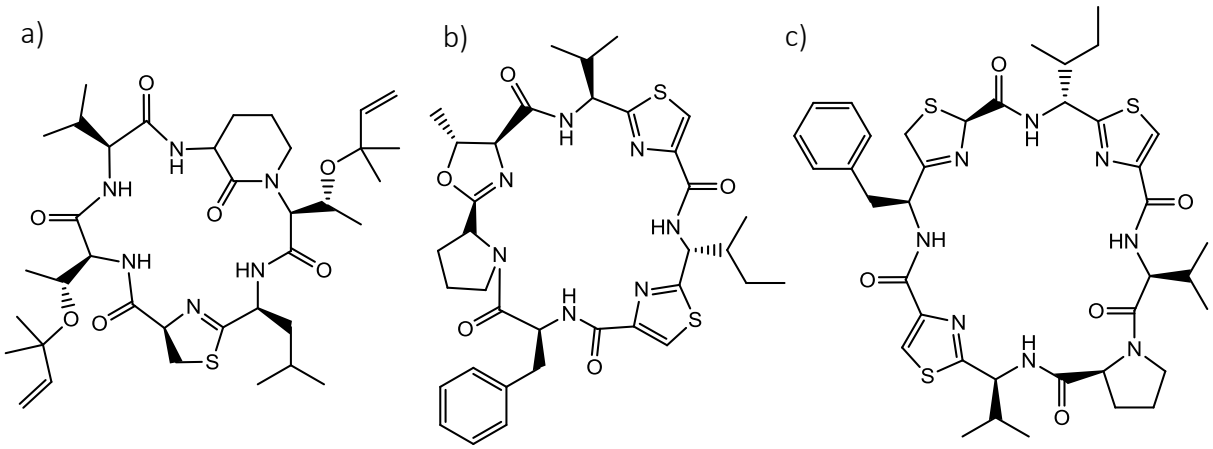

Figure 1.6: Structures of Patellin 1 (a), Lissoclinamide 1 (b), Tawicyclamide A (c).

Studies of the chemistry of the patellamides were encouraged by their known antibacterial, cytotoxic and antiviral activities. [13,32-41,50] The patellamides from *L. Patella* are low weight cyclic peptides and can be described as macrocyclic azacrowns with eight possible N-donors, with the potential to bind metal ions within this macrocyclic cavity. .(Figure 1.6, Table 1.1). Since these cyclic peptides are possible ligands for transition metal ions, it is necessary to have a look at

their diversity, biosynthesis, the combination of amino acids, the azacrown ring size, the peptide conformation and the overall configurations of the patellamides.

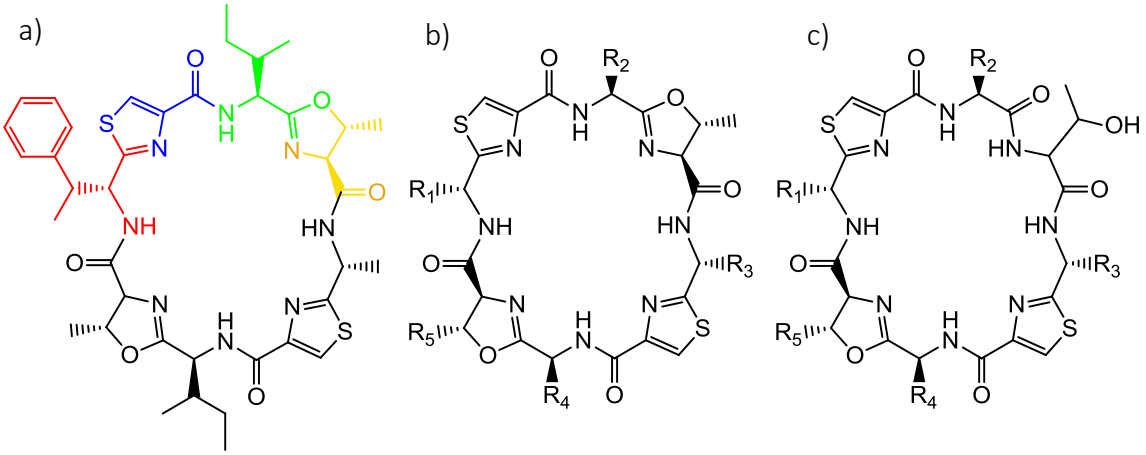

Figure 1.7: Structures of Patellamide D (a) (red: Phe, blue: Cys, green: Ile, yellow: Thr), Patellamide skeleton (b), Prepatellamide skeleton (c).

The patellamides are designated as *pseudo*-octapeptides because, formally, their scaffold of alternating azoles/azolines with amides originates from the condensation of eight amino acids[24,35,50-52] (Figure 1.7 colored patellamide D for visualization).

Tabel 1.1: Structural variations in the patellamide scaffold.[9,11,12,15,37,53-55]

Pseudo-octapeptides	R_1	R_2	R_3	R_4	R_5
A	D-Val	L-Ile	D-Val	L-Ile	H
B	D-Phe	L-Ile	D-Ala	L-Leu	CH_3
C	D-Phe	L-Ile	D-Ala	L-Val	CH_3
D	D-Phe	L-Ile	D-Ala	L-Ile	CH_3
E	D-Phe	L-Ile	D-Val	L-Val	CH_3
F	D-Val	L-Val	D-Phe	L-Val	H
G	D-Ala	L-Leu	D-Phe	L-Ile	CH_3
Ascidiacyclamide	D-Val	L-Ile	D-Val	L-Ile	CH_3
Prepatellamide A	D-Val	L-Ile	D-Val	L-Ile	H
Prepatellamide B	D-Phe	L-Ile	D-Ala	L-Leu	CH_3

The condensation of eight amino acids is the first ribosomal step of the native patellamide synthesis. Biosynthesis starts with the ribosomal formation of a propeptide, which is initiated by a gene cluster with seven genes, called Pat A-G, but only five genes are required for the patellamide synthesis. The resulting propeptide has at its beginning a start-cyclization sequence

that is a pentapeptide and at its end a stop-cyclization-sequence which is a tripeptide.[56] The heterocycles, i. e. thiazols, thiazolines and oxazolines are produced by cyclic condensation of serine, threonine and cysteine and, in some cases subsequent oxidation (Figure 1.8). The thiazoles/thiazolines are produced prior to the commencement of oxazoline condensation. Both steps are post translational modifications.[43,57] The biosynthesis ends with a macrocyclic condensation of both peptide ends. This final step is directed by the start and end sequences and is presumably enzyme-driven.[58,59] Due to the fact that all steps occur in *prochloron* ribosomes the synthesis is classified as ribosomal production and post-translational modification (RIPP).

Until now no imidazole-containing cyclic pseudo-peptide has been discovered in *L. Patella*. This may be the case because the necessary 2,3-diaminopropionic acid is not abundant in the ribosome.[60,61] However, considering the various metabolic roles of the imidazole-groups as side chains of histidine containing peptides and proteins, this fact increases curiosity about the natural role of the patellamides even more.

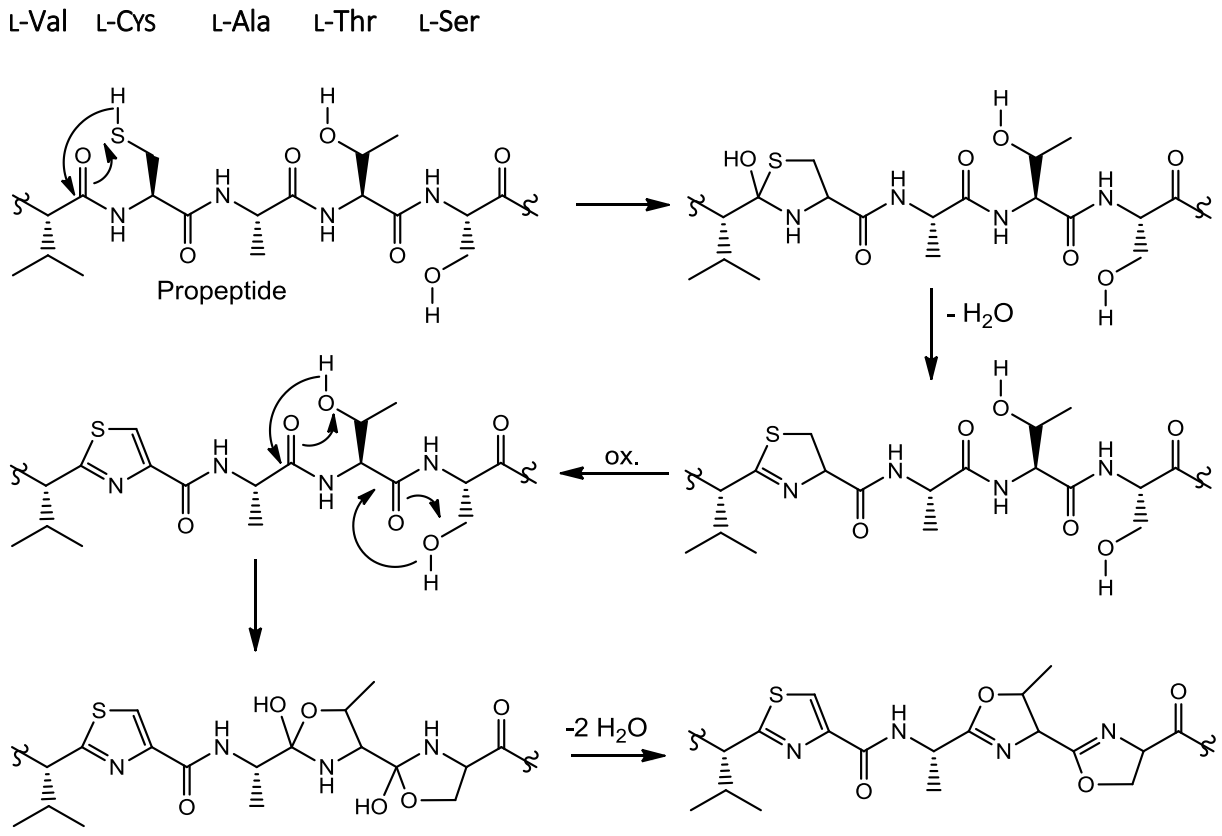

Figure 1.8: Post transalational heterocyclization of a hypothetical linear propeptide.

The absolute configuration (R* or S*) of the amides-stereo centers is another characteristic feature of this peptide family. The potential for the differences in absolute configuration at Cα is illustrated in Figure 1.6 and Table 1.1 and shown in Figure 1.9.

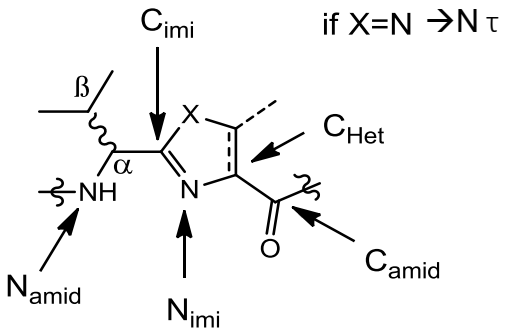

Figure 1.9: Visualization of C_α and $C_ß$.

It is known that peptides containing D-amino acids are protease resistant and less immunogenic than their stereoisomers with only L-amino acids.[62,63] Therefore, it is understandable that studies were able to show that D-amino acids and D-peptides have high potential for improving selectivity and maintaining activity of therapeutic agents[64] Investigation of the dynamics of the glycopeptide peptidoglycan (Figure 1.10), an essential component of the bacterial cell wall, showed that the substitution of one single L-alanine with D-alanine lead to a significant change in the biological response.[65]

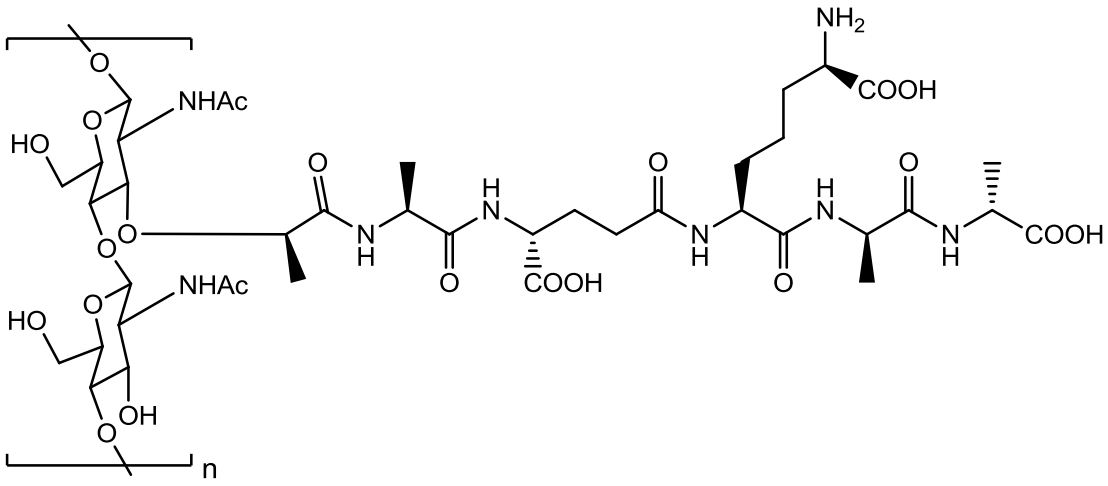

Figure 1.10: modified Peptidoglycan.

Thus, the consequent use of D-amino acids in a ribosomally produced peptide presumably plays a key-role in the biological function of the patellamides. Furthermore, the fact that

amino acid residues that are opposite to each other adopt the same absolute configuration is the mainly influencing feature for the whole peptides structure.

Another key feature of the patellamides is their structure, both, in solid state and in solution. Due to the heterocycles and the amides, the structure of the macrocycles is relativly rigid.[66,67] The dihedral angle χ [N_{amide}-C_α-C_{imi}-X] is an indicator for the extension of deviation from planarity of the complete macrocycle (χ=0, 180° indicates planarity) and is the decisive factor for the macrocycles final structure. It has been shown with DFT calculations (Figure 1.11) that χ depends on the kind of azole-system and the size of the amino acid residues.[68,69] By comparing the small-residue cyclic peptides (Figure 1.11a) it is obvious that the thiazol reference system has one minimum more than the oxazole and the imidazole reference system, which leads to the suggestion that thiazole-containing macrocycles have a higher flexibility than oxazole- or imidazole-containing macrocycles.[66,69] The second observation from the data in figure 11 is that while changing to a sterically more demanding residue (Figure 1.11b), the rotational activation barrier increases and so there is for all three reference systems just one minimum left in the less planar range from 100°- 150°. Investigations of the crystal structures and DFT calculations on imidazole and oxazole containing cyclic octapeptides confirmed, by comparing the structures of C_2- and C_4-symmetric cyclic octapeptides, that the final structure of these peptides depends on the kind of azole used and not on the symmetry of the system.[69]

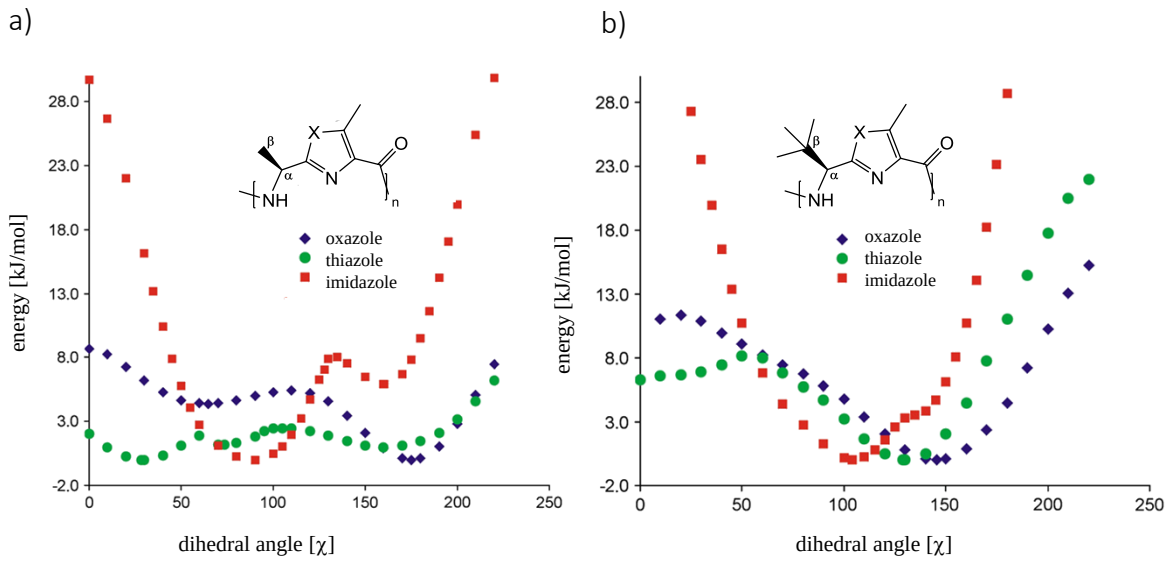

Figure 1.11: Energy profiles – DFT calculated of the oxazole- , thiazole- and imidazole- reference systems, respectively, in relation to the dihedral angle.[66,67,70]

The solution structures of the patellamides are determined by NMR Spectroscopy[52,71,72] in combination with molecular mechanics, molecular dynamics and Monte Carlo[9 71,72] as well as DFT calculations.[73] A mixed NOE-NMR and circular dichroism study indicated a figure-of-eight structure for patellamides A and C in non-polar solvents; in contrast in polar solvents the pseudo-symmetric patellamide A adopts the known saddle-shaped conformation whereas the non-C_2-symmetric patellamide C remains in an figure-of-eight conformation.[74]

All structural investigations in solution indicate that there are two main types of conformation in solution the "saddle-shaped" (square) and the "figure-of-eight" geometry (Figure 1.12), which depend on the degree of symmetry as well as on the polarity of solvents used. Additionally the NMR studies pointed out that most patellamides adopt in general in solution the same conformations as they adopt in the solid state.[10,13,69,71,75] Within the saddle-shaped conformation the thiazoles and the oxazolines occupy the corners of a rectangle. The most important feature of this conformation is that all nitrogens are directed towards the center of the macrocycle. The figure-of-eight conformation therefore is characterized by a twist within the two opposite amide sides.

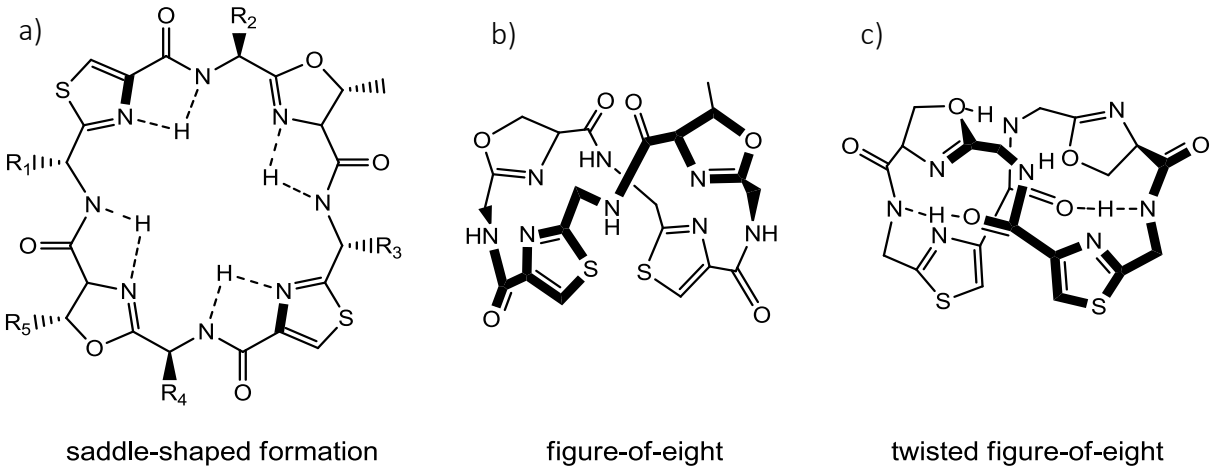

Figure 1.12: Visualisation of possible conformations; drawings of all possible conformations.

In 1988 the X-ray structure of ascidiacyclamide (Figure 1.13b) was reported by Ishida et al.[9] In later work the same group reported the X-ray structures of Patellamide A and D.[73,76] Both Patellamide A and D seem on the first view to have similar rectangular structures, but on closer inspection, the C_2-symmetric asciacyclamide (as the C_2 symmetric patellamide A) crystallized in a so called saddle-shape conformation (Figure 1.13b) whereas patellamide D, which is less symmetric, crystallized in a so called twisted figure-of-eight form (Figure 1.13a).

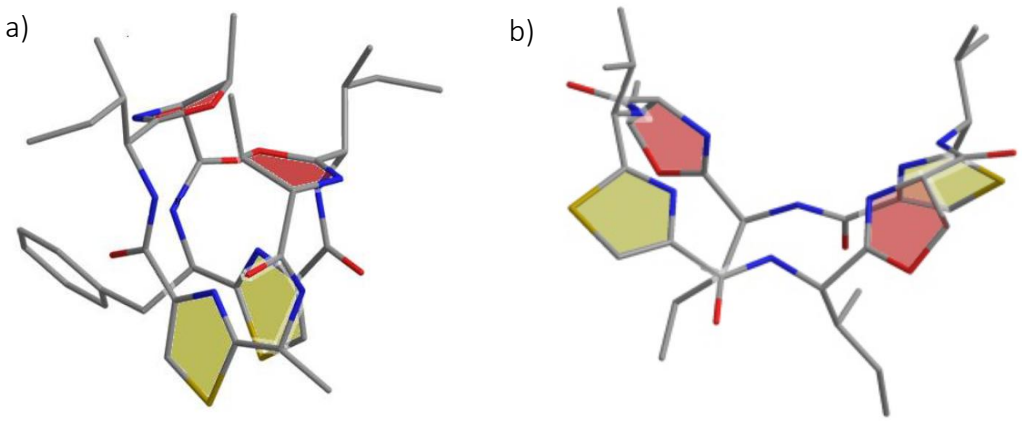

Figure 1.13: crystalstructures of Patellamide D (a)[77] and Ascidiacyclamid (b).[9,70]

Also, patellamide B and C which have a lower than C_2-symmetry, were later found to crystallize in a twisted figure-of-eight configuration.[71] The different solid state conformations of the patellamides are related to the type of symmetry.[54]

1.4 Patellamides and their Metal Complexes

The last sections indicate that there are a number of attempts to discover the natural role of the patellamides. These approaches include investigations of their synthesis,[53,69,78-80] finding the genetic information responsible for their production[16,17] and also investigations towards their ability to coordinate metal ions. [1,70,81-85] The fact that transition metals like copper(II), vanadium(III) and zinc(II) are highly concentrated in the ascidians leads, together with the [18]- and [24]-azacrown structure of the cyclic peptides, to the assumption that coordination chemistry may play a major role for the cyclic peptides found in *Lissoclinum Patella*.[86-88] However, investigations of the metal ion coordination by marine secondary metabolites was rarely considered before 1993 when a review of the field by Pattenden stimulated greater interest in the topic.[89]

In 1996 Jaspars *et al.* collectecd samples of *Lissoclinum Patella,* which revealed, after solvent extraction, that the concentration of copper(II) and the concentration of zinc(II) was approximately four orders of magnitude higher than in the surrounding seawater. Interestingly, the highest concentrations were detected in the dichloromethane extract,

which indicated that the metal ions must have been complexed.[88] One suggestions for the biological function of the patellamides, considering the high copper enrichment, was copper(II) complexation, transport, storage or detoxificationor.[88] The high copper(II) concentrations found in the ascidiacea *Lissoclinum patella* would be toxic for most organisms as toxicity towards copper(II) can be observed for most organisms at a concentration in a range from 10^{-7} to 10^{-6} M.[1,41,88,90]

The copper(II) complexes of the patellamides have been investigated extensively [1,70,81-85] In addition, the zinc(II), calcium(II), magnesium(II) and potassium(I) complexes have been investigated.[41,82,91-93 94] While comparing the calcium binding ability of patellamides A, B, C and D with synthetic analogues, via NMR and CD spectroscopy, it was concluded that only the conformationally more flexible peptides exhibit a significant affinity for calcium(II) ions. [91,93] The calcium(II) ions were proposed to be coordinated by the amides oxygen, preferring to form 1:1 complexes with these ligands.[91,93] The crystallization of a potassium complex (Figure 1.14) with a twice hydrolyzed ascidiacyclamide was also reported.[82] The hydrolysis of the oxazoline moieties led to a more flexible macrocycle and thus, it was possible for potassium to coordinate to two heterocyclic nitrogens and two carbonylic oxygens. Astonishingly this potassium complex was able to form by addition of copper(II) perchlorate a purple compound which had an EPR spectrum indicative of two different mononuclear copper(II) complexes.[82]

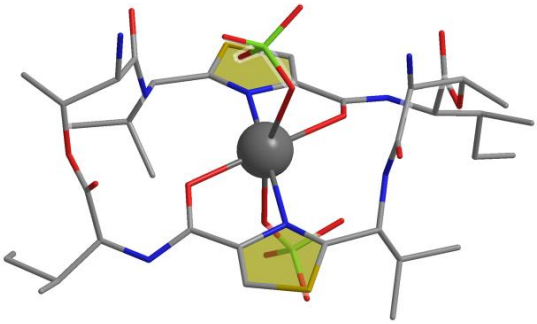

Figure 1.14: Potassium complex of Ascidiacyclamide. (carbon=grey, sulfur=yellow, nitrogen = blue, oxygen=red)[70,82]

Comparison of the zinc(II) coordination properties of ascidiacyclamide with those of an synthetic analogue showed the formation of three species, depending on the nature of the anion and the presence or absence of base.[92] Complex formation by zinc(II) triflate, perchlorate and chloride led to the formation of two different mononuclear species. The NMR spectrum of the mononuclear species indicated C_2 symmetric complexes. Only the use of zinc(II) chloride resulted in a dinuclear species, characterized by mass spectrometry.

Freeman and Pattenden studied the coordination preferences of patellamides A,B and E and showed that all three have no affinity for the coordination of calcium(II) or magnesium(II).[95] However, the patellamides investigated showed a high affinity for the coordination of zinc(II) ions and an even higher affinity for the coordination of copper(II) ions. Interestingly, all investigations showed that the patellamides bind up to two metal ions. In the case of copper(II) and zinc(II) the binding constants for the first metal were in the range 2×10^4 to 3×10^5 and for the second metal ion in the range from 20 to 230. It was also confirmed that patellamides B and E underwent a conformational change from figure-of-eight to a saddle-shaped conformation while complexing copper(II) ions.[95]

While for the patellamides there is no report of the formation of sandwich-type complexes nor clusters, Wipf *et al.* reported for the smaller analogue westiellamide (Figure 1.2) the formation of a silver(I) complex harboring four silver(I) ions with a sandwich-like structure.[96] Bertram and Pattenden studied the possibilities of template-synthesis and reported the discovery of a sandwich complex with five silver(I) ions in between two four-thiazole containing patellamide-model peptides.[97]

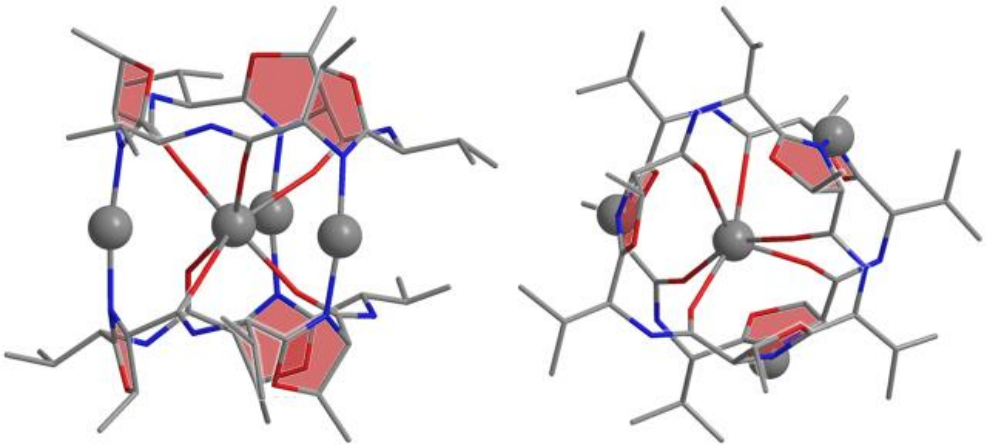

Figure 1.15: Silver(I) complex of Ascidiacyclamide. (carbon=grey, nitrogen = blue, oxygen=red)[70,96]

In 1988 Hawkins *et al.* published circular dichroism studies of the interaction of the patellamides with copper(II). It was shown that mono- and dinuclear complexes were formed.[1,81] One of the most significant discoveries was that the dinuclear copper(II) complexes of ascidiacyclamide reacted with carbon dioxide to form a carbonato-bridged complex (Figure 1.16). This was characterized by X-ray crystallography, as well as through magnetic susceptibility measurements and ion-spray mass spectrometry.[1] In this complex the two copper(II) ions are separated by a bridging carbonate and embedded in the saddle-shaped ligand. Each cpper(II) ion is coordinated by two heterocyclic nitrogen atoms (N_{imi}), one amide nitrogen atom (N_{amid}), the carbonate and a water molecule. This crystal structure lead the first time to the idea that potentially existing dinuclear copper(II) complexes of the patellamides in *vivo* might be involved in the fixation of CO_2. [1]

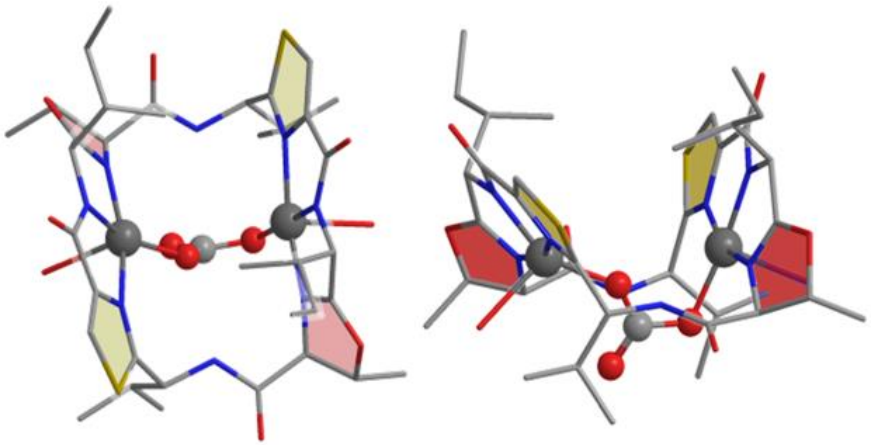

Figure 1.16: Carbonato-bridged dinuclear Copper(II) complex of ascidiacyclamide; Top view (left), side view (right) (carbon=grey, sulfur=yellow, nitrogen = blue, oxygen=red).[1,70]

There was also an electronic paramagnetic resonance (EPR) mass spectrometry (MS) and circular dichroism (CD) study in 1994 investigating the copper(II) binding properties of patellamide D.[81] The study showed the formation of two mononuclear and three dinuclear complexes, one of which was a carbonato-bridged complex.[81] The copper(II) coordination depended on the choice of the copper(II) salt, on the solvent employed and on the presence of base. Furthermore, it was concluded that in the dinuclear carbonato-bridged copper(II) complex of patellamide D, the ligand had a saddle-shape conformation as it does in the same complex with ascidiacyclamide. In later work the results were reinterpreted with the help of molecular modeling which showed that the coordination of metal ions could change the conformation of the cyclic peptide if necessary.[98] Similar results were obtained by Jaspars et al. while investigating the copper(II) coordination properties of patellamide A, C and ulithiacyclamide with circular dichroism and mass spectrometry. Patellamide C showed a higher affinity for copper(II) ions than patellamide A. This finding was assigned to the greater willingness of a conformational change from figure-of-eight to saddle-shaped by patellamide C. Furthermore, this result indicated a cooperative effect of the macrocycle: that is, the coordination of the first metal ion preorganizes the macrocycle for the coordination of the second metal ion.[41,88] Jaspars et *al.* studied the metal ion selectivity of these peptides and found out that there was no binding of cobalt(II), nickel(II) or mecury(II) and that patellamide C (as well as ulithiacyclamide) had a higher selectivity for copper(II) than patellamide A, in comparison to zinc(II).[88] The higher selectivity of copper(II) over zinc(II) could be assigned to the ability of copper(II) ions to induce the conformational necessary change, for the uptake of

a second metal ion, in patellamide C earlier than zinc(II) does. Copper(II) favours a square planar or a square pyramidal coordination environment, which is provided for two metal ions when patellamide C adopts a saddle-shaped conformation. On the contrary zinc(II) is geometrically highly flexible (as in Chapter 4 described; zinc(II) could easily adopt tedrahedral, octahedral or trigonal bipyramidal geometries). From all their studies jaspars *et al.* concluded that it is more likely that copper(II) is the biologically relevant metal for the patellamides.[94]

Tabel 1.2: Published complex stabilities of the patellamides.[70]

Peptide	Metal ion	K_1	K_2	method	reference
Patellamide A	Cu(II)	$2.00*10^4$	$7.76*10^2$	CD	41,95
		$3.31*10^4$	$1.00*10^4$	MS	41
	Zn(II)	$3.02*10^4$	$1.00*10^3$	CD	41
		$2.82*10^3$	$3.89*10^3$	MS	41
Patellamide B	Cu(II)	$3.02*10^5$	$2.29*10^2$	CD	95
	Zn(II)	$3.02*10^4$	$1.19*10$	CD	95
Patellamide C	Cu(II)	$6.70*10^4$		CD	41
		$6.31*10^4$	$6.03*10^3$	MS	41
	Zn(II)	$1.78*10^4$	$8.13*10^2$	CD	41
		$2.40*10^3$	$2.57*10^3$	MS	41
Patellamide D	Ca(II)	$7.94*10^2$		NMR, CD	91
Patellamide E	Cu(II)	$1.51*10^4$		CD	95
	Zn(II)	$7.94*10^4$	$2.00*10$	CD	95
Ascidiacyclamide	Ca(II)	$7.94*10^2$		NMR	91

The complex stabilities discussed above and in the literature are listed in Table 2. While interpretation of these values one has to keep in mind that different analytical methods were used.

1.5 Model Peptides and their Copper(II)-Complexes

In order to model structural features of the patellamides and to investigate possible biological activities of probably naturally occurring patellamide-metal complexes, a range of artificial occurring cyclic peptides were synthesized. [69,70,83-85,99] The main focus for the design of new ligands was on the stereochemistry of the amino acid residues and the donor strengh of the azoles and azolines. A set of synthetic peptides was developed, labeled H_4pat^1 to H_4pat^5 and H_4ascA (Figure 1.17).

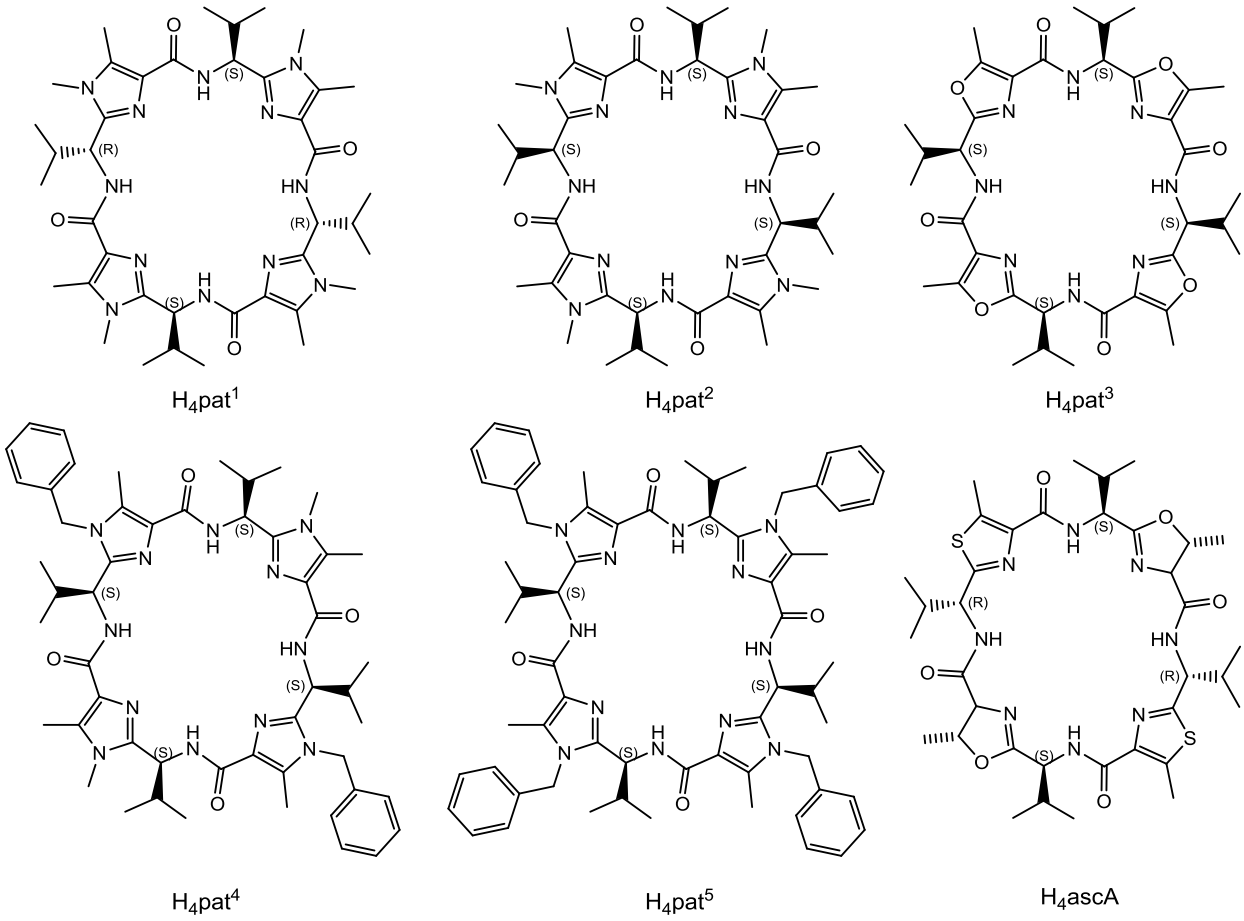

Figure 1.17: Synthetic *pseudo* octapeptides.[100,101] [69,99]

Even if imidazole-containing patellamides were not found in *Lissoclinum patella*, diamino propionic acid is not abundant in *prochlorons* ribosomes, they were chosen for this set of ligands. [99] Imidazoles are less hydrolytically sensitive than oxazoles, thiazoles and oxazolines.[102-

[104] and offered the possibility of varying the electronic effect of the second hetero-atom by substitution of the residue at the nitrogen N_τ. The pK_A values of the heterocyclic nitrogen donor of N-methylimidazole is 7.0, which is considerably higher than the pK_A values of; oxazoles (pK_A: 0,8), oxazolines (pK_A: 4.8) and thiazolines (pK_A: 2.5).[105]

All synthetic ligands have valine side chains. The ligands H_4pat^1 and H_4pat^2 have the same chemical composition but in contrast to H_4pat^2, H_4pat^1 adopts the native configuration (R*,S*,R*,S*) of the amino acid residues. The configurational change makes H_4pat^1 a C_2 symmetric ligand and H_4pat^2 a C_4 symmetric ligand. The C_4 symmetric ligand H_4pat^3 has the same configuration as H_4pat^2 but instead of four methyl-imidazoles there are four oxazoles. H_4pat^4, has a 4S* configuration, harbors two methyl imidazoles alternating with two benzyl imidazoles and therefore has C_2 symmetry. In addition, there is the four benzyl-imidazole containing ligand H_4pat^5 with C_4 symmetry. The most biomimetic ligand is H_4ascA which differs from ascidiacyclamide only by substitution of two isoleucine- to two valine- side chains.

Cyclic pseudo octapeptides are highly preorganized for the coordination of copper(II), and these artificial macrocycles show a strong cooperativity in the binding of two copper(II) ions. [70,99,106] Various experiments and computational analyses illustrated the cooperativity of the binding event of two copper(II) ions, and it was possible to detect a dinuclear copper(II) complex via EPR-spectroscopy in at 10-fold excess of the macrocyclic ligand H_4pat^2.[100 85] The equilibrium of copper(II) complexes of the artificial patellamides was experimentally explored in methanolic solutions because most of the artificial *pseudo*-peptides have only a low solubility in water, and also to keep all systems comparable. The equilibria can be described as follows (Figure 1.18):

1.) All cyclic *pseudo*-peptides considered here prefer to coordinate two copper(II) ions. The preorganization by the coordination of the first metal ion leads to a change in conformation which facilitates the coordination of the second metal ion, and is thus described as cooperativity.
2.) Due to the large number of possibile mono- and dinuclear complexes (co-ligands: solvent, deprotonated solvent, OH-, bridging or terminal), there is an complex equilibrium between different species for all cyclic *pseudo* peptides (Figure 1.18). This makes the spectroscopic characterization of a distinct single species difficult,

compared to ligands which do form under diverse conditions selectively distinct complexes. And also, crystallization of a single species has only rarely been achieved.[99]

3.) The copper(II) ions are always coordinated to two heterocyclic nitrogen atoms and one deprotonated amide nitrogen atom. The formation of mono- and dinuclear complexes with copper(II) involves two metal ion assisted deprotonation steps of the amide nitrogen donors, the resulting drop in pH makes it necessary to add base for a complete complexation.

4.) Nevertheless, the equilibria of the different cyclic *pseudo* peptides are characteristic.

The copper(II) complexation equilibria of all ligands are described by various spectroscopically monitored titration experiments (EPR, UV/vis-NIR, CD, MS), as a function of copper(II)- and base- (OMe^-) concentration. The native configuration (R*,S*,R*,S*) of H_4pat^1 results in the most stable copper(II) complexes.[106] Also, this ligand forms directly dinuclear complexes without evidence of any mononuclear species.. It was possible to trap the hydroxo bridged $[Cu_2H_2pat^1(\mu\text{-}OH)]^+$ species and to structurally characterize it.[99,101] The 4S* configured ligand H_4pat^2 forms a mononuclear copper(II) complex as well as a higher concentrated dinuclear copper(II) complex at low copper(II) and base ratios.[85,100] With H_4pat^2 it was also possible to detect a carbonato-bridged species in contrast to H_4pat^1. Interestingly, H_4pat^2 forms a pink species upon addition of water to titration at a low base ratio. The ligand H_4pat^3, which has four oxazoles instead of four imidazoles shows at low copper(II) concentrations the formation of a 2:1 ligand/copper(II) complex, a so-called outside-coordination. (Figure 1.18) UV/vis and CD spectroscopic monitored titration studies of the ligands H_4pat^4 and H_4pat^5 with copper(II) have been reported.[107] Ligand H_4ascA as a close analogue of ascidiacyclamide has a similar copper(II) coordination equilibrium as H_4pat^1 and H_4pat^2. Addition of copper(II), even without base, shows a d-d absorption band at 687 nm that increases rapidly with the addition of two equivalents of base. The fact that there is only one d-d band which does not shift upon addition of base suggests that both copper(II) ions have an identical coordination sphere, even if there would be a mononuclear species in solution, this would have the same coordination sphere. The corresponfding CD-spectrum shows an expected change in conformation upon addition of copper(II) which is visible below 400 nm. Addition of a third equivalent of base leads to a decreasing intensity and to a shift to higher wavelengths of the d-d absorption. Upon addition of a fourth equivalent of base the d-d band shifts to 660 nm. This result can be explained by

the formation of a dihydroxo complex and of a bridged hydroxo species at higher base ratios. The copper(II) coordination chemistry of H_4pat^4 will be in chapter 3 of this thesis. At low copper(II) concentrations, H_4pat^4 forms a single existing mononuclear copper(II) complex.

Thermodynamic stabilities of all dinuclear copper(II) complexes with the patellamide derivatives were determined by isothermal titration calorimetry (Table 1.3). H_4pat^1 forms the most stable dinuclear copper(II) complex. The high thermodynamic stability of H_4pat^1 indicates that the alternating configuration promotes formation of dinuclear copper(II) complexes.

Table 1.3. Copper(II) stability constants, entropies and enthalpies of complexation of the patellamide derivatives (standard deviations in brackets), obtained from ITC.[106]

	$[H_2pat^1Cu_2]^{2+}$	$[H_2pat^2Cu_2]^{2+}$	$[H_2pat^3Cu_2]^{2+}$	$[H_2pat^4Cu_2]^{2+}$	$[H_2pat^5Cu_2]^{2+}$
N [a)]	1.90 (0.09)	1.84 (0.08)	1.99 (0.02)	2.03 (0.02)	1.89 (0.02)
K	$1.71x10^6$ (0.71)	$4.03x10^4$ (0.55)	$2.27x10^5$ (0.14)	$1.43x10^5$ (0.08)	$1.50x10^5$ (0.09)
Δ*H* [kJ/mol]	46.8 (4.6)	84.52 (7.7)	62.7 (0.8)	74.8 (0.8)	73.5 (1.8)
Δ*S* [J/(mol K)]	278.6	371.5	313.8	349.3	344.7

[a)] computed Cu^{II} : (H_2pat^n) ratio

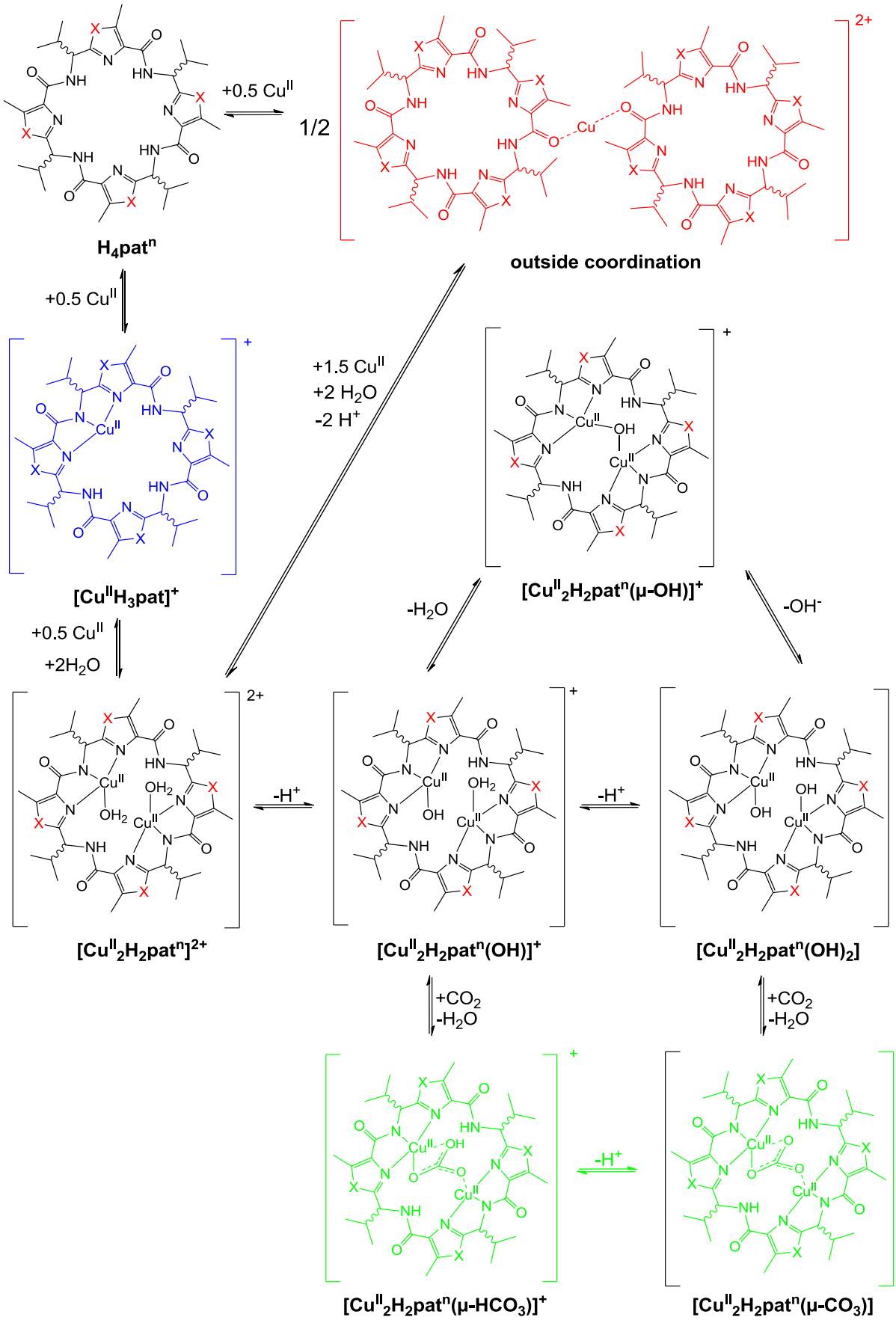

Figure 1.18: Scheme of all possible complex structures in *Pseudo* octapeptide copper(II) equilibrium. [70]

1.6 Hydrolase Activity by Model Complexes

Since potentially existing copper(II) complexes of the patellamides assumably fullfil their metabolic role in a hydrophilic environment, its likely that this metabolic role is hydrolysis chemistry. Regarding the ubiquitious occurrence of CO_2 and its various metabolic functions, it is obvious that nature needs various strategies to fix and to hydrolyse CO_2.

Hydrolysis of CO_2 is important in context of climate change and the acidification of the oceans. The development of technologies that are able to fix and to hydrolyze atmospheric CO_2 are thus important environmental questions. [108-110] The mechanistic and kinetic analysis of the carbonic anhydrase activity of dinuclear copper(II) complexes of patellamide derivatives has recently been described.[111] The dinuclear copper(II) complex of the ligand H_4pat^1 was the most active [k_{cat}=7.3 × 10^3 s^{-1} (uncatalyzed: 3.7 × 10^{-2} s^{-1})][111] and is, thus far, the most potent copper(II)-based model complex for the enzyme carboanhydrase.

Phosphoester-hydrolysis is also an interesting reaction with respect to the structures of the dinuclear copper(II) complexes of the patellamide derivatives. Phosphoester have numerous biological functions as being part of the DNA, RNA, phospholipids, ADP, ATP and pyrophosphates. Nature needs substances and strategies to hydrolyze phosphoesters catalytically under various conditions, in hydrophobic pockets, in cytoplasm, at different temperatures and different pH values. Since there are numerous CO_2 hydrolyzing systems that are also active in phosphoesters hydrolysis, this could also be a relevant reaction for the dinuclear transition metal complexes of the patellamides. Therefore, the copper(II) complexes of the Ligands H_4pat^1 and H_4pat^2 have been shown to hydrolyze the model phosphoester BDNPP (2,2´,4,4´-bis(dinitrophenyl)phosphate).[70,112]

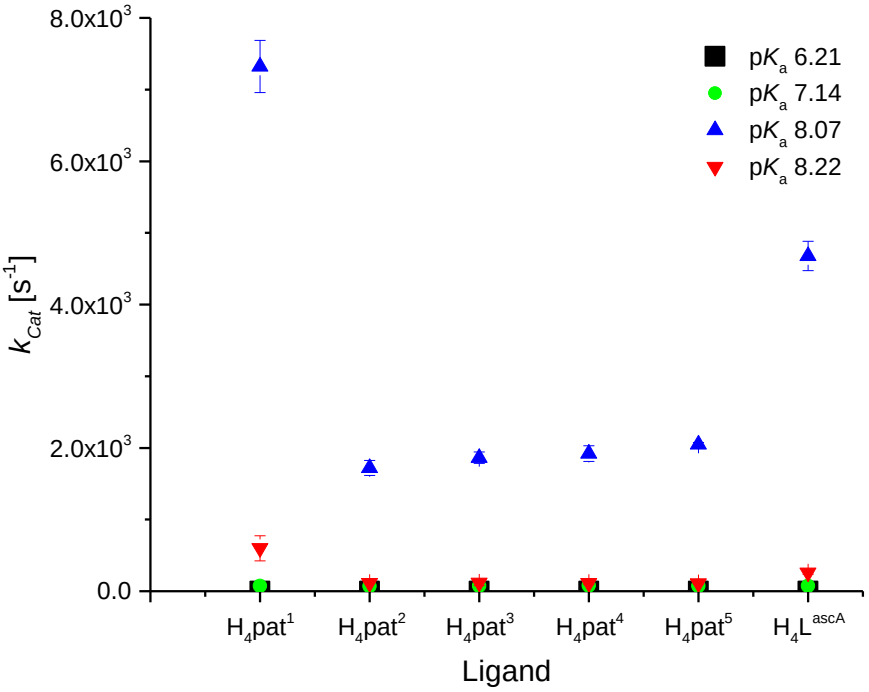

Figure 1.19: Graphical comparison of the catalytic effencies in CO_2 hydrolysis, of the patellamide derivatives dinuclear copper(II) complexes, at various pK_A values.[107,111]

1.7 Aims

On the continuous search for the natural role of the patellamides and ascidiacyclamide the coordination chemistry of specific derivatives shall be further investigated. Copper(II) is considered to play an important role in the natural chemistry of the patellamides. The copper(II) solution chemistry of a library of designed patellamide derivatives has been studied spectroscopically and thermodynamically. The first aim of this thesis was to study the electrochemical behavior of the corresponding copper(II) complexes. The electrochemical description of the copper(II) solution equilibria shall help to determine whether redox chemistry of potentially existing complexes under biological conditions is relevant.

Zinc(II) is also highly concentrated in the ascidians[88] and, in addition, it plays a key role in most hydrolyzing metallo enzymes. Thus, the focus of Chapters 4 and 5 lies on zinc(II) coordination

chemistry of the cyclic *pseudo*-octapeptides. Three peptides of the already existing library were chosen to explore their zinc(II) chemistry.

The coordination chemistry of zinc(II) containing cyclic *pseudo* peptides in the present thesis was explored with the objective focus on catalytic hydrolysis chemistry. The challenging question the present thesis is whether the characterized dinuclear zinc(II) containing cyclic *pseudo* peptide complexes are able to hydrolyze phosphoesters under physiologic conditions? Thus, all described complexes were tested using phosphoester model assays.

2 Synthesis of Patellamide Derivatives

The intention to describe the formation of zinc(II) complexes with patellamide derivatives required first the selection of appropriate ligands from an existing library (see Figure 1.17). The decision was made to explore the zinc(II) chemistry with the imidazole containing *pseudo*-octapeptides H_4pat^1, H_4pat^2 and H_4pat^4 (Figure 2.1). By altering the configuration of the valine-residues and the residues at N_τ of the imidazoles, it should be possible to determine which structural features are essential for the formation of the zinc(II) peptides.

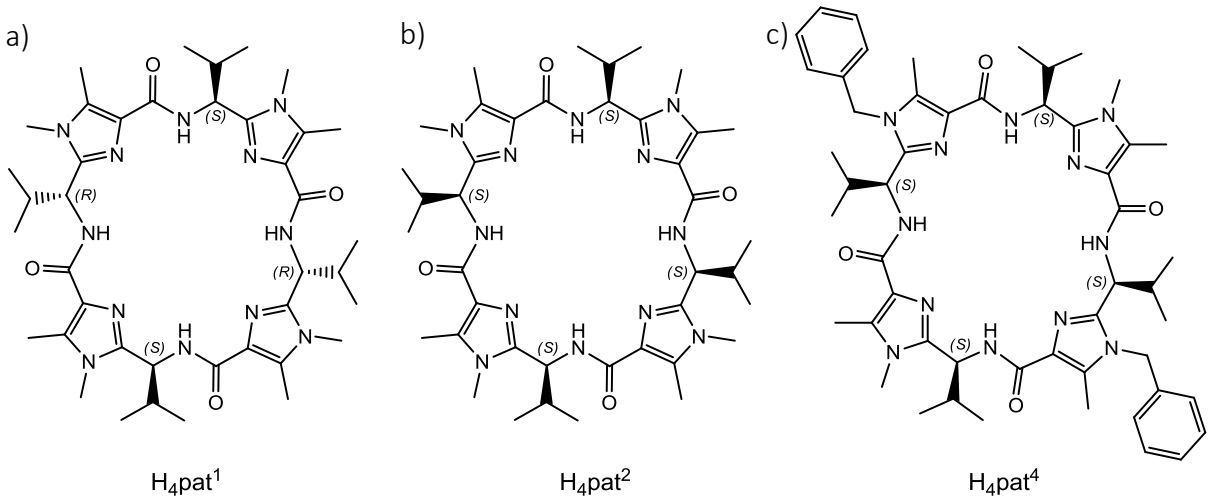

Figure 2.1: Structures of selected ligands: H_4pat^1 (a), H_4pat^2 (b) and H_4pat^4 (c).

The three patallamide derivatives chosen for this study have similar donor sets (N-methylimidazoles or N-benzylimidazols and amides) but are different in symmetry: H_4pat^2 is C_4 symmetric and H_4pat^1 and H_4pat^4 are C_2 symmetric. In case of H_4pat^1, the C_2 symmetry is a result of the alternating R*,S* configuration of the valine side chains, while in case of H_4pat^4, the C_2 symmetry is the result of the alternation of N-methylimidazoles with N-benzylimidazoles. The conformation adopted by these artificial cyclic *pseudo* octapeptides depends mainly on the stereochemistry of the amino acid residue (C_α) between the imidazole moieties. From

comparison of the X-ray structures (Figure 2.2) of all three ligands it appears that all may be described as saddle-shaped. Comparison of NMR studies with X-ray crystallography indicated that in solution and in solid state these peptides adopt the same saddle-shaped conformation.[101]

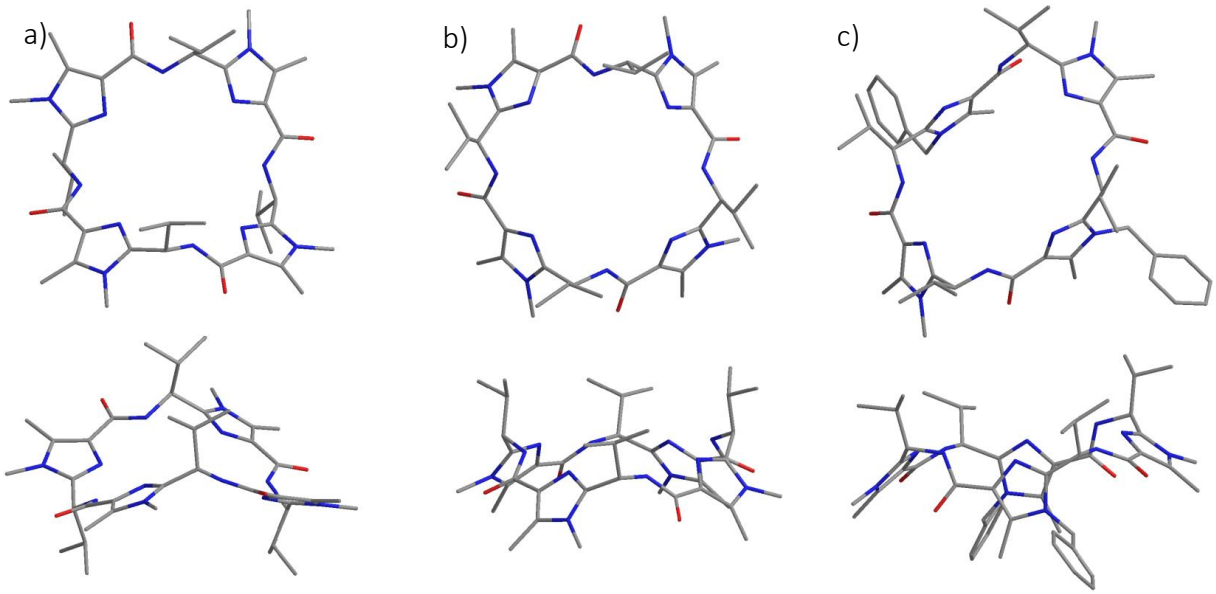

Figure 2.2: Crystal Structures of H_4pat^1 (a),[101] H_4pat^2 (b)[100,101] and H_4pat^4 (c)[101].

Although, all three crystal structures are assigned as saddle-shape conformed, there is a remarkable difference between them. The crystal structur of H_4pat^1 shows four imidazols that are oriented in a zig-zag fashion (Figure 2.2a). Contrary, in the the crystal structures of H_4pat^2 and H_4pat^4 the imidazoles are more conical oriented.[70,101]

2.1 Synthesis Strategy

The patellamide derived cyclic *pseudo* octapeptides were prepared following a modular synthesis route.[69,71,113,114] First heterocyclic building block were prepared (Figure 2.3), these were then formed to the final peptides in a cascade of deprotection- and coupling steps (Figure 2.4).

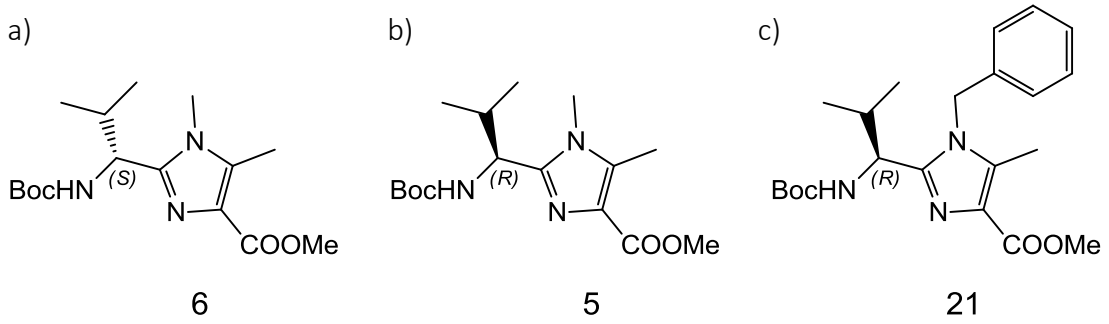

Figure 2.3: Structures of protected monomers H_4pat^1 (a), H_4pat^2 (b) and H_4pat^4 (c).

With this general approach it is possible to tune the final properties of the peptides while changing the type of heterocycle or the configuration of the amino acid side chain.[66,69,85,99,105,113] In this thesis all cyclic *pseudo*-peptides were synthesized *via* a double dimerization to avoid the formation of trimers.[100,101]

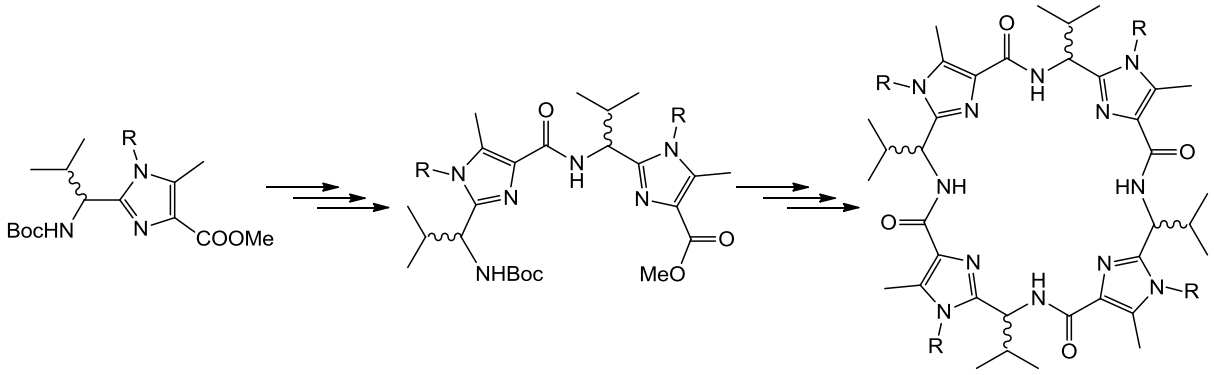

Figure 2.4: Schematic drawing of the modular synthesis route to the artificial cyclic *pseudo* peptides.

First two deprotected *pseudo* dipeptides were coupled, and the resulting product was subsequently deprotected and cyclodimerized. All reactions are known in the literature and only slight modifications to the published procedures will be highlighted.[6966,106]

2.2 Monomer Synthesis

The preparation of all three heterocyclic building blocks **5**, **6** and **21** (Figure 4.5) starts with the same molecule; the oxime **1**, which was prepared by the reaction of methyl 3-oxobutanoate

with sodium nitrate in glacial acetic acid. The oxide obtained was reduced in a methanolic HCl solution under a hydrogen atmosphere using 10% palladium on charcoal as catalyst. The resulting ammonium chloride salt **2** is the starting material for all three monomeric building blocks. Using isobutyl chloroformate and *n*-methyl morpholine (NMM) as coupling agent and base, the ammonium chloride salt **2** was converted into peptides**.** Ammonium chloride salt **2** was converted by coupling with Boc-protected R-valine into peptide **4**, by coupling with Boc-protected S-valine into peptide **3**, or into peptide **18** by coupling with Cbz-protected R-valine.

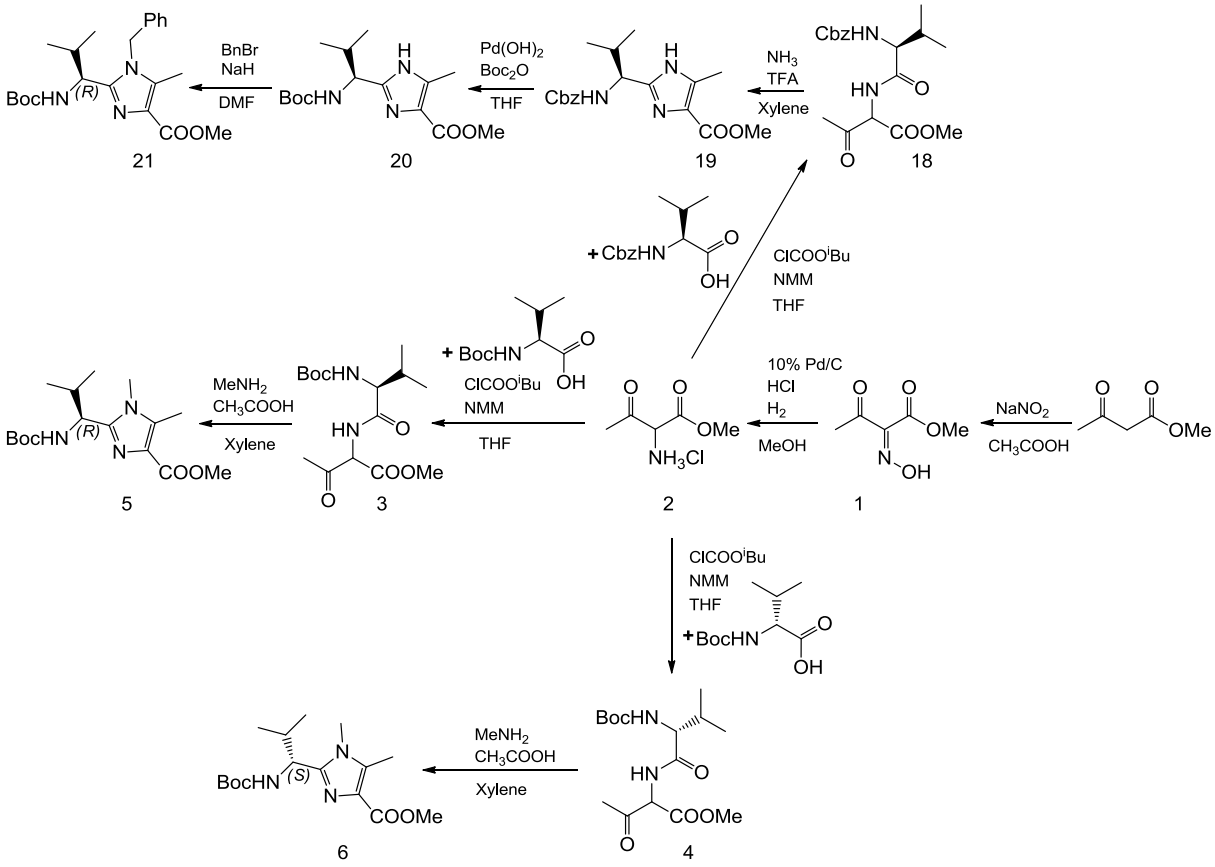

Figure 2.5: Scheme of monomer synthesis.

The heterocyclic building blocks **5** and **6**, the monomer subunits of H_4pat^1 and H_4pat^2, were prepared in a hetero-cyclization reaction (cyclo-Mannich condenzation) with methylamine and acetic acid. The benzyl imidazole building block **19** was obtained by hetero-cyclization with ammonia and trifluoroacetic acid. The formation of the benzyl imidazole building block required two additional steps. First the Cbz protecting group had to be substituted by a Boc protecting group via deprotection with palladium hydroxide and subsequent protection with Boc_2O. A benzyl group was then attached by the addition benzyl bromide and sodium hydride

in DMF. All heterocyclic building blocks were obtained as crystalline white solids: the R-valine methyl imidazole **5** was obtained in 63.6%, the S-valine methyl imidazole **6** in 86.6% and the R-valine benzyl imidazole **21** in 80.1% yield.

2.3 Peptide Coupling and Cyclization

For the preparation of the final cyclic peptides it was necessary that monomer **a** (Figure 2.6) was deprotect at one site. Deprotection of the carboxylate ester was achieved by hydrolysis with sodium hydroxide and Boc-deprotection by trifluoroacetic acid. The resulting deprotected monomers **b** and **c** were coupled using COMU as coupling agent and EDIPA as base.

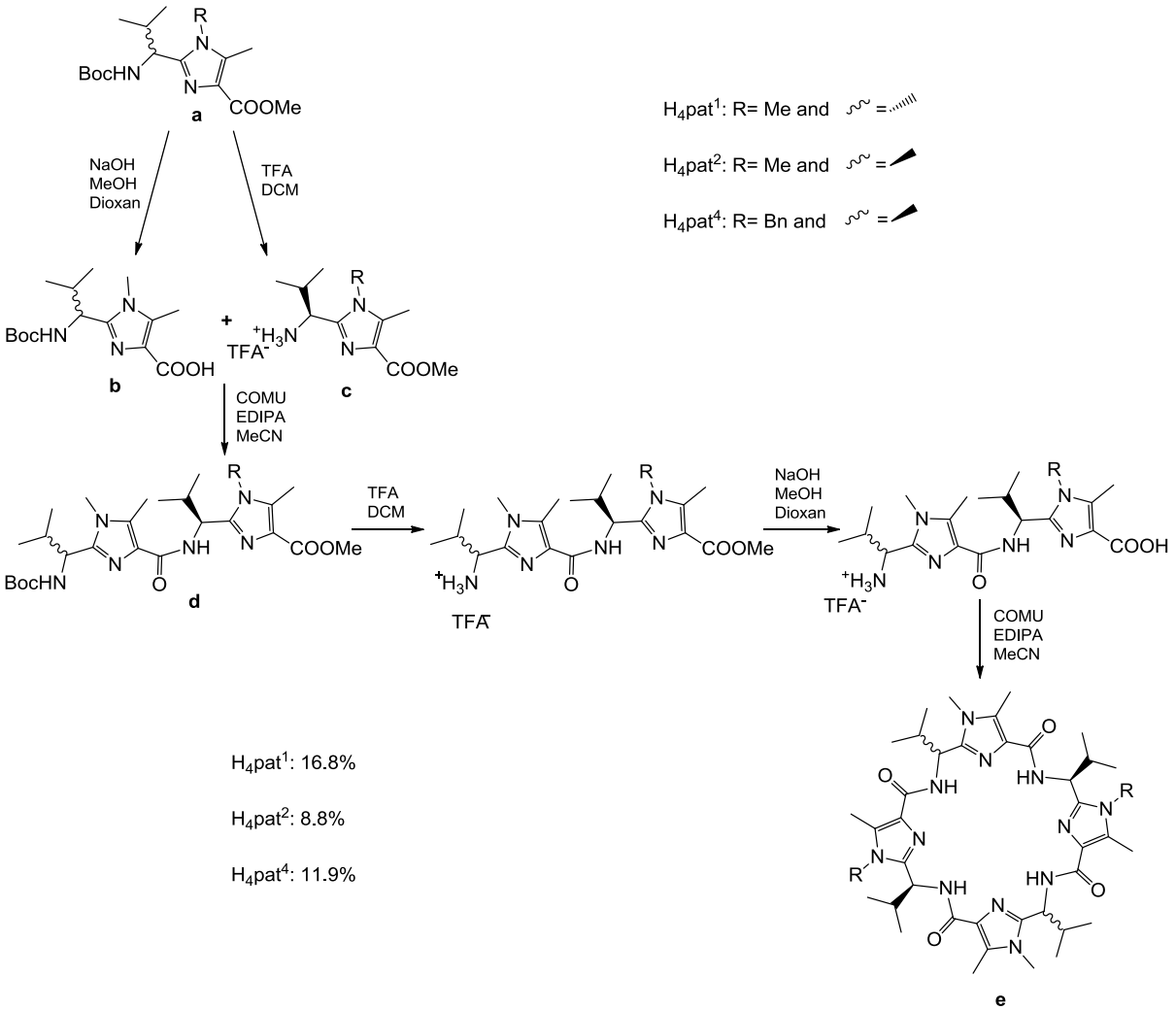

Figure 2.6: Schematic representation of the cyclo-peptide coupling.

The dipeptide building block **d** was first Boc-deprotected using TFA and subsequently methyl deprotected using NaOH. Finally, coupling to the desired cyclic *pseudo*-peptide **e** was achieved using COMU as coupling agent and EDIPA as base. After an extensive purification procedure by column chromatography and repetitive recrystallization all cyclic *pseudo*-octapeptides were obtained as crystalline white solids: yield of H_4pat^1 16.8%, H_4pat^2 8.8% and H_4pat^4 11.9%.The main influencing change in the cyclic *pseudo*-peptide synthesis was the use of COMU® as coupling reagent instead of FDPP. The uronium-type coupling reagent is less expensive, has a higher solubility and it is additionally easier to handle because of its stability. The herein reported yields are the result from the purification of only a part of the crude product after recrystallization and column chromatography. Nevertheless, with further time consuming purification steps it was possible to purify more of the crude product, which increases yields by approximately 2 to 3 time

Parts of the following chapter are published in “Copper Solution Chemistry of Cyclic Pseudo-Octapeptides”; Peter Comba, Nina Dovalil, Gebhard Haberhauer, Klaus Kowski, Nina Mehrkens, *Zeitschrift für anorganische und allgemeine Chemie* 2013, *639* (8-9), 1395-1400.

3 Copper(II) Complexes of Patellamide Derivatives

Since the biological function of the patellamides and ascidiacyclamide remains unknown and the donor set provided, as well as the shape of the macrocyclic peptides, appear to be suitable, copper(II) coordination chemistry is assumed to be of importance. Therefore, the copper(II) coordination chemistry of the patellamides and of their derivatives has been widely investigated.[1,52,70,81-85,99] The biological role of potentially existing copper(II) complexes might be copper(II) transport and storage, oxygen activation, CO_2 hydrolysis, carbonate transport, phosphoester hydrolysis, *ß*-lactam hydrolysis and glycoside hydrolysis.[52,85,112,115-117] Biologically relevant electron transfer reactions, oxygenations and oxidations by copper proteins (tyrosinase, hemocyanine, plastocyanine, catechol oxidase) usually occur in a hydrophobic microenvironment provided by a protein.[118] Considering the fact that the patellamides were isolated from ascidian cytoplasm together with high concentrations of copper(II) and zinc(II),[88] the suggestion that potentially existing copper(II) complexes of the patellamides acting as small molecular systems in an hydrophilic environment as hydrolysis catalysts seems very likely. To combine structural properties and thermodynamic stabilities of the known copper(II) complexes of cyclic *pseudo*-octapeptides with the electrochemical properties of the corresponding complexes, cyclo voltammetry (CV) measurements and square wave voltammetry (SQW) experiments were performed. Furthermore, knowing the reduction potentials E_{red} of dinuclear copper(II) complexes should give information about the stability of the according copper(I) species, and thus be able to answer the question whether there is a sufficiently stable copper(I) species which could be involved in biologically relevant electron transfer, oxygenation or oxidation reactions.

Furthermore, the complexation equilibrium of the copper(II) complexes of H_4pat^4 were investigated by electron paramagnetic resonance (EPR) spectroscopy to provide important information about possible heterodinuclear complexes discussed in Chapter 5.

3.1 Electrochemical Studies

Electrochemical properties of the copper(II) complexes of the ligands H_4pat^1-H_4pat^5 were investigated by voltammetry. Cyclic voltammetry was performed under anaerobic conditions in methanol (1mM complex) with ferrocene as the internal reference.[119,120]

Table 3.1 (S. 42) lists all redox potentials of the copper(II) complexes of the patellamide derivatives H_4pat^1-H_4pat^5. Cyclic voltammetry proved to be inconclusive, since the processes studied are electrochemically irreversible (Figure 3.1). Based on the known structures and stabilities of the copper(II) complexes, chemically reversible processes were not expected. The donor set provided by the macrocyclic peptides consists of two heterocyclic nitrogen atoms and one amide per copper(II) center, and the ligand sphere is completed by two solvent molecules, hydroxide or methoxide (terminal or bridging) and is thus not expected to stabilize copper(I).[121-124] Electrochemistry reveals in all cases that the copper(II) complexes of the cyclic *pseudo*-peptides do exist in equilibria. Thus, there is a number of different species in solution (Chapter 1, Figure 1.18) that can be electrochemically reduced. Moreover, the dinuclear copper(II) complexes with *K* values around 10^5 are only moderately stable.[106,107] Therefore, it is not unexpected that complicated voltammograms are obtained as shown (Figure 3.1). These voltammograms are depending on the concentration of all species involved (ligand, copper(II), base),[119] and exclude a simple assignment of the observed processes.

The cyclic voltammograms of solutions of H_4pat^4 with two equivalents of copper(II), that have been taken upon addition of various equivalents of base, show a number of irreversible reduction waves (Figure 3.1). Since the cyclo voltammograms did not change significantly with multiple scans, it can be supposed that no decomposition occurs. The first CV (Figure 3.1 a) is of a solution with 0.5 equivalents of base, with a ligand-copper(II) ratio of 1:2. The irreversible reduction at -370 mV belongs to solvated copper(II) ions (in methanol solvated copper(II) triflate shows an intense and irreversible reduction potential at -430 mV, which shifts to -350 mV upon addition of base). However, the signal assigned to free solvated copper(II) disappears upon further addition of base. The reduction potential of the solvated copper(II) is already disappeared at a ligand/copper(II)/

base ratio of 1:1:2. Moreover, irreversible reduction potentials at 363 and 773 mV appear and grow in intensity with increasing addition of base. The assignment of these positive reduction potentials is this way not possible, because of various different reasons. First, according to mass spectrometry (Section 3.3) there are different mono- and dinuclear species in solution. Second, even if there would be a single hydroxo coligated dinuclear copper(II) complex in solution (which is according to MS the main component), it wold be hard to assigne the potentials. One one hand it is not clear wether the hydroxo coligand is bridging or terminal, and on the other hand for both kinds of species are some options possible. A hydroxo-bridged species for example could have one, two or three reduction potentials.[121] Moreover, it is possible that both copper(II) ions are reduced at the same potential. Thus, a dinuclear copper(II) complex with a terminal hydroxid could have one or two reduction potentials.

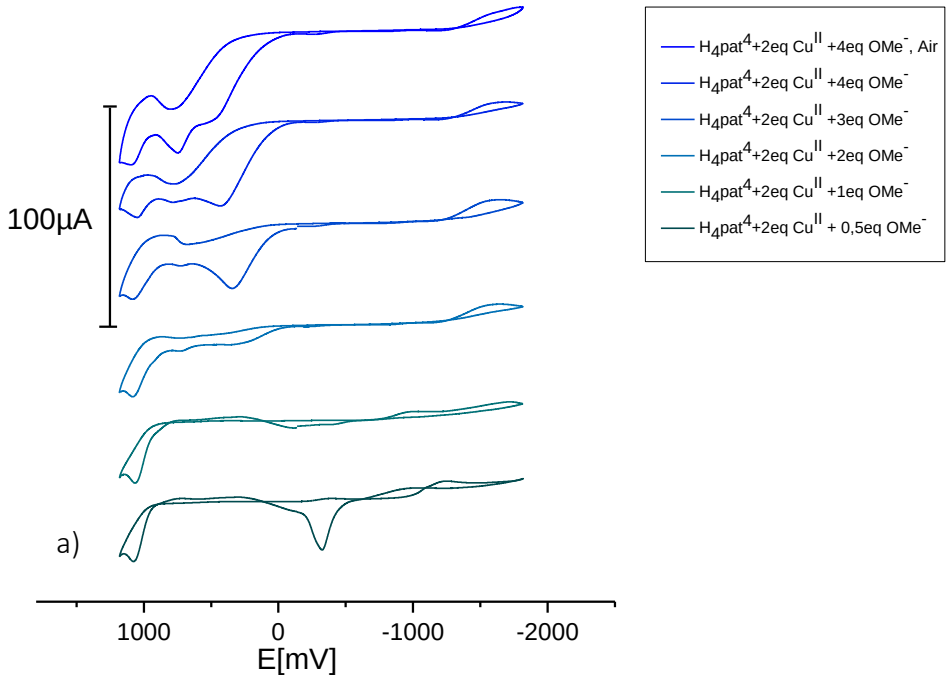

Figure 3.1: CV traces for selected copper(II) complexation-steps of H_4pat^4 (1mM in methanol with 0.1M $(t\text{Bu})_4NPF_6$ and vs. Fc/Fc^+, 100 mV/s, $Ag/AgNO_3$ 0.01M, 25°C)

Redox potentials of dinuclear hydroxo-bridged copper(II) complexes which are comparable to the copper(II) complexes of cyclic *pseudo*-octapeptides have been studied by Krebs *et al.*[125,126]. Casella *et al.* studied the differences between terminal or bridging coordinated hydroxides and water molecules at dinuclear copper(II) complexes and stated, that hydroxo-bridged dinuclear copper(II)

complexes have a poor ability to bind the electro-generated copper(I), and therefore, the processes have higher potentials.[127]

To simplify the analysis, square wave voltammetry (SQW) measurements were undertaken in 0.1 mM methanolic solution. Data reported in table 3.1 (s. 42) are those of the more sensitive SQW experiments. The higher-resolution of the square wave voltammetric titration (Figure 3.2) shows a very negative potential (-1242 mV) after flushing with CO_2 for five minutes. This leads to the assumption that the formation of carbonato-bridged species stabilizes coordinated copper(I).

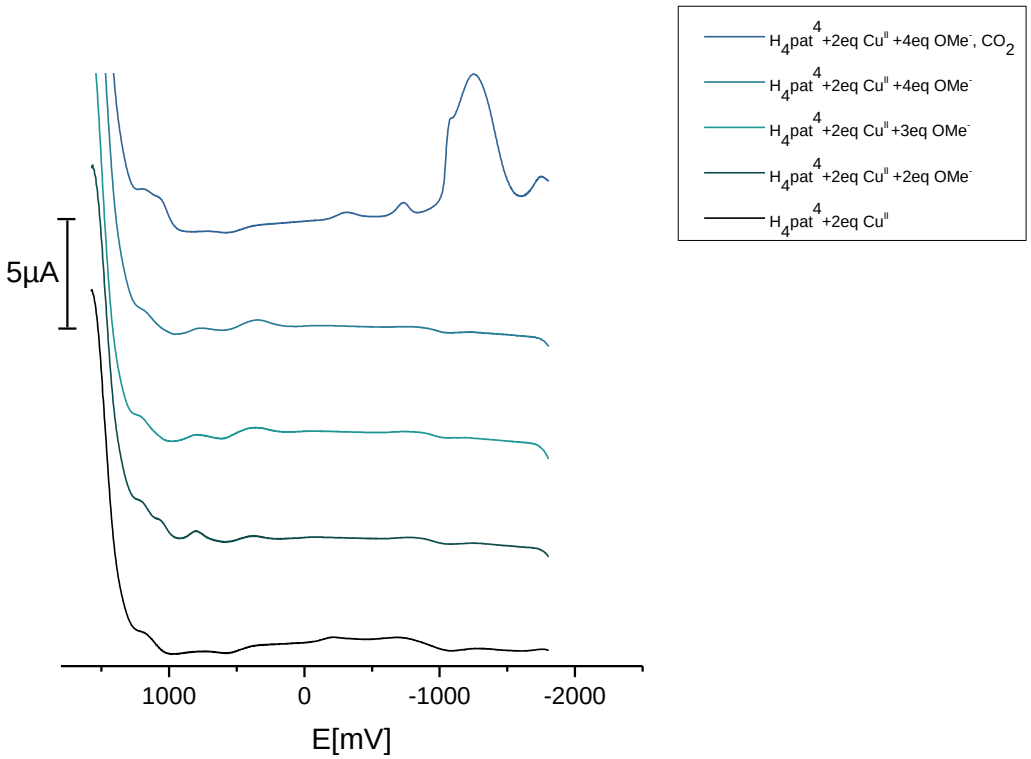

Figure 3.2: SQW traces for selected copper(II) complexation-steps of H_4pat^4 (0.1mM in methanol with 0.1M $(t\text{Bu})_4NPF_6$ and vs. Fc/Fc^+, 25°C).

The redox potential of a carbonato-bridged dinuclear copper(II) complex was determined to be -620 mV vs Ag/Ag^+.[128] Thus, the negative potentials at -302, -750, -1086 and -1242 mV obtained upon flushing with CO_2 can presumably be assigned to different species with coordinated carbonate or bicarbonate.After flushing with CO_2 the complex solutions of all ligands show a characteristic voltammogram (Appendix). All ligand-copper(II) solutions have the formation of a quite negative reduction potentials (-714 to -1289 mV) in common, which could presumably be assigned to the reduction of dinuclear copper(II) carbonato or bicarbonato species

Based on literature derived data of mono and dinuclear copper(II) complexes,[121,126,127,129] and the square wave voltammograms of the copper(II) complexes of all five ligands H_4pat^1-H_4pat^5 (see Figure 3.2 and Appendix) reduction potentials around 350 -450 mV are tentatively assigned to the reduction of one of the central copper(II) ions to result in an unstable copper(II)-copper(I)-complex. These rather positive reduction potentials are in agreement with the only moderate stability constants and the complex equilibria in solution.

Considering the expected instability of the reduced systems and the positive reduction potentials in agreement with the only moderate complex stabilities, it is unlikely that copper(II)/(I) based oxygen activation may be of importance in neutral aqueous solution.

Table 3.1. Redox potentials of the copper(II) complexes of the patellamide derivates.

Ligand	Cu^{II}	Base	reduction potentials [mV] vs. Fc/FC^+ 0.1M TBA-PF_6 in MeOH									
H_4Pat^4	2eq							-214	354	746		1162
	2eq	2eq					-750		382	784	1062	1218
	2eq	3eq					-754		368	798	1054	1214
	2eq	4eq					-778		350	764	1070	1210
CO_2			-1938	-1758	-1242	-1086	-750	-302			1054	1171
			-1938	**-1758**	**-1242**	**-1086**	**-750**	**-258**	**363(13)**	**773(20)**	**1060(7)**	**1195(24)**
H_4Pat^2	2eq									770	1186	1294
	2eq	2eq							486	775	1178	1305
	2eq	3eq							494	772	1187	1301
	2eq	4eq							506	783	1178	1295
CO_2					-1289		-714				1178	
					-1289		**-714**		**495(8)**	**777(5)**	**1181(4)**	**1299(4)**
H_4Pat^1	2eq											1239
	2eq	2eq		-1402		-1102			466	794		1259
	2eq	3eq		-1387		-1101			394	819		1259
	2eq	4eq		-1378		-1094			411	836		1270
CO_2			-1762		-1168		-766		352	828		1254
			-1762	**-1389**	**-1168**	**-1099**	**-766**		**405(41)**	**819(16)**		**1256(10)**
H_4Pat^3	2eq								390	810	1038	1294
	2eq	2eq							383	865	1042	1298
	2eq	3eq							402	782	1117	1286
	2eq	4eq			-1216				391	771	1107	1287
CO_2			-1806		-1202		-726	-354				1290
			-1806		**-1207**		**-726**	**-354**	**392(7)**	**807(36)**	**1076(36)**	**1291(5)**
H_4Pat^5	2eq										1154	
	2eq	2eq							291	794	1163	
	2eq	3eq							378	781	1152	
	2eq	4eq							439	776	1138	
CO_2			-1709			-880	-728	-239			1154	
			-1709			**-880**	**-728**	**-239**	**369(61)**	**784(8)**	**1152(8)**	

3.2 Oxygenation Properties of $[Cu_2(H_4pat^1)(OH)]^+$

Although, the electrochemical results indicate that in a hydrophilic environment at physiological pH no stable copper(I) species can be formed, under basic conditions and after flushing with CO_2, low reduction potentials are visible. Considering the possibility that a naturally existing dinuclear copper(II) complex of a patellamide derivative may act as a cofactor in a protein, i.e. in a hydrophobic microenvironment, copper-based redox chemistry seems possible. Furthermore, this scenario may involve amino acid side chains of the protein acting as a base. Thus, it appears to be worth to check, whether a dinuclear copper(II) complex of a patellamide derivative could act as oxygenase or oxidase.

There are biologically relevant oxygenation, oxidation and electron transfer reactions which have dinuclear copper centers in the active sides of the appropriate enzyme.[118,130] For instance, the copper type-3 proteins tyrosinase, catechol oxidase and hemocyanine are important copper-type-3 proteins. While catecholase catalyzes the oxidation from catechol to quinone, tyrosinase catalyzes the oxygenation from the phenol derivative tyrosine to the corresponding quinone.[131,132] Hemocyanine is the oxygen transporting protein of mollusks. Even if hemocyanine does not oxygenate phenols or oxidize catechols it was spectroscopically shown that oxygen binds in a side-on fashion between the two copper centers in μ-η^2:η^2-geometry, which is comparable to the *oxy*-forms of tyrosinase and catecholoxidase.[133] All three proteins are structurally related and contain a dinuclear copper(II) center in their "resting state" (the *met*-form, Figure 3.3). The *met*-form is hydroxo-bridged and features a copper(II)-copper(II) distance from 2.9 Å to 3.5 Å. The metal site is antiferromagnetically coupled and thus EPR silent.[118,131,134] The literature-described mechanism of tyrosinase is illustrated in Figure 3.5.[135,136] The monophenolase cycle (creolase cycle) shown in blue can be described as a hydroxylation reaction and is the rate determining step.[137] The second part of the catalystic cycle, the diphenolase cycle (catecholase cycle), displays a two-electron transfer process with a subsequent proton transfer.[135,136]

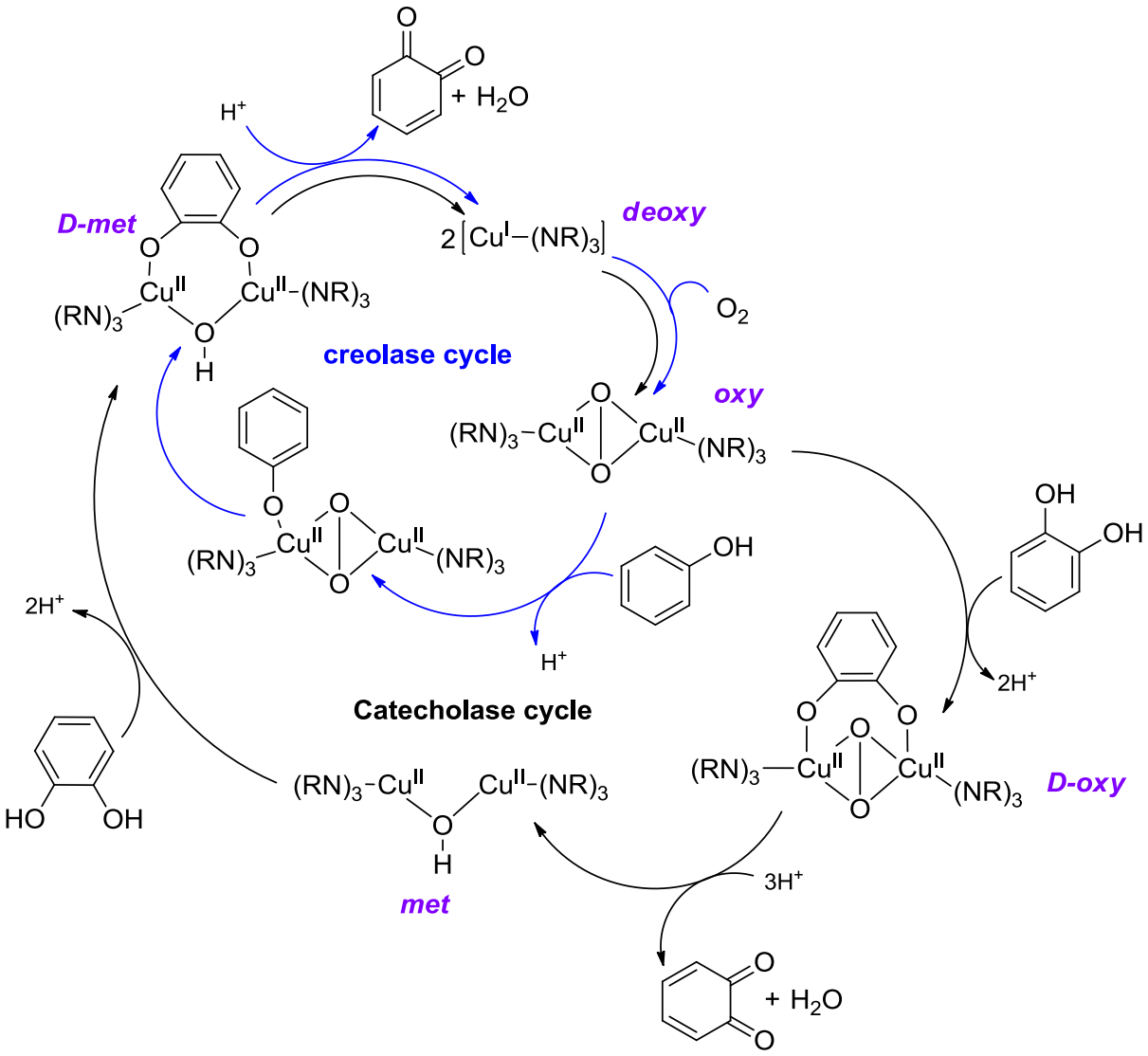

Figure 3.3: Schematic drawing of the tyrosinase catalysis.[135,136]

Koval *et al*. published in 2006 a carbonato-bridged dinuclear copper(II) complex of a macrocyclic ligand with a copper(II)-copper(II) distance of 4.5 Å, that showed catecholase activity. [128] The reduction potential of this species was detected at -620mV (vs. Ag/Ag^+) (-707 mV vs. Fc/Fc^+)[120] which is comparable to the reduction potentials detected for all ligands at -714 to -766 mV (Tabel 3.1).[128] The copper(II)-copper(II) distance in the previously published crystal structure of $[Cu_2[H_2pat^1)(OH)(H_2O)_2]^+$ is about 3.6 Å.[85] Thus, a similar reactivity is imagineable, the ability to oxygenate or oxidize a distinct model substrate. It is also possible that a bridging or terminal co-ligand may act as a radical and generate Copper(I).[128,129,138,139] In 2010 Kaizer and Speier reported a dinuclear hydroxyl-bridged Copper(II) complex that was able to act as catechol oxidase mimic, *via* the radical semiquinone.[140]

The chosen oxygenation assay is well established.[137,141,142] The model substrate 2,4-ditertbutylphenole (DTBPH) (Figure 3.7a) was dissolved under anaerobic and basic conditions in methanol. The previously prepared catalyst solution (anaerobic conditions, to avoid the formation of carbonato species) was added before the reaction was started by flushing with air. The formation of the product was monitored via UV/Vis-NIR spectroscopy (Figure 3.6).

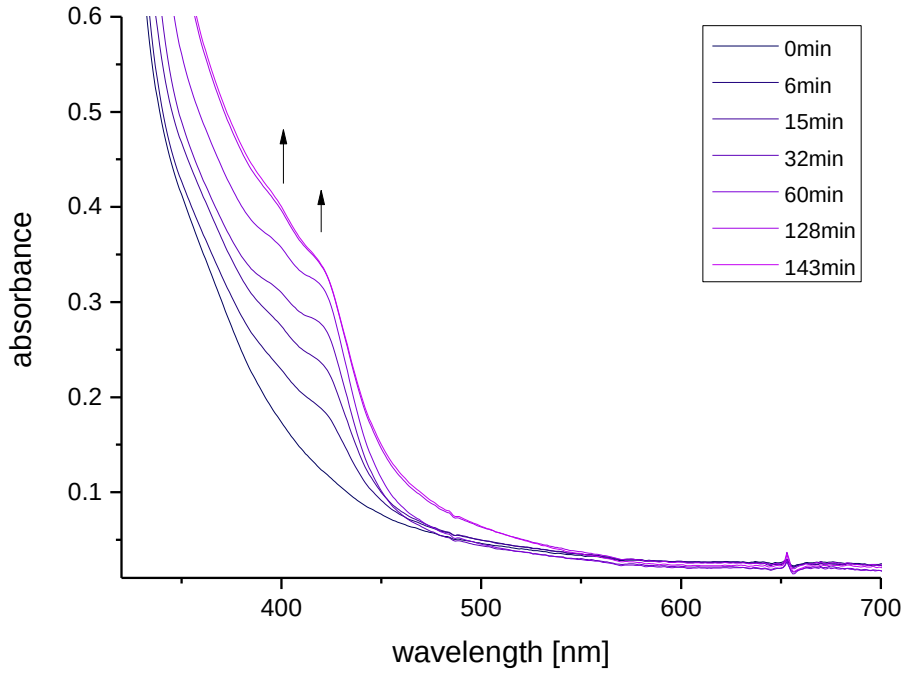

Figure 3.4: Time dependent change in the UV/Vis spectrum, of the oxygenation solution.

The formed 3,5-ditertbutylquinone (Figure 3.7b) has an absorption maximum at 407 nm (ε= 1830 L*mol^{-1}*cm^{-1}),[137] and it was possible to calculate the turnover number (equation 1, Figure 3.7 a), which shows the number of catalytic cycles a catylyst performs till it gets inactive. Furthermore, it is possible to calculate the turnover frequency (equation 2, Figure 3.7 b), which displays the efficiency of the catalyst.

$$TON = \frac{[product]}{[\text{catalyst}]} \qquad (1)$$

$$TOF = \frac{TON}{time} \qquad (2)$$

The second observed absorption maximum at 421 nm belongs presumably to the formation of the corresponding semiquinone. The formation of semiquinone is characteristic for catalytic model systems with a radical intermediate.[137]

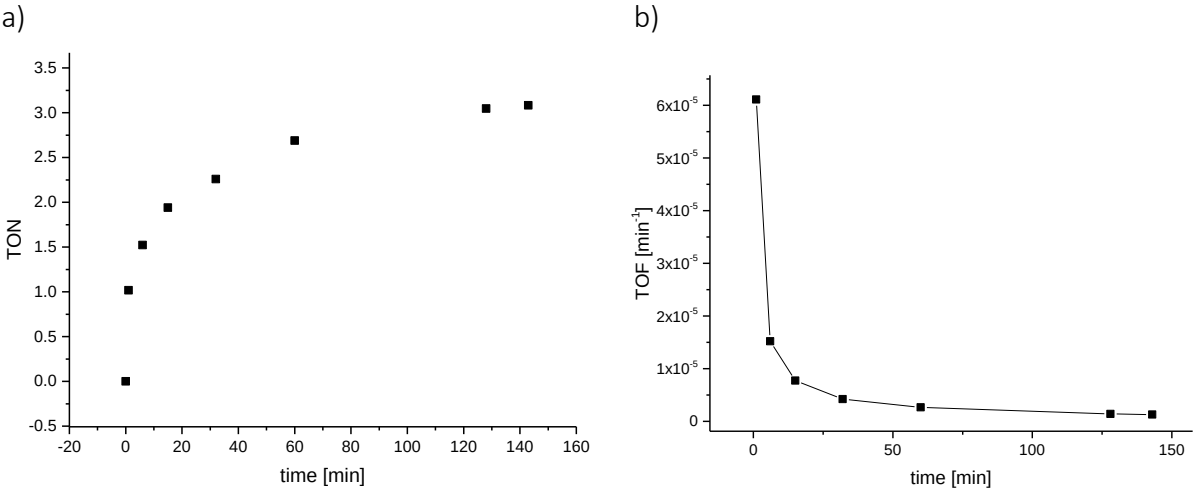

Figure 3.5: Plot of the TON (a) and of the TOF (b) of the generation of DTBQ.

The turnover number of this reaction is 3 after 2 hours, which indicates that the reaction is better described as a stoichiometric reaction rather than as catalytic. From the plot of the turnover frequency (Figure 3.7 b) it is obvious that the catalyst is deactivated within one hour.

An interesting observation is that the reaction can be interrupted by flushing the solution with CO_2 (Figure 3.8). When changing back from CO_2 to O_2 the reaction proceeds again. The behavior of CO_2 as inhibitor leads to the assumption that both molecules be of co-ligands and CO_2, i.e. CO_2 may displace O_2.

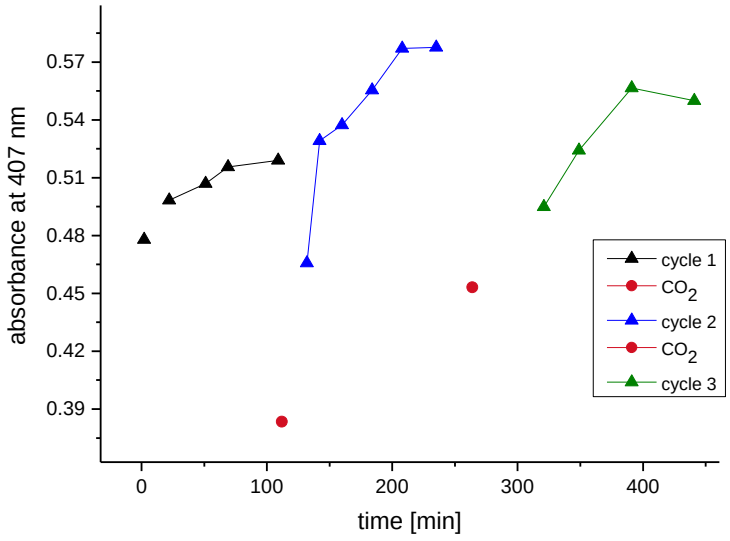

Figure 3.6: Plot of the change in absorbance at 407 nm by time, interrupted by CO_2.

To obtain more information about the reaction, the oxygenation products were characterized. The desired products were isolated by quenching the reaction with 6 M HCl, and extracting oxygenation products with dichloromethane. To identify the oxygenation products, the resulting brownish precipitate was investigated with mass spectrometry (Figure 3.9) and NMR spectroscopy (Figure 3.10).

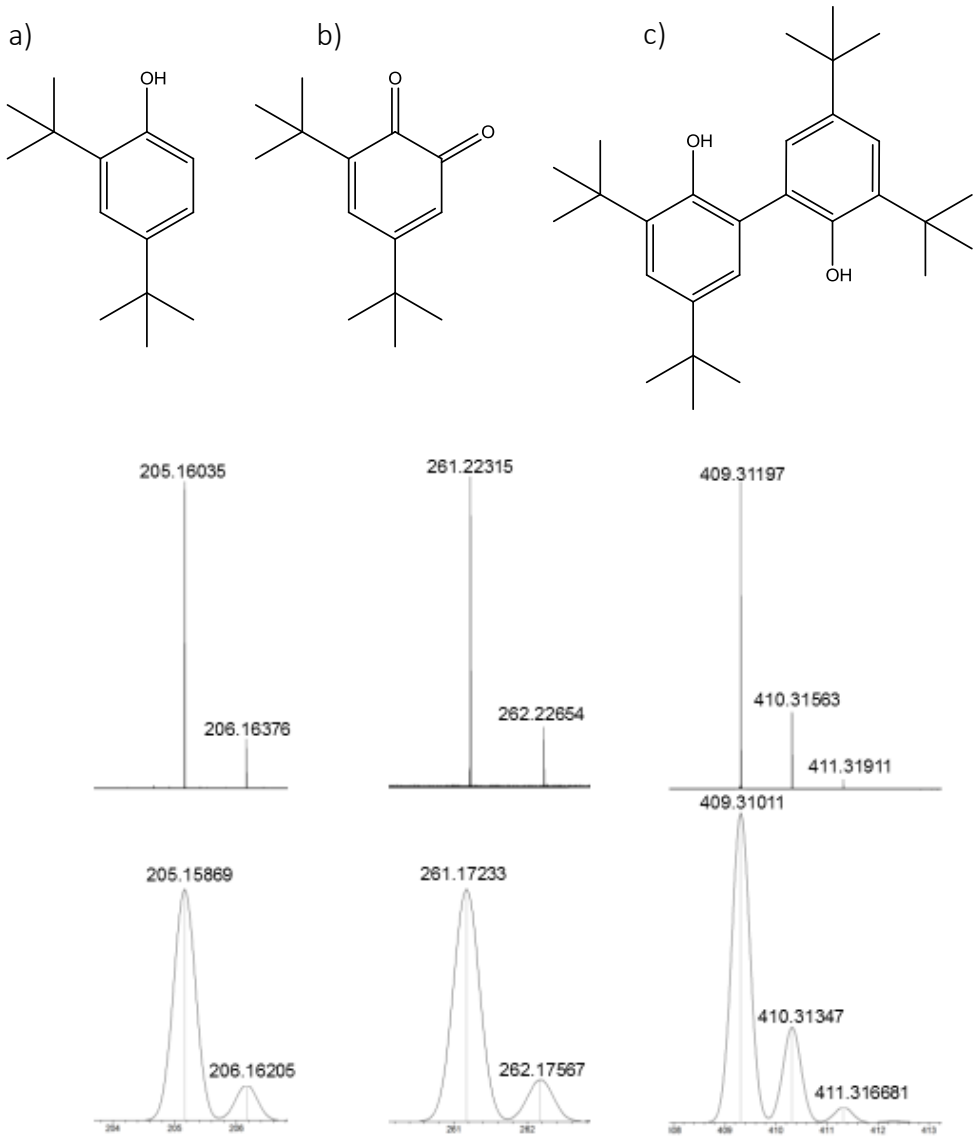

Figure 3.7: HR $^{-}$ESI mass spectra of a) DTBPH, b) DTBQ+Cl^{-} and c) BDTBPH; observed (top) calculated (bottom).

The mass spectra of the oxygenation products show as highest mass the oxygenation substrate DTBPH (Figure 3.7 a), the quinone DTPQ (Figure 3.7 b) and the coupling product 3,3,5,5-bis(di*tert*butylphenole) BDTBPH (Figure 3.7 c).

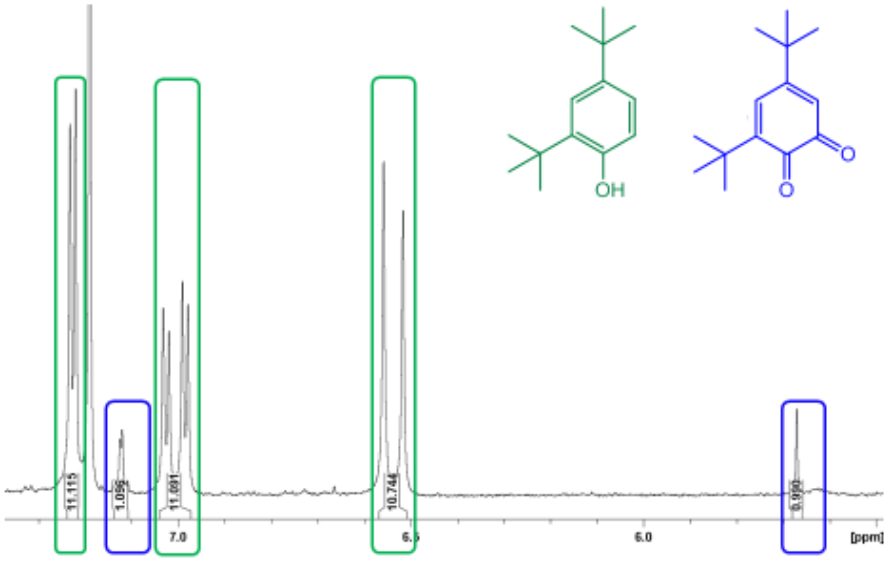

Figure 3.8: aromatic region of the ^{1}H NMR of the oxygenation products at 25°C in $CDCl_3$.

Due to the coupling product BDPBPH a radical pathway seems likely. However, in contrast to the mass spectrum, the ^{1}H-NMR spectrum of the oxygenation products (Figure 3.10) shows the unreacted oxygenation substrate DTBPH and the quinone product in a ratio of 11:1. Also, the ^{1}H-NMR spectrum does not exhibit the coupling product BDTBPH. There is the possibility that BDTBPH evolved during the mass spectrometric analysis from a semiquinone intermediate which is paramagnetic and thus NMR silent.

To obtain further mechanistic information mass spectra from the original oxygenation solution were also measured (Figure in appendix). Further an EPR spectrum of the concentrated reaction solution was measured (Figure 3.11). The EPR experiment at 113 K shows a spectrum that is typical for a dinuclear copper(II) complex. However, due to the fact that there is a copper(II) complex EPR signal detectable, there is definitely no dinuclear *met*-form-like copper(II) center in solution, which indicates that the oxygenation starts from a different type of species.

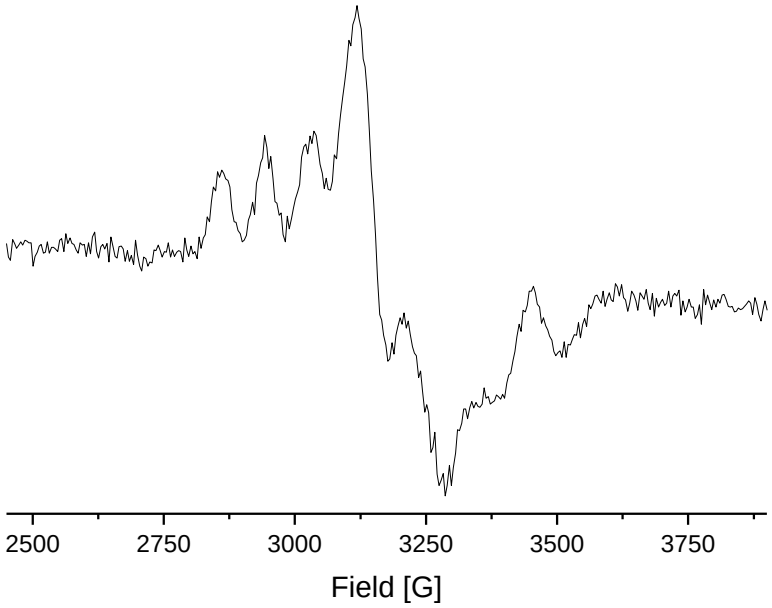

Figure 3.9: EPR spectrum of the frozen oxygenation solution at 113K (~.0.3 mM in MeOH, ν = 9.439058 GHz)

The mass spectrum of the oxygenation solution shows an intense signal for the complex $[Cu_2(H_2pat^1)(OH)]^+$. All other signals are far less intense except for those of the substrate and of the base ($(n\text{Bu})_4N^+$).

In order to identify a putative dinuclear copper(II) dioxygen species, paramagnetic NMR measurements were performed. Koval *et al* published in 2005 a temperature-dependent ^{1}H-NMR experiment of an antiferromagnetically coupled dinuclear copper(II) complex.[143] The signal of the μ-OH co-ligand of their sample shifts with decreasing temperature (from rt decreasing to -40°C) from -50 ppm to -30 ppm.

A sample of $[Cu_2(H_2pat^1)(OH)]^+$ that was originally prepared for an nmr experiment was stored under air for some weeks. The paramagnetic ^{1}H NMR spectrum did not change with time but the sample was EPR silent after the long storage time. Interestingly, while freezing in liquid nitrogen the sample color changed from green to blue. This observation might be explained with the formation of an antiferromagnetically coupled dinuclear copper(II) complex, that was formed while freezing. In order to monitor the change from the paramagnetic dinuclear copper(II) complex to the antiferromagnetically coupled species (virtually diamagnetic) a low temperature ^{1}H-NMR experiment was performed (Figure 3.10). The number of signals increases as well as broad signals become narrower and better resolved with decreasing

temperatures. This indicates that the sample loses its paramagnetism with decreasing temperatures which might be due to coordination of coordination of a bridging hydroxid which was terminal coordinated at room temperature. Furthermore, at -80°C there is a broad doublet visible at -1ppm with an integral of one compared to the valine-H´s which might belong to a bridging hydroxo-species. Nevertheless, this interpretation is tentative and needs further experimental support.

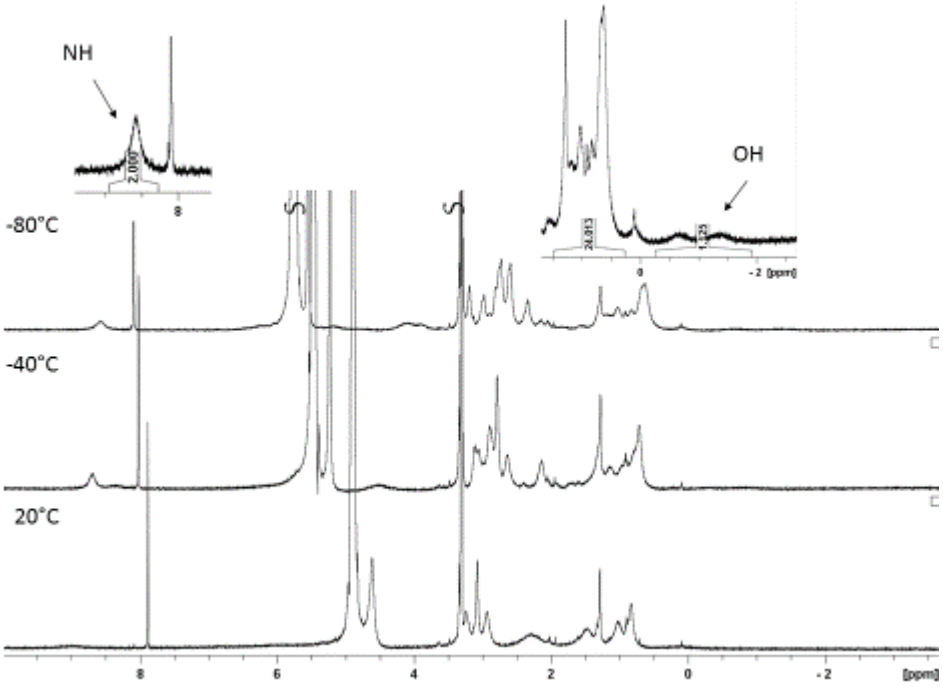

Figure 3.10: ^{1}H NMR spectra of the blue EPR-silent copper(II) complex of H_4pat[1] at various temperatures: a) 25°C, b) at -40°C and c) at -80°C.

A suggested preliminary proposal of the oxygenation mechanism is given by Figure 3.13.

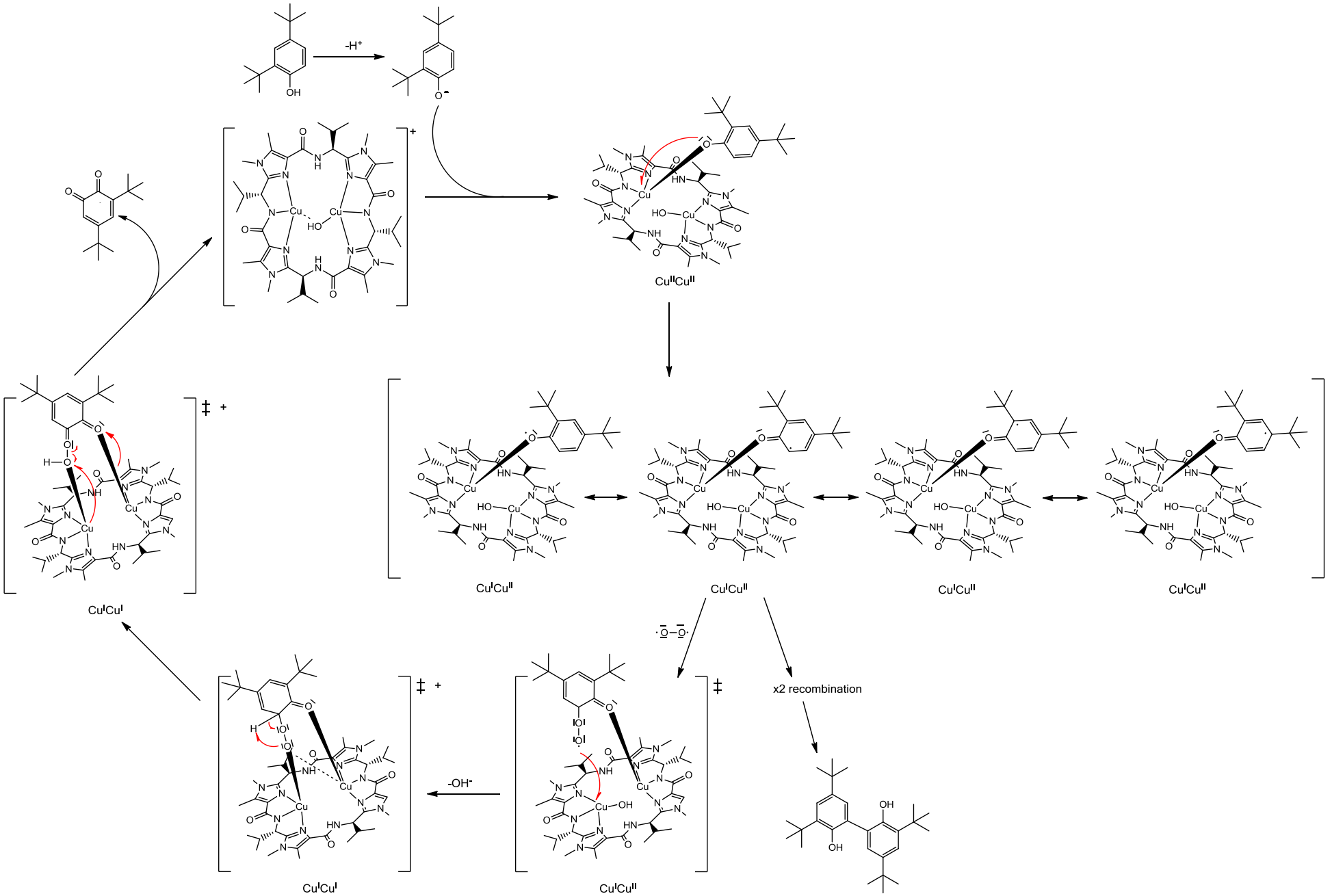

Figure 3.11: Sceme of the proposed mechanism.

Assuming the deprotonated substrate as an electron donor, it may coordinates to one of the copper(II) centers and reduce the first copper(II) while forming a phenyl radical. The stabilized radical intermediate might undergo a recombination and form the coupling product BDTBPH, or react with dioxygen. The peroxo phenyl radical might coordinate to and reduce the second copper(II). Both copper(I) centers may react with O_2 and form a dicopper(II) peroxophenyl complex, that rebuilds the starting form under the release of DTBQ.

For a complete more throuout mechanistic understanding of the reaction additional experiments are necessary, e.g. $^{18}O_2$ labeling, low temperature UV/Vis-NIR spectroscopy, Raman spectroscopy and variations in the reaction such as a change of substrate and study the reaction stoichiometry might also be helpful, as well as support by quantum chemical calculations. Recently, Solomon, Tolman and Cramer *et al.* published a macrocyclic hydroxo-bridged dinuclear copper(II) complex, which was oxidized to a copper(II)-copper(III) species and further to a copper(III)-copper(III) species that was able to act as an oxidation catalyst.[144]. They have been able to measure an EPR spectrum of the mixed valent species which looks *pseudo*-mononuclear. Thus, it smight also be tested whether in our system a copper(III) species may play an important role.

3.3 Copper(II) Coodination Chemistry of H_4pat^4

The coordination chemistry of the ligand H_4pat^4 was investigated previously by UV/Vis-NIR and CD spectroscopy[107] but not by EPR spectroscopy. EPR gives crucial information about the relative orientation of the two copper(II) centers and their distance.

Copper(II) has a d^9 electron configuration with a S = 1/2 ground state. The magnetic energy levels (described by the magnetic quantum number m_s) split when a magnetic field is applied (Zeeman phenomenom). The energy difference between the two levels m_s=-1/2 and m_s=1/2 can be described by $hv = g\beta_e B$. The magnetic tensor g reflects the ligand field and the coordination environment around the copper(II) ions. Furthermore, the interaction of the unpaired electron with the nucleus results in a hyperfine structure of the spectrum obtained. The hyperfine coupling

(A_{HF}) originates from the nuclear spin (copper(II) *I = 3/2*) and leads to four allowed transitions. Well resolved spectra of mononuclear copper(II) complexes may have additionally coupling, especially the so-called superhyperfine coupling (A_{SHF}), which results from the interaction of the unpaired electron with the nuclei of donor atoms. All interactions are described with the spin Hamiltonian given in equation 3.[145]

$$H = \sum_{i=x,y,z}(ß_e B_i g_i S_i + S_i A_{HF_i}(Cu)\, I_i\,(Cu) - g_n ß_n B_i I_i) + \sum_{i=1}(S_i A_i(N)\, I_i(N) - g_n ß_n B_i I_i(N)) \qquad (3)$$

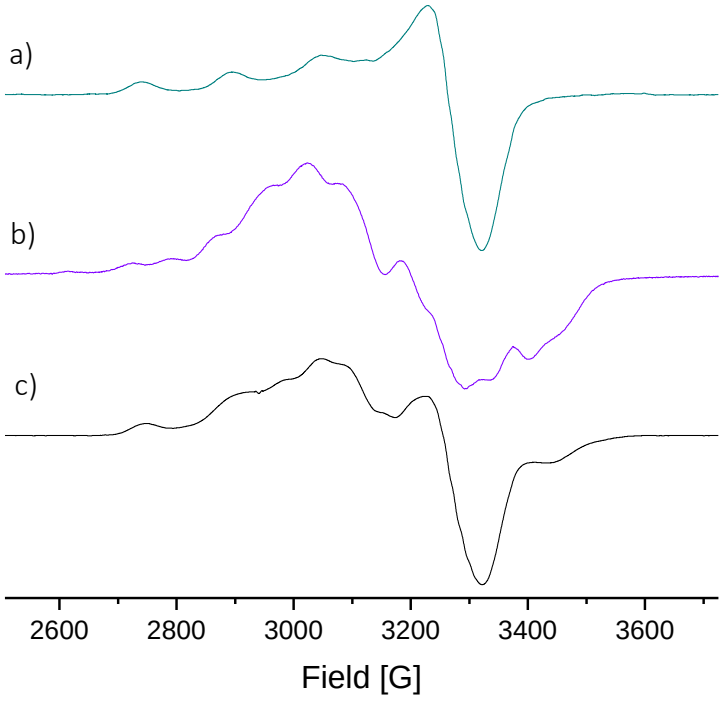

Figure 3.12: Traces of selected EPR spectra (X-Band, 140k, 1 mM in MeOH) at distinct ligand: copper(II) : OMe^- ratios; a)1:05:0.5 and v = 9.445927 GHz, b) 1:2:2 and v = 9.440451 GHz and c) 1:2:4. v = 9.452096 GHz.

In order to study the copper(II) complexation equilibrium with ligand H_4pat^4, EPR spectra of frozen methanolic solutions (140 K) were taken at different ligand/copper(II)/base ratios (Figure 3.12). Surprisingly, at low copper(II) and low base concentrations (below one equivalent) it is possible to detect a mononuclear species (Figure 3.12 a). Comparing the detected EPR spectra with the copper(II) complexation equilibria of the other patellamide derivatives,[85] which show at low copper(II) and low base ratios solvated copper(II) in addition to mononuclear and dinuclear copper(II) species or only dinuclear species, the spectra in figure 3.12 indicate that the in the

cooperative effect is less pronounced for H_4pat^4. When the copper(II) ratio exceeds 0.5 equivalents the formation of dinuclear species is also detectable.

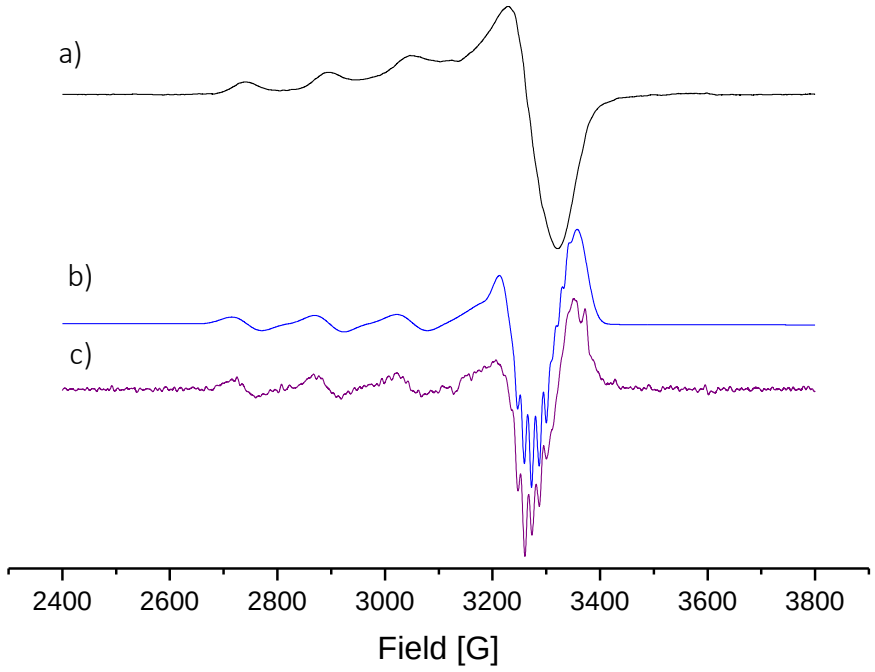

Figure 3.13: EPR spectra of [Cu(H_3pat^4)(OH]; first derivative a) second derivative b) and simulated second derivative of [Cu(H_3pat^4)(OH]. (X-Band, 140K, 1 mM in MeOH, v = 9.445927 GHz)

The spectrum of the mononuclear complex and its simulation performed with the program Xsophe[145] are displayed in figure 3.13, and the EPR parameters obtained are given in table 3.2. The well resolved spectrum (Figure 3.13 a) exhibits superhyperfine coupling constants (second derivative; Figure 3.13 b). The superhyperfine coupling which is more precisely displayed in the second derivative (Figure 3.13 b) was simulated assuming that the copper(II) is coordinated to two different types of nitrogen atoms (one amide and two imidazoles).

Table 3.2. Simulated EPR parameter.

	$[Cu^{II}(H_3pat^4)(OH)]$	Superhyperfine $[10^{-4}cm^{-1}]$	
g_x	2.048	$A_x(N_{im})$	7.2
g_y	2.076	$A_y(N_{im})$	11.6
g_z	2.269	$A_z(N_{im})$	13.0
A_x $[10^{-4}cm^{-1}]$	6.3	$A_x(N_{am})$	12.1
A_y $[10^{-4}cm^{-1}]$	6.8	$A_y(N_{am})$	7.9

A_z [$10^{-4}cm^{-1}$]	159.0	$A_z(N_{am})$	13.1

The simulation of the dinuclear copper(II) complex (Figure 3.12 b) was performed using the program MoSophe.[146] The simulation with MoSophe includes the relative orientation and the distance of both copper(II) ions (Figure 3.14).[146]

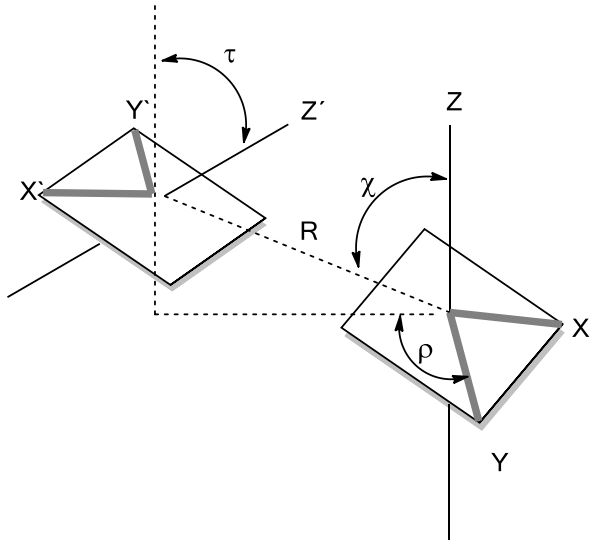

Figure 3.14: schematic representation of the Euler angles ρ, τ and χ used for EPR simulations with the program MoSophe.[146]

At a ligand / copper(II) / base ratio of 1:2:2, H_4pat^4 shows an EPR spectrum of a single dinuclear copper(II) complex (Figure 3.15 b black spectrum). It´s stoichiometry $[Cu_2(H_2pat^4)(OH)]^+$ emerges from mass spectrometry (Figure 3.15). The formally forbidden $\Delta m_S = 1$ transition, which is typical for dinuclear copper(II) complexes, is also detected (Figure 3.15 a black spectrum) but had a poor resolution. The simulated spin hamiltonian parameters are given in table 3.3 and are comparable to the parameters of the respective species by other patellamides derivatives[85]. The copper(II)···copper(II) distance of 5.16 Å is too long for a bridging hydroxide. [99] Thus the hydroxide is believed to coordinated terminally at one copper(II) ion. It is convincible that a bidentate co-ligand such as bicarbonate or phosphate might coordinate in a bridging fashion at this metal-metal distance.

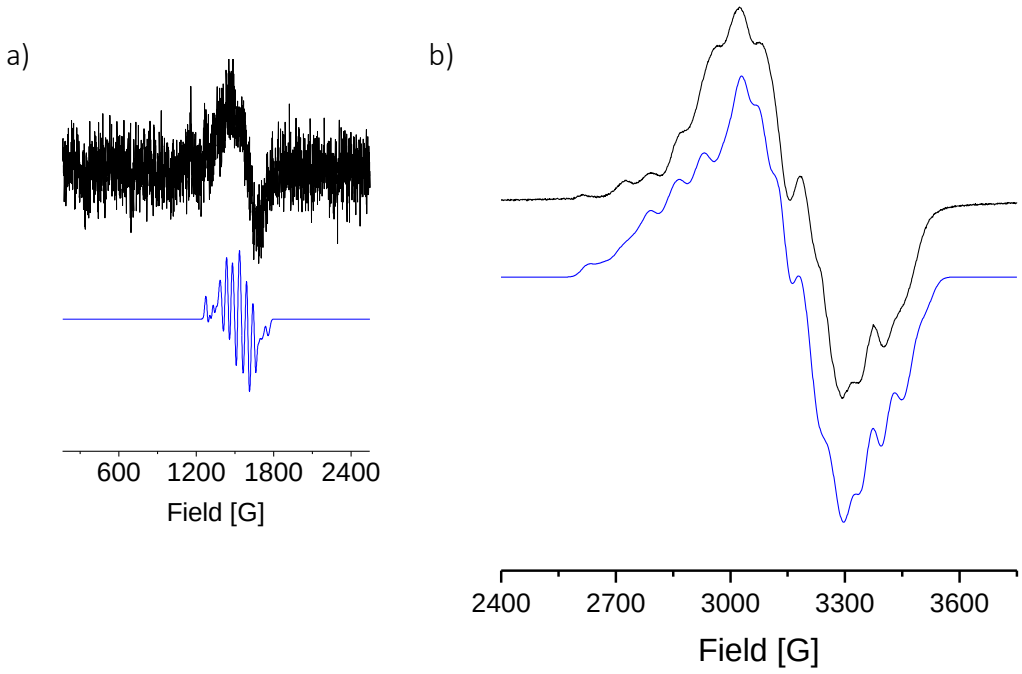

Figure 3.16: EPR spectra of $[Cu_2(H_2pat^4)(OH)]^+$; a) Δm_S = 1 region and b) Δm_S=1/2 region; measured (black) and simulated (blue). (X-Band, 140K, 1 mM in MeOH, ν = 9.440451 GHz)

Table 3.3. Simulated EPR parameter.

	Cu_a	Cu_b	R [Å]	5.210
g_x	2.035	2.055		
g_y	2.150	2.155	χ [°]	17
g_z	2.286	2.215		
A_x [$10^{-4}cm^{-1}$]	125	25	τ [°]	47
A_y [$10^{-4}cm^{-1}$]	65	110		
A_z [$10^{-4}cm^{-1}$]	212	120	ρ [°]	17

The EPR spectrum of a ligand / copper(II) / base ratio of 1:2:4 (Figure 3.14 c) is interpreted as containing a mixture of more than one species. It appears to be a mixture of spectrum a) and b). However, subtraction of neither spectrum a) nor subtraction of spectrum b) leads to satisfactory results that could be simulated.

High-resolution mass spectra of all methanolic solutions were measured. Figure 3.17 shows two selected mass spectra with a distinct pattern for dinuclear copper(II) complexes. It is possible to

detected more masses belonging to mononuclear and dinuclear complexes (solvent, H_2O, OH^-, MeO^-).

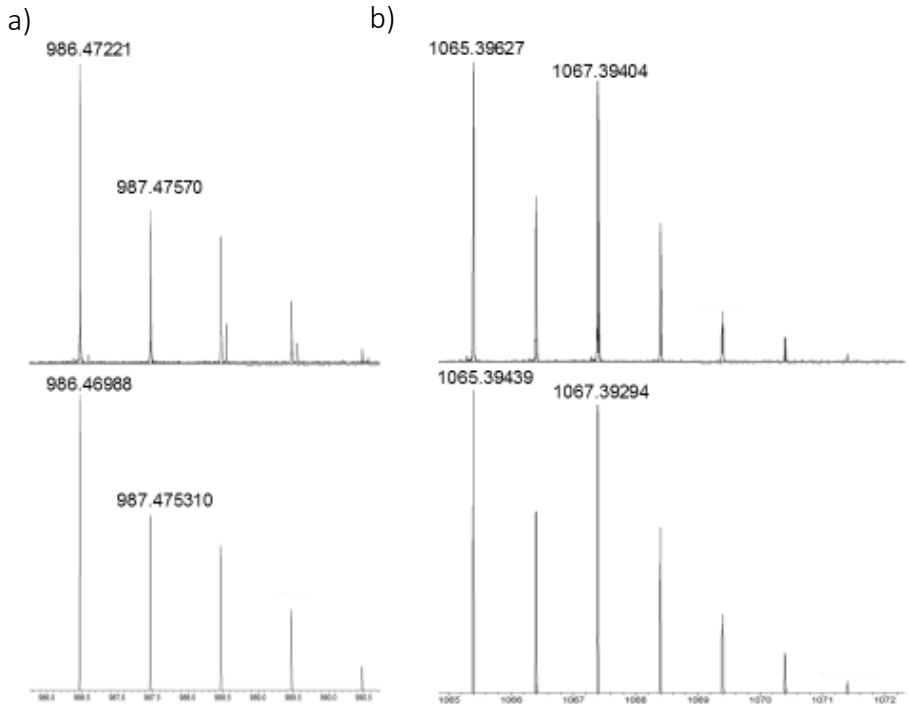

Figure 3.17: Selected recorded mass spectra (top) and calculated (bottom) isotopic pattern for a) $[Cu(H_3pat^4)]^+$ and b) $[Cu_2(H_2pat^1)(OH)]^+$ in methanol.

Considering the findings described in this study by EPR spectroscopy, mass spectrometry and electrochemistry (Figure 3.1 and Figure 3.2) and the findings of published ITC, UV/Vis and CD-based studys[107] the proposed complexation equilibria are displayed in figure 3.18.

H_4pat^4 forms at low copper(II) and low base concentrations, in contrast to the other ligands a distinct mononuclear species. Starting with 0.75 equivalents of both copper(II) and base, the formation of a dinuclear species is detecable. At a copper(II) and base concentration of two equivalents, only one dinuclear copper(II) species with is detectable (Figure 3.16). The addition of higher base ratios leads to formation of further species.

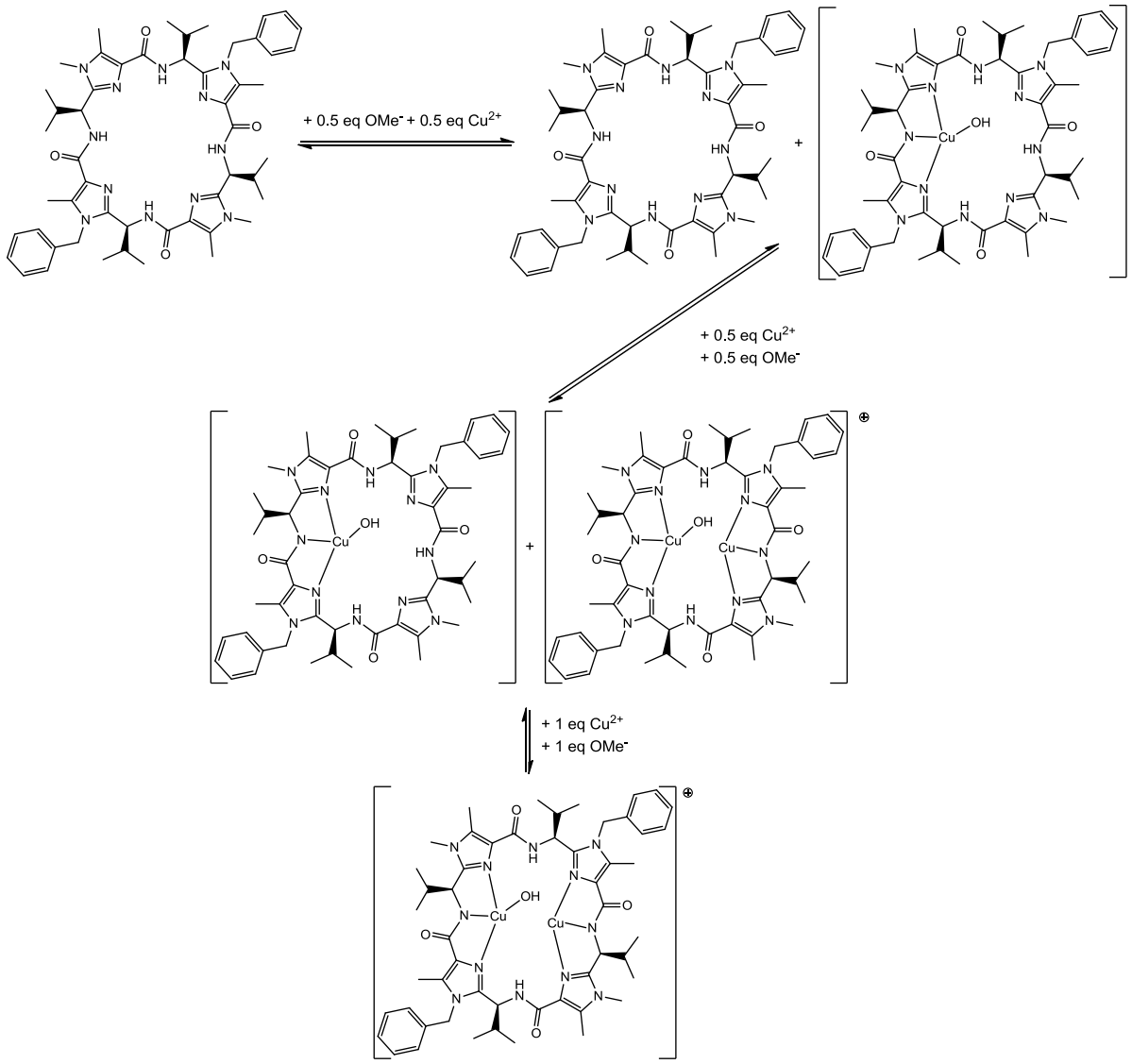

Figure 3.18: Proposed copper(II) complexation equilibrium of H_4pat^4.

Parts of the following chapter are to be published in a manuscript entitled: “Dinuclear Zinc(II) and Copper(II)/Zinc(II) complexes of artificial Patellamides as Phosphatase models”; Peter Comba, Annika Eisenschmidt, Lawrence R. Gahan, Graeme R. Hanson, Nina Mehrkens, Michael Westphal, *manuscript in preparation*, 2015

4 Zinc(II) Coordination Chemistry

4.1 Zinc(II) Hydrolases

4.1.1 Zinc(II) enzymes – a general introduction

In biological coordination chemistry there is no other metal known which has as many biological roles as zinc.[147] Nevertheless, zinc(II) is often ironically described as "boring". The d^{10} electronic configuration leads to the absence of ligand field stabilization energy with the consequence of a high geometric flexibility. It exchanges its ligands rapidly and prefers both hard and soft donors.[147-149] In 2007 Heinrich Vahrenkamp described the chemistry of zinc(II) and it´s lack of properties in the following way: "*in essence, the non-properties of zinc(II) are the basis of its success: no redox chemistry, no ligand field effects, no typical coordination numbers or geometries, no stability or inertness of its complexes, no typical hard or soft characteristics. For generations of chemists zinc(II) was the boring element.*"[147 150] However, this unspectacular reputation is completely undeserved. Zinc(II) is the second most abundant inorganic transition metal in human bodies, and it is indispensable to all forms of life.[147] Nature uses it in structural functions as well as in catalytic processes.[150] Zinc(II) occurs in all enzyme classes; in 2007 it was reported that the number of known enzymes that contain zinc(II) in their active center exceeded 1000.[151] There are about 5000 further proteins known in which zinc(II) plays a role.[152] The role of zinc(II) ions and proteins is, in the majority of cases, a structural one, comparable to the role of hydrogen bonds.[147] A well-known example of this structural role is zinc(II)-finger proteins. Zinc(II) is necessary for effective growth and development due to its various functional roles.[147] Zinc(II) can be 6, 5 or 4 coordinate,

depending on the ligands, solvent and possible co-ligands. In proteins in which zinc(II) plays a structural role, it is usually tetrahedrally coordinated by cysteine and histidine side chains (N_2S_2 motif).[149]

If the native role of zinc(II) is not structural it is mostly acting as a hydrolytic agent. Examples of zinc(II) containing hydrolyzing enzymes include alcohol hydrolases, phosphoesterases, carbonic anhydrases, carboxypeptidases, and metallo-ß-lactamases (Table 2.1).[149] In hydrolyzing enzymes, the zinc(II) ion is tetrahedrally coordinated, usually coordinated by three amino acid side chains and one site occupied by a water molecule. The amino acid side chains are mainly provided by histidine and cysteine, the carboxylates of glutamine and asparagine can also be involved.[149] When it comes to dinuclear or even trinuclear hydrolyzing zinc(II) enzymes, such as alkaline phosphatase, nuclease P1 or phospholipase C, it is often observed that the zinc(II) center is pentacoordinated in a trigonal bipyramidal geometry.[149] Glutamate and aspartate are especially known to bind in a bridging manner between two zinc(II) centers, mainly besides a bridging hydroxide.[153-155] For the whole group of zinc(II) enzymes the pK_A value of a coordinated and activated OH_2 molecule is the main influencing factor for the activity. Zinc(II) acts as a Lewis acid and lowers the pK_A value of the coordinated water molecule, causing the nucleophilic OH^- group to be available at physiological pH.[156,157], [158] The Lewis acidic zinc(II) is thus neither involved in reactions with high energetic changes nor does it have colorful chemistry but it rather exhibits an ubiquitous hydrolysis chemistry.[147,149,159,160]

Tabel 4.1: Examples of zinc(II) based hydrolases.

enzyme	active side metal center	Metabolic functions	Zinc(II) coordination motif	ref.
purpel acid phosphatase (PAP)	Fe(III)-Zn(II)*	bone resorption iron transport generation of ROS	His, Asn, His	[161], [162], [163]
carbonic anhydrase (CA)	Zn(II)	hydration of CO_2 respiration, pH control fluid secretion	His, His, His	[164], [149], [165], [166].
Metallo-ß-lactamase	Fe(II)-Zn(II)*[2]	transduction of neuronal signals	His, His, His	[167]
carboxypeptidase	Zn(II)-Zn(II)	protein decomposition amino acid synthesis	His, His, Glu	[149]
alkaline phosphatase (AP)	Zn(II)-Zn(II)-(Mg(II))	bone mineralisation	Asp, His, His Ser,His, Asp	[168]
nuclease P1	Zn(II)-Zn(II)-Zn(II)	hydrolysis of single strain DNA and RNA	His, His, μ-Asp His, His, Asp His, Trp, μ-Asp	[169]

*PAPs are also known with Fe(III)-Fe(II) and Fe(III)-Mn(II)
*[2]Metallo-ß-lactamases are also known with Mn(II)-Mn(II)

Possibly the most abundant zinc(II) based hydrolyzing enzyme is carbonic anhydrase, a mononuclear zinc(II) enzyme. Carbonic anhydrase is one of the most effective enzymes known, it accelerates the uncatalyzed hydration of CO_2 approximately 10^8-fold.[170] Human carbonic anhydrase II (HCA II) is predominantly found in red blood cells where it catalyzes the hydration of respirated CO_2 to HCO_3^-. The first crystal structure of HCA II was published in 1988 with 2.0 Å resolution.[171] Figure 4.1 shows the crystal structure of the engineered wild type variant of HCA II, which has an additional disulfide bond, that shall provide a higher stability for industrial reaction conditions.[164]

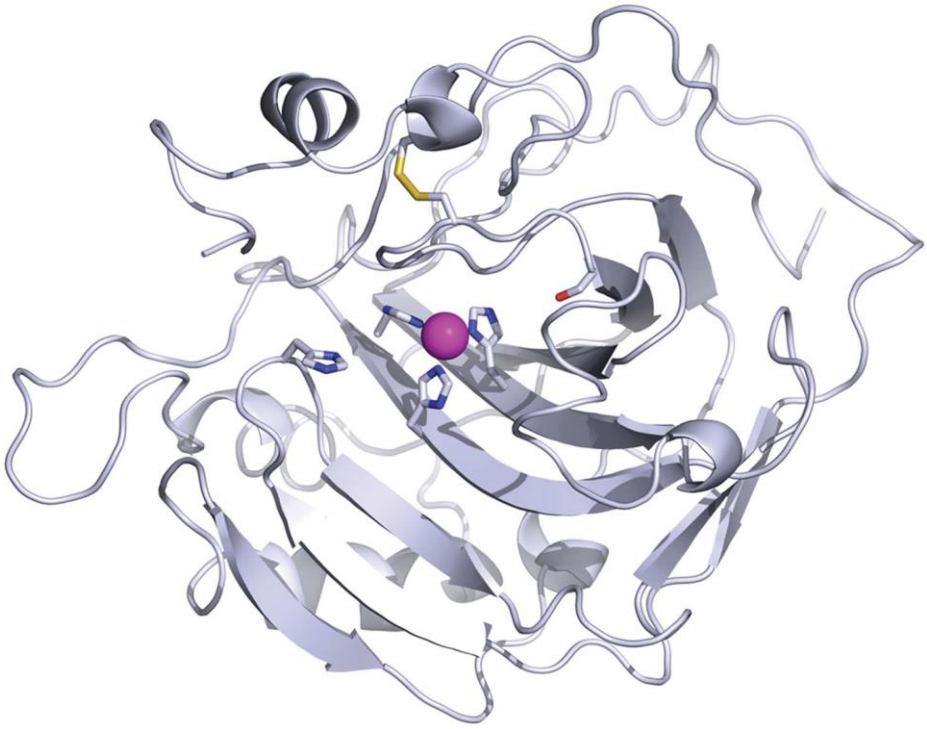

Figure 4.1: The X-ray structure of the disulfide-containing human carbonic anhydrase II with a silver backbone and an active site in ball and stick view. Colors; violet: zinc(II), blue: nitrogen, red: oxygen and yellow: sulfur.[164], (Reproduced with permission from IUCr), (pdb: 4hba), (http://onlinelibrary.wiley.com/iucr/10.1107/S0907444913008743)

Due to the various metabolic functions of carbonic anhydrases (e.g. respiration and pH regulation in the stomach) there are various isoenzymes, whose structures show only slight differences in contrast to their catalytic efficiency, which can differ greatly depending on the pH.[118] The active site contains a tetrahedrally configured zinc(II) ion coordinated by three histidine residues (His94, His96, His119) and a water molecule.

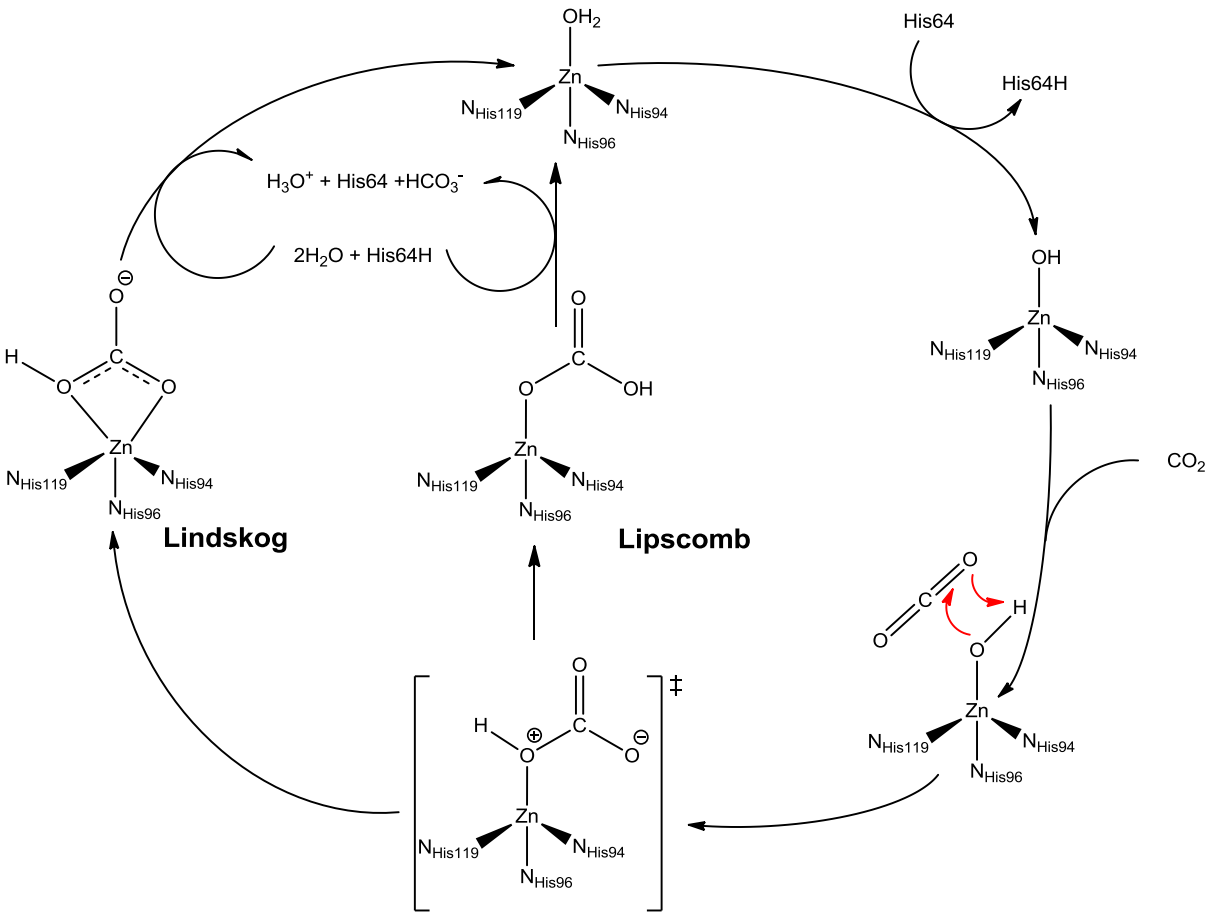

Figure 4.2: Scheme of the catalytic hydration of CO_2.[118,164,172]

The mechanism of carbonic anhydrase is briefly described, because the dinuclear copper(II) complexes of the patellamide derivatives, described in this thesis, have recently been shown to act as efficient carbonic anhydrase models.[111] While exploring the zinc(II) chemistry of the patellamides the possibility of carbonic anhydrase activity was considered and will be discussed in Section 4.2.4 of this Chapter. For the mechanism of CO_2 hydration by HCA II (Figure 4.2) there are two possible pathways; the Lipscomb-mechanism (internal proton transfer) and the Lindskog-mechanism (pentacoordinated bidentate intermediate).[118,172] Theoretical studies assume the Lindskog mechanism to be the naturally relevant mechanism.[173,174].Carbonic anhydrases could generally work in two directions; clockwise from CO_2 to bicarbonate (as displayed in Figure 4.2), relevant for the CO_2 uptake in green plants chloroplasts and in the uptake of produced CO_2 from human body cells to blood plasma; and anticlockwise, which takes places when bicarbonate from blood plasma goes into pulmonary alveoli as CO_2.

The pK_A value of the zinc(II) bound water molecule in carbonic anhydrase in the enzyme´s resting state is ≈ 7. Catalysis starts with the deprotonation of the coordinated water by histidine 64. Due to a later step, in which this proton is given back to the catalytic cycle, histidine 64 could be described as proton shuttle.

Besides the broad range of mononuclear zinc(II) complexes, there is a smaller range of dinuclear zinc(II) complexes that catalytically hydrolyze CO_2 via a nucleophilic attack of coordinated water or hydroxide have been described in the literature.[149,175,176], [177-180] As well as some dinuclear copper(II) complexes are also known that hydrolyse CO_2.[181,182] But the most efficient copper(II) based model complexes known so far are those of the patellamides. [111]

4.1.2 Zinc(II) in the active site of hydrolases

Nature appears to have selected zinc(II) in the majority of the hydrolyzing enzymes because of the capacity of the metal ion to promote the deprotonation of a coordinated water molecule in the physiological pH range. This ability is tunable by slight changes in the first coordination sphere of the metal ion as well as by the hydrogen bond network, provided from the second coordination sphere.[183-187] Thus, zinc(II) acts as a Lewis acid and lowers the pK_A value of the water molecule so that a nucleophilic OH^- group is available at physiological pH.[188] The relatively high ionization potential, displayed in its Lewis acidity, gives the zinc(II) ion the ability to polarize H_2O, C-O and P-O bonds easily.[189] There are many examples biomimetic approaches to model the hydrolytic active zinc(II) sites in these zinc(II) hydrolases. The key factor is the acidity displayed in the pK_A value of the zinc(II) bond water molecule. The pK_A value, therefore, is known to depend on the number and on the nature of the zinc(II) coordinating ligands.[190]

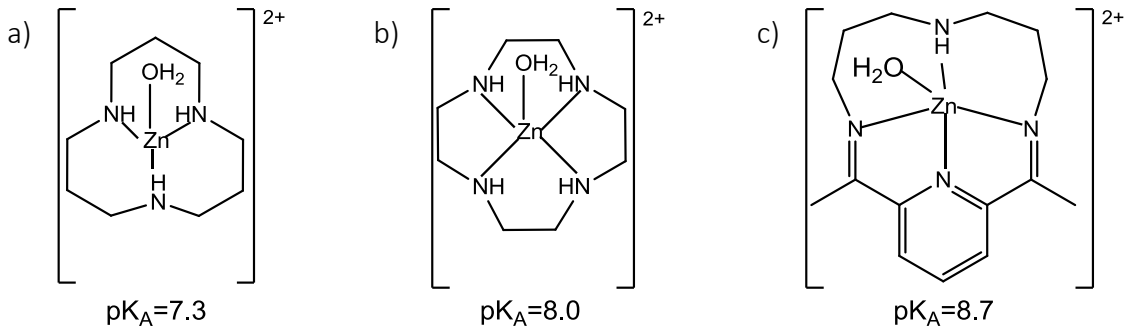

Figure 4.3: Structures of $[Zn([12]aneN_3)H_2O]^{2+}$ (a)[191], $[Zn([12]aneN_4)H_2O]^{2+}$ (b)[160] and $[Zn(cadip)H_2O]^{2+}$ (c)[192].

The first model complex (based on a macrocyclic ligand) for carbonic anhydrase was reported in 1975 by Woolley *et al.* (Figure 2.3 c).[192,193] Kimura *et al.,* whose research was focused on mononuclear zinc(II) complexes of macrocyclic tri- and tetramines, reported that while the coordination number of zinc(II) decreased from 5 to 4, the pK_A value of the zinc(II) bound water molecule decreased from 8.0 to 7.3 (Figure 4.3 a and b).[194, 195, 191] This feature could be explained by the decreasing charge on the zinc(II) ion with a decreasing coordination number, which consequently increases the zinc(II) ions capacity to polarize the coordinated water molecule.[188] Furthermore, while comparing $[Zn([12]aneN_4)H_2O]^{2+}$ (Figure 4.3b) with $[Zn(CR)H_2O]^{2+}$ (Figure 4.3c) the influence of the ligand's geometry was studied. The change from a cyclen platform (Figure4.3 b) to the more rigid ligand cadip (Figure 4.3c) leads to a higher pK_A of the zinc(II) bound water.[196]

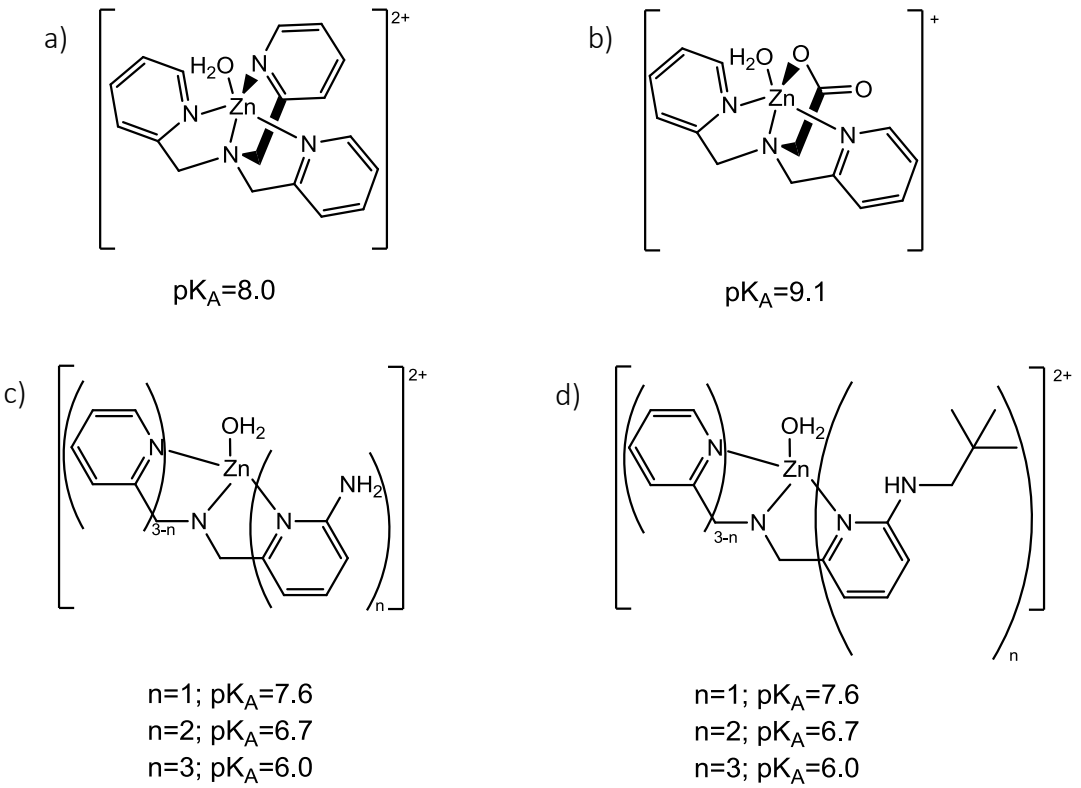

Figure 4.4: Structures of $[Zn(tpa)H_2O]^{2+}$ (a), $[Zn(bpg)H_2O]^{2+}$ (b), $[Zn(tapa)H_2O]^{2+}$ (c) $[Zn(tnpapa)H_2O]^{2+}$ (d).[184.]

The substitution of a neutral pyridine (Figure 4.4 a) by an anionic carboxylate (Figure 4.4b) also results in a higher pK_A value.[197] This can be explained with the decrease of the Lewis acidity of the zinc(II) ion by coordination to a carboxylate, which results in a lower ability to polarize/ionize the coordinated water molecule. The effect of hydrogen bonding donors was investigated by Mareque-Rivas *et al.* (Figure 4.4 c). N-H hydrogen bonding donors can polarize the O-H bond of the zinc(II) coordinated water molecule, which results in a decrease of the pK_A value with an increasing number of coordinating amino pyridyl residues (Figure 4.4 c).[184] However, the ability of hydrogen-bonding donors to decrease the pK_A value of the zinc(II) coordinated water is limited. Due to the effect of greater stabilization of the zinc(II) bound hydroxide by the H-bond network, the pK_A value of zinc(II) coordinated water starts to increase again when the number of coordinating aminopyridyl residues exceeds 2, or 3.[184]

Peptide zinc(II) complexes that functionally and structurally mimic the active site of zinc(II) hydrolases are rare.[189] In order to model the biologically relevant zinc(II) coordination sphere by histidine side chains Ichikawa *et al.* and Ibrahim *et al.* investigated the benzyl imidazole containing *pseudo*-peptides L_1 and L_2 (Figure 4.5). With the use of benzyl imidazoles, they achieved an increase in the hydrophobicity of the zinc(II) center's microenvironment. Additionally, the benzyl residues were expected to help aromatic hydrolysis substrates by π-stacking, which could be confirmed by high hydrolysis rates of model phosphoesters in the physiological relevant pH range.[198]

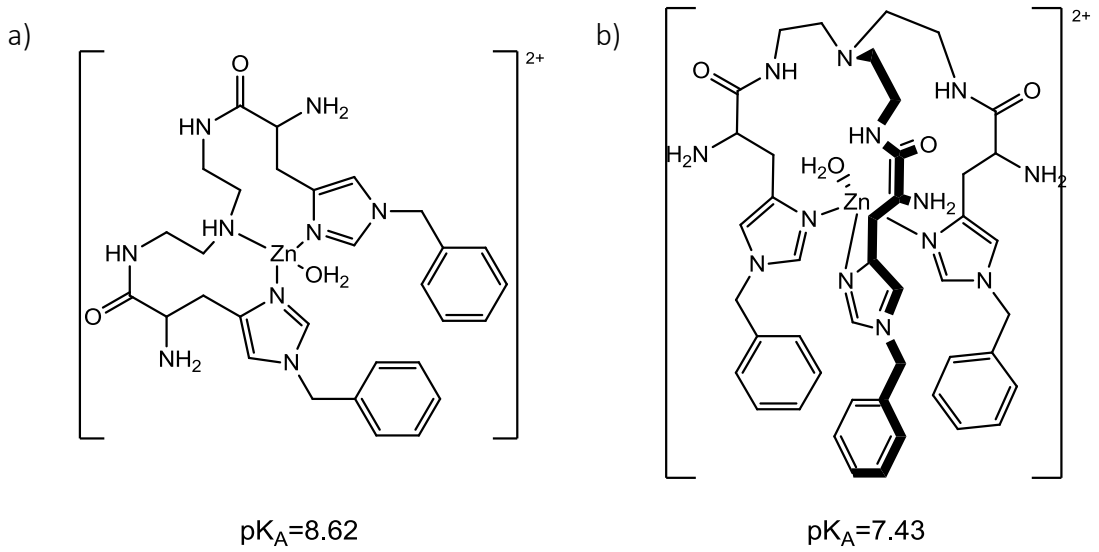

Figure 4.5: Structures of $[Zn(L_1)H_2O]^{2+}$ (a) and $[Zn(L_2)H_2O]^{2+}$ (b):[198,199, 200]

Coordinated imidazoles are more labile then amines.[159] This leads to a decreasing pK_A value of the coordinated water when comparing $[Zn(L_1)H_2O]^{2+}$ (Figure 4.5 a) with $[Zn(L_2)H_2O]^{2+}$ (Figure 4.5 b). The more flexible tripodal ligand L_2 provides an optimum geometry for a tetrahedrally coordinated zinc(II) ion.[198]

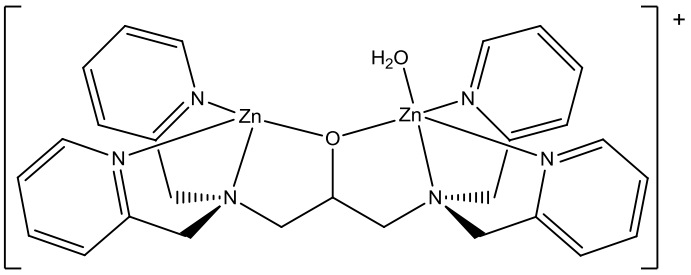

Figure 4.6: Structure of $[Zn_2(BBPAP)H_2O]^+$.[201]

Model systems containing two metal centers were in general found to cleave various substrates faster than the corresponding mononuclear species. Bringing two zinc(II) centers in close distance leads to the possibility of cooperation; either by double Lewis acid activation of the substrate or by Lewis acid activation of the substrate coupled with the provision of a metal bound hydroxide nucleophile. Additionally, in the dinuclear case the pK_A value of the Zn- OH_2 moiety is the main influencing factor for the ability of zinc(II) complexes to hydrolyze specific substrates under defined conditions (see also section 4.1.3).[202-206] Therefore, dinucleating ligand systems based on the skeleton of bis(bipyridylamino) isopropane (HBBPAP) (Figure 4.6) were developed.[201] This ligand scaffold inspired further investigations towards the use of bridging phenols or imidazolates as linkers between bipyridylamines.[207-210], [211-218]

4.1.3 Zinc(II) based Phosphatases

The present thesis aims to identify and characterize zinc(II) and zinc(II)/copper(II) complexes of the model peptides H_4pat^1, H_4pat^2 and H_4pat^4 and to investigate their ability to hydrolyze the model phosphoester BDNPP. Therefore, the impact of phosphatases shall be discussed. Due to the fact that the literature described dinuclear copper(II) complexes of patellamides derivatives, which actias hydrolase models,[107,111,112] the focus of this section is on dinuclear phosphatases.

Phosphoesters are ubiquitous and have various key functions in biological chemistry for all forms of life.[189] They are found in the linkage of nucleotides in deoxyribonucleic acid (DNA) and ribonucleic acid (RNA), phospholipids in cell membranes, secondary messengers and they are part of several organic cofactors (the most important being adenosine triphosphate (ATP), the universal biological energy carrier). Phosphoesters are highly stable as illustrated, for example, by DNA, which has a half-life of 30 million years.[219] Thus one could imagine that nature has evolved various phosphoester cleaving strategies. The necessity to understand the chemistry of phosphatases has thus various reasons including understanding diseases, understanding ecosystems and development of artificial phosphatases for agricultural and pharmaceutical uses.

Alkaline phosphatases (AP) are also omnipresent and encompass a whole class of enzymes with various metabolic roles. The class of phosphomonoesterases described in the literature is quite substrate unspecific and has its highest catalysis rates at pH > 7.5. AP has a homodinuclear zinc(II) center in its active site.[220] The active center of *E. coli* AP is schematically displayed in figure 4.7a.[221] In addition to the two different coordinated zinc(II) ions a magnesium(II) ion is bridged to one of the zinc(II) ions by an aspartate. The metal-metal distances within the trinuclear active site are 3.94 Å, 4.88 Å, and 7.09 Å.[220] The role of the magnesium ion is not completely understood.

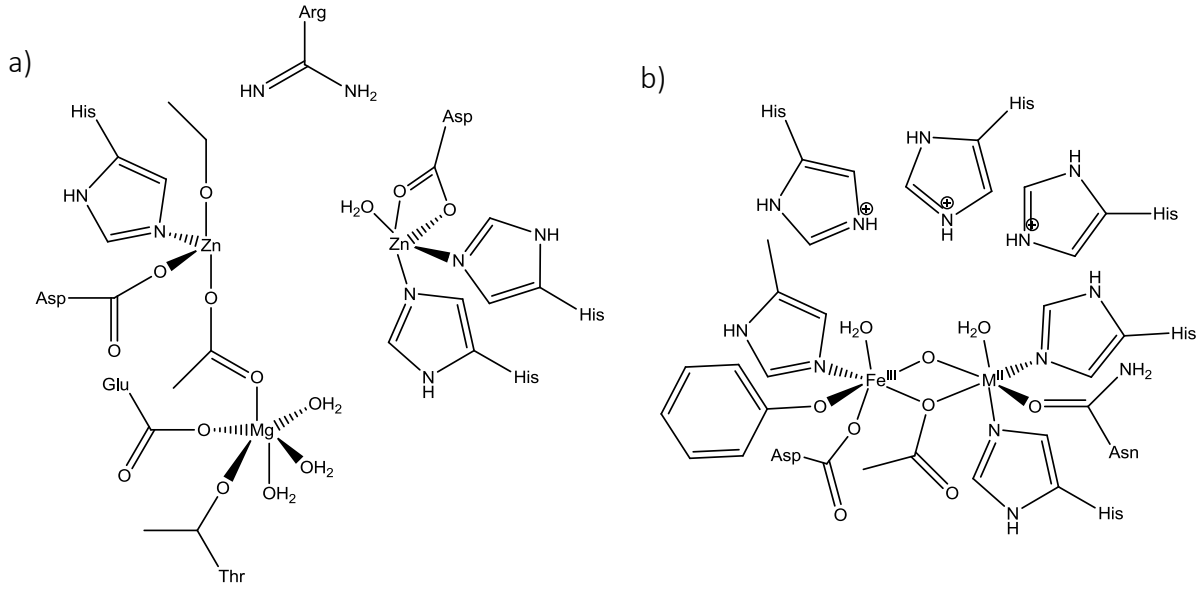

Figure 4.7: Schematic representation of the active sides of AP a) and PAP b) in their resting state.[163,203,220,221]

Purple acid phosphatases (PAP) are also a ubiquitous class of enzymes with a dinuclear metal center. However, in contrast to AP, PAP has an acidic to neutral pH optimum and always contains iron(III) in its active site (Figure 4.7 b). The enzyme's purple color derives from a CT band from tyrosine-Fe(III).[183,222-225] PAP is involved in osteoporosis and therefore is a very interesting target for pharmaceutical industry.[162,163,226,227] While iron(III) is always present in PAP the second divalent metal ion depends on the kind of organism[204,228] While in mammalian PAP iron(II) is the second metal ion, in plant PAP zinc(II) or manganese(II) were found.[185,229-232], Despite these differences the active site is structurally the same in all types of PAP (Figure 4.7b).[185,233]

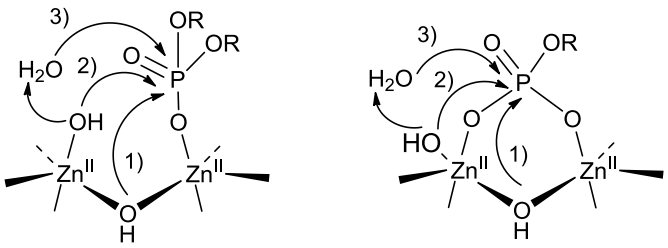

Figure 4.8: Schematic representation of possible phosphoester activation routes/mehanisms by dinuclear zinc(II) complexes.[159,203-206]

For dinuclear zinc(II) complexes there are three possible hydrolyzing scenarios of a phosphoester: first a bridging hydoxide could hydrolyze the substrate, secondly a terminal hydroxide bound at the second zinc(II) center could hydrolyze the substrate, and the third option occurs by hydrolysis of a coordinated substrate through a non-coordinated hydroxide activated by a coordinated hydroxide (Figure 4.8). The pK_A values of the hydrolysis is dependent on the scenario.[159,203-206]

Since the naturally occurring patellamides were isolated from ascidian cytoplasm, it is likely that their supposed transition metal complexes existing in a hydrophilic environment are acting as hydrolases. Indeed, the dinuclear copper(II) complexes of H_4pat^1 and H_4pat^2 have been shown to act as phosphatase models as well as carbonaic anhydrase . However, in nature the most common hydrolyzing transition metal in metallo-hydrolase centers is zinc(II). While keeping in mind that zinc(II) is also highly concentrated in the ascidians (see chapter 1.4)[88] one aim of this thesis was to determine if dinuclear zinc(II) complexes of patellamide derivatives could act as artificial phosphatases. Furthermore, the question of whether this hydrolyzing scenario may play a biological role arises. Answering this question might help to identify the biological role of the patellamides.

4.2 Zinc(II) Coordination by Patellamide Derivatives

4.2.1 Isothermal Calorimetric Titrations

The thermodynamic stability of zinc(II) complexes of the ligands H_4pat^1 and H_4pat^2 was determined by isothermal calorimetric titrations (ITC) with zinc(II) triflate towards the ligands (Figure 4.9). ITC is a commonly used method that delivers thermodynamic data like enthalpy *ΔH*, entropy *ΔS*, reaction stoichiometry *N* and stability constant *K*.[234,235] During the experiment one reactant (solvated metal) is titrated into a sample solution containing the other reactant (ligand). The temperature of the reaction vessel is kept constant by the calorimeter. Thus the heat which is released or absorbed which each titration step had to be compensated by the calorimeter, which measures the voltage needed and calculates the compensated energetic difference. [236,237] All experiments were performed with an experimental procedure according to a previous study in which copper(II) triflate was titrated towards the same ligands.[106]

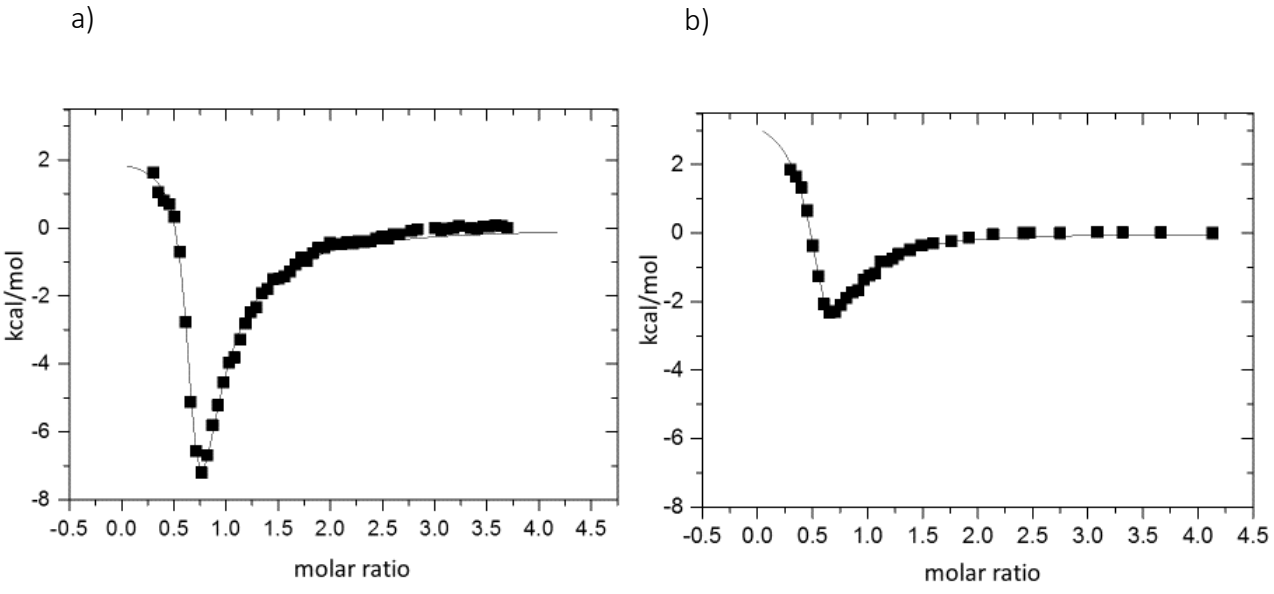

Figure 4.9: Isothermal titration calometry plots of a zinc(II) titration to the ligands H_4pat^1 (a) and H_4pat^2 (b).

Table 4.2. Zinc(II) and Copper(II) stability constants, entropies and enthalpies of complexation of the patellamide derivatives H_4pat^1 and H_4pat^2 (standard deviations in brackets), obtained from ITC.[106]

	$[H_2pat^1Cu_2]^{2+}$	$[H_2pat^1Zn_2]^{2+}$	$[H_2pat^2Cu_2]^{2+}$	$[H_2pat^2Zn_2]^{2+}$
N [a)]	1.90 (0.09)	1.51 (0.16)	1.84 (0.08)	1.69 (0.78)
K	$1.71x10^6$ (0.71)	$1.03x10^5$ (0.30)	$4.03x10^4$ (0.55)	$3.34x10^4$ (0.57)
Δ*H* [kJ/mol]	46.8 (4.6)	-40.86 (0.77)	84.52 (7.7)	-7.686 (3.644)
Δ*S* [J/(mol K)]	278.56	-41.04	371.53	60.67

[a)] computed Zn^{II}/Cu^{II} : (H_2pat^n) ratio[238]

Interpretation of the resulting ITC data leads first to the conclusion that zinc(II) complexes with the naturally configured ligand H_4pat^1 and the 4S* configured ligand H_4pat^2 are less stabile than the formation of the corresponding copper(II) complexes. The trend between the ligands is for the zinc(II) coordination the same as for the copper(II) coordination; H_4pat^1 forms a more stable complex as H_4pat^2. Beyond that, the coordination of zinc(II) is, in contrast to the coordination of copper(II), directed by the enthalpy and not by the entropy. The low enthalpy while complexing zinc(II) displays a change in coordination sphere of the metal ion from tetrahedral to trigonal bipyramidal or even octahedral, which involves at least one solvent molecule more than with the ligand-"free" zinc(II), and thus leads to a higher degree of organization in the whole system. In consequence; the low stabilities of the zinc(II) complexes compared to the corresponding copper(II) complexes, is a result of the zinc(II) ions adaption of an uncommon coordination sphere. This effect was already described for the native peptides by Jaspars *et al*. [41,94] With both ligands, H_4pat^1 and H_4pat^2, the simulations of the ITC data lead only to one stability constant per ligand with a ligand to metal ratio of approximately 1:2, which supports a cooperative binding event. The cooperative effect was already described in the copper(II) chemistry of both ligands; the coordination of the first metal ion preorganizes the ligand for the coordination of the second metal ion.[99] From crystal structures and NMR spectra of previous studies it is known that both ligands (as well as H_4pat^4)[101] are exist in a saddle-shaped conformation. The angle between both binding sides in case of H_4pat^1 is more ideal for the coordination of two metal ions, which is displayed in the higher stability of $[Cu_2H_2pat^1]^{2+}$ compared to $[Cu_2H_2pat^2]^{2+}$. The naturally configured ligand

H_4pat^1 has to undergo less structural change while coordinating metal ions than H_4pat^2. The same effect explains the higher stability of $[Zn_2H_2pat^1]^{2+}$ compared to $[Zn_2H_2pat^2]^{2+}$. Interestingly, both ligand ^1H NMR spectra show only very small changes when base is added, which indicates that the ligand conformation does nearly not change with increasing pH- value (Figure 4.10 b). Thus, it is obvious that every necessary structural change occurs while the coordination of metal ions, and not due to the addition of base, which can be explained with a metal assisted deprotonation.

4.2.2 Nuclear Magnetic Resonance

The coordination chemistry of zinc(II) with the patellamide derivatives was studied using by NMR-spectroscopic titrations in combination with high resolution mass spectrometry. The d^{10} character of zinc(II) allows the observation of the complex formation via NMR spectroscopy.

Titration of zinc(II) triflate to H_4pat^1 in the presence of base leads to the formation of a complex. A pure single existing species can be observed under water-free and highly basic conditions (Figure 4.11a). High-resolution mass spectrometric experiments (see Section 4.2.3) show even at low zinc(II) concentrations and at low base concentrations the dinuclear zinc(II) complexes $[Zn_2(H_2pat^1)(OH)]^+$ and $[Zn_2(H_2pat^1)(OMe)]^+$. The species shown in Figure 4.11 a) was investigated by 2D-NMR (HMBC), which indicates that this species with the formula $[Zn_2(H_2pat^1)(OH)]^+$ (the most intense signal in mass spectrometry) is a C_2-symmetric complex with two chemically different imidazoles (Figure 4.12). ^1H-^{13}C HBMC shows that upon zinc(II) coordination, the evolving signals in the ^1H NMR are not resulting from a splitting, but they do belong to aromatic ^{13}C resonances that have been developed during the coordination of zinc(II) and can thus be assigned as “new” imidazole signals. The existence of two chemically distinguishable imidazoles may be interpreted in two ways: First, both zinc(II) ions have a different coordination environment, i.e. means that one zinc(II) coordinates one solvent molecule more than the other. Second; if the hydroxide (or methoxide) is terminally coordinated to one of the zinc(II) ions both coordination sides (imidazoles) would have a different chemical shift in the NMR experiment. A third option is the coordination of both zinc(II) ions in an $N_{amid}N_{imidazole}N_{amid}$ binding motif, but MM and DFT calculations indicate that this option is unlikely.[117] Moreover, the direct formation of a dinuclear zinc(II) complex supports

the assumption of a cooperative effect while H_4pat^1 is coordinating zinc(II). Unfortunately, the existence of this species occurs only under absolutely water-free conditions, which makes it impossible for this species to act as a hydrolysis catalyst.

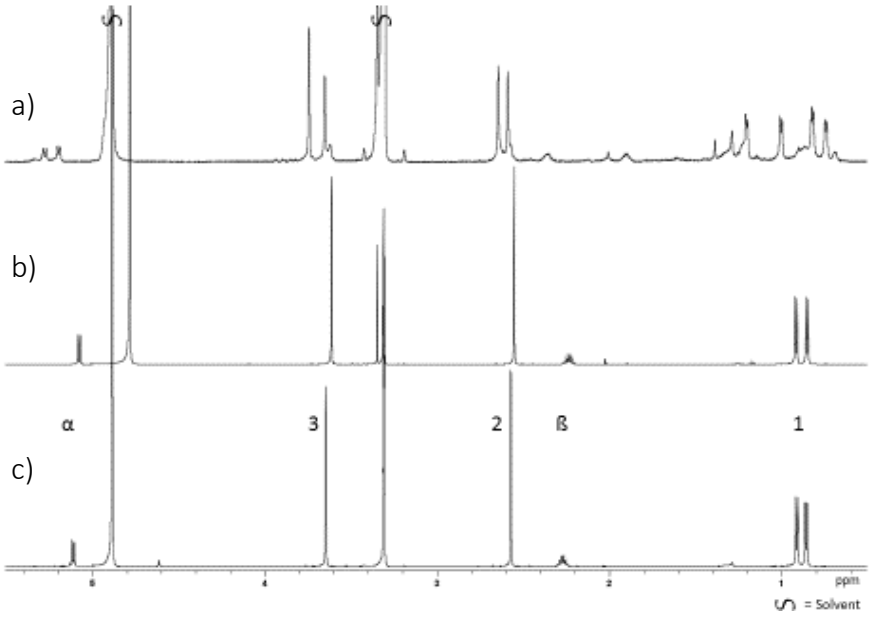

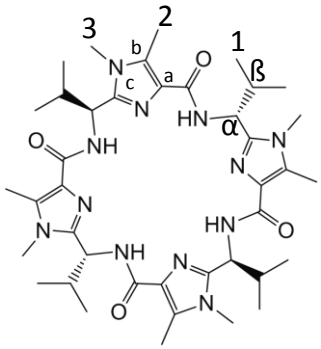

Figure 4.10: ^{1}H-NMR spectra of a) H_4pat^1, b) H_4pat^1+7.5 equivalents of NaOMe and c) $[Zn_2(H_2pat^1)(OH)]^+$ in CD_3OD (10mM), ν = 600 MHz, 25°C.

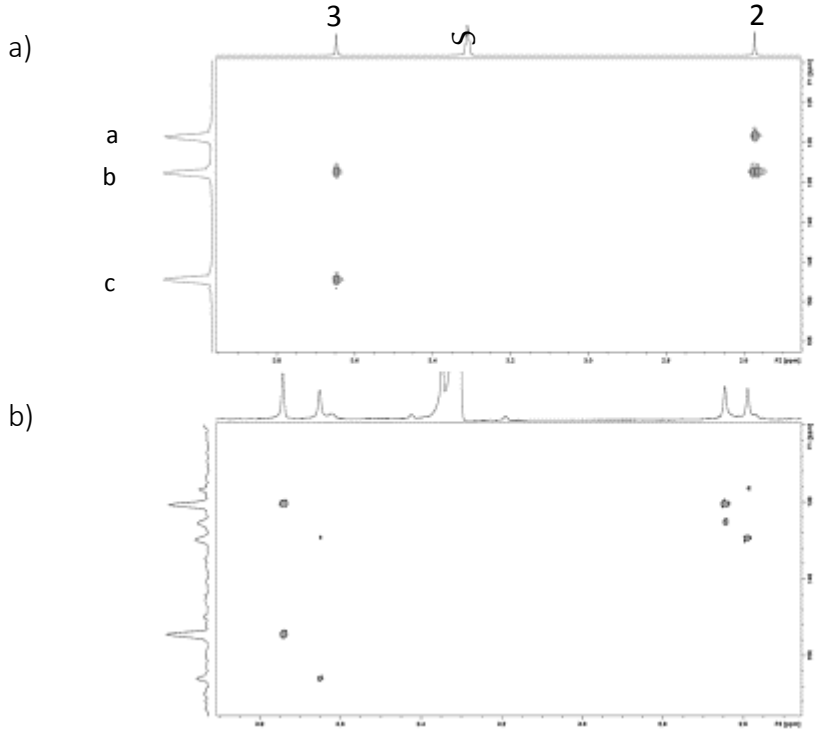

Figure 4.11: ^{13}C-^{1}H HMBC NMR spectra of a) H_4pat^1 and b) $[Zn_2(H_2pat^1)(OH)]^+$ in CD_3OD (10mM) and ν = 600 MHz, 25°C.

The phenomenon, that the stability of zinc(II) complexes depends significantly on the presence or absence of water in solution is literature known.[147] Recently, a mononuclear calixarene zinc(II) complex with three methyl imidazole donors was published, that coordinates zinc(II) under a massively increased *ΔH* and *ΔS* upon the addition of 0.1%$_{Vol}$ water to the in acetonitrile solvated complex.[239]

When it comes to the 4S* configured ligand H_4pat^2, addition of zinc(II) (triflate or acetate) does not lead to the formation of spectroscopically detectable complexes. Addition of an excess of base leads to new signals in the ^{1}H NMR spectrum. This can be assigned to the formation of new species. However, But the uncoordinated ligand is always the main component in solution and neither addition of an excess of zinc(II) nor of an excess of base, not even the absence of water in solution, leads to a single complex. This result reflects the relatively weak stability determined by ITC. H_4pat^2 shows in the calculated ITC data a stability constant which is approximatively only one third of the stability with H_4pat^1. Since the thermodynamic stability of the zinc(II) complex of H_4pat^1 could only be described as moderate, the formation of stable zinc(II) complexes by H_4pat^2 is even more unlikely.

A completely different result is obtainede by analyzing the ^{1}H-NMR titration of zinc(II) triflate and sodium methanolate with the ligand H_4pat^4 (Figure 4.12). The 4S* configured ligand with C_2 symmetry (due to two benzyl residues at two opposite imidazoles) coordinates zinc(II) even without added base. Moreover, it starts to quantitatively form new species after the addition of small amounts of methanolate. There is no clean endpoint in this titration, neither with an excess of zinc(II) nor with an excess of base. Thus, there must be an equilibrium of various species. This coordination behavior was also observed when titrating copper(II) to the same ligand in EPR experiments (see Chapter 3, Section 3). Due to the fact that both, copper(II) and zinc(II) ions, show a similar behavior with H_4pat^4 and both deliver mass-spectrometrically the same stoichiometric composed species, it can be proposed that both metals form similar thermodynamically stable complexes with H_4pat^4.

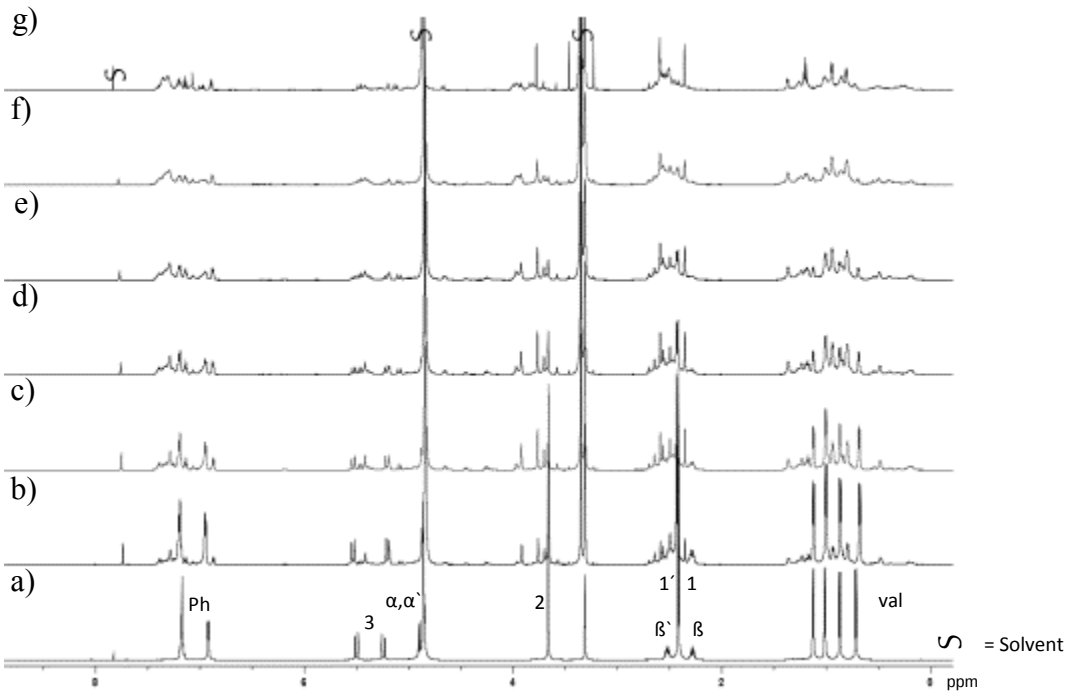

Figure 4.12: ^{1}H-NMR spectra of a) H_4pat^4, b) H_4pat^4 + 2eq $ZnOTf_2$, c) H_4pat_4 + 2eq $ZnOTf_2$ + 2eq OMe^-, d) H_4pat^4 + 2eq $ZnOTf_2$ + 4eq OMe^-, e) H_4pat^4 + 2eq $ZnOTf_2$ + 6eq OMe^-, f) H_4pat^4 + 2eq $ZnOTf_2$ + 8eq OMe^- and g) H_4pat^4 + 2eq $ZnOTf_2$ + 10eq OMe^- in a $CD_3OD/CDCl_3$ mixture of 3:1 (10mM), ν = 600 MHz, 25°C.

The described hydrolytcally active species (see Chapter 6) is already present at a ligand / zinc(II) / base ratio of 1:2:2 and its intensity grows with the addition of base. Due to the formation of solid zinc(II) hydroxide at a ligand / zinc(II) / base ratios larger than 1:2:4, it was not possible to distinguish or characterize a single species via NMR spectroscopy under these highly basic conditions. However, at a ligand / zinc(II) / base ratio of 1:2:4 it is possible to distinguish between the pure ligand and one main species (according to mass spectrometry $[Zn_2(H_2pat^4)(OH)]^+$, see next Section). Characterization of this main species was also done by 2D-NMR spectroscopy (^{15}N-^{1}H HMBC, Figure 4.13). The ^{15}N-^{1}H HMBC measurement of the ligand / zinc(II) / base-1:2:4-mixture produces a 2D-NMR spectrum of a mixture, in which it is difficult to distinguish between species (Figure 4.13b). The ^{15}N-^{1}H HMBC experiment was detected under the same conditions the pure ligand was measured (Figure 4.13a). A reduction of the number of scans leads to a 2D-NMR spectrum, that shows the pure ligand in addition to the main species (Figure 4.13c). This low resolution spectrum shows only the cross couplings of the outer imidazole nitrogens N_b and N_c

with the methyl groups 1,1` and 2 (Figure 4.13 right). Due to the fact that HR-ESI$^+$ mass spectrometry of this component (Figure 4.14 and table 4.3) leads to a main species with the stoichiometry $[Zn_2H_2pat^4(OH)]^+$ it is concluded that the main species is a dinuclear zinc(II) complex, that has structurally two different types of imidazoles. Further, these cross couplings as well as the corresponding resonances in the ^{1}H spectrum do not seem to split, which leads together with the fact that the ligand has also two chemically different types of imidazoles, to the conclusion that this complex has also C_2 symmetry.

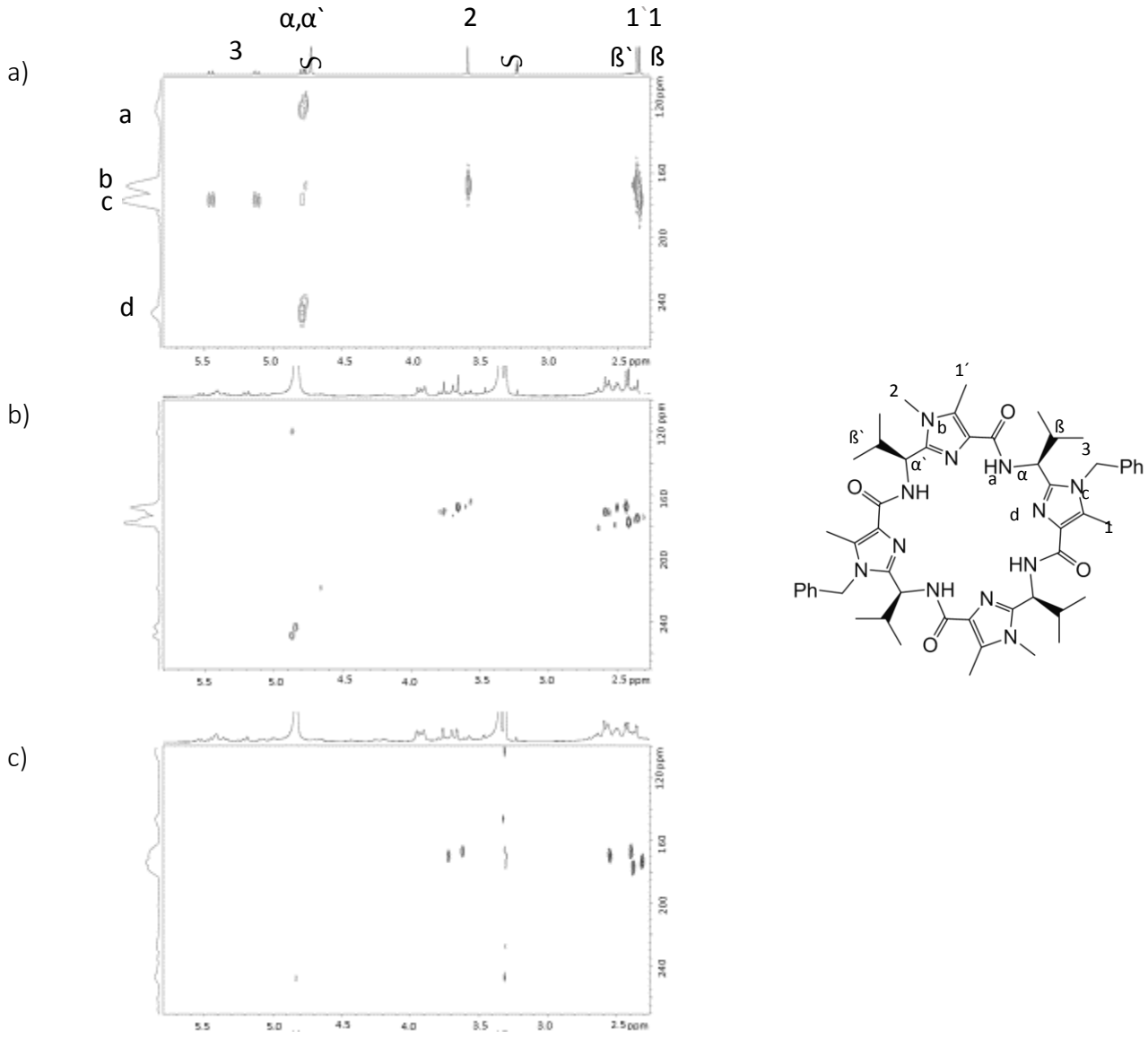

Figure 4.13: ^{15}N-^{1}H HMBC NMR spectra of a) H_4pat^4, b) H_4pat^4 + 2eq $ZnOTf_2$ and c) H_4pat^4 next to $[Zn_2(H_2pat^4)(OH)]^+$ (measured with a smaller number of scans) in a $CD_3OD/CDCL_3$ mixture of 3:1 (10mM), ν = 600 MHz, 25°C..

4.2.3 Mass Spectrometry

In order to study the complex structure of the dinuclear zinc(II) complexes in solution, mass spectra (High-resolution electron-spray ionisation (HR-ESI$^+$), fast atom bombardement (FAB) and matrix-assisted laser-desorption/ ionization (HR-MALDI$^+$) were measured. All the zinc(II) species described here are positively charged complex cations; negatively charged complexes were not detected. It was possible to identify, besides the signals belonging to the species listed in table 4.3, also a number of further species whose signals have a distinct pattern. In case of H_4pat^4, there was also a mononuclear zinc(II) species present. The interpreted spectra were obtained from 1mM methanolic solutions with varying macrocycle: zinc(II) (OTf): base (OMe^-) ratios (see Table 4.3 and Appendix). Identified charged complexes of all three macrocycles are summarized in table 4.3. All mass peaks show the distinctive isotopic pattern of dinuclear zinc(II) complexes (Figure 4.14) except the mononuclear species of H_4pat^4.

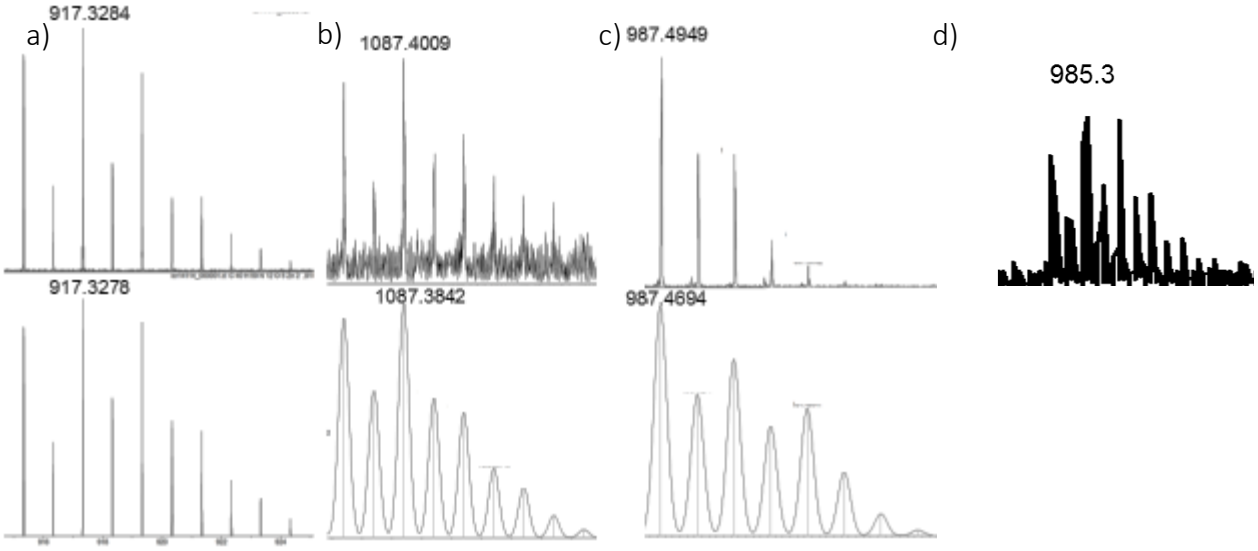

Figure 4.14: Recorded (top) and calculated (bottom) isotopic pattern for a) $[Zn_2(H_2pat^1)(OH)]^+$ b) $[Zn_2(H_2pat^4)(OH)(H_2O)]^+$ c) $[Zn(H_3pat^4)]^+$ in methanol and d) $[Zn_2(H_2pat^2)(CO_2)(H_2O)]+Na^+$ (odd mass).

Table 4.3: Detected Mass peaks in (HR-) ESI^+ mass spectrometric measurements of various different ligand / zinc(II) / base mixtures of all three ligands.

Ligand	Complex	detection ratio/ conditions ligand / zinc(II) / OMe^-	peak found [m/z]	assigned to calc. [m/z]
H_4pat^1	$[Zn_2(H_2pat^1)(OH)]^+$	all 1:2:OMe^->>2	917,3284	917,3282
	$[Zn_2(H_2pat^1)(OMe)]^+$		931,3442	931,3439
	$[Zn_2(H_3pat^1)]^+$		835,4069	835,4068
H_4pat^2	$[Zn_2(H_2pat^2)(OH)]^+$	all obtained with ecxess zinc(II)	917,3	917,3
	$[Zn_2(H_2pat^2)(CO_2)(H_2O)]+Na^+$	occurs only under OMe^- ecxess	985,3	985,3
H_4pat^4	$[Zn_2(Hpat^4)]^+$	in all samples	1051,4282	1051,3798
	$[Zn_2(H_2pat^4)(OH)]^+$	1:Zn>1:OMe^->1	1083.4	1083.4
	$[Zn_2(H_2pat^4)(OMe)]^+$	1:Zn>1:OMe^->1	1069.4	1069.4
	$[Zn(H_3pat^4)]^+$	in all samples	987,4949	987,4649

As expected, the detection of dinuclear zinc(II) complexes and the relative intensities of the m/z peaks depends strongly on the concentration of base, especially for H_4pat^1 and H_4pat^2. While H_4pat^1 exhibited NMR spectra of dinuclear zinc(II) complexes only under highly basic and dry conditions, the same ligand exhibits under mass spectroscopic conditions evidence for the formation of various dinuclear zinc(II) complexes. With an increasing concentration of base (>>4 equivalents) the dinuclear complex $[Zn_2H_2pat^1(OH)]^+$ (917.3284 m/z) represented the most intense peak. Interestingly the 4S*configurated ligand H_4pat^2, which does not exhibit ^1H NMR spectra identicative of complex formation, gave mass spectra with a few signals that are assignable to dinuclear zinc(II) species with a distinct pattern). Upon the addition of an excess of methanolate, it was possible to detect a species, which may assidned to a carbonato complex. In contrast the mass spectra of all zinc(II) / H_4pat^1 mixtures, those of H_4pat^2 do not show any doubly charged species. When it comes to H_4pat^4, the number of species in all experiments increases. Neither the existence nor the absence of some species does depend on the concentration of base. The mononuclear species $[ZnH_3pat^4]^+$ could always be found in solution (with more or less intensity). As well as the dinuclear species $[Zn_2H_3pat^4]^+$. Therefore, all dinuclear zinc(II) species, which contain co-ligands (solvent and/or base) do only exist if zinc(II) and methanolate have larger concentrations

than the ligand, and relative intensities of their peaks increasing with zinc(II) and methanolate concentration.

4.2.4 Complexation Equilibrium of the Patellamide Derivatives with Zinc(II)

A general scheme for zinc(II) complexation equilibria (Figure 4.15) for all three peptides can be proposed, based on the results discussed in this chapter and supported by MM and DFT calculations. The calculations, which are not part of this thesis, confirmed the coordination of two zinc(II) ions in an $N_{imidazole}N_{amide}N_{imidazole}$ binding motif and were performed by Annika Eisenschmidt.[117]

Addition of zinc(II) to a solution of cyclic *pseudo* peptide leads to the formation of mononuclear and dinuclear zinc(II) complexes, which are spectroscopically detectable and could be characterized in the cases of H_4pat^1 and H_4pat^4. While H_4pat^4 forms an equilibrium with various complexes existing next to each other, H_4pat^1 forms a stable and solely existing dinuclear zinc(II) complex, which is assumed to be hydroxo bridged. This species exists only under dry and basic conditions (Figure 4.15red). Even if it was not possible to characterize any zinc(II) complexes of the unnatural 4S* configured ligand H_4pat^2 via NMR spectroscopy, mass spectrometry indicates the formation of carbonato and/or hydrogen carbonato dinuclear zinc(II) complexes (figure 4.15 green). However, for all ligands investigated, there is a clear preference to form dinuclear zinc(II) complexes, which can be explained with the cooperative effect as it is already known from the copper(II) chemistry of the cyclic *pseudo* peptides[85,99,101,106] and supported by ITC. With the ligand with the benzyl residues, H_4pat^4, it is possible to observe mononuclear zinc(II) complexes at low zinc(II) concentrations. While H_4pat^1 and H_4pat^2 show a zinc(II) coordination behavior which differs fundamentally from their copper(II) coordination behavior, H_4pat^4 shows a similar behavior for both metal ions. (see also Chapter 3.3).

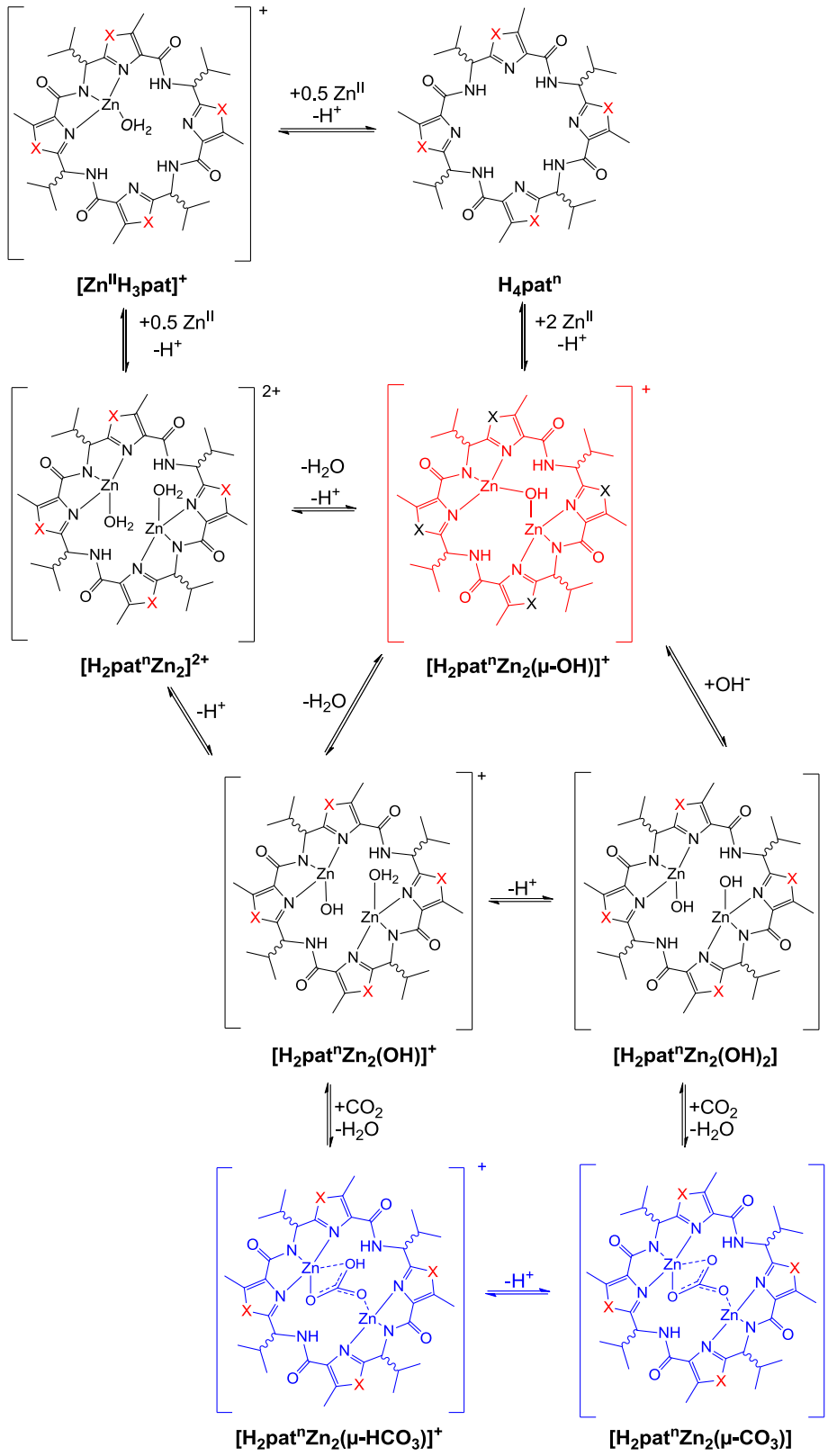

Figure 4.15: Scheme of all complex described structures in *pseudo* octapeptide zinc(II) equilibrium.

Parts of the following chapter are to be published in a manuscript entitled: “Dinuclear Zinc(II) and Copper(II)/Zinc(II) complexes of artificial Patellamides as Phosphatase models”; Peter Comba, Annika Eisenschmidt, Lawrence R. Gahan, Graeme R. Hanson, Nina Mehrkens, Michael Westphal, *manuscript in preparation*, 2015

5 Heterodinuclear Complexes

One major result of the studies described in Chapters 3 and 4, is that the 4 S* configured and two benzyl residues containing ligand H_4pat^4 forms stable dinuclear complexes with both copper(II) and zinc(II). Titration experiments with the two metal ions show the development of complexation equilibria. While H_4pat^1 and H_4pat^2 interact with zinc(II) only weakly or under special and unphysiological (hydrophobic and highly basic) conditions, H_4pat^4 forms with both metal ions structurally comparable complexes. Additionally, H_4pat^4 is the only ligand known from the patellamide-derivative-library (Chapter 1 Figure 1.17), which forms a single mononuclear species at low copper(II) and low base concentrations. Due to the fact, that H_4pat^4 shows with both metal ions (titrations with the corresponding salts) a similar complexation behavior, it seems likely that both copper(II) and zinc(II) have similar stability constants, which lead to the idea that this ligand may form heterodinuclear copper(II)-zinc(II) complexes. Descriptions in the literature of approaches to heterodinuclear copper(II)-zinc(II) complexes, in which the binding sites for both metal ions are chemically identical, are rare.[240-242] The combination of the facts that H_4pat^4 forms a mononuclear copper(II) complex and that both metals seem to have a comparable thermodynamic stability could make sequential coordination of both metal ions possible.

A mixed strategy of EPR spectroscopy, UV/Vis-NIR spectroscopy and paramagnetic ^1H NMR in combination with high resolution mass spectrometry was chosen in order to investigate this complexation. Paramagnetic NMR on one hand delivers the opportunity to have a closer look on the complexation equilibrium at room temperature and therefore makes it possible to compare the obtained results to those of the only-zinc(II) titration. EPR spectroscopy on the other hand gives information about changes in coordination sphere of the copper(II) ion which makes it possible to compare the copper(II)-zinc(II) titration to the only-copper(II) titration.

Additionally, same experiments were carried out with the 4S* configured ligand H_4pat^2. Even if H_4pat^2 does not form stable, spectroscopically detectable zinc(II) complexes (weak interaction), this ligand exhibits a cooperative effect in copper(II) coordination. Since H_4pat^2 forms less stable complexes with copper(II) than the naturally configured ligand H_4pat^1, there is the chance that due to the cooperative effect it may be possible with H_4pat^2 to obtain heterodinuclear copper(II)-zinc(II) complexes with an excess of zinc(II).

The enzyme PAP (described in Chapter 4) isolated from kidney beans, has a heterodinuclear iron(III)/ zinc(II) center in its active side.[243] The major reason for studying the formation of heterodinuclear copper(II)/ zinc(II) complexes is, that all in this thesis described complexes were tested phosphatase activity (chapter 6) and thus the formation of heterodinuclear complexes delivers a higher comparability to enzymes like PAP.

5.1 Cu^{II}/Zn^{II} Complexation by H_4pat^4

5.1.1 Electron paramagnetic resonance

Before commencing the formation of heterodinuclear copper(II)-zinc(II) complexes, it was important to investigate the exact concentration at which the formation of a homodinuclear copper(II) complex starts. As already mentioned in Chapter 3, at a ligand / copper(II) / base ratio of 1:0.5:0.5 a single mononuclear copper(II) species, $[Cu(H_3pat^4)(OH)]^+$, was identified. The formation of dinuclear copper(II) complexes starts upon adding further 0.25 equivalents of each copper(II) and base. Thus the starting point chosen for the addition of zinc(II) was at a ligand / copper(II) / base / ratio of 1:0.5:0.5. A mixed copper(II)/ zinc(II) complex was obtained by addition of 0.5 equivalents of zinc(II). In figure 5.1 the EPR spectra of the mononuclear copper(II) complex (black, discussed in chapter 3.3) as well as of the copper(II) / zinc(II) complex (blue) are overlaied. Since zinc(II) is a d^{10} ion with nuclear spin of zero all changes in an EPR spectrum are due to

geometric changes and thus changes in the coordination sphere of the precoordinated copper(II) ion occurring by the coordination of the second metal ion into the same ligand. Indeed, the g values of the mononuclear copper(II) species and the heterodinuclear copper(II) / zinc(II) complexes are very similar, while the hyperfine splitting differs.

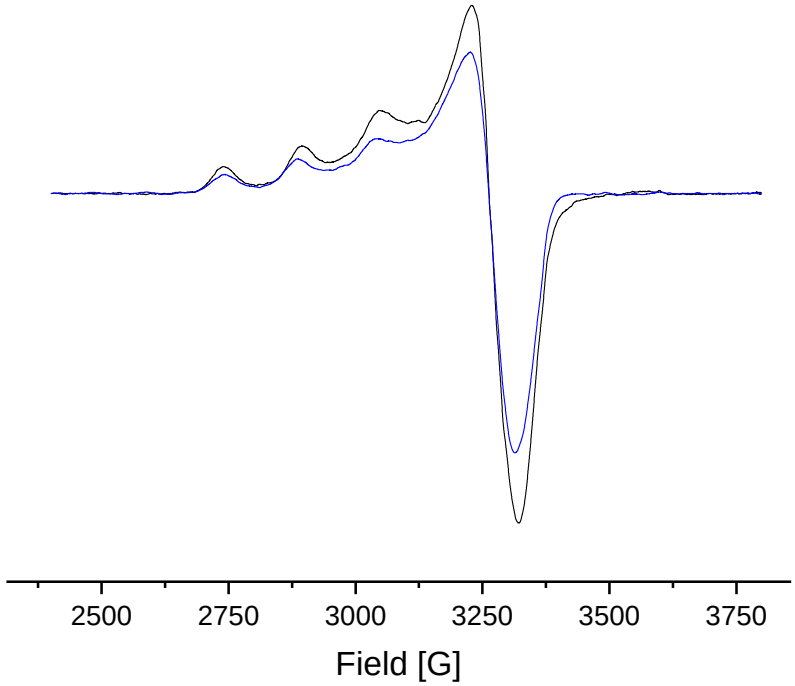

Figure 5.1: EPR spectra of $[Cu(H_3pat^4)(OH)]$ (black) and $[CuZn(H_3pat^4)(OH]^+$ (blue). (X-Band, 140K, 1 mM in MeOH, ν = 9.446309 GHz)

The well resolved spectrum delivers a superhyperfine coupling (Figure 5.2 b), which could be simulated (Table 5.1), involving two different types of nitrogen ($N_{imidazole}N_{amide}N_{imidazole}$). The superhyperfine coupling of the mononuclear copper(II) complex (Chapter 3, Table 3.2) is smaller than that of the heterodinuclear copper(II)-zinc(II) species, it is enlarged with the addition of zinc(II). This enlargement can be explained by slight changes in distances and in angulars from the copper(II) ion to the ligand. The simulated spin Hamiltonian parameters $g_{II} > g_{\perp}$ and $A_{II} >> A_{\perp}$ are suggestive of a distorted square pyramidal coordination sphere of the copper(II) ion and in good agreement with the parameters obtained from previously investigated patellamide derivative copper(II) complexes.[85,100,101] Another influencing factor for the ligandssphere, and thus, for the spectral differences, is the charge; $[Cu(H_3pat^4)(OH)]$ has no charge, while$[CuZn(H_2pat^4)(OH)]^+$ is +1 charged.

Table 5.1. Simulated EPR parameter.

	$[Cu^{II}Zn^{II}(H_2pat^4)(OH)]^+$	$[Cu^{II}(H_3pat^4)(OH)]$	Superhyperfine $[10^{-4}cm^{-1}]$		
g_x	2.046	2.048	$A_x(N_{im})$	12.1	7.2
g_y	2.078	2.076	$A_y(N_{im})$	7.0	11.6
g_z	2.280	2.269	$A_z(N_{im})$	12.9	13.0
A_x $[10^{-4}cm^{-1}]$	13.4	6.3	$A_x(N_{am})$	6.7	12.1
A_y $[10^{-4}cm^{-1}]$	11.5	6.8	$A_y(N_{am})$	11.0	7.9
A_z $[10^{-4}cm^{-1}]$	155.0	159.0	$A_z(N_{am})$	13.2	13.1

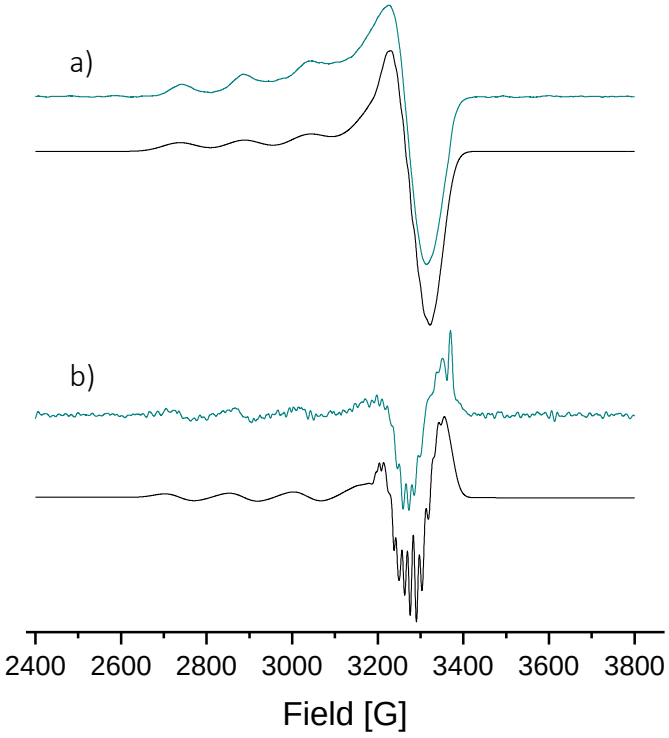

Figure 5.2: EPR spectra of $[CuZn(H_2pat^4)(OH]^+$: a) first derivative and b) second derivative (detected:turquoise and simulated:black, X-Band, 140K, 1 mM in MeOH, ν = 9.446309 GHz).

The coordination of copper(II) can also be followed via UV/Vis-NIR spectroscopy. In case of the ligand H_4pat^4 a complete complexation of both either solvated copper(II) as of solvated zinc(II) occurs with the addition of base, thus to a 1 mM methanolic solution of ligand plus one equivalent zinc(II) triflate, first a solution of copper(II) triflate was added stepwise (Figure 5.3 green), then base was added in 0.1 equivalent steps (Figure 5.3 blue). With the addition of base all solvated copper(II) is complexed (absorption > 800nm decreases) and the formation of two new d-d- bands is observable. In agreement with previous studies the absorption at approximatively 660 nm

belongs to a homodinuclear copper(II) species, while the absorption at 520 nm might belong to a new species, probably the expected copper(II)-zinc(II) species.

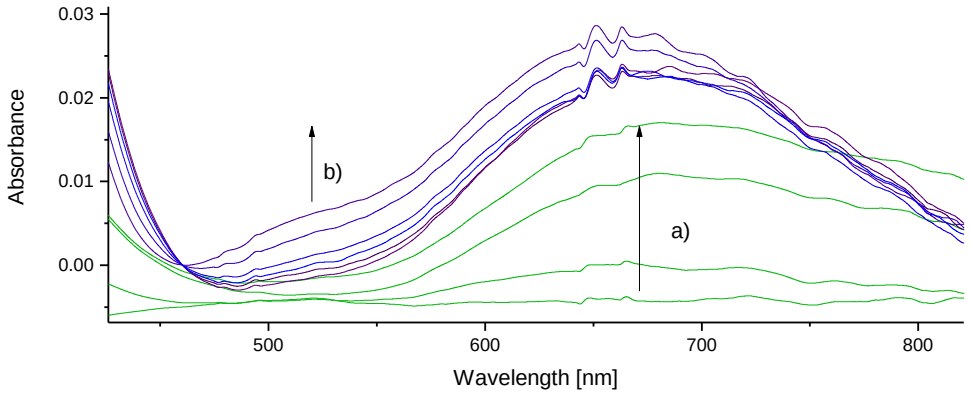

Figure 5.3: UV/Vis titration of a) 0-0.5 eq. $Cu(OTf)_2$ to H_4pat^4 1 eq. $Zn(OTf)_2$ and b) 0-1.5 equivalents $(n\text{-}Bu)_4OMe$.

To obtain further information about the complexation equilibrium, paramagnetic ^1H NMR spectra were measured. The spectra were measured while zinc(II) triflate was titrated into a ligand / copper(II) solution (Figure 5.4). As expected ^1H NMR spectroscopy shows a complexation equilibrium and the signals get broadened with the addition of zinc(II), indicating the cooperative coordination of copper(II) with increasing zinc(II) concentration. The expected shift or formation of new resonances in the low field region was first visible in spectrum d). The paramagnetic signal displayed in figure 5.4 f) belongs to H_α, the closest proton to the paramagnetic copper(II) ion. Surprisingly this grows with addition of zinc(II). This observation further indicates a cooperative effect. The addition of zinc(II) preorganizes the ligand for the coordination of a copper(II) ion.

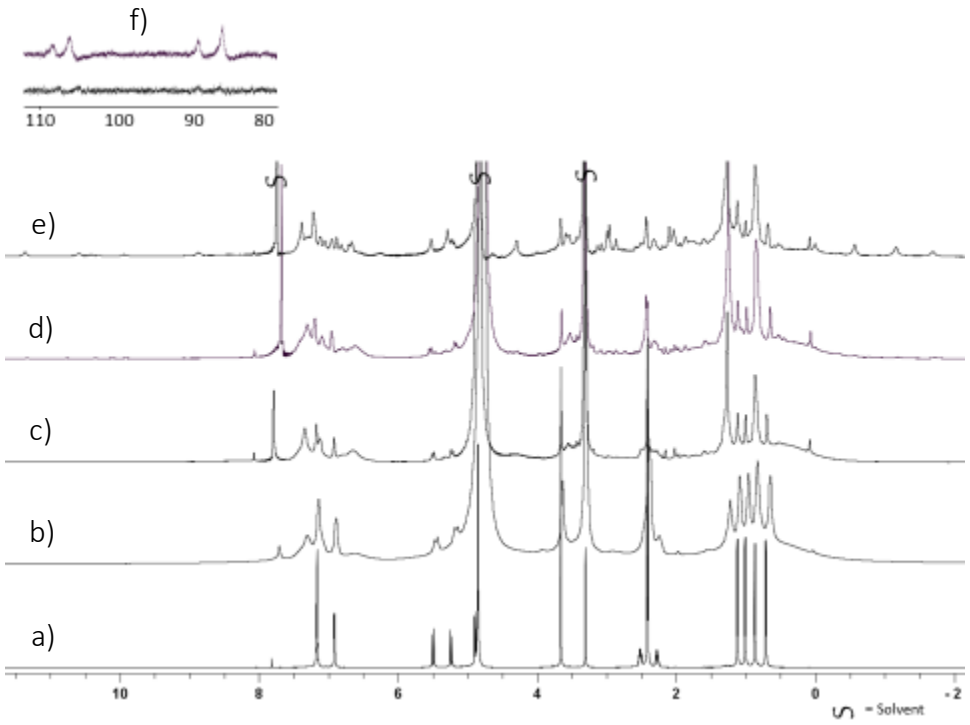

Figure 5.4: Paramagnetic ^{1}H NMR of H_4pat^4/ $Cu(OTf)_2$/ OMe^-/ $Zn(OTf)_2$: a) pure Ligand, b) 1:0.5:0.5:0, c)1:0.5:1:0.5, d) 1:0.5:1.25:0.75, e) 1:0.5:2:1.5 and f) paramagnetic shifted signal of H_α in MeOD-d_4 and $CDCl_3$ 3:1.

High-resolution mass spectra of each solution were taken and a copper(II)/ zinc(II) species with an additional zinc(II) ion which gives both even and odd masses could be identified (Figure 5.5).

The complexation equilibria that involve both metal ions, copper(II) and zinc(II), are proposed in Figure 5.6. From comparison with the copper(II)-only and the zinc(II)-only equilibria (see Chapters 3 and 4) a mixture of both equilibria is evident. This indictates further, that both metals have a similar stability constant with H_4pat^4, as it was proposed at the beginning of this chapter.

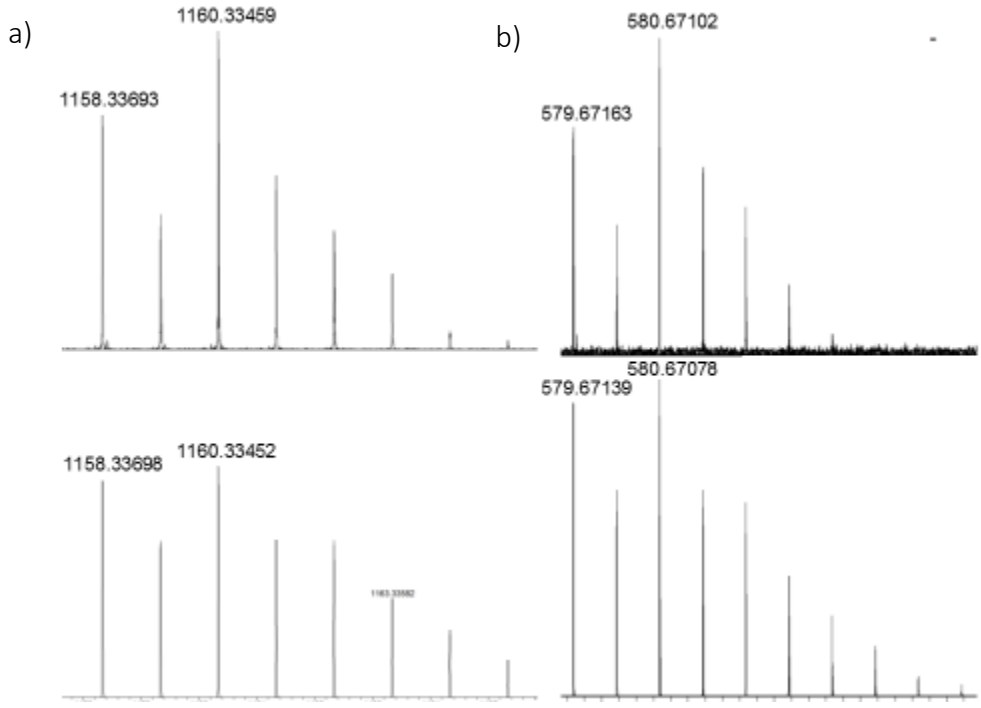

Figure 5.5: Hr-ESI$^+$ mass spectra of: a) [[CuZn(H_2pat^4)(OH)(OMe)]+Zn]$^+$ (odd) and b) [CuZn(H_2pat^4)(OH)(OMe)]+Zn]$^{2+}$ (even)

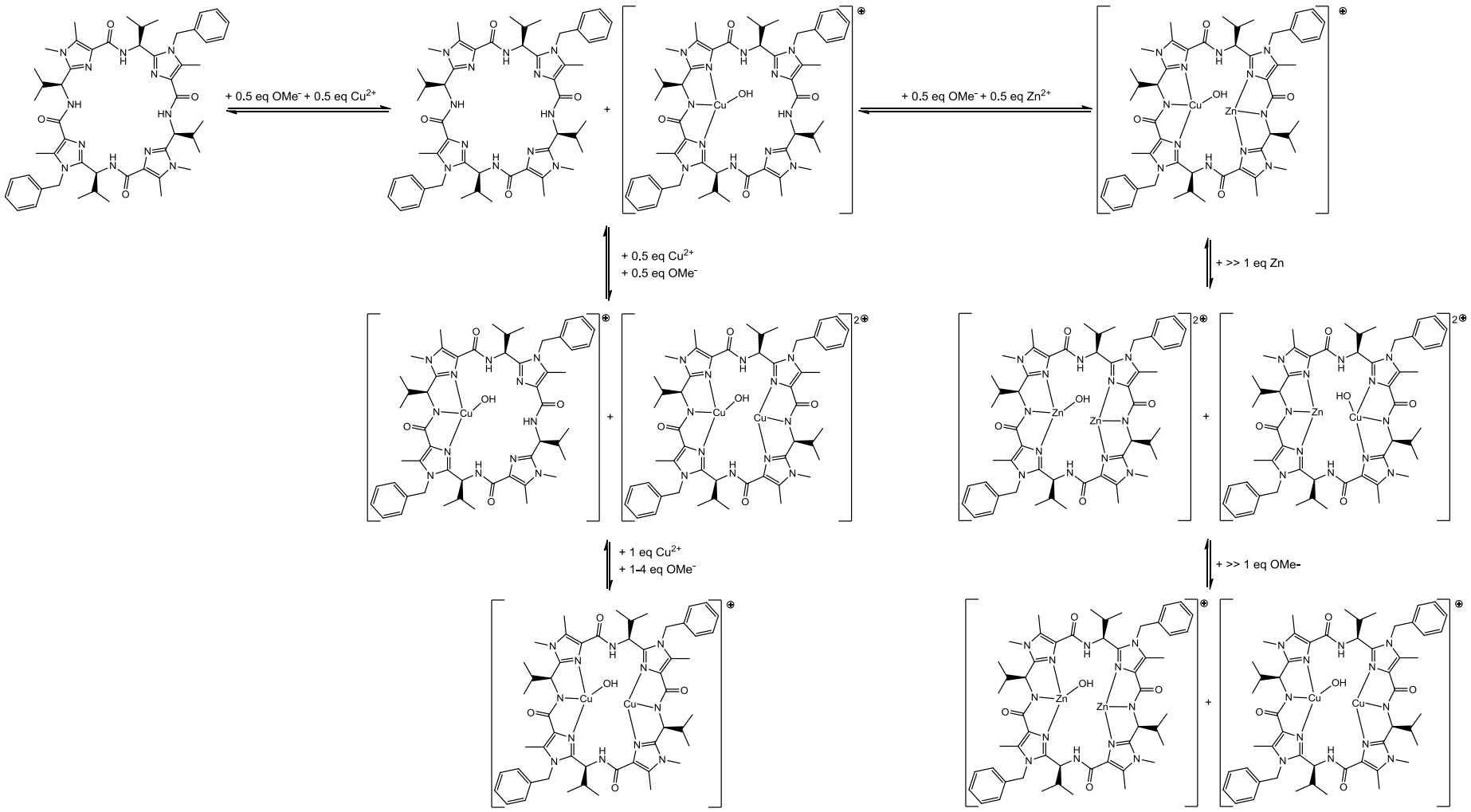

Figure 5.6: Proposed copper(II)/ zinc(II) complexation equilibrium of H_4pat^4.

5.2 Cu^{II}/Zn^{II} Complexation by H_4pat^2

For the formation ofheterodinuclear copper(II)-zinc(II) complexes with the 4 S* configured ligand H_4pat^2, which forms less stable dinuclear copper(II) complexes than the naturally configured ligand H_4pat^1 but exhibits also a high preorganization for the coordination of two metal ions, a different strategy had to be applied. With H_4pat^2 a single mononuclear species was not expected to be found[85,100,101], and zinc(II) triflate was therefore titrated to a solution that already contained a mixture of mononuclear and dinuclear copper(II) complexes (Figure 5.7 blue).

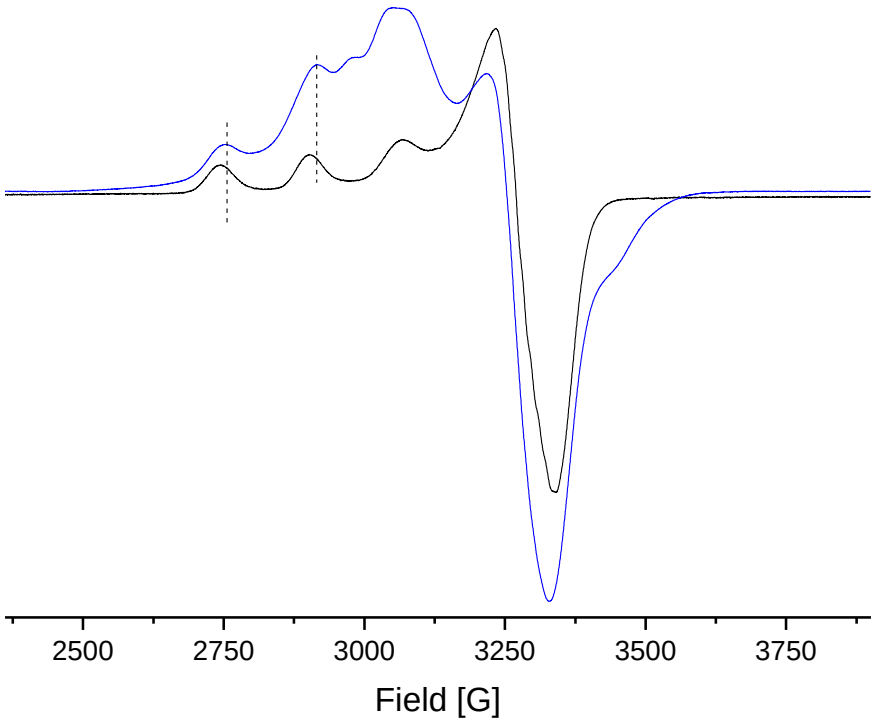

Figure 5.7: Overlay of selected EPR spectra at distinct ligand / Cu^{II}/ Zn^{II} / OMe^- ratios: 1:1:0:1(blue, ν = 9.447735 GHz) and 1:1:4:2 (black, ν = 9.446188 GHz) (X-Band, 140K, 1 mM in MeOH).

The blue spectrum displayed in figure 5.7 shows according to previous studys a mixture of a dinuclear copper(II) species and a mononuclear copper(II) species.[100,101] Upon addition of 4 equivalents of zinc(II) and one more equivalent of base, the black spectrum displayed in Figure 5.7

was detected. The spectrum has the characteristical shape belonging to a mononuclear copper(II) complex, but due to the fact that it was obtained by the addition of an excess of zinc(II) to a solution with mono and dinuclear copper(II) complexes it can be assigned to a heterodinuclear copper(II)-zinc(II) complex. Spin Hamiltonian parameter obtained by simulation with Xsophe differ significantly from the parameters obtained by simulation (table 5.2) for the mononuclear copper(II) complex (which was obtained by spectral substraction, parameter are purple in Table 5.2).[100]

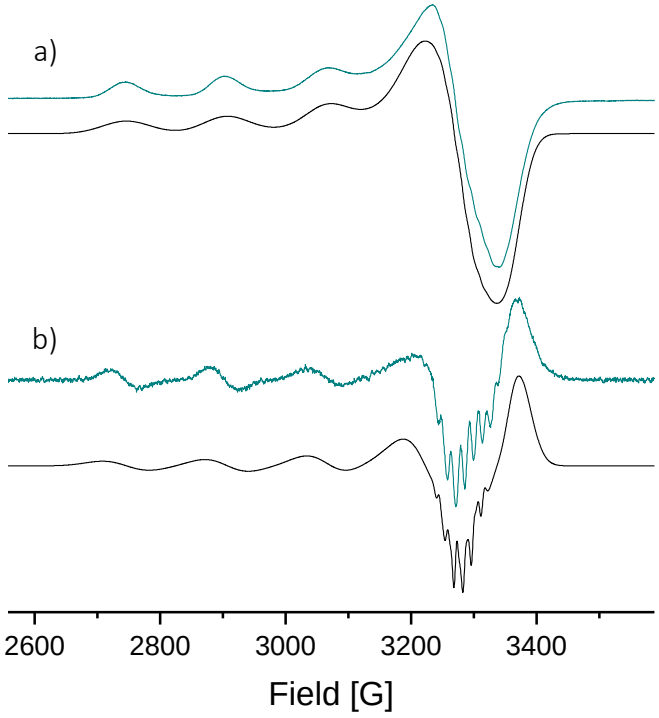

Figure 5.8: EPR spectra of $[CuZn(H_2pat^2)(OH]^+$: a) first derivative and b) second derivative (detected:turquoise and simulated:black). 2:4 (ν = 9.446188 GHz, X-Band, 140K, 1 mM in MeOH).

Table 5.2. Simulated EPR parameter.

	$[Cu^{II}Zn^{II}(H_2pat^2)(OH)]$	$[Cu(H_3pat^2)(OH)]$	Superhyperfine $[10^{-4}cm^{-1}]$	
g_x	2.082	2.074	$A_x(N_{im})$	11.8
g_y	2.045	2.051	$A_y(N_{im})$	12.6
g_z	2.260	2.259	$A_z(N_{im})$	10.8
A_x $[10^{-4}cm^{-1}]$	13.8	14.2	$A_x(N_{am})$	11.3
A_y $[10^{-4}cm^{-1}]$	15.2	14.7	$A_y(N_{am})$	7.2
A_z $[10^{-4}cm^{-1}]$	168.6	150.0	$A_z(N_{am})$	15.4

The spectrum obtained also exhibits a well resolved superhyperfine coupling, which could be simulated involving two different types of nitrogen donors as already described for H_4pat^4. Due to the fact that the spectrum obtained has similar spin Hamiltonian parameters as obtained for the complexes of H_4pat^4 the constitutional formula $[CuZn(H_2pat^2)(OH)]^+$ was tentatively proposed for this species. Comparison of the copper(II)/ zinc(II) species with the previously described mononuclear copper(II) species[85,100,101] shows that the hyperfine splitting in Z- direction in this case is enlarged, while the g values are nearly the same.

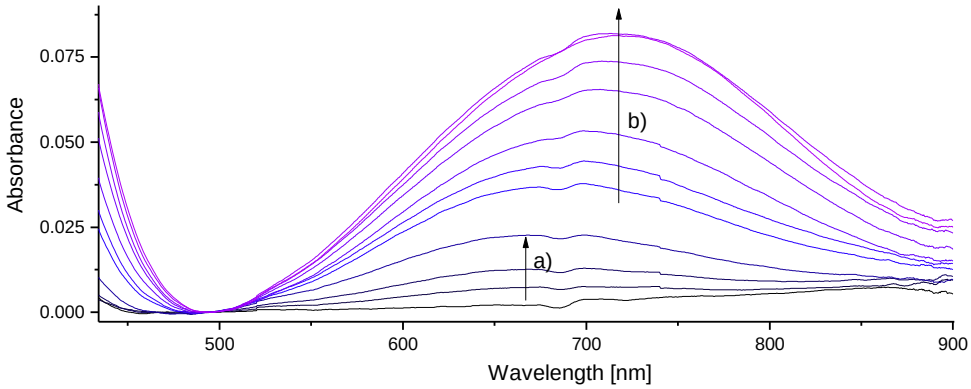

Figure 5.9: UV/Vis titration of a) 0-0.5 equivalents $Cu(OTf)_2$ to H_4pat^2 1 equivalent $Zn(OTf)_2$ and b) 0-1.5 equivalents $(n\text{-}Bu)_4OMe$.

Performing the same UV/Vis-NIR titration experiment as in case of H_4pat^4, leads in case of H_4pat^2 to a different result. The first steps of the stepwise addition of copper(II) to the zinc(II) containing ligand solution shows a d-d band at about 650 nm which might belong to a mixed species (Figure 5.9 a). However, further addition of copper(II) leads to the formation of the known dinuclear copper(II) complexes.[101] (Figure 5.9 b).

A preliminary complexation equilibrium based on the EPR results could be proposed and is shown in figure 5.10. Addition of an excess of zinc(II) leads to the formation of a mononuclear looking EPR spectrum (Figure 5.10 black), which can be assigned to the formation of a heterodinuclear complex, because this ligand does not exhibit any point in the copper(II) complexation equilibrium were a single mononuclear copper(II) species exists.

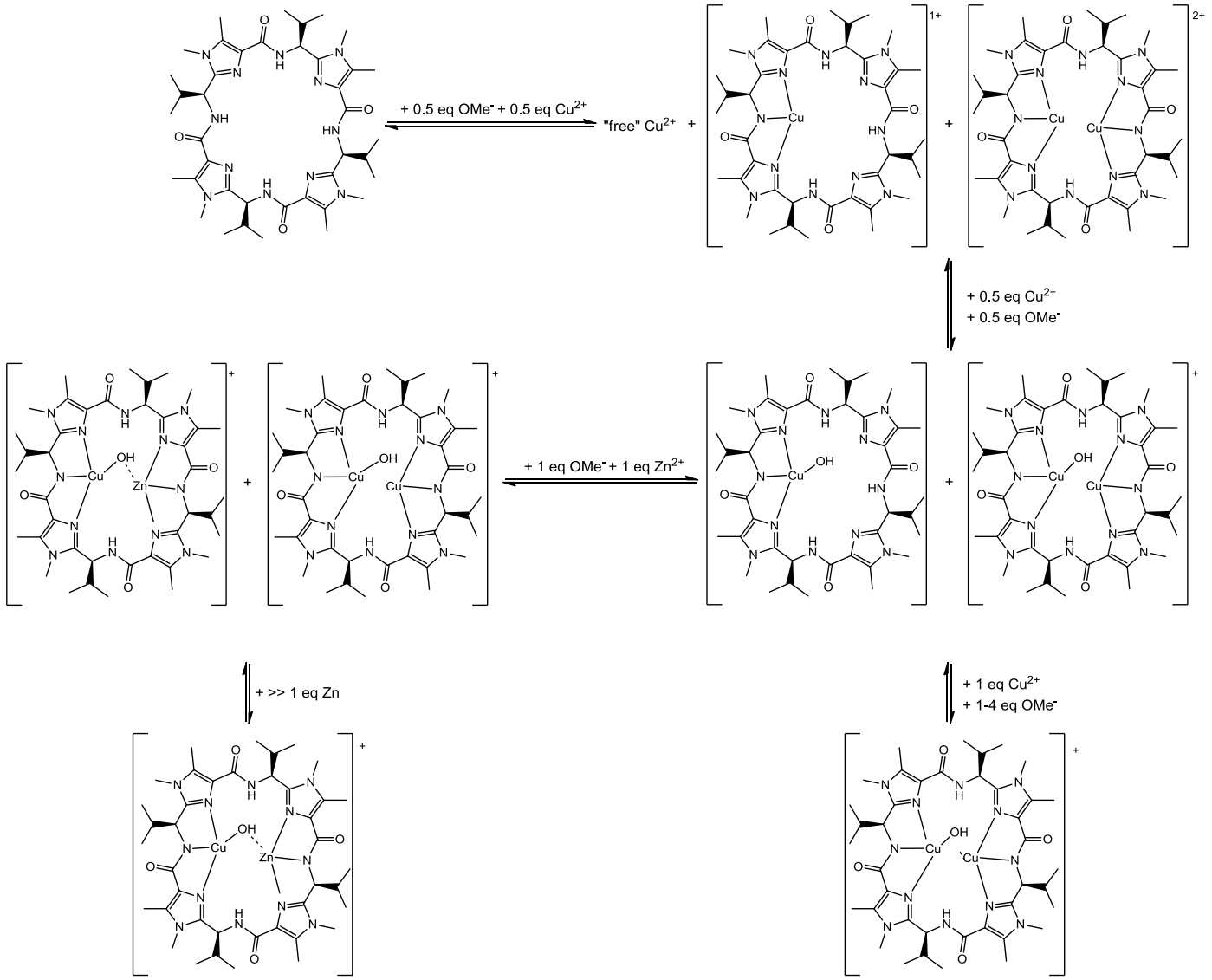

Figure 5.10: Proposed copper(II)/ zinc(II) complexation equilibrium of H_4pat^2.

Parts of the following chapter are to be published in a manuscript entitled: “Dinuclear Zinc(II) and Copper(II)/Zinc(II) complexes of artificial Patellamides as Phosphatase models”; Peter Comba, Annika Eisenschmidt, Lawrence R. Gahan, Graeme R. Hanson, Nina Mehrkens, Michael Westphal, *manuscript in preparation*, **2015**

6 Hydrolysis of Phosphoesters

Phosphoesters are omnipresent in nature, and thus, nature has evolved various strategies to cleave them. Many Artificial model catalysts that are capable of hydrolyzing CO_2 often exhibit the ability to hydrolyze phosphoesters as well.[112,202] For example, the dinuclear copper(II) complexes of the patellamide derivatives are very efficient carbonic anhydrase models[107,111] and these complexes also act as phosphatase models[112]. It therefore seems likely that zinc(II) containing complexes of the patellamide analogues might act as even more efficient phosphatases. A well known phosphatase that has a dinuclear metal center and is active at neutral pH is the enzyme purple acid phosphatase (PAP). The active site of PAP has a dinuclear heterovalent metal center, which is in some cases also heterodinuclear (Chapter 4, Table 4). Enzymatic mimics for the hydrolysis of phosphoesters have the advantage that they have the ability to hydrolyze various substrates, which can be used in further applications. For example the hydrolytic degradation of organophosphate pesticides or nerve agents, both of which are often phosphotriesters and, due to their high stability, accumulated in nature.[244,245]

The phosphoester hydrolyzing dinuclear copper(II) complexes of the patellamide derivatives function most efficiently at neutral pH and in a narrow pH range[112], thus a mechanistic scenario similar to that of PAP is quite likely. In order to determine whether the dinuclear complexes described in chapters 3, 4 and 5 have the ability to hydrolyze phosphoesters catalytically, they were tested in a hydrolysis assay which is widely applied in PAP research.[208] However, it is not the focus of this chapter to go deeply into the mechanistic scenario of the phosphodiester cleavage, but instead provide an overview about the hydrolytic abilities of homo- and heterodinuclear copper(II)-zinc(II) complexes of patellamide derivatives.

Phosphoester cleavage was followed by monitoring the concentration of the hydrolysis product 2,4-dinitrophenolate, which has a strong absorption at 400 nm (ε = 12,100 $M^{-1}cm^{-1}$) at 25°C *via* UV/Vis-NIR spectroscopy (Figure 6.1).[208,209] The multicomponent buffer used for the pH dependence of the initial rate is described in detail in Chapter 8. The complexes tested were prepared in methanol for solubility reasons and for keeping the results comparable to the results from previous studies. The model substrate BDNPP was dissolved in acetonitrile. All measurements were performed in solutions with the final solvent ratio of H_2O : MeCN : MeOH 50:45:5. The final catalyst concentration and the BDNPP concentration are described separately for each measurement in the respective section. To prevent inhibition by carbonate all solutions were carefully degassed and kept under argon. Autohydrolysis of BDNPP was determined in duplicate and subtracted from the observed catalyzed hydrolysis rates, these were determined in triplicate.

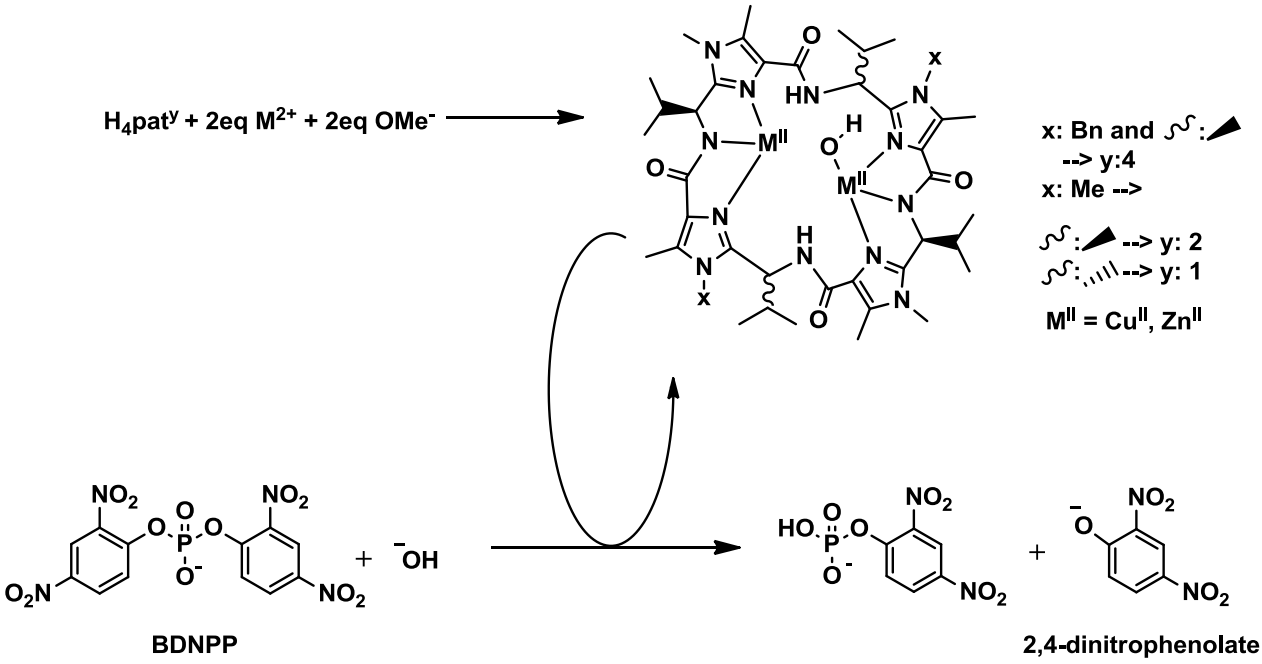

Figure 6.1: Reaction scheme of the dinuclear metal(II)-patellamide catalyzed BDNPP hydrolysis.

The activity in hydrolyzing BDNPP was measured at constant BDNPP concentration at different pH values from pH = 4.5 to pH = 11. The data obtained were fitted with equation 6.1 to produce a pH profile. Equation 6.1, is based on a model for diprotic systems, with two active intermediates E^n and E^{n-1}, and gives equilibrium constants K_{AI} and K_{AII} for two deprotonation steps, which are tabulated as pK_{AI} and pK_{AII}. V_{0max}, the maximum initial rate, is also defined in equation 6.1. The value γ indicates whether, E^n (the active catalyst) is more active (γ < 1) or E^{n-1} (the protonated form)(γ > 1). [246]

$$V_0 = V_{0,max} * \frac{\left(1+\frac{\gamma * K_A II}{[H^+]}\right)}{\left(1+\frac{[H^+]}{K_A I}+\frac{K_A II}{[H^+]}\right)} \quad (6.1)$$

$$V = \frac{V_{max} * [S]_0}{K_M + [S]_0} \quad (6.2)$$

$$k_{cat} = \frac{V_{max}}{[K]_0} \quad (6.3)$$

To obtain further kinetic information, substrate dependent measurements were performed at the pH value with the maximum rate. The data obtained were fitted according the Michaelis-Menten approach (equation 6 .2 and 6.3), where V_{max} is the maximum rate at saturation conditions and K_M the Michaelis-Menten constant. The catalytic efficiency k_{cat} (equation 6.3) can be used to compare different catalysts.

6.1 Dinuclear Complexes of H_4pat^4

The ligand H_4pat^4 is the only ligand of the set investigated which forms both a homodinuclear copper(II) and zinc(II) complexes and in addition also a heterodinuclear copper(II)-zinc(II) complex. The homodinuclear complexes of H_4pat^4 $[M^{II}_2(H_2pat^4)OH]^+$ (M = Cu, Zn) were investigated in pH - dependent scans of the initial catalysis rate (Figure 6.2).

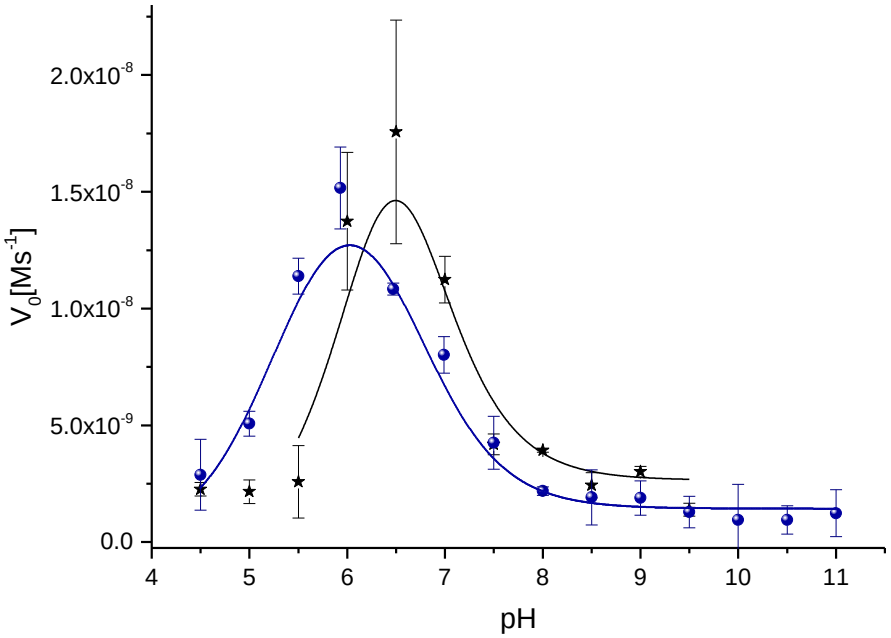

Figure 6.2: pH profiles of the BDNPP hydrolysis with $[Zn_2(H_3pat^4)(OH)]^+$ (blue) and $[Cu_2(H_3pat^4)(OH)]^+$ (black); [BDNPP] 5mM and [cat.] 40µM, 25°C.

The resulting pH profile Figure 6.2 is similar to those obtained in the previous study for $[Cu_2(H_2pat^1)OH]^+$ and $[Cu_2(H_2pat^2)OH]^+$.[70,107,112] Both complexes hydrolyze BDNPP with a narrow pH profile. The dinuclear copper(II) complex has its maximum initial rate at pH 6.50, while the dinuclear zinc(II) complex has its maximum initial rate at pH 6.02, 0.5 pH units lower and has a broader pH activity range than the compared copper(II) complex. Both complexes function efficiently under neutral to slightly acidic conditions. The difference of 0.5 pH units between the

copper(II) and the zinc(II) complexes may be explained by the fact that macrocyclic N-donated coordinated zinc(II) is the better Lewis acid in comparison to corresponding copper(II) species and has the ability to deprotonate coordinated water at lower pH. (comparison of $[Zn[12]aneN_3(H_2O)]^{2+}$: pK_A = 7.3 (Figure 4.3a) and the corresponding $[Cu[12]aneN_3(H_2O)]^{2+}$: pK_A = 8.4)[159]

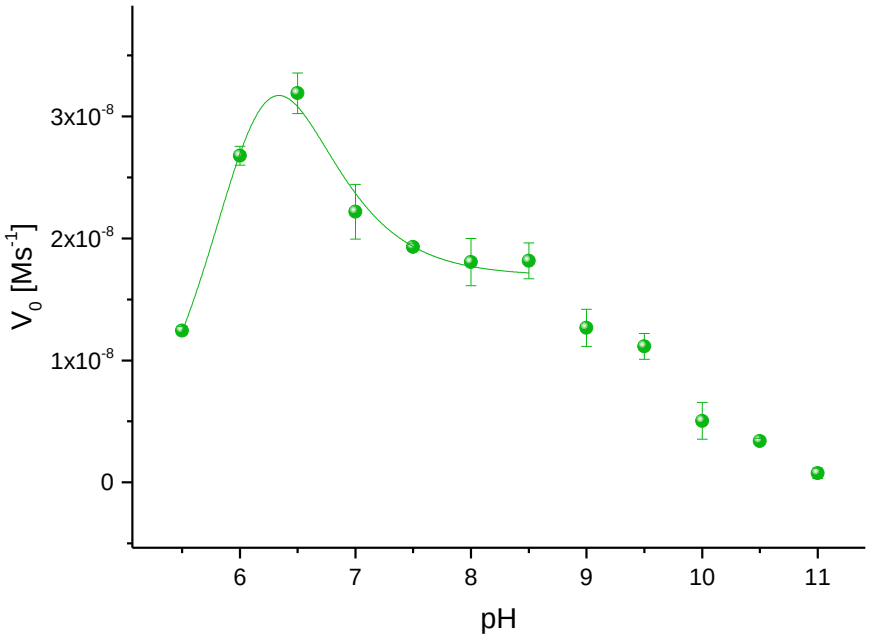

Figure 6.3: pH profiles of the BDNPP hydrolysis with $[CuZn(H_3pat^4)(OH)]^+$ (green), [BDNPP] 8mM and [cat.] 15µM, 25°C.

However, the mixed heterodinuclear copper(II)-zinc(II) complex was tested under slightly different conditions (Figure 6.3). The detected EPR spectrum of the mixed metal complex was detected at a ligand / copper(II) / zinc(II) / base ratio of 1:0.5:0.5:1 (Chapter 5). Therefore, this species is less concentrated by taking the same or a similar amount of stock solutions while *in situ* complex formation (compared to the homodinuclear complexes). The pH profile displayed in Figure 6.3 was obtained with a higher concentration of BDNPP. The pH value at which the catalyst exhibits its maximum rate is pH 6.41, as expected, between the pH_{max} values of the two homodinuclear complexes. Furthermore, there might be a second maximum in the pH profile at approximatively pH 8.5. There are various possible interpretations for this reproducible observation: (i) The active species could be a complex with three pK_A values, which would consequently lead to a different

model and fitting equation (see ref.).[247] (ii) The reaction solution might contain two different structural forms of the catalyst with different pH maxima. (iii), the active species at pH 6.5 could be the same as at pH 8.5 but hydrolysis of BDNPP at higher pH values might follow a different mechanism. An overview of the pH-dependend hydrolysis results obtain by fitting with equation 6.1 is given in table 6.1.

Table 6.1: Hydrolysis data of the dinuclear complexes of H_4pat^4 obtained by fitting with eq. 6.1.

	pH_{max}	$V_{0,max}$ [Ms^{-1}]		pK_a(I)		pK_a(II)	
$[Cu_2(H_2pat^4)(OH)]^+$	6.50	$3.45x10^{-8}$	$\pm 6.28x10^{-8}$	6.32	± 0.57	6.58	± 0.52
$[Zn_2(H_2pat^4)(OH)]^+$	6.02	$1.78x10^{-8}$	$\pm 2.24x10^{-9}$	5.32	± 0.69	6.68	± 0.71
$[CuZn(H_2pat^4)(OH)]^+$	6.41	$9.21x10^{-8}$	$\pm 1.97x10^{-8}$	5.79	± 0.12	6.59	± 0.20

In order to investigate this, EPR spectra in methanol / buffer mixtures were detected (buffer / methanol = 1:3, 5mM complex). Figure 6.4 shows the EPR spectrum of a mononuclear copper(II) compound at pH = 6.5 b) and a different more complex spectrum at pH = 9.5 a). The spectrum detected at pH = 9.5 (Figure 6.4a) could not be satisfactorily simulated and might be the result of a mixture of various species. Comparison to literature known complexes[1,101] tentatively indicates that there is probably a carbonato bridged species in solution.

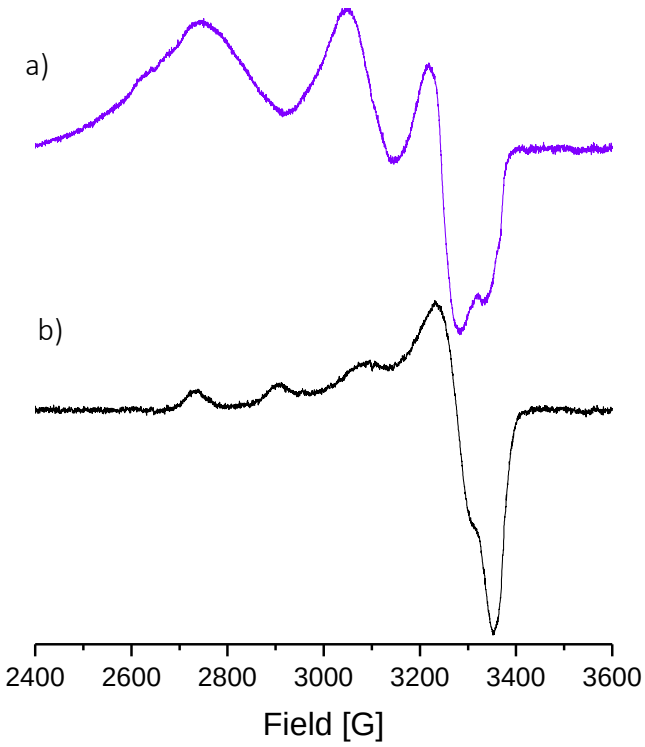

Figure 6.4: EPR spectra of 5 mM frozen solutions of H_4pat^4 + 0.5eq. of copper(II) triflate and 1.5eq. of zinc(II) triflate in methanol/ buffer mixtures; a) pH 6,5, ν = 9.444516 GHz and b) pH 9.5, ν = 9.445288 GHz, (X-Band, 140 K, 5 mM in buffer / MeOH 1:3)

Due to the fact that frozen buffer solutions are poor glasses, the spectra of the buffer solvent mixtures have poor resolution, no half field transitions and no superhyperfine coupling could be detected. The EPR spectrum at pH 6.5 shows a signal looking like a mononuclear copper(II) species, which is in table 6.2 compared to the spectrum obtained complex in pure methanol (Chapter 5, Figure 5.2). Spin Hamiltonian parameters obtained upon simulation are given in table 6.2. Mass spectrometry of the buffer solutions did not show any complexes. Thus spectral parameters are displayed without a proposed formula for the complexes. However, the g values and hyperfine splitting are in the expected range for patellamide derivative copper(II) complexes.[85,100,101]

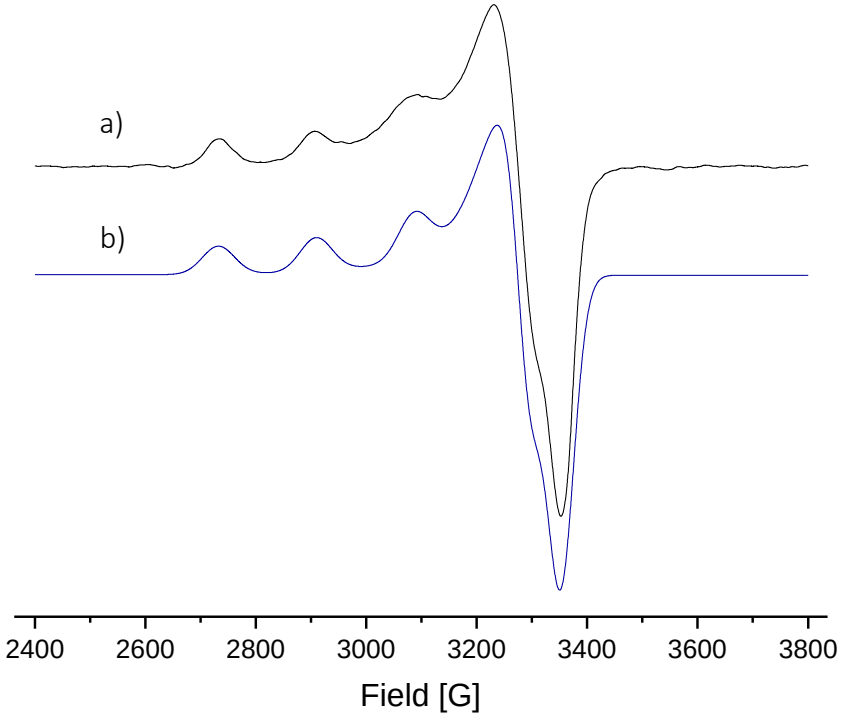

Figure 6.5: EPR spectrum of H_4pat^4 + 0.5eq. of copper(II) triflate and 1.5eq. zinc(II) triflate at pH 6,5: a) measured and b) simulated (X-Band, 140 K, 5 mM in buffer / MeOH 1:3, ν = 9.444516 GHz).

Table 6.2: EPR parameters obtained by simulation with Xsophe.

	pH 6.5	$[Cu^{II}Zn^{II}(H_2pat^4)(OH)]^+$
g_x	2.054	2.046
g_y	2.077	2.078
g_z	2.250	2.280
A_x [$10^{-4}cm^{-1}$]	4.7	13.4
A_y [$10^{-4}cm^{-1}$]	17.1	11.5
A_z [$10^{-4}cm^{-1}$]	185.7	155.0

The by simulation obtained spin Hamiltonian parameters of the spectrum obtained at pH = 6.5, are different form those, of the spectrum detected from a methanolic solution in chapter 5. Due to the different solvent environment, the copper(II) center might be coordinated by a different coligand, which would explain the shifted g_z and the enlarged A values (except A_y). The assumption that $[CuZn(H_2pat^4)OH]^+$ is the active species at pH 6.5, could this way neither be confirmed nor be excluded. But this spectrum indicates that there is presumably no dinuclear copper(II) complex in

solution, which acts as hydrolysis catalyst. Thus, the fit (eq. 6.1) for a diprotic hydrolysis system was used, assuming $[CuZn(H_2pat^4)OH]^+$ is the active species at pH 6.5. Following this assignment, all active species containing the ligand H_4pat^4 would have the same constitutional formula $[M^{II}_2(H_2pat^4)OH]^+$.

To compare the catalytic abilities of all dinuclear complexes of H_4pat^4, as efficiency and rate, a Michaelis Menten experiment was performed. The dependence of the initial rate on the substrate concentration was determined for each catalyst at its previously determined pH maximum ($[Cu_2(H_2pat^4)OH]^+$ at pH = 6.51, $[Zn_2(H_2pat^4)OH]^+$ at pH = 6.00 and $[CuZn(H_2pat^4)OH]^+$ at pH = 6.37). The substrate concentration was varied between 0.25 mM and 8 mM. Equation 6.2 and equation 6.3 were used to obtain kinetic data, which are listed in table 6.3. It appears that the homodinuclear zinc(II) complex catalyzes the hydrolysis of BDNPP with a higher catalytic efficiency k_{cat} as the corresponding homodinuclear copper(II) complex, and the highest catalytic efficiency is observed with the heterodinuclear copper(II)/ zinc(II) complex of H_4pat^4. Therefore, the same species has a small value of K_M, which indicates that the catalyst-substrate intermediate of the heterodinuclear complex is less stable than thoses of the corresponding homodinuclear complexes.

a)

b)

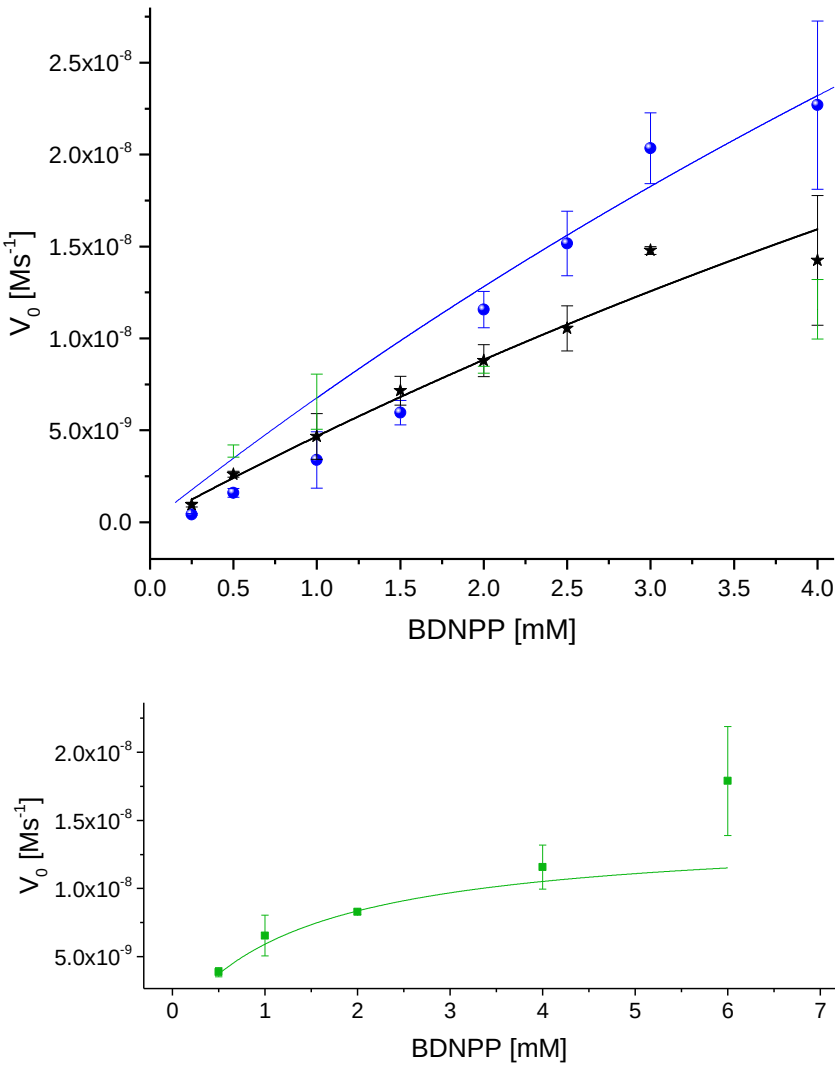

Figure 6.6: Michaelis-Menten measurement fitted with equation 6.2; a) $[Zn_2(H_3pat^4)(OH)]^+$ (blue) and $[Cu_2(H_3pat^4)(OH)]^+$ (black). (both with [cat.] 40µM, 25°C) and b) $[CuZn(H_3pat^4)(OH)]^+$ (green) ([cat.] 15µM, 25°C).

Table 6.3: Michaelis Menten parameter of the dinuclear complexes of H_4pat^4 obtained by fitting with eq. 6.2 and eq. 6.3.

	k_{cat}		K_M		k_{cat}/K_M	
	$[s^{-1}]$ *10^{-3}		[mM]		$[M^{-1}s^{-1}]$	
$[Cu_2(H_2pat^4)(OH)]^+$	2.34	± 0.07	16.56	± 1.61	0.14	± 0.04
$[Zn_2(H_2pat^4)(OH)]^+$	4.89	± 0.00	16.98	± 0.05	0.29	± 0.02
$[CuZn(H_2pat^4)(OH)]+$	4.72	± 0.04	13.93	±0.17	0.34	± 0.23

6.1 Dinuclear Complexes of H_4pat^1 and H_4pat^2

With the ligands H_4pat^1 and H_4pat^2, the homodinuclear zinc(II) complexes are not expected to act as hydrolases due to the low complex stabilities in a wet environment (see chapter 4). They were tested anyway (Figure 6.7 and Appendix), but did not show any activity. The phosphatase activity of the proposed heterodinuclear complex (Chapter 5.2) was also examined. Figure 6.8 shows the pH profile obtained (blue trace). As there are reproducible two maxima, the pH profile is overlaid with the pH profile of $[Cu_2(H_2pat^2)(OH)]^+$ (black trace). A comparison of the spectra leads to the conclusion that there are two species present in solution, capable of hydrolyzing BDNPP; presumably $[Cu_2(H_2pat^2)(OH)]^+$ and $[CuZn(H_2pat^2)(OH)]^+$.

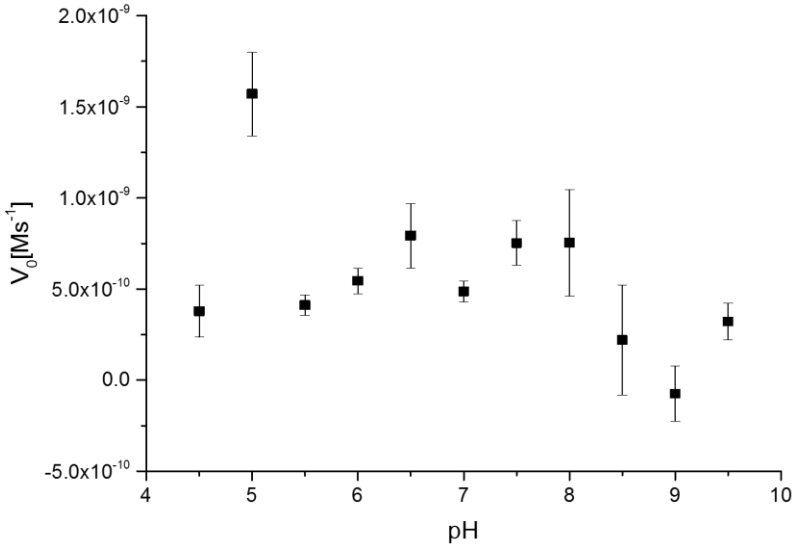

Figure 6.7: pH-profiles of the BDNPP hydrolysis with "$[Zn_2(H_2pat^2)(OH)]^+$".

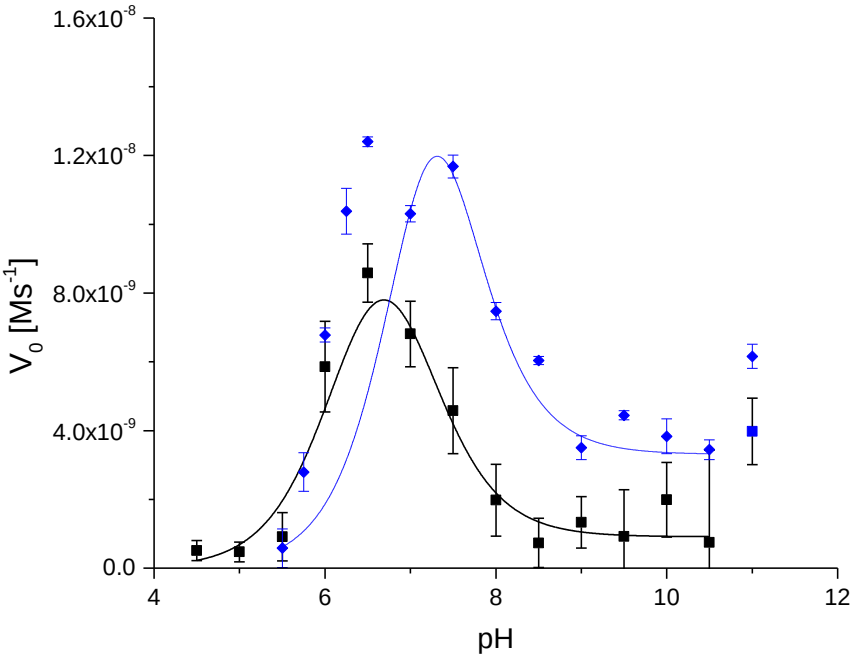

Figure 6.8: Overlaid pH profiles of the BDNPP hydrolysis with $[Cu_2(H_2pat^2)(OH)]^+$ (black, [BDNPP] 6.25mM and [cat.] 40µM, 25°C.)[70,107] and $[CuZn(H_2pat^2)(OH]^+$ (blue,. [BDNPP] 5.25 mM and [cat.] 30µM, 25°C).

To obtain the desired hydrolysis data of the pH dependent hydrolysis by the proposed heterodinuclear complex $[CuZn(H_2pat^2)(OH)]^+$ by fitting with equation 6.1 the detected initial rates from pH = 6.0 to pH = 6.5 had to be ignored, to avoid a obviously falsified result. The obtained data as well as those for $[Cu_2(H_2pat^2)(OH)]^+$ are displayed in table 6.4. Both complexes have narrow pH profiles and both do hydrolyse BDNPP with the maximum rate at pH values close to neutral. Interrestingly, the heterodinuclear complex of H_4pat^2 has a higher pHMax as the corresponding homodinuclear complex, which will be discussed in the next section.

Table 6.4: Hydrolysis data of the dinuclear complexes of H_4pat^4 obtained by fitting with eq. 6.1.

	pH_{max}	$V_{0,max}$ [Ms^{-1}]		pK_a(I)		pK_a(II)	
$[Cu_2(H2pat2)(OH)]^+$	6.69	1.57x10-8	±1.24x10-9	6.37	± 0.40	7.25	± 0.65
$[CuZn(H2pat2)(OH)]^+$	7.31	2.89x10-8	±1.55x10-8	7.58	± 0.52	6.76	± 0.14

6.3 Mechanistic Discussion

To summarize, all obtained pH profiles show a bell-shaped maximum close to neutral pH. This leads together with the facts that the obtained pK_A values are in all cases approximatively separated by one unit (narrow profile) to the proposal of a mechanism similar to that of PAP.[112,218] The obtained pK_A values were assigned to belong to two deprotonation steps that are possible when considering a dinuclear aqua species as catalyst (Figure 6.9). In water solvated copper(II) ions are stronger lewis acids as zinc(II) ions. ($[Cu(H_2O)_6]^{2+}$: pK_A = 8.0 and $[Zn(H_2O)_6]^{2+}$: pK_A = 9.0).[248] But, upon coordination to macrocyclic N-donating ligands this effect turns back, and Zinc(II) becomes compared to copper(II) the better lewis acid ($[Zn[12]aneN_4(H_2O)]^{2+}$: pK_A = 7.9 (Figure 4.3b) and the corresponding $[Cu[12]aneN_4(H_2O)]^{2+}$: $pK_A > 10$).[159] In PAP mechanism the substrate coordinates to one metal center and is attacked by the generated hydroxide from the other metal center.[112,218] If this or a similar scenario, is the hydrolysis pathway (see Figure 4.8) used by the dinuclear patellamide derivative complexes, it is expected that the pK_A values of water coordinated to a zinc(II) ion is lower in comparison to a water molecule coordinated by a copper(II) ion.

The two pK_A values of $[Zn_2(H_2pat^4)OH]^+$ obtained by fitting the data to equation 6.1 are pK_{AI} = 5.32 and pK_{AII} = 6.68. Thus, pK_{AI} of the dinuclear zinc(II) species is lower as that of the respective dinuclear copper(II) species (pK_{AI} = 6.32), in contrast to the pK_{AII} of the dinuclear zinc(II) species which higher compared to that of the respective copper(II) complex (pK_{AII} = 6.58). This leads to a broadened pH-profile of hydrolysis catalyzed by the dinuclear zinc(II) complex (Figure 6.2). The broader pH profile can be explained by the zinc(II) ions slower exchange rates compared to copper(II) (Zn^{2+}; ~ $6x10^8$ and Cu^{2+}; $4.4*10^9$ s^{-1} (water exchange in water at 25°C)),[249] and thus the active aqua species might be available over a broader pH range.

The corresponding heterodinuclear complex $[CuZn(H_2pat^4)OH]^+$ has a pH maximum between the pH maxima of both homodinuclear complexes. The by fitting with equation 6.1 obtained pK_{AII} value pK_{AII} = 6.59 is close to that of the homodinuclear copper(II) species, and might thus be assigned to

the deprotonation of a copper(II) coordinated water molecule. In consequence pK_{AI} = 5.79 can be assigned to the deprotonation of an aqua coligand coordinated by the zinc(II) ion, which is in agrrement with the zinc(II) ions higher lewis acidity in macrocyclic azacrown ligands.[159]

The proposed heterodinuclear copper(II)-zinc(II) complex of the 4S* configured ligand H_4pat^2 (Chapter 5) is also shown to act as phosphatase. Interestingly, this complex seems to exist in solution along with the corresponding homodinuclear copper(II) complex. Surprisingly, in this case the pH maximum of the heterodinuclear species lies slightly higher than that of the respective homodinuclear copper(II) complex.

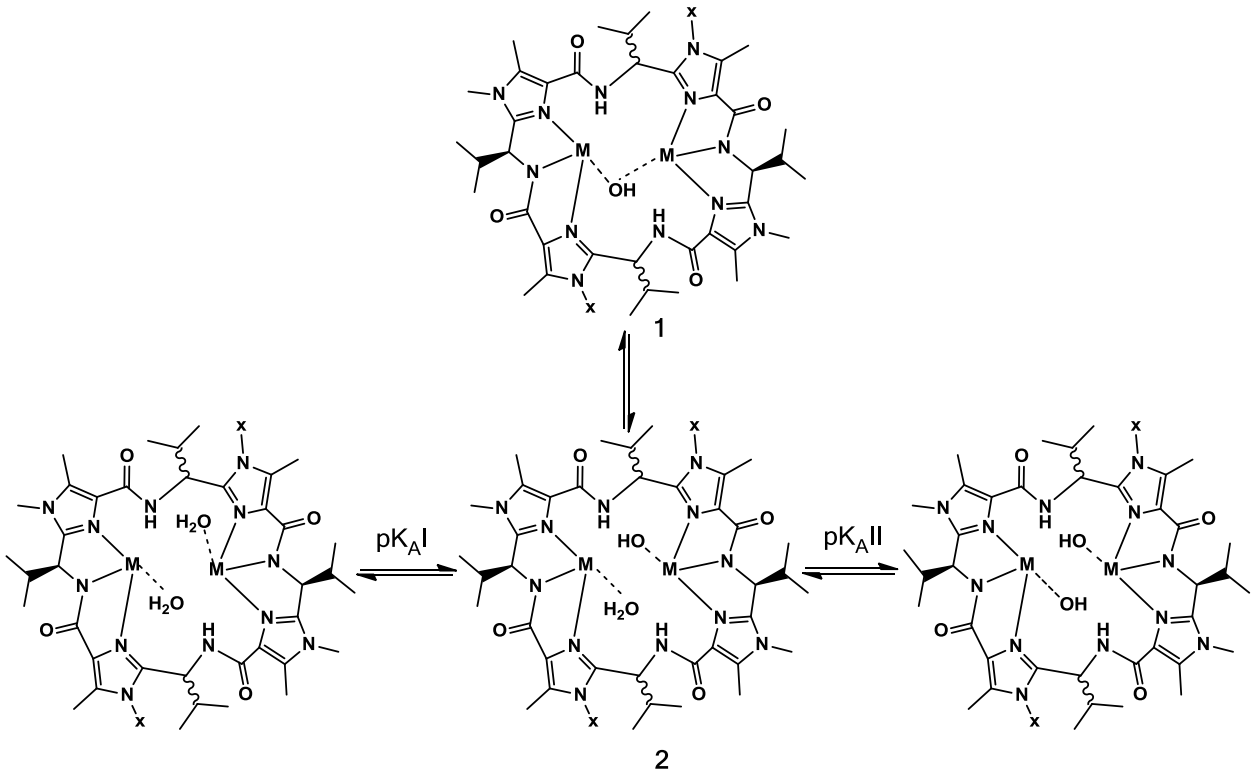

Figure 6.9: Schematic representation of the pK_A values in relation to the considered active species (blue).

While comparing the results listed in table 6.2 it appears that the zinc(II) containing complexes of the benzyl residue containing ligand H_4pat^4 show the highest catalytic efficiency. In addition the heterodinuclear zinc containing complexes of the ligand H_4pat^4 exhibits a the smallest Michaelis-Menten constant, meaning that this complex has the highest affinity towards the substrate BDNPP. The most efficient catalyst remains the homodinuclear zinc(II) complex of H_4pat^4. The question arises then: why is the unnatural 4S* configurated ligand H_4pat^4 the fastest? Eventually due to the

benzyl residues which may help the substrate to coordinate by π-stacking. Another reason may be that a more hydrophobic microenvironment surrounds the dinuclear metal center due to the large benzyl residues and thus stabilizes the zinc(II) complexes of H_4pat^4. In the case of the tripodal benzyl histidine ligands investigated by Ichikawa and Ibrahim,[198] the effect of the benzyl groups is just described as that of a bulky substituent.[198]

Table 6.5. Kinetic Properties of $[M_2(H_2pat^y)(OH)]^+$ in BDNPP-hydrolysis.

Catalyst	pH_{max}	$V_{0,max}$ [Ms^{-1}]		pK_a(I)		pK_a(II)		k_{cat} [s^{-1}] *10^{-3}		K_M [mM]		k_{cat}/K_M [$M^{-1}s^{-1}$]		ref
$[Cu_2(H_2pat^1)(OH)]^+$	7.21	$1.58x10^{-7}$	$\pm 3.00x10^{-9}$	6.91	± 0.21	7.31	± 0.20	3.95	± 0.07	26.4	± 2.20	0.15	± 0.03	70,107,112
$[Cu_2(H_2pat^2)(OH)]^+$	6.69	$1.57x10^{-8}$	$\pm 1.24x10^{-9}$	6.37	± 0.40	7.25	± 0.65	0.39	± 0.03	5.5	± 0.64	0.07	± 0.05	70,107
$[CuZn(H_2pat^2)(OH)]^+$	7.31	$2.89x10^{-8}$	$\pm 1.55x10^{-8}$	7.58	± 0.52	6.76	± 0.14	0.34	± 0.30	5.74	± 1.74	0.06	± 0.17	
$[Cu_2(H_2pat^4)(OH)]^+$	6.50	$3.45x10^{-8}$	$\pm 6.28x10^{-8}$	6.32	± 0.57	6.58	± 0.52	2.34	± 0.07	16.56	± 1.61	0.14	± 0.04	
$[Zn_2(H_2pat^4)(OH)]^+$	6.02	$1.78x10^{-8}$	$\pm 2.24x10^{-9}$	5.32	± 0.69	6.68	± 0.71	4.89	± 0.00	16.98	± 0.05	0.29	± 0.02	
$[CuZn(H_2pat^4)(OH)]^+$	6.41	$9.21x10^{-8}$	$\pm 1.97x10^{-8}$	5.79	± 0.12	6.59	± 0.20	4.72	± 0.04	13.93	±0.17	0.34	± 0.23	

7 Summary and Outlook

The biological function of the naturally occurring cyclic peptides patellamide A-F and ascidiacyclamide, found in the ascidians of the Pacific and Indian oceans, is still unclear. Since the discovery of a carbonato-bridged dinuclear copper(II) complex of ascidiacyclamide,[1] there has been a discussion about metal ions playing a key role in the chemistry these peptides.[18] Due to the the high concentration of copper(II) found in ascidians,[88] the copper(II) coordination chemistry of the patellamides has been extensively investigated.[70] A library of easily accessible patellamide derivatives has been designed to study their copper(II) chemistry.[85] Recently, dinuclear copper(II) complexes of these artificial cyclic *pseudo*-peptides have been shown to act as extremely efficient hydrolases at neutral pH. The complex $[Cu_2(H_2pat^1)(OH)]^+$ has, on one hand, been shown to hydrolyze very efficiently CO_2[111] and, on the other hand, this complex is also able to hydrolyze the model phosphodiester BDNPP.[112]

The aim of this thesis was to explore the zinc(II) coordination chemistry of these cyclic *pseudo*-octapeptides regarding biologically relevant hydrolysis chemistry. A further question was; whether the patellamide derivatives, known to preferably form dinuclear complexes, have the ability to form heterodinuclear copper(II) and zinc(II) complexes? Finally, this thesis aimed to test all explored complexes in a phosphoester hydrolysis assays. Besides this, the electrochemical properties of the patellamide derivative copper(II) complexes were investigated.

The electrochemical results displays the equilibrium chemistry of the Patellamide derivative copper(II) complexes, and lead thus to the conclusion, that copper(I/II) based biological relevant redox chemistry is rather unlikely in neutral aqueous solution. Nevertheless, the complex $[Cu_2(H_2pat^1)(OH)]^+$ has been shown to take part in an oxygenation reaction under basic conditions. Kinetic properties were shortly discussed and oxygenation products have been identified *via* NMR spectroscopy and mass spectrometry.

The complexation equilibrium of the ligand H_4pat^4 was investigated by EPR spectroscopy in combination with high-resolution mass spectrometry. So far, H_4pat^4 is the only ligand of the of the patellamide derivative library that forms under specific conditions a pure mononuclear copper(II) complex. EPR simulations, cooperativity and the resulting copper(II) complexation equilibria have been discussed in Chapter 3.

The zinc(II) chemistry of the patellamide derivatives is discussed in Chapter 4. Isothermal calorimetric titration (ITC) experiments show, that a homodinuclear zinc(II) complex of the naturally configured ligand H_4pat^1 has a higher thermodynamic stability than a homodinuclear zinc(II) complex of the 4S* configured ligand H_4pat^2. ITC experiments show that H_4pat^1 and H_4pat^2 prefer to coordinate two metal ions at once and exhibit a cooperative effect. In addition, the ITC experiment shows that zinc(II) coordination is rather enthalpy driven, in contrast to the corresponding copper(II) coordination. This is interpreted as a result of a change from a tetrahedral to a trigonal bipyramidal or octahedral coordination sphere, upon zinc(II) coordination by a patellamide derivative. This is believed to be one of the reasons for the lower stability of the zinc(II) complexes in comparison to the corresponding copper(II) complexes.

The complexation behavior of zinc(II) by H_4pat^1 and H_4pat^4 was investigated by NMR spectroscopy, especially with the help of 2D methods i.e. ^{13}C-^{1}H HMBC and ^{15}N-^{1}H HMBC. The results, are interpreted in combination with HR mass spectrometry and lead to the proposal of a complexation equilibrium.

Regarding the results of both, of copper(II) and of zinc(II) coordination by the ligand H_4pat^4, results of Chapters 3 and 4 indicate that H_4pat^4 forms similarly stable complexes with either metal ion. Under comparable conditions H_4pat^4 forms various species in equilibria with both metal ions. Thus, the formation of a heterodinuclear species was investigated in Chapter 5. Specifically, the 4S* configured ligand H_4pat^2 was examined in the formation of a heterodinuclear copper(II)-zinc(II) complex. Even if for both ligands, H_4pat^2 and H_4pat^4, heterodinuclear complexes were found, different strategies have been applied. Both ligands heterodinuclear complexes deliver EPR spectra that have been simulated and analyzed in combination with UV/Vis spectroscopy and mass spectrometry.

In Chapter 6, all complexes were tested in a phosphoester hydrolysis assay. The kinetics were measured as function of pH and of as function of the substrate concentration. Results were analyzed considering a model for dinuclear hydrolyzing enzymes and considering Michaelis

Menten kinetics. All three dinuclear complexes of H_4pat^4 (Cu_2^{II}, Zn_2^{II}, $Cu^{II}Zn^{II}$) were shown to act as phosphatases. The in chapter 5 proposed heterodinuclear copper(II)-zinc(II) complex of H_4Pat^2 has been shown to act as phosphatase as well. The pH profiles and Michaelis Menten plots are discussed with respect to their biological relevance. It could be shown, that all zinc(II) containing complexes are slightly more active than the corresponding copper(II) complexes.

Having the biological relevance of these results in mind, a first conclusion is that, if possibly existing dinuclear copper(II) complexes of patellamides fulfill a metabolic function in the ascidian cytoplasm, it is likely that this is a hydrolytic reaction rather than any role involving a copper(I) state. The results of the zinc(II) chemistry, especially that of H_4pat^2 and H_4pat^1, lead to the conclusion that, if a metal ion has biological relevance for the patellamides, it is more likely that copper(II) is the relevant metal ion. However, regarding the zinc(II) chemistry of H_4pat^4 , these results deliver an interesting insight into the solution chemistry of the patellamide derivatives complexes from a diamagnetic point of view. The zinc(II) complexes of H_4pat^4 are efficient phosphoester hydrolysis catalysts, working in a neutral pH range. And in addition the zinc(II) chemistry showed, that the cooperativity i.e. the preferential formation of dinuclear complexes seems to be more important than metal selectivity.

The exact mechanistic description of phosphoester hydrolysis, catalyzed by dinuclear complexes of the patellamide derivatives is in the focus of computational studies.[117] The hydrolysis ability towards further substrates as *ß*-lactams and glycosides are aims of ongoing investigations as well.[117]

The most challenging question is, whether copper(II)-patellamide derivative hydrolysis chemistry in vivo is possible. Therefore, a suitable imaging strategy is required, which is in the focus of an ongoing study.[117]

The biological role of the patellamides and ascidiacyclamide remains thus a mystery, but this open question can be regarded from various perspectives and creates great scientific ideas. This way, I hope that this question remains still unsolved for a while.

8 Experimental Section

8.1 Materials, Methods and Instruments

8.1.1 Materials

All solvents and reagents (absolute, *p.a*. grade and *purum* grade) were purchased and used without further purification. Dry solvents were kept over molecular sieves. MilliQ water (R > 18MΩ) was used for the kinetic assays. Phosphoryl chloride was distilled and 2,4-dinitrophenol was three times recrystallized from ethanol before use. The cyclic peptides H_4pat^3 and H_4L^{AscA} were obtained from Dr. Michael Westphal. The peptide H_3L^1 was provided by Dr. Nina Dovalil. Both were used without further purification.

8.1.2 Chromatography

Thin layer chromatography (TLC) on silica gel 60 F254 plates (POLYGRAM® SIL G/UV, Macherey-Nagel) was conducted in order to monitor reactions. Detection was accomplished with a UV-lamp (λ=254 nm). Flash chromatography was performed using silica gel 60 (230-400 mesh) purchased from Macherey-Nagel.

8.1.3 Microanalyses

Quantitative microanalysis was performed at the microanalytical laboratory of the University of Heidelberg with a Vario EL and a Vario MICRO cube instrument (Elementar).

8.1.4 Mass Spectrometry

Electrospray ionization mass spectra (ESI) were measured on a Finnigan LCQ spectrometer at the institute of Organic Chemistry of the University of Heidelberg. High-resolution electrospray ionization mass spectra (ESI-HR MS) were measured on a Bruker Apex-Qe hybrid 9.4 T FT-ICR instrument with an Apollo II MTP ion source in the positive-ion and negative-ion mode, respectively, at the Institute of Organic Chemistry of the University of Heidelberg. External mass calibration was performed on $[arginine_n+H]^+$ cluster ions prior to analysis. A mass accuracy of 1ppm was achieved. The instrument was controlled by the Bruker ApexControl 2.0.0 beta software. At the School of Chemistry and Molecular Biosciences of the University of Queensland, high-resolution mass spectra were measured on a Bruker microTOF ESI-MS spectrometer. High-resolution fast atom bombardement (FAB) mass spectrometric measurements were performed on a Finnigan TSQ 700 instrument at the institute of Organic Chemistry of the University of Heidelberg. The matrix used was nitrobenzylalcohol. High-resolution direct-analysis-in-real-time (HR-DART) mass spectra were measured on a Bruker Apex-Qe hybrid 9.4 T FT-ICR instrument in the positive-ion mode, at the Institute of Organic Chemistry at the University of Heidelberg.

Data analysis was performed with the Bruker Compass Data Analysis 3.4 software.

8.1.5 NMR Spectroscopy

^{1}H, ^{13}C, ^{15}N and ^{31}P nuclear magnetic resonance (NMR) measurements as well as; two dimensional correlation spectroscopy (COSY), heterodinuclear single quantum correlation (HSQC), heterodinuclear multiple bound correlation (HMBC) and nuclear Overhauser-effect spectroscopy NOESY) were performed with a Bruker 200 MHz DRX, a Bruker 400 MHz Advance-II, a Bruker 600 MHz Advance-II or a Bruker 900 MHz Advance-III spectrometer, respectively. Chemical shifts (δ) in ppm are calculated relative to TMS. For ^{1}H and ^{13}C NMR spectra the deuterated solvent peaks are indicated in brackets in the analytical data. For ^{31}P NMR spectra 85% H_3PO_4 (0 ppm) was used as reference for the chemical shifts δ. All reported coupling constants are ^{1}H-^{1}H couplings. Signal multiplicities are described by the following abbreviations: s = singlet, d = doublet, t = triplet, q = quartet, quin = quintet, dd = doublet of doublets, dt = doublet of triplets, tt = triplet of triplets, o = octet, m = multiplet and b = broad. In peptides the H-atom next to the N-amide is assigned with H_α and the second H-atom is assigned with $H_ß$.The Bruker software package TopSpinTM was used to analyze the recorded data. All measurements were performed at 25°C, unless a different temperature is designated at the respective points, and the solutions for complex titrations were kept under Argon, unless carbonato-complexes were desired.

8.1.6 EPR Spectroscopy

X-Band continuous wave (CW) EPR spectra were recorded with a Bruker Biospin Elexsys E500 at the University of Heidelberg or with an Elexis E580 spectrometer at the University of Queensland, fitted with either a super high Q cavity or an ER 4118X resonator. The microwave frequency and the magnetic field were calibrated with a Bruker ER 036TM Teslameter and a Bruker microwave frequency counter, respectively. Temperatures of 110 - 140 K at the sample position were achieved by a flow-through cryostat in conjunction with a Eurotherm B-VT-2000 variable temperature controller. The Bruker Xepr software (version 2.4b.12) was used for Spectrometer tuning, signal averaging and visualization. Simulations of the mononuclear

copper(II) complexes and of the copper(II)-zinc(II) complexes were carried out with the Xsophe software from Bruker.[145] The simulation of the dinuclear copper(II) complex spectrum was obtained using the Bruker software Molecular Sophe.[146]. All measurements were performed at 140 K, unless a different temperature is designated at the respective points, and the solutions kept under Argon unless carbonato-complexes were desired.

8.1.7 Spectrophotometric Titrations

Spectrophotometric titrations were carried out with 1 mM cyclic peptide solutions in MeOH. Metal and base solutions ($Cu^{II}(CF_3SO_3)_2$, $Cu^{II}(CH_3COO)_2$, $Zn^{II}(CF_3SO_3)_2$, $Zn^{II}(OMe)_2$, (nBu)$_4$N(OMe), NaOMe)) in methanol (25 mM or 10 mM) were added in 0.1 equivalent steps and NIR-UV/vis-NIR and CD spectra were recorded. The spectra obtained were corrected with respect to the dilution factor. All measurements were performed at 25°C and the solutions kept under Argon unless carbonato-complexes were desired.

8.1.8 NIR-UV/Vis-NIR and CD-Spectroscopy

A Jasco V-570 spectrophotometer equipped with a JASCO ETC-505T cryostat, a TIDAS II spectrophotometer or a Varian Cary 50 Bio UV/Vis-NIR spectrometer with a peltier temperature controller were used to record UV/Vis-NIR spectra in the range of 200-900 nm, as well as time-course measurements at fixed wavelengths. All measurements were performed at 25°C and the solutions kept under Argon unless carbonato-complexes were desired.

8.1.9 CD-Spectroscopy

Circular Dichroism (CD) spectra were measured with a JASCO J-170 spectropolarimeter equipped with a JASCO ETC-505T cryostat. A Jasco CD spectrometer with a peltier temperature controller were used to record CD spectra in the range of 200-900 nm. All measurements were

performed at 25°C and the solutions kept under Argon unless carbonato-complexes were desired.

8.1.10 IR Spectroscopy

A Perkin Elmer 16C FTIR spectrometer was used to record infrared (IR) spectra of solid samples in KBr pellets as well as of liquid samples in an irtran4 (CaF_2) cuvette. Liquid samples were prepared from methanolic or deutero methanolic stock solutions. IR spectroscopic titrations were performed by stepwise addition of 0.5 equivalents of metal ion or base solution. IR spectra in solution were recorded between 450 and 4000 cm^{-1} at 25°C, and the solutions kept under Argon unless carbonato-complexes were desired.

8.1.11 Electrochemistry

Electrochemical properties were studied by cyclic voltammetry (CV) and square wave voltammetry (SQW) in methanol using (nBu)$_4$N(PF_6) as supporting electrolyte. All measurements were performed with a CH Instruments CHI660D electrochemical workstation, equipped with a CH Instruments Picoamp booster and Faraday cage, with a three-electrode setup consisting of a glassy-carbon working electrode, a Pt wire as auxiliary electrode and a $Ag/AgNO_3$ reference electrode (0.01 M Ag^+, 0.1 M (Bu_4N)(BF_4) in methanol). The solutions were thoroughly degassed and measured with a slight argon-flow was above the solution during the measurement. A scan rate of 100 mVs^{-1} was applied.

The Copper(II) complex solutions were prepared *in situ* according to the spectrophotometric titrarions as follows: First a 25 mM $Cu^{II}(CF_3SO_3)_2$ methanolic solution was added in 0.1 equivalent steps to 0.1 mM ligand solution into the electrochemical cell (7ml). Afterwards, a 10 mM (nBu)$_4$N(OMe) methanolic solution was added in 0.1 equivalent steps to the electrochemical cell. In a final step a slight stream of CO_2 was set above the solution for 10 minutes, to generate carbonato complexes. After each step a CV and a SQW scan were recorded.

8.1.12 Isothermal Titration Calometry (ITC)

ITC measurements were performed with a MicroCal ITC 200 instrument at the School of Chemistry and Molecular Biosciences of the University of Queensland. All experiments were done in methanolic solutions containing 0.1 M $(nBu)_4N(ClO_4)$ for control of the ionic strength during each measurement. Initially, the reaction vessel contained 200 µL of a 1mM ligand solution in methanol. A 20 mM Zinc(II) triflate solution in methanol was added either in 38 steps of 1 µL or in 76 steps of 0.5 µL by an injection syringe to the ligand solution. The spectra obtained were analyzed by the program Origin 7® with the plugin *Microcal LLC – VPViewer 2000 ITC*®.

8.1.13 pH Measurements

A Metrohm 713 pH-meter equipped with a KCl electrode was used to adjust pH values at 25°C. The pH meter was calibrated with pH standard solutions at pH 4, pH 7 and pH 9. Reported pH values of buffer/ solvent mixtures refer to the aqueous component. The pH value of a 1:1 mixture of buffer and acetonitrile was the same as the corresponding buffer solution itself. [250,251]

8.1.14 Preparation of Buffers

A multicomponent buffer was used to measure the pH-dependent and Michaelis-Menten kinetics. The aqueous buffers consisted of :

CAPS, *N*-cyclohexyl-3-aminopropanesulfonic acid, pK_A = 10.40

CHES, 2-(*N*-cyclohexylamino)ethanesulfonic acid, pK_A = 9.30

HEPES, 4-(2-hydroxyethyl)-1-piperazinylethanesulfonic acid, pK_A = 7.55

MES, 2-(*N*-morpholino)ethanesulfonic acid, pK_A = 6.15

Each component was dissolved in Milli-Q water. The final concentration of each buffer was 50 mM. The ionic strength was adjusted with $LiClO_4$ (250mM) to μ = 0.45. Afterwards the multicomponent buffer solution was separated in 40 ml aliquots and their pH values were adjusted with 2 M NaOH. Metal ions were removed by stirring the adjusted buffers with Chelex 100 overnight, and filtration through 45 μm syringe filters.

8.1.15 Phosphoester Hydrolysis Assay

The phosphatase-like activity was determined by measuring the hydrolysis of the model substrate bis(2,4-dinitrophenyl)phosphate (BDNPP). Phosphoester cleavage of BDNPP produces 2,4-dinitrophenolate, which can be detected by monitoring the increase of a strong absorbance at 400 nm (ε = 12100$M^{-1}cm^{-1}$) via UV/Vis spectroscopy at 25°C (settings see section 8.1.8). Initial rates were obtained by the initial rate method, which leads to an assay-design where the initial linear portion of data can be reproducibly used for analysis. The reported rates are averages with standard deviations from triplicates. Each assay was corrected for autohydrolysis, which was also determined in triplicates. The substrate BDNPP was dissolved in acetonitrile. The catalysts $[M^{II}(H_2pat^n)(OH)]^+$ (M^{II} = Cu^{II}, Zn^{II}) were prepared *in situ* from stock solutions (ligand 1mM, $M^{II}OTf_2$ 25mM, $(n\text{Bu})_4\text{N(OMe)}$ 25mM) in methanol (for solubility reasons). The aqueous multi component buffer described in section 8.1.14 was used for pH-

dependent kinetics. All assays were carried out in a mixture as follows: H_2O/MeCN/MeOH = 50:45.5; $[M^{II}(H_2pat^n)(OH)]^+$ = 40µM, [buffer] = 25mM. To prevent the formation of CO_3^{2-} (and consequently the formation of inhibiting carbonato-species), it was necessary to use freshly degassed solutions. The pH-dependence of the hydrolysis rate was measured in the range of pH 4.5 - 11.5. While measuring the substrate concentration dependence at a distinct pH the BDNPP concentration was varied between 0.25 - 10 mM. The resulting data were plotted with the program Origin (OriginLab) and fitted to Equation 7.1 (chapter 7.2).[246] Reported pH values refer to the aqueous component. The pH value of a 1:1 mixture of buffer and acetonitrile was the same as the corresponding buffer solution itself.[250,251]

8.1.16 Oxygenation Assay

The oxygenation properties of $[Cu_2(H_2pat^1)OH]^+$ were studied according to a literature known procedure, which was performed as follows: 236.7 mg (1.149 mmol) of 3,5-di*tert*butylphenol (DTBPH) were dissolved in 10 mL dry and degassed methanol. After the addition of one equivalent of base ($(n\text{Bu})_4\text{NOMe}$, 1.92 mL of a 20% methanolic solution) under argon, 600 µL of the catalyst solution (1 mM in methanol under Ar) were added. Subsequently, a first UV/Vis spectrum was recorded. A slight flow of pressed air was conducted through the reaction solution while stirring, UV/Vis spectra were recorded as a function of time. The formation of the oxygenation product 3,5-di*tert*butylquinone DTBQ was monitored at the increasing absorption at 407 nm (1830L mol^{-1} cm^{-1}). After each spectrum taken, the measured solution was returned to the reaction mixture. Before each measurement the volume of the reaction mixture was corrected to the initial volume with dry and degassed methanol, to keep initial concentrations constant.

8.2 General Procedures

Cyclic Peptides and their precursors were prepared according to known literature procedures with slight modifications. All moisture or air sensitive reactions were performed applying Schlenk-techniques.

8.2.1 General Procedure for Methyl Ester Cleavage (GP1):[113]

The methyl-protected amino acid (1eq) or methyl–protected peptide was dissolved in a MeOH/dioxane mixture = 10:7 (resulting in a 0.1 M solution) and cooled to 0°C. Then, a 2M NaOH solution (10 eq) was slowly added. The reaction mixture was allowed to warm up to rt. While stirring for at least one day, the reaction progress was monitored by TLC. After the consumption of all starting material, brine and 1 M HCl solution were added until a neutral pH value was reached. The reaction solution was extracted with DCM. The combined organic phases were dried over Na_2SO_4 and concentrated *in vacuo* to yield the desired acidic product.

8.2.2 General Procedure for Boc Group Cleavage (GP2):[113]

The respective of the Boc-protected Amine (1eq) was dissolved in DCM (resulting in a 0.1 M solution), and cooled to 0°C. At this temperature concentrated TFA (3ml/1mmol) was added slowly. After stirring for further 30 min at 0°C, the ice bath was removed, and the reaction mixture was stirred at rt while monitoring the reaction progress by TLC. After complete conversion, solvent and TFA were removed *in vacuo*. The remaining TFA was removed through repetitive stripping with EtOAc. Finally the deprotected amine was dried to yield a colorless foam.

8.2.3 General Procedure for Peptide Coupling with COMU (GP3):[113,252]

The methyl deprotected acidic building block (1mM) was dissolved under Ar atmosphere in dry MeCN (100ml/ 10mmol). After addition of EDIPA (10eq) the reaction mixture was cooled to 0°C and the coupling reagent COMU (0.95eq) was added. After further stirring for 30 min the amine building block was added. The reaction mixture was permitted to warm slowly until rt was reached. The reaction mixture was stirred at rt until a TCL showed consumption of all starting materials. Solvent and base were removed *in vacuo*, and the resulting residue was dissolved in EtOAc and then extracted with H_2O, 1M HCl solution and brine (each at least twice). The combined organic layers were concentrated *in vacuo* and then purified by flash chromatography with silica gel.

8.2.4 General Procedure for Cyclic Peptide Coupling with COMU (GP4): [113,252]

The respective deprotected dimeric building block (1eq) was dissolved in dry MeCN (0.1 M) mixed with EDIPA (10 eq) and cooled to 0°C while stirring under Ar atmosphere. Then COMU (1.95 eq) was added before the reaction mixture was allowed to slowly warm to rt. The reaction progress was monitored by TLC until all starting material was consumed. Solvent and base were removed *in vacuo*. The resulting residue was dissolved in EtOAc and then extracted with H_2O, 1M HCl solution and brine (each at least three times). The combined organic layers were concentrated *in vacuo* and purificated by column chromatography with silica gel.

8.2.5 General Procedure for the preparation of dinuclear transition metal complexes of the Peptides (GP5):

Complexes for all experiments were prepared *in situ* from stock solutions in dry and degassed MeOH, which has been stored under an Ar atmosphere. The concentration of the ligand solutions was 1 mM. For deprotonation, a methoxide base was used, either sodium methanolate or tetra butyl-ammonium methoxide salt ((*n*Bu)$_4$NOMe) was added.

8.3 Synthesis of H_4pat[1]

8.3.1 (*E*)-methyl-2-(hydroximo)-3-oxobutanoate (1):

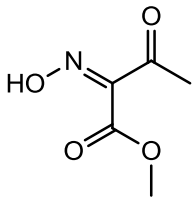

1

Molecular formula: $C_5H_7NO_4$

Molecular weight: 145.11 g/mol

Following known literature procedures,[113,253] methyl acetoacetate (103.13 g, 936.57 mmol) was dissolved in glacial acetic acid (140 ml) and cooled to -5°C. While stirring at a temperature ranging from -5 to -10°C, 200 ml of aqueous sodium nitrite solution (148.55 g, 2152.09 mmol) were added slowly. The reaction mixture was stirred for 3 h at -5 °C and afterwards for 1.5h at rt. The reaction mixture was poured on 800 g ice. After extraction with diethyl ether (3x) the combined organic phases were washed with saturated $NaHCO_3$ solution until CO_2 production ended, dried over Na_2SO_4, and concentrated *in vacuo* to yield **1** (95.67 g, 659.28 mmol, 70.39%) as a white solid.

^{1}H NMR: (200 MHz, $CDCl_3$): δ = 2.35 (s, 3H, $COCH_3$); 3.85 (s, 3H, CO_2CH_3); 10.80 (bs, 1H, NOH) ppm.

8.3.2 1-Methoxy-1,3-dioxobutan-2-ammonium chloride (2):

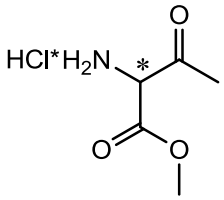

2

Molecular formula: $C_5H_{10}ClNO_3$

Molecular weight: 167.59 g/mol

Compound **2** was prepared according to known literature procedures.[113,253] The oxime **1** (50.43 g, 347.53 mmol) was dissolved in EtOH (800 ml). Palladium on charcoal was suspended (10 %, 25g) before 348 ml 3 M methanolic HCl (1040 mmol, 3eq) were slowly added. The reaction mixture was stirred for 3 days under a H_2-atmosphere. Afterwards the mixture was filtered twice over Celite and the solvent was removed *in vacuo*. The crude product was dissolved in EtOAc, recrystallized at -20°C from EtOAc, filtered and washed with ice cold DCM. The ammonium chloride salt **2** (46.43 g, 277.05 mmol, 79.72%) was isolated as a white crystalline solid.

Microanalysis: $C_5H_{10}ClNO_3$: calc. (%): C 35.41, H 7.13, N 8.26; found (%): C 34.08, H 7.03, N 7.89 (Report No. 33726)

^{1}H NMR: (200 MHz, DMSO - d_6): δ = 2.38 (s, 3H, $COCH_3$); 3.81 (s, 3H, CO_2CH_3); 5.30 (s, 1H, $CHNH_3$), 8.91 (bs, 3H, NH_3) ppm.

^{13}C NMR: (50 MHz, DMSO - d_6): δ = 28.34 ($COCH_3$); 53.92 (OCH_3); 61.52 ($CHNH_3$), 164.61 ($COCH_3$), 197.15 (CO_2CH) ppm.

HR-FAB$^+$ MS: m/z calc. for $C_5H_{10}NO_3^+$ 132.062, found 132.066.

8.3.3 Methyl 2-((*S*)-2-(*tert*-butoxycarbonylamino)-3-methylbutanamido)-3-oxobutanoate (3):

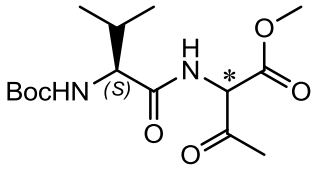

Molecular formula: $C_{15}H_{26}N_2O_6$

Molecular weight: 330.38 g/mol

3

Following known literature procedures,[66,113] (*S*)-Boc-valine (18.31 g, 84.27 mmol) and NMM (8.59 g, 84.27 mmol, 1 eq) were dissolved in anhydrous THF (450 ml) and cooled to -25°C. Then, isobutyl chloroformate (11.68 g, 84.27 mmol, 1 eq) was added carefully. After stirring the reaction mixture for 1h at -25°C, the ammonium chloride salt **2** (28.23 g, 168.54 mmol, 2 eq) was added. Subsequently, the reaction mixture was treated with NMM (8.59 g, 84.27 mmol, 1eq) and the the cooling bath was removed (over 2h) slowly. The reaction mixture was stirred for another day at rt before the solvent was removed *in vacuo*. The crude product was dissolved in EtOAc and extracted with brine, dried over Na_2SO_4, and concentrated *in vacuo* to a colorless oil. After addition of *n*-hexane, colorless crystals were obrtained on standing overnight at -20°C. Filtration yielded **3** (23.69 g, 71.78 mmol, 85.17%) as a white crystalline solid.

Microanalysis: $C_{15}H_{26}N_2O_6$: calc. (%): C 54.53, H 7.93, N 8.48; found (%): C 54.67, H 7.57, N 8.80 (Report No. 33435)

^{1}H NMR: (200 MHz, $CDCl_3$): δ = 0.89 (d, 3H, $CH(C\underline{H}_3)_2$, $^3J_{H-H}$ = 6.7 Hz); 0.96 (d, 3H, $CH(C\underline{H}_3)_2$, $^3J_{H-H}$ = 6.8Hz); 1.43 (s, 9H, $C(C\underline{H}_3)_3$), 2.15 – 2.25 (m, 1H, $C\underline{H}(CH_3)_2$), 2.37 (s, 3H, $COC\underline{H}_3$), 3.79 (s, 3H, CO_2CH_3), 4.09 (m, 1H, $NHC\underline{H}CO$), 4.95-4.99 (m, 1H, $CO_2N\underline{H}$), 5.21 (d, 1H, $BocNHC\underline{H}CO$), 7.01-7.12, (m, 1H, $N\underline{H}$) ppm.

HR-DART$^+$ MS: m/z calc. for $[M+H]^+$: 331.182, $[M+NH_4]^+$ = 348.213, $[2M+H]^+$ = 661.365, $[2M+NH_4]^+$ = 678.392; found: 331.186, 348.213, 661.365, 678.392.

8.3.4 Methyl 2-((R)-2-(*tert*-butoxycarbonylamino)-3-methylbutanamido)-3-oxobutanoate (4):

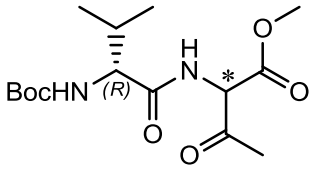

4

Molecular formula: $C_{15}H_{26}N_2O_6$

Molecular weight: 330.38 g/mol

Following known literature procedures,[66,113] (*R*)-Boc-valine (5.00 g, 22.90 mmol) and NMM (2.33g, 22.90 mmol, 1 eq) were dissolved in anhydrous THF (300 ml) and cooled to -25°C. Then, isobutyl chloroformate (3.18 g, 22.90 mmol, 1eq) was added slowly. After stirring the reaction mixture for 1h at -25°C, the ammonium chloride salt **2** (7.67 g, 45.80 mmol, 2 eq) was added. Subsequently NMM (2.33 g, 22.90 mmol. 1eq) was added to the reaction mixture and the cooling bath was removed (over 2h) slowly. The reaction mixture was stirred for another day at rt before the solvent was removed *in vacuo*. The crude product was dissolved in EtOAc and extracted with H_2O and brine, dried over Na_2SO_4, and concentrated *in vacuo* to a colorless oil. After addition of *n*-hexane, colorless crystals formed on standing overnight at -20°C. Filtration and subsequent washing with ice- cold n-Hexane yielded **4** (4.81 g, 14.81 mmol, 63.61%) as a white crystalline solid.

Microanalysis: $C_{15}H_{26}N_2O_6$: calc. (%): C 54.53, H 7.93, N 8.48; found (%): C 54.55, H 7.89, N 8.72 (Report No. 33436)

^{1}H NMR: (200 MHz, $CDCl_3$): δ = 0.89 (d, 3H, $CH(C\underline{H}_3)_2$, $^3J_{H\text{-}H}$ = 7.1 Hz); 0.95 (d, 3H, $CH(C\underline{H}_3)_2$, $^3J_{H\text{-}H}$ = 6.7Hz); 1.42 (s, 9H, $C(C\underline{H}_3)_3$), 2.09 – 2.28 (m, 1H, $C\underline{H}(CH_3)_2$), 2.36 (s, 3H, $COC\underline{H}_3$), 3.78 (s, 3H, CO_2CH_3), 4.04 (m, 1H, $NHC\underline{H}CO$), 4.93-5.04 (m, 1H, $CO_2N\underline{H}$), 5.21 (d, 1H, $BocNHC\underline{H}CO$), 7.02-7.14, (m, 1H, $N\underline{H}$) ppm.

^{13}C NMR: (200 MHz, $CDCl_3$): δ = 17.47 ($CH(\underline{C}H_3)_2$); 19.23($CH(\underline{C}H_3)_2$); 28.01 ($COC\underline{H}_3$); 28.29 ($C(\underline{C}H_3)_3$), 30.88 ($\underline{C}H(CH_3)_2$), 53.29 ($CO_2\underline{C}H_3$), 62.95 ($NH\underline{C}HCO_2$), 80.23 ($\underline{C}(CH_3)_3$), 166.34 ($NH\underline{C}OC(CH_3)_3$), 171.44 ($\underline{C}O_2CH_3$), 180.25($NH\underline{C}O$), 197.98 ($\underline{C}OCH_3$) ppm.

HR-DART$^+$ MS: m/z calc. for $[M+H]^+$: 331.182, $[M+NH_4]^+$ = 348.213, $[2M+H]^+$ = 661.365, $[2M+NH_4]^+$ = 678.392; found: 331.188, 348.213, 661.371, 678.400.

8.3.5 Methyl 2-((S)-2-(*tert*-butoxycarbonylamino)-2-methylpropyl)-1,5-dimethyl-imidazole-4-carboxylate (5):

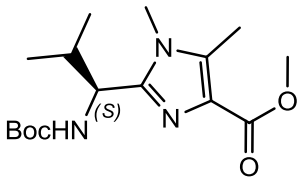

Molecular formula: $C_{16}H_{27}N_3O_4$

Molecular weight: 325.40 g/mol

5

Following known literature procedures,[66,113] the amide **3** (23.69 g, 71.78 mmol) was dissolved in xylene (450 ml) and glacial acetic acid (28.6 ml) and $MeNH_2$ (25.6 ml) were added to the solution. The reaction mixture was refluxed for 3 h at 155°C. Then, further 19.7 ml glacial acetic acid and 9.85 ml $MeNH_2$ were added, and the reaction mixture was refluxed for another 5 h. After cooling to rt the solvent, $MeNH_2$ and acetic acid were removed *in vacuo*. The crude product was purified by flash chromatography with silica gel (5 x 30 cm, EtOAc/PE= 4:1) to yield **5** (20.21 g, 62.19 mmol, 86.63%) as a white solid.

Microanalysis: $C_{16}H_{27}N_3O_4$: calc. (%): C 59.06, H 8.36, N 12.91; found (%): C 58.97, H 7.94, N 13.04 (Report No. 33487)

^{1}H NMR: (200 MHz, $CDCl_3$): δ = 0.78 (d, 3H, $CH(C\underline{H}_3)_2$, $^3J_{H-H}$ = 6.6 Hz); 1.02 (d, 3H, $CH(C\underline{H}_3)_2$, $^3J_{H-H}$ = 6.5 Hz); 1.38 (s, 9H, $C(C\underline{H}_3)_3$), 2.08 – 2.46 (m, 1H, $C\underline{H}(CH_3)_2$), 2.53 (s, 3H, imi$C\underline{H}_3$), 3.54 (s, 3H, $CO_2C\underline{H}_3$), 3.85 (s, 3H, $NC\underline{H}_3$), 4.53 (t, 1H, $NHC\underline{H}$, $^3J_{H-H}$ = 9.4Hz), 5.35 (bs, 1H, $N\underline{H}$) ppm.

HR-DART$^+$ MS: m/z calc. for $[M+H]^+$: 326.207, $[2M+H]^+$ = 651.407, found: 326.208, 651.409.

8.3.6 Methyl 2-((*R*)-2-(*tert*-butoxycarbonylamino)-2-methylpropyl)-1,5-dimethyl-imidazole-4-carboxylate (6):

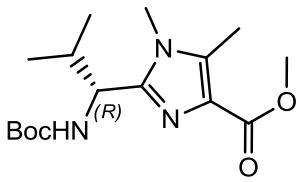

Molecular formula: $C_{16}H_{27}N_3O_4$

Molecular weight: 325.40 g/mol

6

Following a known literature procedures,[66,113] the amide **3** (4.81 g, 14.58 mmol) was dissolved in xylene (92 ml). Glacial acetic acid (5.8 ml) and $MeNH_2$ (5.2 ml) were added, before the reaction mixture was refluxed for 3 h at 155°C. Then, additional 2 ml glacial acetic acid and 4 ml $MeNH_2$ were added, and the reaction mixture was refluxed for another 5 h. After cooling the mixture to rt, the solvent, MeNH2 and acetic acid were removed in vacuo. The crude product was purified by flash chromatography with silica gel (3 x 25 cm, EtOAc/PE 3:1) to yield **6** (3.02 g, 9.28 mmol, 63.65%) as a white solid.

Microanalysis: $C_{16}H_{27}N_3O_4$: calc. (%): C 59.06, H 8.36, N 12.91; found (%): C 58.86, H 8.46, N 12.74 (Report No. 33486)

^{1}H NMR: (200 MHz, $CDCl_3$): δ = 0.80 (d, 3H, $CH(C\underline{H}_3)_2$, $^3J_{H\text{-}H}$ = 6.5 Hz); 0.99 (d, 3H, $CH(C\underline{H}_3)_2$, $^3J_{H\text{-}H}$ = 6.8Hz); 1.38 (s, 9H, $C(C\underline{H}_3)_3$), 2.11 – 2.30 (m, 1H, $C\underline{H}(CH_3)_2$), 2.51 (s, 3H, imi$C\underline{H}_3$), 3.54 (s, 3H, CO_2CH_3), 3.85 (s, 3H, $NC\underline{H}_3$), 4.50 (t, 1H, NHC$\underline{H}$, $^3J_{H\text{-}H}$ = 9.1Hz), 5.35 (d, 1H, N$\underline{H}$, $^3J_{H\text{-}H}$ = 9.4Hz) ppm.

HR-DART$^+$ MS: m/z calc. for $[M+H]^+$: 326.207, $[2M+H]^+$ = 651.407, found: 326.208, 651.408.

8.3.7 (*S*)-1-(4-(methoxycarbonyl)-1,5-dimethyl-imidazole-2-yl)-2-methylpropan-1-ammonium trifluoro acetat (7):

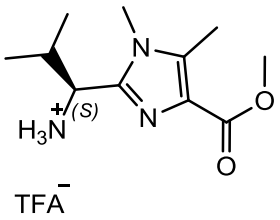

7

Molecular formula: $C_{13}H_{20}F_3N_3O_4$

Molecular weight: 339.31 g/mol

The imidazole building block **5** (4.50 g, 13.83 mmol) was converted into **7** (4.71 g, 13.88 mmol) according to general procedure GP2 using TFA (27.5 ml) and DCM (210 ml). In this way, **7** was obtained quantitatively as a white solid foam.

^{1}H NMR: (200 MHz, $CDCl_3$): δ = 0.80 (d, 3H, CH($C\underline{H}_3$)$_2$, $^3J_{H\text{-}H}$ = 6.4 Hz); 0.98 (d, 3H, CH8($C\underline{H}_3$)$_2$, $^3J_{H\text{-}H}$ = 6.7 Hz); 2.08 – 2.46 (m, 1H, $C\underline{H}(CH_3)_2$), 2.50 (s, 3H, imi$C\underline{H}_3$), 3.54 (s, 3H, CO_2CH_3), 3.85 (s, 1H, $NC\underline{H}_3$), 4.50 (t, 1H, NHC$\underline{H}$, $^3J_{H\text{-}H}$ = 9.1Hz), 5.35 (d, 1H, N$\underline{H}$, , $^3J_{H\text{-}H}$ = 9.6 Hz) ppm.

^{13}C NMR: (200 MHz, $CDCl_3$): δ = 10.57 (imi$\underline{C}H_3$), 18.66 (CH($\underline{C}H_3$)$_2$); 18.96(CH($\underline{C}H_3$)$_2$), 31.21 ($\underline{C}H(CH_3)_2$),33.63 (N$\underline{C}H_3$), 51.92 ($CO_2\underline{C}H_3$), 53.48 ($NH_3^+\underline{C}H$), 125.93 ($\underline{C}_{imi}CO_2$), 139.17 ($\underline{C}_{imi}NCH_3$), 144.04 ($\underline{C}_{imi}CH_3$), 169.85 ($\underline{C}O_2CH_3$), 180.25(NH$\underline{C}$O) ppm.

HR-DART+ MS: m/z calc. for [2Mamine+H]+ = 451.303, [3Mamine+H]+ = 676.450, found: 451.303, 676.452.

8.3.8 (*R*)-2-(1-(*tert*-butoxycarbonylamino)-2-methylpropyl)-1, 5-dimethyl-imidazole-4-carboxylic acid (8):

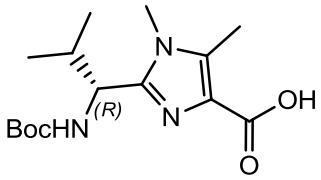

Molecular formula: $C_{15}H_{25}N_3O_4$

Molecular weight: 311.38 g/mol

8

According to general procedure GP1, the imidazole building block **6** (4.95 g, 15.20 mmol) was converted into **8** (3.77 g, 12.11 mmol, 79.65%) as a white solid. Using 2M NaOH (77 ml) and 174 ml of a dioxane/MeOH mixture.

^{1}H NMR: (200 MHz, $CDCl_3$): δ = 0.81 (d, 3H, $CH(C\underline{H}_3)_2$, $^3J_{H\text{-}H}$ = 6.3 Hz); 1.17 (d, 3H, $CH(C\underline{H}_3)_2$, $^3J_{H\text{-}H}$ = 6.4 Hz); 1.37 (s, 9H, $C(C\underline{H}_3)_3$), 2.70 – 2.88 (m, 1H, $C\underline{H}(CH_3)_2$), 2.63 (s, 3H, imi$C\underline{H}_3$), 3.85 (s, 3H, NCH_3), 4.62 (t, 1H, NHC<u>H</u>, $^3J_{H\text{-}H}$ = 9.5Hz), 5.27 (s, 1H, N<u>H</u>) ppm.

HR-DART$^+$ MS: m/z calc. for $[M+H]^+$: 312.192, $[2M+H]^+$ = 623.376, found: 312.193, 623.381.

8.3.9 Methyl 2-((*S*)-1-(2-((*R*)-1-(*tert*-butoxycarbonylamino)-2-methylpropyl)-1, 5-dimethyl-imidazole-4-carboxamido)-2-methylpropyl)-1.5-dimethyl-imidazole-4-carboxylate (9):

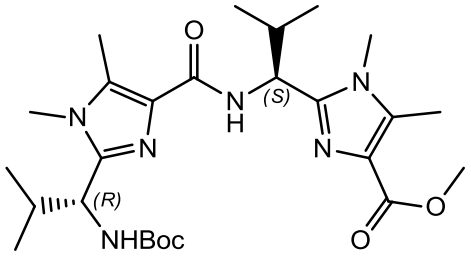

Molecular formula: $C_{26}H_{42}N_6O_5$

Molecular weight: 518.64 g/mol

9

Following general procedure GP3, the methyl deprotected building block **8** (3.11 g, 9.99 mmol) was coupled with the boc deprotected building block **7** (4.06 g, 11.97 mmol) to yield **9** (5.18 g, 9.99 mmol). After purification by flash chromatography with silica gel (3 x 30 cm, EtOAc/DCM/MeOH 70:29:1) **9** *w*as obtained as a lightly yellow powder. Coupling was done using 100 ml MeCN, 8.56 g (20.00 mmol) COMU, and 3.84 ml EDIPA (2.85 g, 22.04 mmol).

^{1}H NMR: (200 MHz, $CDCl_3$): δ = 0.73 (d, 3H, $CH(C\underline{H}_3)_2$, $^3J_{H\text{-}H}$ = 6.6 Hz); 0.83 (d, 3H, $CH(C\underline{H}_3)_2$, $^3J_{H\text{-}H}$ = 7.1 Hz); 0.88 (d, 3H, $CHC\underline{H}_3$, $^3J_{H\text{-}H}$ = 6.7 Hz); 1.01 (d, 3H, $CHC\underline{H}_3$, $^3J_{H\text{-}H}$ = 7.03 Hz); 1.40 (s, 9H, $C(C\underline{H}_3)_3$), 2.01 – 2.27 (m, 1H, $C\underline{H}(CH_3)_2$), 2.48 (s, 3H, imi$C\underline{H}_3$), 2.50 (s, 3H, imi$C\underline{H}_3$), 3.06 – 3.20 (m, 1H, $C\underline{H}(CH_3)_2$), 3.46 (s, 3H, $NC\underline{H}_3$), 3.56 (s, 3H, $NC\underline{H}_3$), 3.85 (s, 3H, CO_2CH_3),4.58 (t, 1H, NHC<u>H</u>, $^3J_{H\text{-}H}$ = 9.4Hz), 4.94 (d, 1H, NHC<u>H</u>, $^3J_{H\text{-}H}$ = 9.2Hz), 5.50 (d, 1H, N<u>H</u>Boc), 8.10 (bs, 1H, N<u>H</u>) ppm.

8.3.10 2-((*S*)-1-(2-((*R*)-1-(*tert*-butoxycarbonylamino)-2-methylpropyl)-1,5-dimethyl-imidazole-4-carboxamido)-2-methylpropyl)-1.5-dimethyl-imidazole-4-carboxylic acid (10):

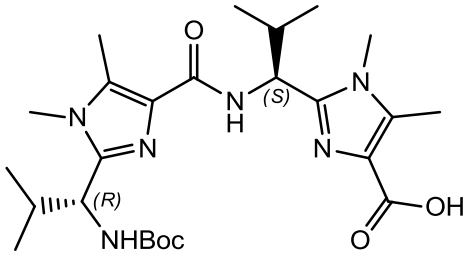

Molecular formula: $C_{25}H_{40}N_6O_5$

Molecular weight: 504.62 g/mol

10

According to general procedure GP1, the dimeric building block **9** (5.18 g, 9.99 mmol) was converted into **10** (4.83 g, 9.57 mmol, 95.81%) as a yellowish solid. 2M NaOH (80.6 ml) and 180 ml of a dioxan/MeOH mixture were used.

^{1}H NMR: (200 MHz, $CDCl_3$): δ = 0.74 (d, 3H, CH($C\underline{H}_3$)$_2$, $^3J_{H-H}$ = 7.3 Hz); 0.88 (d, 3H, CH($C\underline{H}_3$)$_2$, $^3J_{H-H}$ = 6.7 Hz); 0.96 (d, 3H, CHC$\underline{H}_3$, $^3J_{H-H}$ = 6.7 Hz); 1.09 (d, 3H, CHC$\underline{H}_3$, $^3J_{H-H}$ = 7.1 Hz); 1.40 (s, 9H, C($C\underline{H}_3$)$_3$), 2.06 – 2.22 (m, 1H, C$\underline{H}$(CH_3)$_2$), 2.30 – 2.53 (m, 1H, C$\underline{H}$(CH_3)$_2$), 2.60 (s, 3H, imiC$\underline{H}_3$), 2.63 (s, 3H, imiC$\underline{H}_3$), 3.22 (bs, 3H, NC$\underline{H}_3$), 3.66 (s, 3H, NC$\underline{H}_3$), 4.49- 4.82 (m, 2H, NHCßH), 5.24- 5.46 (m, 1H, N$\underline{H}$Boc), 6.8 (bs, 1H, N$\underline{H}$), 9.92 (bs, 1H, COOH) ppm.

8.3.11 (*R*)-1-(4-(((*S*)-1-(4-carboxy-1,5-dimethyl-imidazol-2-yl)-2-methylpropyl)carbamoyl)-1,5-dimethyl-imidazol-2-yl)-2-methylpropan-1-ammonium trifluoroacetat (11):

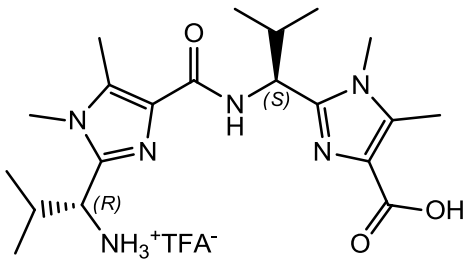

Molecular formula: $C_{22}H_{33}N_6O_5F_3$

Molecular weight: 518.53 g/mol

11

The methyl deprotected dimeric building block **10** (4.83 g, 9.57 mmol) was converted into the twice deprotected dimeric building block **11** (4.92 g, 9.49 mmol) following general procedure GP2. Compound **11** is isolated as a yellowish foam. TFA (18.33 ml) and DCM (80 ml) were used. The crude product was used without further purification.

8.3.12 H_4pat^1 (12):

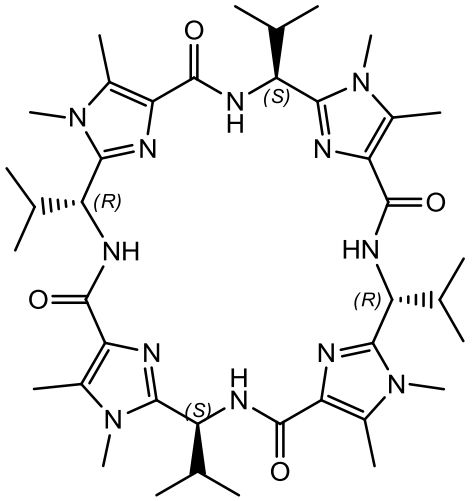

Molecular formula: $C_{40}H_{60}N_{12}O_4$

Molecular weight: 772.98 g/mol

12

The cyclic *pseudo* octapeptide H_4pat^1 was prepared according to general procedure GP3. The deprotected peptidic building block **11** (4.67g, 9.00 mmol) was converted into **12** (1.17 g, 1.51mmol, 16.80%) and obtained as a white solid. After purification by repetitive recrystallization from a MeOH / diethyl ether mixture and flash chromatography with silica gel (3 x 20 cm, EtOAc/DCM/MeOH 70:29:1) the product was obtained as a white powder. Coupling was performed, using 90 ml MeCN, 7.72 g (18 mmol) COMU, and 11.63 ml EDIPA (90 mmol).

^{1}H NMR: (600 MHz, MeOD-d_4): δ = 0.86 (d, 12H, CH(C$\underline{H}_3$)$_2$, $^3J_{H\text{-}H}$ = 6.8 Hz); 0.91 (d, 12H, CH(C$\underline{H}_3$)$_2$, $^3J_{H\text{-}H}$ = 6.8 Hz); 2.27 (o, 4H, C$\underline{H}$(CH$_3$)$_2$), 2.57 (s, 12H, imiC$\underline{H}_3$), 3.65 (s, 12H, NC$\underline{H}_3$), 5.11 (bd, 4H, C$\underline{H}$, $^3J_{H\text{-}H}$ = 7.1 Hz), 8.68 (d, 0.9 H, N$\underline{H}$, $^3J_{H\text{-}H}$ = 9.0 Hz) ppm.

^{13}C NMR: (150 MHz, MeOD-d_4): δ = 10.14 (C$_{Het}$C$\underline{H}_3$); 19.10, 19.98 (CH(C$\underline{H}_3$)$_2$); 31.67 (NC$\underline{H}_3$), 35.07 (C$_ß$), 51.47 (C$\underline{}_α$), 130.46 (C$\underline{}_{Het}$-CO), 135.04 (C$\underline{}_{Het}$-NCH$_3$), 148.57 (C$\underline{}$=N), 165.76 (C$\underline{}$O) ppm.

^{15}N NMR: (60 MHz, MeOD-d_4): δ = 115.6 (N$\underline{}$H); 166.0 (N$\underline{}$CH$_3$), 246.0 (C=N$\underline{}$) ppm.

HR-ESI$^+$ MS: m/z calc. for $[M+H]^+$: 773.493, $[M+Na]^+$ = 795.475; found: 773.49, 795.476.

8.4 Synthesis of H_4pat^2

8.4.1 (*S*)-2-(1-(*tert*-butoxycarbonylamino)-2-methylpropyl)-1,5-dimethyl-imidazole-4-carbox-ylic acid (13):

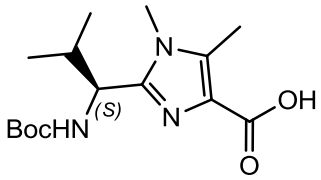

Molecular formula: $C_{15}H_{25}N_3O_4$

Molecular weight: 311.38 g/mol

13

According to general procedure GP1, the imidazole building block **5** (3.10 g, 9.57 mmol) was converted into **13** (2.90 g, 9.31 mmol, 97.28%) as a white solid. 46.7 ml 2M NaOH and 112.5ml of the dioxan/MeOH mixture were used.

^{1}H NMR: (200 MHz, $CDCl_3$): δ = 0.78 (d, 3H, $CH(C\underline{H}_3)_2$, $^3J_{H\text{-}H}$ = 6.3 Hz); 1.11 (d, 3H, $CH(C\underline{H}_3)_2$, $^3J_{H\text{-}H}$ = 6.4 Hz); 1.37 (s, 9H, $C(C\underline{H}_3)_3$), 2.39 – 2.55 (m, 1H, $C\underline{H}(CH_3)_2$), 2.58 (s, 3H, imi$C\underline{H}_3$), 3.68 (s, 3H, NCH_3), 4.55 (t, 1H, $NHC\underline{H}$, $^3J_{H\text{-}H}$ = 9.5Hz), 6.81 (bs, 1H, $N\underline{H}$) ppm.

HR-DART$^+$ MS: m/z calc. for $[M+H]^+$: 312.192, $[2M+H]^+$ = 623.376, found: 312.193, 623.381.

8.4.2 Methyl 2-((*R*)-1-(2-((*R*)-1-(*tert*-butoxycarbonylamino)-2-methylpropyl)-1,5-dimethyl-imidazole-4-carboxamido)-2-methylpropyl)-1.5-dimethyl-imidazole-4-carboxylate (14):

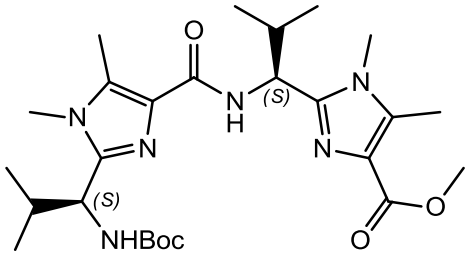

Molecular formula: $C_{26}H_{42}N_6O_5$

Molecular weight: 518.64 g/mol

14

Following general procedure GP3, the methyl deprotected building block **13** (2.96 g, 9.51 mmol) was coupled with the boc deprotected building block **7** (3.78 g, 11.14 mmol) to yield **14** (4.04 g, 7.79 mmol, 81.90%), after purification by flash chromatography with silica gel (3 x 30 cm, EtOAc/DCM/MeOH 75:25:1) as a light yellow powder. Coupling was done, using 130 ml MeCN, 8.57 g (20.01 mmol) COMU, and 3.84 ml EDIPA (3.88 g, 30.02 mmol).

^{1}H NMR: (200 MHz, $CDCl_3$): δ = 0.73 (d, 3H, $CH(C\underline{H}_3)_2$, $^3J_{H\text{-}H}$ = 7.3 Hz); 0.81 (d, 3H, $CH(C\underline{H}_3)_2$, $^3J_{H\text{-}H}$ = 6.8 Hz); 0.91 (d, 3H, $CHC\underline{H}_3$, $^3J_{H\text{-}H}$ = 7.2 Hz); 0.99 (d, 3H, $CHC\underline{H}_3$, $^3J_{H\text{-}H}$ = 7.5 Hz); 1.38(s, 9H, $C(C\underline{H}_3)_3$), 2.00 – 2.31 (m, 1H, $C\underline{H}(CH_3)_2$), 2.44 (s, 3H, imi$C\underline{H}_3$), 2.45 (s, 3H, imi$C\underline{H}_3$), 3.08 – 3.21 (m, 1H, $C\underline{H}(CH_3)_2$), 3.42 (s, 3H, $NC\underline{H}_3$), 3.56 (s, 3H, $NC\underline{H}_3$), 3.81 (s, 3H, $CO_2C\underline{H}_3$),4.32- 4.55 (m, 2H, NHC<u>H</u>), 5.20 (d, 1H, N<u>H</u>Boc, $^3J_{H\text{-}H}$ = 9.0Hz), 7.62 (d, 1H, N<u>H,</u> $^3J_{H\text{-}H}$ = 9.5Hz) ppm.

8.4.3 2-((*S*)-1-(2-((*S*)-1-(*tert*-butoxycarbonylamino)-2-methylpropyl)-1,5-dimethyl-imidazole-4-carboxamido)-2-methylpropyl)-1.5-dimethyl-imidazole-4-carboxylic acid (15):

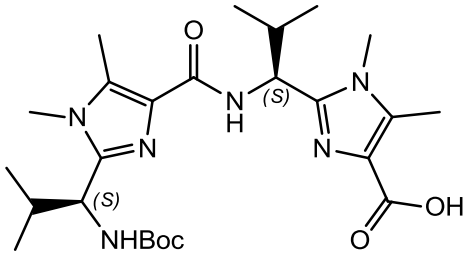

Molecular formula: $C_{25}H_{40}N_6O_5$

Molecular weight: 504.62 g/mol

15

According to general procedure GP1, the dimeric building block **14** (4.04 g, 7.79 mmol) was converted into **15** (1.11 g, 2.20 mmol, 28.80%), which was obtained as a yellowish solid. 63 ml 2M NaOH and 138 ml of the described dioxan/MeOH mixture were used.

^{1}H NMR: (200 MHz, $CDCl_3$): δ = 0.80 (d, 3H, CH($C\underline{H}_3$)$_2$, $^3J_{H\text{-}H}$ = 7.2 Hz); 0.82 (d, 3H, CH($C\underline{H}_3$)$_2$, $^3J_{H\text{-}H}$ = 7.1 Hz); 0.90 (d, 3H, CHC$\underline{H}_3$, $^3J_{H\text{-}H}$ = 6.7 Hz); 1.03 (d, 3H, CHC$\underline{H}_3$, $^3J_{H\text{-}H}$ = 7.0 Hz); 1.39 (s, 9H, C($C\underline{H}_3$)$_3$), 2.10 – 2.41 (m, 1H, C$\underline{H}$(CH_3)$_2$), 2.54 (bs, 6H, imiC$\underline{H}_3$), 3.21 (bs, 3H, NC$\underline{H}_3$), 3.62 (s, 3H, NC$\underline{H}_3$), 3.87- 4.39 (bm, 1H, C$\underline{H}$(CH_3)$_2$), 4.55 (q, 1H, NHCß$\underline{H}$, $^3J_{H\text{-}H}$ = 8.7 Hz), 5.08 (t, 1H, 1H, NHCß$\underline{H}$, $^3J_{H\text{-}H}$ = 10.0 Hz), 6.59 (d, 1H, N$\underline{H}$Boc, $^3J_{H\text{-}H}$ = 8.3 Hz), 8.65 (bs, 1H, N$\underline{H}$) ppm.

8.4.4 (*S*)-1-(4-(((*S*)-1-(4-carboxy-1,5-dimethyl-imidazol-2-yl)-2-methylpropyl)carbamoyl)-1,5-dimethyl-imidazol-2-yl)-2-methylpropan-1-ammonium trifluoroacetat (16):

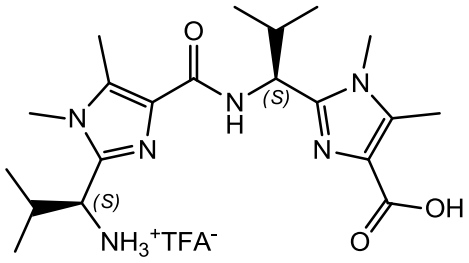

Molecular formula: $C_{22}H_{33}N_6O_5F_3$

Molecular weight: 518.53 g/mol

16

According to general procedure GP2, the methyl deprotected dimeric building block **15** (1.55 g, 3.07 mmol) was converted into **16** (1.58 g, 3.04 mmol) as a yellowish foam. Using 5.9 ml TFA and 25 ml DCM, a quantitative yield was reached and the product was used without further purification.

^{1}H NMR: (200 MHz, DMSO d_6): δ = 0.80 (d, 3H, CH(C<u>H</u>$_3$)$_2$, $^3J_{H\text{-}H}$ = 5.9 Hz); 0.86 (d, 3H, CH(C<u>H</u>$_3$)$_2$, $^3J_{H\text{-}H}$ = 7.0 Hz); 0.95 (d, 3H, CHC<u>H</u>$_3$, $^3J_{H\text{-}H}$ = 6.8 Hz); 1.01 (d, 3H, CHC<u>H</u>$_3$, $^3J_{H\text{-}H}$ = 6.7 Hz); 2.10 – 2.39 (m, 1H, C<u>H</u>(CH$_3$)$_2$), 2.44 (s, 3H, imiC<u>H</u>$_3$), 2.47 (s, 3H, imiC<u>H</u>$_3$), 3.50 (bs, 3H, NC<u>H</u>$_3$), 3.09- 3.20 (bm, 1H, C<u>H</u>(CH$_3$)$_2$), 3.53 (bs, 3H, NC<u>H</u>$_3$), 4.02 (q, 1H, NHCß<u>H,</u> $^3J_{H\text{-}H}$ = 7.2 Hz), 4.42 (bs, 1H, N<u>H</u>$_2$), 5.07 (t, 1H, 1H, NHCß<u>H,</u> $^3J_{H\text{-}H}$ = 9.9 Hz), 8.02 (bs, 1H, N<u>H,</u> $^3J_{H\text{-}H}$ = 9.9 Hz), 8.43 (bs, 1H, COO<u>H</u>) ppm.

8.4.5 H_4pat^2 (17):

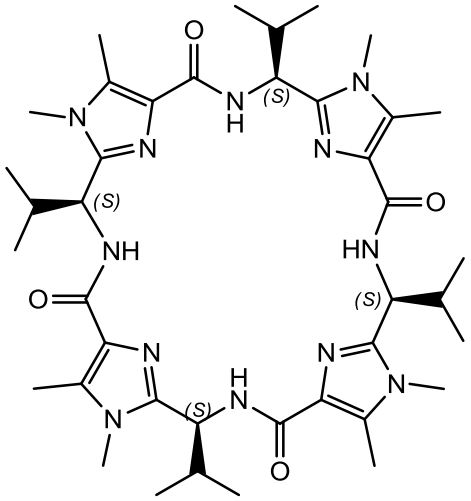

Molecular formula: $C_{40}H_{60}N_{12}O_4$

Molecular weight: 772.98 g/mol

17

The cyclic *pseudo* octapeptide H_4pat^1 was prepared according to general procedure GP3. The twice deprotected peptidic building block **16** (1.68 g, 3.32 mmol) was converted into **17** (0.22 g, 0.28 mmol, 8.79%) as a white solid. After purification by repetitive recrystallization from a methanol / diethyl ether mixture and flash chromatography with silica gel (3 x 20 cm, EtOAc/DCM/MeOH 70:29:1) the product yielded as a white powder. Coupling was done, using 35 ml MeCN, 2.78 g (6.48 mmol) COMU, and 5.6 ml EDIPA (32.4 mmol).

^{1}H NMR: (600 MHz, MeOD-d_4): δ = 0.88 (d, 12H, CH(C<u>H</u>$_3$)$_2$, $^3J_{H\text{-}H}$ = 6.7 Hz); 1.10 (d, 12H, CH(C<u>H</u>$_3$)$_2$, $^3J_{H\text{-}H}$ = 6.7 Hz); 2.36- 2.45 (m, 4H, <u>H</u>ß), 2.49 (s, 12H, imiC<u>H</u>$_3$), 3.66 (s, 12H, NC<u>H</u>$_3$), 4.92 (d, 4H, <u>H</u>α, $^3J_{H\text{-}H}$ = 7.1 Hz), 7.89 (d, 0.1 H, N<u>H</u>, $^3J_{H\text{-}H}$ = 9.0 Hz) ppm.

^{13}C NMR: (150 MHz, MeOD-d_4): δ = 10.20 (C_{Het}<u>C</u>H$_3$); 19.83, 20.08 (CH(<u>C</u>H$_3$)$_2$); 30.98 (N<u>C</u>H$_3$), 34.24 (Cα), 51.63 (<u>C</u>H(CH$_3$)$_2$), 130.08 (<u>C</u>$_{Het}$-CO), 135.05 (<u>C</u>$_{Het}$-NCH$_3$), 149.01 (<u>C</u>=N), 165.69 (<u>C</u>O) ppm.

^{15}N NMR: (60 MHz, MeOD-d_4): δ = 114.1 (<u>N</u>H); 165.5 (<u>N</u>CH$_3$), 241.5 (C=<u>N</u>) ppm.

HR-ESI$^+$ MS: m/z calc. for $[M+H]^+$: 773.493, $[M+Na]^+$ = 795.475; found: 773.493, 795.477.

8.5 Synthesis of H_4pat^4

8.5.1 Methyl 2-((*S*)-2-(benzyloxycarbonylamino)-3-methylbutanamido)-3-oxobutanoat (18):

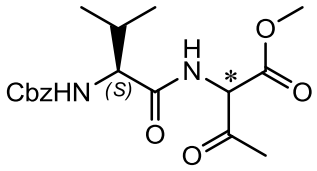

Molecular formula: $C_{18}H_{24}N_2O_6$

Molecular weight: 364.39 g/mol

18

According to literature known procedures, [66,113] (*S*)-Cbz-valine (10.00 g, 39.79 mmol) and NMM (4.05 g, 39.79 mmol, 1eq) were dissolved in 520 ml dry THF and cooled to -25°C. Then, 1 eq. of isobutyl chloroformate (5.53 g, 39.79 mmol) was added carefully. After stirring the reaction mixture for 1h at -25°C, the ammonium chloride salt **2** (6.66 g, 39.79 mmol, 1eq) was added. The reaction mixture was treated subsequently with NMM (4.05 g, 39.79 mmol, 1eq). Afterwards, the cooling bath was removed slowly (over 2h), and the reaction mixture was stirred for another day at rt, before the solvent was removed *in vacuo*. The crude product was dissolved in EtOAc and extracted with H_2O and brine, dried over Na_2SO_4, and concentrated *in vacuo* to a colorless oil. Colorless crystals were obtained on standing overnight at -20°C. Filtration and subsequent washing with ice-cold *n*-hexane yielded **18** (9.50 g, 26.07 mmol, 65.52%) as a white crystalline solid.

Microanalysis: $C_{18}H_{24}N_2O_6$: calc. (%): C 59.33, H 6.64, N 7.69; found (%): C 59.61, H 7.22, N 6.68 (Report No. 33724)

^{1}H NMR: (200 MHz, $CDCl_3$): δ = 0.85 – 1.07 (m, 6H, $CH(C\underline{H}_3)_2$); 1.88- 2.29 (m, 1H, $C\underline{H}(CH_3)_2$), 2.36 (s, 3H, $COC\underline{H}_3$), 3.79 (s, 3H, $CO_2C\underline{H}_3$), 4.05 (d, 1H, $NHC_\alpha\underline{H}$, $^3J_{H\text{-}H}$ = 6.6 Hz), 5.09 (s, 2H, $C\underline{H}_2$-Ar), 5.19 (d, 1H, $NHC\underline{H}COOMe$, $^3J_{H\text{-}H}$ = 6.6 Hz), 5.25- 5.35 (m, 1H, $N\underline{H}CHCOOMe$), 6.99 (bt, 1H, $N\underline{H}$, $^3J_{H\text{-}H}$ = 6.6 Hz), 7.26- 7.38 (m, 5H, H_{arom}) ppm.

ESI$^+$ MS: m/z calc. for $[M+H]^+$: 365.0, $[M+Na]^+$ = 387.1; found: 365.0, 387.1

8.5.2 Methyl 2-((*S*)-1-(benzyloxycarbonylamino)-2-methylpropyl)-5-methyl-1H-imidazole-4-carboxylate (19):

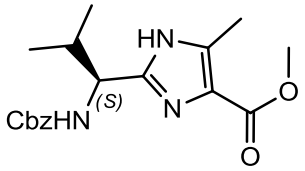

Molecular formula: $C_{18}H_{23}N_3O_4$

Molecular weight: 345.39 g/mol

19

Compound **19** was prepared following known literature procedures.[67] The twice protected oxo-peptide **18** (4.40 g, 12.07 mmol) was suspended in 200 ml xylene, before 1.85 ml TFA (2 eq, 24.15 mmol, 2.75 g) and 0.53 ml ammonia in methanol (2 eq, 24.15 mmol, 0.41 g) were added. The reaction mixture was refluxed for 6h, with azeotropic removal of water. Then a further 2 ml of TFA and 1 ml of ammonia were added, and the reaction mixture was refluxed for another 6 h. After cooling to rt, solvent, ammonia and TFA were removed *in vacuo*. The crude product was purified by flash chromatography with silica gel (5 x 30 cm, EtOAc/PE 1:1) to yield **19** (1.60 g, 4.63 mmol, 38.36%) as a white foam.

^{1}H NMR: (200 MHz, $CDCl_3$): δ = 0.90 – 1.01 (m, 6H, CH($C\underline{H}_3$)$_2$); 2.08- 2.25 (m, 1H, C$\underline{H}$(CH_3)$_2$), 2.15 (s, 3H, COOC$\underline{H}_3$), 3.59 (s, 3H, imiC$\underline{H}_3$), 3.93- 4.13 (m, 1H, NHC$_\alpha\underline{H}$), 5.09 (s, 2H, C$\underline{H}_2$-Ar), 5.25- 5.50 (m, 1H, N$\underline{H}$), 7.34 (m, 5H, H_{arom}) ppm.

HR-ESI$^+$ MS: m/z calc. for $[M+H]^+$: 346.176, $[M+Na]^+$ = 368.158; found: 346.177, 368.158

8.5.3 Methyl 2-((*S*)-1-(*tert*-butoxycarbonylamino)-2-methylpropyl)-5-methyl-1H-imidazole-4-carboxylate (20):

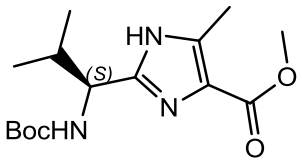

Molecular formula: $C_{15}H_{25}N_3O_4$

Molecular weight: 311.18 g/mol

20

According to known literature procedures,[67] 9 the cbz- protected imidazole building block **19** (4.03 g, 11.68 mmol) was dissolved in THF (200 ml). Then palladium hydroxide (45g) and Boc_2O (1 eq, 2.55 g, 11.70 mmol) were suspended. The reaction mixture was stirred for 1 day under a H_2-atmosphere before the mixture was filtered over celite. The solution was concentrated *in vacuo*. The crude product was dissolved in EtOAc, purified by flash chromatography with silica gel (5 x 25 cm, PE/EtOAc 2:3) and yielded the boc- protected imidazole **20** as a white foam (4.03 g, 12.95 mmol,).

^{1}H NMR: (600 MHz, $CDCl_3$): δ = 0.78 (d, 3H, $CH(C\underline{H}_3)_2$, $^3J_{H\text{-}H}$ = 5.5 Hz), 0.99 (d, 3H, $CH(C\underline{H}_3)_2$, $^3J_{H\text{-}H}$ = 5.5 Hz), 1.41 (s, 9H, $C(C\underline{H}_3)_3$), 2.40 – 2.53 (m, 1H, $C\underline{H}(CH_3)_2$), 2.49 (s, 3H, $imiC\underline{H}_3$), 3.81 (s, 3H, $CO_2C\underline{H}_3$), 4.29 (bs, 1H, Cα$\underline{H}$) ppm.

HR-DART$^+$ MS: m/z calc. for $[M+H]^+$: 312.192, $[2M+H]^+$ = 623.376, found: 312.193, 623.381.

8.5.4 Methyl-1-benzyl-2-((*S*)-1-(*tert*- butoxycarbonylamino)-2-methylpropyl)-5-methyl-imidazole-4-carboxylate (21):

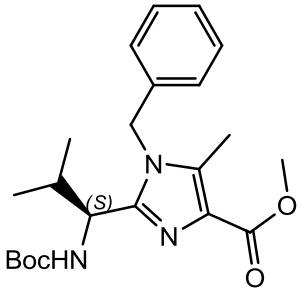

21

Molecular formula: $C_{22}H_{31}N_3O_4$

Molecular weight: 401.50 g/mol

Following known literature procedures,[67] the boc- protected imidazole building block **20** (4.03 g, 12.95 mmol) was dissolved in dry DMF (400 ml) and cooled down to 0°C. At this temperature NaH (60% dispersion in mineral oil: 1.5eq, 777g, 19.42 mmol) was suspended. Subsequently 1.5 eq. of benzyl bromide (3.33 g , 19.429 mmol) was added to the reaction mixture. Afterwards the mixture was stirred for 3h at 0°C, before it was allowed to warm up to rt. At rt the reaction mixture was stirred overnight. The next day the reaction mixture was slowly poured on Ice (1000 g). After allowing the mixture to warm up to rt the resulting solid was filtered off. The crude product was dissolved in DCM and extracted with H_2O and brine, dried over Na_2SO_4, and concentrated *in vacuo* to yield as a yellowish solid **21** (4.16 g, 10.37 mmol, 80.07%).

^{1}H NMR: (600 MHz, $CDCl_3$): δ = 0.64 (d, 3H, CH($C\underline{H}_3$)$_2$, $^3J_{H-H}$ = 6.8 Hz), 0.96 (d, 3H, CH($C\underline{H}_3$)$_2$, $^3J_{H-H}$ = 6.8 Hz), 1.38 (s, 9H, C($C\underline{H}_3$)$_3$), 2.15 – 2.25 (m, 1H, C$\underline{H}$(CH_3)$_2$), 2.45 (s, 3H, imi$C\underline{H}_3$), 3.89 (s, 3H, $CO_2C\underline{H}_3$), 4.47 (d, 1H, Cα$\underline{H}$, $^3J_{H-H}$ = 9.6Hz), 5.38 (d, 1H, Cα$\underline{H}_2$-Ph, $^3J_{H-H}$ = 5.0Hz), 7.06-7.37 (m, 5H, $C_{Ar}\underline{H}$) ppm.

HR-DART$^+$ MS: m/z calc. for $[M+H]^+$: 402.239, $[2M+H]^+$ = 804.470, found: 402.239, 804.476.

8.5.5 Methyl 2-((*S*)-1-(*tert*- butoxycarbonylamino)-2-methylpropyl)-5-methyl-imidazole-4-carboxylic acid (22):

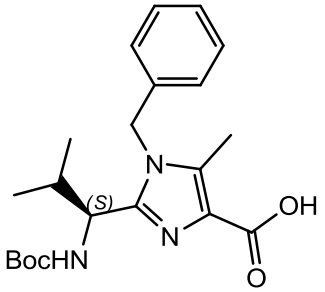

22

Molecular formula: $C_{21}H_{29}N_3O_4$

Molecular weight: 387.47 g/mol

Methyl deprotected building block **22** was prepared according to general procedure GP1 from the imidazole building block **21** (4.16 g, 10.37 mmol). Compound **22** (4.87 g, 12.57 mmol, quantitative) yielded as a white solid foam. 53 ml 2M NaOH and 126 ml of the dioxane/MeOH mixture were used.

^{1}H NMR: (600 MHz, $CDCl_3$): δ = 0.42 (d, 3H, $CH(C\underline{H}_3)_2$, $^3J_{H\text{-}H}$ = 6.8 Hz), 0.68 (d, 3H, $CH(C\underline{H}_3)_2$, $^3J_{H\text{-}H}$ = 7.1 Hz), 1.10 (s, 9H, $C(C\underline{H}_3)_3$), 2.04 – 2.10 (m, 1H, $C\underline{H}(CH_3)_2$), 2.31 (s, 3H, imi$C\underline{H}_3$), 4.14 (t, 1H, Cα$\underline{H}$, $^3J_{H\text{-}H}$ = 9.2Hz), 5.10 (s, 1H, $C\underline{H}_2$-Ph), 6.80-7.19 (m, 5H, $C_{Ar}\underline{H}$) ppm.

HR-DART$^+$ MS: m/z calc. for $[M+H]^+$: 388.223, found: 388.222.

8.5.6 Methyl 2-((*S*)-1-(1-benzyl-2-((*S*)-1- (*tert*-butoxycarbonylamino)-2-methylpropyl)-5-methyl-imidazole-4-carboxamido)-2-methylpropyl)-1.5-dimethyl-imidazole-4-carboxylate (23):

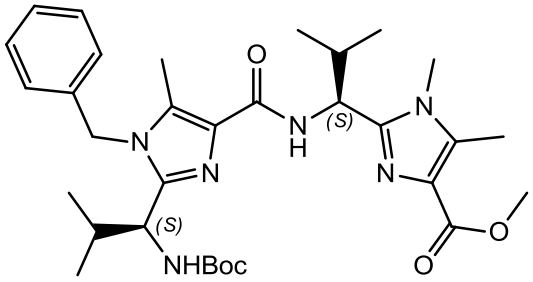

23

Molecular formula: $C_{32}H_{46}N_6O_5$

Molecular weight: 594.75 g/mol

According to general procedure GP3, the methyl deprotected building block **21** (4.87 g, 12.57 mmol) was coupled with the boc deprotected building block **5** (3.58 g, 10.61 mmol) to yield **23** (5.04 g, 8.90 mmol, 85.57%) as a yellowish foam, which was recrystallized a few times in a $CHCl_3$/MeOH mixture. Coupling was performed, using 80 ml MeCN, 4.22 g (9.85 mmol) COMU, and 40 ml EDIPA.

^{1}H NMR: (600 MHz, $CDCl_3$): δ = 0.50-0.61 (m, 3H, CH($C\underline{H}_3$)$_2$); 0.81-0.87 (m, 6H, CH($C\underline{H}_3$)$_2$); 0.91-0.97 (m, 3H, CH($C\underline{H}_3$)$_2$); 1.33 (s, 3H, C($C\underline{H}_3$)$_3$); 2.20 – 2.31 (m, 1H, imi_{Bn}-C$\underline{H}$(CH_3)$_2$), 2.44 (s, 3H, imi_{Bn}-C$\underline{H}_3$), 2.53 (s, 3H, imi-C$\underline{H}_3$), 2.62- 2.78 (s, 1H, C$\underline{H}$(CH_3)$_2$), 3.73 (s, 3H, NC$\underline{H}_3$), 3.89 (s, 3H, $CO_2C\underline{H}_3$), 4.47 (t, 1H, imi_{Bn}-Cß$\underline{H}$, $^3J_{H\text{-}H}$ = 9.1 Hz), 4.96 (t, 1H, imi-Cß$\underline{H}$, $^3J_{H\text{-}H}$ = 9.6 Hz), 5.10-5.43 (m, 2H, C$\underline{H}_2$-Ph) 6.98-7.36 (m, 5H, $C_{Ar}\underline{H}$) ppm.

HR-DART$^+$ MS: m/z calc. for $[M+H]^+$: 595.360, $[2M+H]^+$ = 1189.713, found: 595.358, 1189.704.

8.5.7 Methyl 2-((*S*)-1-(1-benzyl-2-((*S*)-1- (*tert*-butoxycarbonylamino)-2-methylpropyl)-5-methyl-imidazole-4-carboxamido)-2-methylpropyl)-1.5-dimethyl-imidazole-4--carboxylic acid (24):

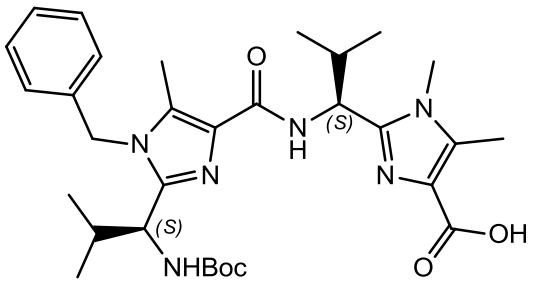

Molecular formula: $C_{31}H_{44}N_6O_5$

Molecular weight: 580.72 g/mol

24

Following to general procedure GP1, the dimeric building block **23** (8.00 g, 14.11 mmol) was converted into the yellowish solid **24** (4.76 g, 8.20 mmol, 58.04%). 2M NaOH (70 ml) and 220 ml of a dioxin/MeOH mixture were used. The crude product **25** was used without further purification.

HR-DART$^+$ MS: m/z calc. for $[M+H]^+$: 581.344, found: 581.344.

8.5.8 (*S*)-1-(4-(((*S*)-1-(4-carboxy-1,5-dimethyl-imidazol-2-yl)-2-methylpropyl)carbamoyl)-1-benzyl-5-methyl-imidazol-2-yl)-2-methylpropan-1-ammonium trifluoroacetat (25):

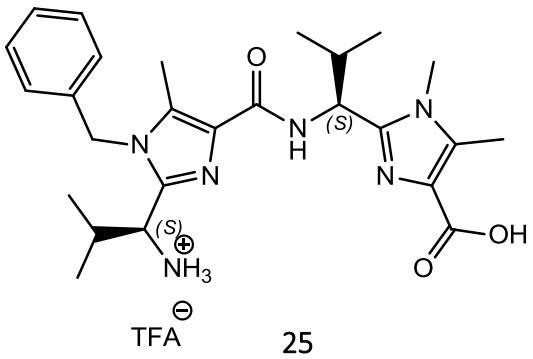

Molecular formula: $C_{28}H_{37}N_6O_4F_3$

Molecular weight: 578.63 g/mol

25

According to general procedure GP2, the methyl deprotected dimeric building block **24** (4.76 g, 8.19 mmol) was converted into **25** (4.90 g, 8.20 mmol), which is isolated as a yellowish resin. 16.36 ml TFA and 160 ml DCM were used. The crude product **25** was used without further purification.

8.5.9 H_4pat^4 (26):

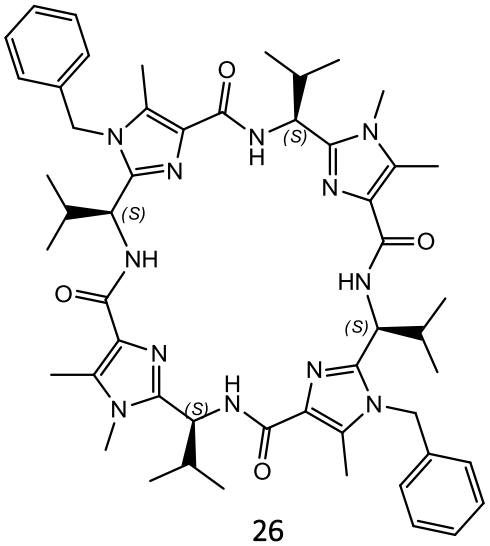

26

Molecular formula: $C_{52}H_{68}N_{12}O_4$

Molecular weight: 924.17 g/mol

The cyclic *pseudo* octapeptide H_4pat^1 **26** (900 mg, 0.93 mmol, 11.86%) was prepared from the deprotected building block **25** (4.90 g, 8.20 mmol), following general procedure GP3. After purification **26** was obtained as a white solid. Purification was done by repetitive recrystallization from a methanol/diethyl ether mixture and flash chromatography with silica gel (3 x 30 cm, EtOAc/DCM 65:35). Coupling was performed, using MeCN (30 ml), COMU (7.02 g, 16.40 mmol), and EDIPA (20 ml).

^{1}H NMR: (600 MHz, MeOD-d_4/$CDCl_3$ 3:1): δ = 0.72 (d, 6H, CH(C$\underline{H}_3$)$_2$, $^3J_{H\text{-}H}$ = 6.58 Hz); 0.87 (d, 6H, CH(C$\underline{H}_3$)$_2$, $^3J_{H\text{-}H}$ = 6.71 Hz); 1.01 (d, 6H, CH(C$\underline{H}_3$)$_2$, $^3J_{H\text{-}H}$ = 6.73 Hz); 1.12 (d, 6H, CH(C$\underline{H}_3$)$_2$, $^3J_{H\text{-}H}$ = 6.62 Hz); 2.28 (m, 2H, Bn-imi-$\underline{H}_ß$); 2.41 (s, 6H, BnN-$C_{Het}C\underline{H}_3$); 2.42 (s, 6H, CH_3N-$C_{Het}C\underline{H}_3$); 2.48-2.56 (m, 2H, CH_3-imi-$\underline{H}_ß$); 3.66 (s, 6H, NC$\underline{H}_3$); 4.89 (d, 4H, $H_α$, $^3J_{H\text{-}H}$ = 9.90 Hz); 5.37 (dd, 4H, C$\underline{H}_2$-Ph, $^2J_{H\text{-}H}$ = 16.98 Hz, $^1J_{C\text{-}H}$ = 154.65 Hz); 6.90- 6.93 (m, 4H, H_{Ph}); 7.14- 7.20 (m, 6H, H_{Ph}) ppm.

^{13}C NMR: (150 MHz, MeOD-d_4/$CDCl_3$ 3:1): δ = 10.32 (CH_3N-$C_{Het}\underline{C}H_3$); 10.35 (BnN-$C_{Het}\underline{C}H_3$); 19.80, 19,84; 19.86; 20.71 (CH($\underline{C}H_3$)$_2$); 30.99 (N$\underline{C}H_3$); 32.95 (CH_3-imi-$\underline{C}_ß$); 34.47 (Bn-imi-$\underline{C}_ß$); 47.60 ($\underline{C}H_2$-Ph); 51.02, 51.93 ($\underline{C}_α$); 127.18 ($\underline{C}_{Ph}$); 128.73 ($\underline{C}_{Ph}$); 129.94 ($\underline{C}_{Ph}$); 130.50 (CH_3N-$\underline{C}_{Het}CH_3$); 134.70 (CH_3-imi$\underline{C}_{Het}$-CO); 134.89 (Bn-imi$\underline{C}_{Het}$-CO); 137.78 (BnN-$\underline{C}_{Het}CH_3$); 148.83 (CH_3-imi$\underline{C}$=N); 149.14 (Bn-imi$\underline{C}$=N); 165.04 (CH_3-imi-$\underline{C}$O); 165.57 (CH_3-imi-$\underline{C}$O) ppm.

^{15}N NMR: (60 MHz, MeOD-d_4/$CDCl_3$ 3:1):δ = 119 ($\underline{N}$H); 167 ($\underline{N}$Bn), 177 ($\underline{N}CH_3$), 248 (C=$\underline{N}$) ppm.

HR-ESI$^+$ MS: m/z calc. for $[M+H]^+$: 926.181, $[M+Na]^+$: 947.537; found: 926.182, 947.538.

8.6 Synthesis of H_4pat^5 (27):

8.6.1 H_4pat^5 (27):

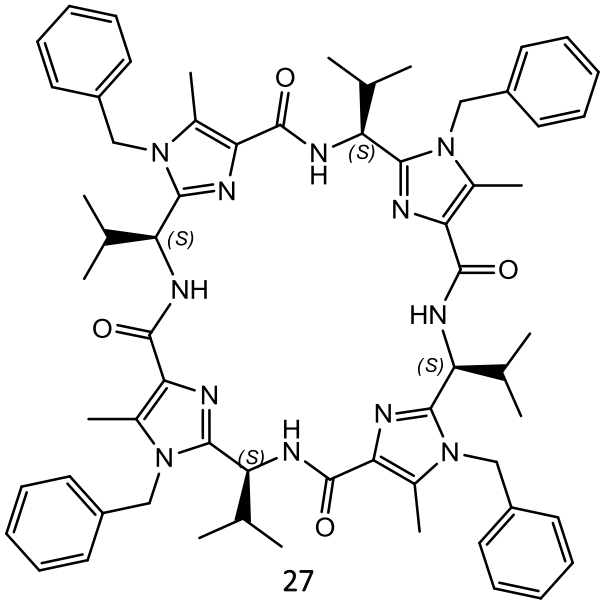

27

Molecular formula: $C_{64}H_{76}N_{12}O_4$

Molecular weight: 1077.366 g/mol

According to general procedure GP2, the methyl deprotected peptidic building block **22** (387.47mg, 1.04mmol) was boc-deprotected using TFA (6.5 ml) and DCM (70 ml) a quantitative Yield was expected, and the crude product was subsequently coupled to a tetramer as described in GP3. After purification by repetitive recrystallization from a methanol / Chloroform / diethyl ether mixture and flash chromatography with silica gel (3 x 30 cm, EtOAc/DCM 20:80) the product **27** was isolated 164.80mg (149.25µmol, 14.35%) as a white powder. Coupling was done, using MeCN (100 ml), FDPP (1.12 g, 2.93 mmol), and EDIPA (0.8 ml, 4.39 mmol).

^{1}H NMR: (600 MHz, MeOD/$CDCl_3$ 3:1): δ = 0.59 (d, 12H, CH($C\underline{H}_3$)$_2$, $^3J_{H\text{-}H}$ = 6.7 Hz); 1.01 (d, 12H, CH($C\underline{H}_3$)$_2$, $^3J_{H\text{-}H}$ = 6.7 Hz); 2.28- 2.38 (m, 4H, C$\underline{H}$(CH_3)$_2$), 2.43 (s, 12H,imiC$\underline{H}_3$), 4.86 (d, 4H, Cß$\underline{H}$, $^3J_{H\text{-}H}$ = 9.70 Hz), 5.43 (dd, 4H, C$\underline{H}_2$-Ph, $^2J_{H\text{-}H}$ = 16.92 Hz, $^1J_{C\text{-}H}$ = 184.06 Hz), 7.05-7.30 (m, 20H, Ph) ppm.

^{13}C NMR: (150 MHz,MeOD/$CDCl_3$ 3:1): δ = 9.18 ($C_{Het}\underline{C}H_3$); 18.30, 19.01 (CH($\underline{C}H_3$)$_2$); 32.08 (Cα), 46.58 ($\underline{C}H_2$-Ph); 49.98 ($\underline{C}_\alpha$); 126.178 ($\underline{C}_{Ph}$); 127.56 ($\underline{C}_{Ph}$); 128.57 ($\underline{C}_{Ph}$); 133.33 (Bn-imi$\underline{C}_{Het}$-CO); 136.28 (BnN-$\underline{C}_{Het}CH_3$); 147.77 (Bn-imi$\underline{C}$=N); 163.60 ($\underline{C}$O) ppm.

^{15}N NMR: (60 MHz, MeOD/$CDCl_3$ 3:1): δ = 118.4 ($\underline{N}$H); 177.6 ($\underline{N}$Bn), 246.9 (C=$\underline{N}$) ppm.

HR-ESI$^+$ MS: m/z calc. for $[M+H]^+$: 1077.619, $[M+Na]^+$ = 1100.608; found: 1077.620, 1100.609.

8.7 Synthesis of Phosphatase model substrate

8.7.1 Pyridinium Bis-(2,4-dinitrophhenyl) phosphate (27): [254]

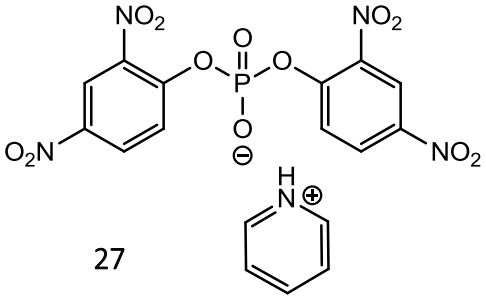

27

Molecular formula: $C_{17}H_{12}N_5O_{12}P$

Molecular weight: 509.28 g/mol

2,4-Dinitrophenol (9.80 g, 53.2 mmol, 3 eq) was dissolved in anhydrous MeCN (100 ml) under an Ar-atmosphere. After addition of anhydrous pyridine (8.6 ml, 106 mmol, 6 eq), the solution was cooled to 0°C and phosphoryl chloride (1.63 ml, 17.7 mmol, 1 eq) was added carefully. The reaction mixture was stirred for 30 minutes at 0°C before it was poured onto 100 g of ice and kept in the fridge over night. The resulting precipitate was filtered off and washed with a small amount of ice cold water. Afterwards, the crude product was recrystallized from acetone to yield BDNPP pyridinium salt **27** (7.62 g, 14.27 mmol, 80.62%) as a white crystalline solid.

Microanalysis: $C_5H_{10}ClNO_3$: calc. (%): C 40.09, H 2.37, N 13.73; found (%): C 40.03, H 2.56, N 13.74 (Report No. 36464)

^{1}H NMR: (400 MHz, Acetone - d_6): δ = 3.04 (bs, 1H, N$\underline{H}^+$); 8.11 (d, 2H, $C_{Ar}\underline{H}_{ortho}$, $^3J_{H\text{-}H}$ = 9.2 Hz); 8.23 (dd, 2H, $C_{Py}\underline{H}_{Meta}$, $^3J_{H\text{-}H}$ = 7.5 Hz, $^3J_{H\text{-}H}$ = 6.6 Hz); 8.51 (dd, 2H, $C_{Ar}\underline{H}_{Meta}$, $^3J_{H\text{-}H}$ = 9.2 Hz, $^4J_{H\text{-}H}$ = 2.8 Hz); 8.71 (d, 2H, $NO_2C\text{-}C\underline{H}\text{-}CNO_2$, $^3J_{H\text{-}H}$ = 2.8 Hz); 8.76 (dd, 1H, $C_{Py}\underline{H}_{Para}$, $^3J_{H\text{-}H}$ = 7.9 Hz, $^4J_{H\text{-}H}$ = 1.5 Hz); 9.01 (d, 2H, $C_{Py}\underline{H}_{Ortho}$, $^3J_{H\text{-}H}$ = 5.4 Hz) ppm.

^{13}C NMR: (100 MHz, Acetone - d_6): δ = 121.73 ($NO_2C_{ortho}\text{-}\underline{C}_{Ar}H$); 124.37 ($\underline{C}_{Ar}H_{ortho}$); 124.40 ($\underline{C}_{Ar}H_{Meta}$); 128.45 ($\underline{C}_{Py}H_{Meta}$); 129.29 ($\underline{C}_{Ortho}NO_2$); 143.26 ($\underline{C}_{Para}NO_2$); 143.30 ($\underline{C}_{Py}H_{Ortho}$); 147.33 ($\underline{C}_{Py}H_{Para}$); 152.15 (PO$\underline{C}$) ppm.

^{31}P NMR: (162 MHz, Acetone - d_6): δ = -14.13 ppm.

HR-ESI$^-$ MS: m/z calc. for $C_{12}H_6N_4O_{12}P^-$ 428.975, found 428.972.

9 Bibliography

(1) Van den Brenk, A. L.; Byriel, K. A.; Fairlie, D. P.; Gahan, L. R.; Hanson, G. R.; Hawkins, C. J.; Jones, A.; Kennard, C. H. L.; Moubaraki, B.; Murray, K. S. *Inorganic chemistry* **1994**, *33*, 3549.

(2) <*www.coml.org_pressreleases_census2010_PDF_German--Census Summary.pdf*>.

(3) Gerwick, W. H.; Moore, B. S. *Chemistry & biology* **2012**, *19*, 85.

(4) Banaigs, B.; Bonnard, I.; Witczak, A.; Inguimbert, N. In *Outstanding Marine Molecules*; Wiley-VCH Verlag GmbH & Co. KGaA: 2014, p 285.

(5) Petit, G. R.; Day, J. F.; Hartwell, J. L.; Wood, H. B. *Nature* **1970**, *229*.

(6) Sigel, M. M. *Food and drugs Proceedings* **1970**.

(7) Ireland, C. M.; Scheuer, P. J. *J. Am. Chem. Soc.* **1980**, *102*, 5688.

(8) Endo, M.; Nakagawa, M.; Hamamoto, Y.; Nakanishi, T. *J. Chem. Soc. Chem. Commun.* **1983**, *6*, 323.

(9) Schmidtz, F. J.; Ksebati, M. B.; Chang, J. S.; Wang, J. L.; Houssain, B.; Van der Helm, D. *J. Org. Chem.* **1989**, *54*, 3463.

(10) Hambley, T. W.; Hawkins, C. J.; Lavin, M. F.; Van den Brenk, A. L.; Watters, D. J. *Tetrahedron* **1992**, *48*, 341.

(11) Ireland, C. M.; Durso, A. M.; Newman, R. A.; Hacker, M. P. *J. Org. Chem.* **1982**, *47*, 1807.

(12) Fu, X.; Do, T.; Schmitz, F. J.; Andrusevich, V.; Engel, M. H. *J. Nat. Prod.* **1998**, *61*, 1547.

(13) Degnan, B. M.; Hawkins, C. J.; Lavin, M. F.; McCaffrey, E. J.; Parry, d. L.; Van den Brenk, A. L.; Watters, D. J. *J. Med. Chem.* **1989**, *32*, 1349.

(14) McDonald, L. A.; Ireland, C. M. *J. Nat. Prod.* **1992**, *55*, 376.

(15) Rashid, M. A.; Gustafson, K. R.; Cardellina, J. H.; Boyd, M. R. *J. Nat. Prod.* **1995**, *58*, 594.

(16) Schmidt, E. W.; Nelson, J. T.; Rasko, D. A.; Sudek, S.; Eisen, J. A.; Haygood, M. G.; Ravel, J. *Proceedings of the National Academy of Sciences of the United States of America* **2005**, *102*, 7315.

(17) Long, P. F.; Dunlap, W. C.; Battershill, C. N.; Jaspars, M. *Chembiochem : a European journal of chemical biology* 2005, *6*, 1760.

(18) Houssen, W. E.; Jaspars, M. *Chembiochem : a European journal of chemical biology* 2010, *11*, 1803.

(19) Behrendt, L.; Larkum, A. W.; Trampe, E.; Norman, A.; Sorensen, S. J.; Kuhl, M. *The ISME journal* 2012, *6*, 1222.

(20) Kwan, J. C.; Tianero, M. D.; Donia, M. S.; Wyche, T. P.; Bugni, T. S.; Schmidt, E. W. *PloS one* 2014, *9*, e95850.

(21) Donia, M. S.; Hathaway, B. J.; Sudek, S.; Haygood, M. G.; Rosovitz, M. J.; Ravel, J.; Schmidt, E. W. *Nature chemical biology* 2006, *2*, 729.

(22) Sings, H. L.; Rinehart, K. L. *J. Industrial Microbiol.* 1996, *17*, 385.

(23) Kuhl, M.; Larkum, A. W. In *Cellular origin and life in extreme habitats Vol. 3: Symbiosis, mechanisms and model systems*; Seckbach, J., Ed.; Kluwer Acad. Publ.: Dordrech, 2002, p 273.

(24) Davidson, B. S. *Chem. Rev.* 1993.

(25) Lewin, R. A. *Phycologia* 1984, *23*, 203.

(26) Maruyama, T.; Hirose, E.; Ishikura, M. *Biol. Bull.* 2003, *204*, 109.

(27) Schreiber, U.; Gademann, R.; Ralph, P. J.; Larkum, A. W. D. *Plant Cell Physiol.* 1997, 945.

(28) Donia, M. S.; Fricke, W. F.; Partensky, F.; Cox, J.; Elshahawi, S. I.; White, J. R.; Phillippy, A. M.; Schatz, M. C.; Piel, J.; Haygood, M. G.; Ravel, J.; Schmidt, E. W. *Proceedings of the National Academy of Sciences of the United States of America* 2011, *108*, E1423.

(29) Chisholm, S. W.; Frankel, S. L.; Goericke, R.; Olson, R. J.; Palenik, B.; Waterburry, J. B.; West-Johnsrud, L.; Zettler, E. R. *Arch. Microbiol.* 1992, *157*, 297.

(30) Lewin, R. A. *Photosynthesis Research* 2002, *73*, 59.

(31) Kuhl, M.; Behrendt, L.; Trampe, E.; Qvortrup, K.; Schreiber, U.; Borisov, S. M.; Klimant, I.; Larkum, A. W. *Frontiers in microbiology* 2012, *3*, 402.

(32) Rosen, M. K.; Schreiber, S. L. *Angew Chem* 1992, *31*, 384.

(33) Lewis, J. R. *Nat. Prod. Rep.* 1986.

(34) Fusetani, N.; Sugawara, T.; Matsunaga, S.; Hirota, H. *J. Am. Chem. Soc.* 1991, *113*, 7811.

(35) Abbenante, G.; March, D. R.; Bergman, D. A.; Hunt, P. A.; Garnham, B.; Dancer, R. J.; Martin, J. L.; Fairlie, D. P. *J. Am. Chem. Soc.* 1995, *117*.

(36) Chakraboty, S.; Ghosh, U. *J. Pharmacy Research* 2010, *3*, 1293.

(37) Degnan, B. M.; Hawkins, C. J.; Lavin, M. F.; McCaffrey, E. J.; Parry, D. L.; Watters, D. J. *J. Med. Chem.* 1989, *32*, 1354.

(38) Milne, B. F.; Long, P. F.; Starcevic, A.; Hranueli, D.; Jaspars, M. *Organic & biomolecular chemistry* 2006, *4*, 631.

(39) Li, Y.-M.; Milne, J. C.; Madison, L. L.; Kolter, R.; Walsh, C. T. *Science* 1996, *274*, 1188.

(40) Wipf, P.; Fritch, P. C.; Geib, S. J.; Sefler, A. M. *J. Am. Chem. Soc.* 1998, *120*, 4105.

(41) Morris, L. A.; Jaspars, M.; Kettens-Van den Bosch, J. J.; Versluis, K.; Heck, A. J. R.; Kelly, S. M.; Price, N. C. *Tetrahedron* 2001, *57*, 3185.

(42) Hirose, E.; Maruyama, T. *Endocytobiosis Cell Res.* 2004, *15*, 51.

(43) Schmidt, E. W.; Donia, M. S.; McIntosh, J. A.; Fricke, W. F.; Ravel, J. *Journal of natural products* 2012, *75*, 295.

(44) Parry, D. L. *Mar. Biol.* 1985, *87*, 219.

(45) Odinstov *Endocytobiosis Cell Res.* 1992, 253.

(46) Koike, I.; Yamamuro, M.; Pollard, P. *Marine and Freshwater Research* 1993, *44*, 173.

(47) Sudek, S., 2006.

(48) Steunou, A. S.; Jensen, S. I.; Brecht, E.; Becraft, E. D.; Bateson, M. M.; Kilian, O.; Bhaya, D.; Ward, D. M.; Peters, J. W.; Grossman, A. R.; Kuhl, M. *The ISME journal* 2008, *2*, 364.

(49) Prinsep, M. R.; Moore, R. E.; Levine, I. A.; Patterson, G. M. L. *J. Nat. Prod.* 1992, *55*, 140.

(50) Faulkner, D. J. *Nat. Prod. Rep.* 1988, *6*, 613.

(51) Lewis, J. R. *Nat. Prod. Rep.* 1989, *6*, 503.

(52) Abbenante, G.; Fairlie, D. P.; Gahan, L. R.; Hanson, G. R.; Van den Brenk, A. L.; Pierrens, G. K. *J. Am. Chem. Soc.* 1996, *118*, 10384.

(53) Hamada, Y.; Kato, S.; Shioiri, T. *Tetrahedron Letters* 1985, *26*, 3223.

(54) Hamada, Y.; Shibata, M.; Shioiri, T. *Tetrahedron Letters* 1985, *26*, 5159.

(55) Hamada, Y.; Shibata, M.; Shiori, T. *Tetrahedron Letters* 1985, *52*, 6501.

(56) Koehnke, J.; Bent, A. F.; Houssen, W. E.; Mann, G.; Jaspars, M.; Naismith, J. H. *Current opinion in structural biology* 2014, *29*, 112.

(57) Koehnke, J.; Bent, A. F.; Zollman, D.; Smith, K.; Houssen, W. E.; Zhu, X.; Mann, G.; Lebl, T.; Scharff, R.; Shirran, S.; Botting, C. H.; Jaspars, M.; Schwarz-Linek, U.; Naismith, J. H. *Angewandte Chemie* 2013, *52*, 13991.

(58) Jaspars, M. *Chemical communications* 2014, *50*, 10174.

(59) Schmidt, E. W.; Donia, M. S.; McIntosh, J. A. *J. Am. Chem. Soc.* 2010, *132*, 4089.

(60) Ikegami, F.; Murkoshi, I. *Phytochemistry* 1994, *35*, 1089.

(61) Wang, M.; Gould, S. J. *J. Org. Chem.* 1993, *58*, 5176.

(62) Schumcher, T. N. M.; Mayr, L. M.; Minor, D. L.; Milhollen, M. A.; Burgess, P. S. K. *Science* 1996, *271*, 1854.

(63) Wiesehan, K.; Willbold, D. *Chembiochem : a European journal of chemical biology* 2003, *4*, 811.

(64) Li, J.; Kuang, Y.; Gao, Y.; Du, X.; Shi, J.; Xu, B. *J Am Chem Soc* 2013, *135*, 542.

(65) Siegrist, M. S.; Whiteside, S.; Jewett, J. C.; Aditham, A.; Cava, F.; Bertozzi, C. R. *ACS chemical biology* 2013, *8*, 500.

(66) Haberhauer, G. *Tetrahedron Letters* 2008, *49*, 2421.

(67) Pintér, Á.; Haberhauer, G. *Tetrahedron* 2009, *65*, 2217.

(68) Haberhauer, G.; Oeser, T.; Rominger, F. *Chemical communications* 2004, 2044.

(69) Haberhauer, G.; Pintér, Á.; Oeser, T.; Rominger, F. *European Journal of Organic Chemistry* 2007, *2007*, 1779.

(70) Comba, P.; Dovalil, N.; Gahan, L. R.; Hanson, G. R.; Westphal, M. *Dalton transactions* 2014, *43*, 1935.

(71) Ishida, T.; In, Y.; Shinozaki, F.; Doi, M.; Yamamoto, D.; Hamada, Y.; Shioiri, T.; Kamigauchi, M.; Sugiura, M. *The Journal of Organic Chemistry* 1995, *60*, 3944.

(72) Ishida, T.; In, Y.; Fumiyoshi, S.; Doi, M.; Yamamoto, D.; Hamada, Y.; Takayuki, S.; Kamigauchi, M.; Sugiura, M. *J. Org. Chem.* 1998, *60*, 3944.

(73) In, Y.; Doi, M.; Inoue, H.; Ishida, T.; Hamada, Y.; Shioiri, T. *Chem. Pharm. Bull.* 1993, *41*, 1686.

(74) Milne, B. F.; Morris, L. A.; Jaspars, M.; Thompson, G. S. *Journal of the Chemical Society, Perkin Transactions 2* 2002, 1076.

(75) Wipf, P.; Miller, C. P. *J. Am. Chem. Soc.* 1992, *114*, 10975.

(76) In, Y.; Inoue, H.; Ishida, T.; Doi, M. *Acta Cryst.* 1994, 432.

(77) Ishida, T.; Inoue, M.; Hamada, Y.; Kato, S.; Shioiri, T. *J. Chem. Soc., Chem. Commun.* 1987, 370.

(78) Wipf, P.; Miller, C. P.; Grant, C. M. *Tetrahedron* 2000, *56*, 9143.

(79) Garcıa-Reynaga, P.; van Nieuwenze, M. S. *Org. Letters* 2008, *10*, 4621.

(80) Sayyadi, N.; Skropeta, D.; Joliffe, K. A. *Org. Letters* 2005, *7*, 5497.

(81) Van den Brenk, A. L.; Fairlie, D. P.; Hanson, G. R.; Gahan, L. R.; Hawkins, C. J.; Jones, A. *Inorganic chemistry* 1994, *33*, 2280.

(82) Van den Brenk, A. L.; Fairlie, D. P.; Gahan, L. R.; Hanson, G. R.; Hambley, T. W. *Inorganic chemistry* 1996, *35*, 1095.

(83) Comba, P.; Cusack, R. M.; Fairlie, D. P.; Hanson, G. R.; Gahan, L. R.; Kazmaier, U.; Ramlow, A. *Inorganic chemistry* 1998, *37*, 6721.

(84) Comba, P.; Fairlie, D. P.; Hanson, G. R.; Gahan, L. R.; Lötzbeyer, L. *Chem. Eur. J.* 2002, *8*, 1527.

(85) Comba, P.; Dovalil, N.; Gahan, L. R.; Haberhauer, G.; Hanson, G. R.; Noble, C. J.; Seibold, B.; Vadivelu, P. *Chemistry* 2012, *18*, 2578.

(86) Kustin, K.; Macare, I. G.; McLeod, G. C. *Comp. Biochem. Physiol.* 1979, *63B*, 299.

(87) Rehder, D.; Woolins, D., Crabtree, B., Atwood, D., Meyer, G., Eds.; Wiley: 2008.

(88) Jaspars, M.; Morris, L. A. *RSC Special Publication* 2000, 140.

(89) Pattenden, G.; Michael, J. P. *Angewandte Chemie* 1993, *32*, 1.

(90) Boitel, F.; Truchot, J. P. *Marine Biol.* 1989, *103*, 495.

(91) Cusack, R. M.; Groendahl, L.; Abbenante, G.; Fairlie, D. P.; Gahan, L. R.; Hanson, G. R.; Hambley, T. W. *J. Chem. Soc. Perkin Trans 2* 2000, 323.

(92) Grøndahl, L.; Sokolenko, N.; Abbenante, G.; Fairlie, D. P.; Hanson, G. R.; Gahan, L. R. *Journal of the Chemical Society, Dalton Transactions* 1999, 1227.

(93) Cusack, R. M.; Grøndahl, L.; Fairlie, D. P.; Gahan, L. R.; Hanson, G. R. *Journal of the Chemical Society, Perkin Transactions 2* 2002, 556.

(94) Morris, L. A.; Milne, B. F.; Thompson, G. S.; Jaspars, M. *Journal of the Chemical Society, Perkin Transactions 2* 2002, 1072.

(95) Freeman, D. J.; Pattenden, G.; Drake, A. F.; Siligardi, G. *J. Chem. Soc. Perkin Trans 2* 1998, *1*, 129.

(96) Wipf, P.; Venkatraman, S.; Miller, C. P.; Geib, S. J. *Angewandte Chemie* 1994, *33*, 1516.

(97) Bertram, A.; Pattenden, G. *Natural product reports* 2007, *24*, 18.

(98) van den Brenk, A. L.; Tyndall, J. D.; Cusack, R. M.; Jones, A.; Fairlie, D. P.; Gahan, L. R.; Hanson, G. R. *Journal of inorganic biochemistry* 2004, *98*, 1857.

(99) Comba, P.; Dovalil, N.; Hanson, G. R.; Linti, G. *Inorganic chemistry* 2011, *50*, 5165.

(100) Seibold, B., 2008.

(101) Dovalil, N., 2010.

(102) Martin, B.; Parcell, A. *J. Am. Chem. Soc.* 1961, *83*, 4830.

(103) Martin, R. B.; Hedrick, R. I.; Parcell, A. *J. Am. Chem. Soc.* 1964, *29*, 3197.

(104) Martin, B.; Parcell, A. *J. Am. Chem. Soc.* 1961, *83*, 4835.

(105) Comba, P.; Gahan, L. R.; Haberhauer, G.; Hanson, G. R.; Noble, C. J.; Seibold, B.; van den Brenk, A. L. *Chem. Eur. J.* 2008, *14*, 4393.

(106) Comba, P.; Dovalil, N.; Haberhauer, G.; Kowski, K.; Mehrkens, N.; Westphal, M. *Zeitschrift für anorganische und allgemeine Chemie* 2013, *639*, 1395.

(107) Westphal, M., 2013.

(108) Parson, E. A. *Science* 1998, *282*, 1053.

(109) Yin, X.; Moss, J. R. *Coordination Chemistry Reviews* 1999, *181*, 27.

(110) Phan, D. T.; Burns, R. C.; Puxty, G.; Williams, M.; Haritos, V. S.; Maeder, M. *International Journal of Greenhouse Gas Control* 2015, *37*, 85.

(111) Comba, P.; Gahan, L. R.; Hanson, G. R.; Maeder, M.; Westphal, M. *Dalton transactions* 2014, *43*, 3144.

(112) Comba, P.; Gahan, L. R.; Hanson, G. R.; Westphal, M. *Chemical communications* 2012, *48*, 9364.

(113) Haberhauer, G.; Rominger, F. *European Journal of Organic Chemistry* 2003, *2003*, 3209.

(114) Haberhauer, G.; Rominger, F. *Tetrahedron* 2002, *43*, 6335.

(115) Kremer, B. P.; Pardy, R.; Lewin, R. A. *Phycologia* 1982, *21*, 258.

(116) Latifi, R.; Bagherzadeh, M.; Milne, B. F.; Jaspars, M.; de Visser, S. P. *Journal of inorganic biochemistry* 2008, *102*, 2171.

(117) Eisenschmidt, A. *unpublished results* 2015.

(118) Kaim, W.; Schwederski, B. *Bioanorganische Chemie*; Vieweg+Teubner Verlag, 2005; Vol. 4.

(119) Labuda, J.; Plaskoň, V.; Pavlishchuk, V. V. *Inorganica Chimica Acta* 1988, *146*, 13.

(120) Pavlishchuk, V. V.; Addison, A. W. *Inorganica Chimica Acta* 2000, *298*, 97.

(121) Rorabacher, D. B. *Chem. Rev.* 2004, *104*, 651.

(122) Zanello, P.; Casella, L.; Gullotti, M.; Pallanzer, G.; Laschi, F. *Polyhedron* 1990, *9*.

(123) Gullotti, M.; Casella, L.; Pintar, A.; Suardi, E.; Zanello, P.; Mangani, S. *Journal of the Chemical Society, Dalton Transactions* 1989, 1979.

(124) Ambundo, E. A.; Deydier, M.-V.; Grall, A. J.; Aguera-Vega, N.; Dressel, L. T.; Cooper, T. H.; Heeg, M. J.; Ochrymowycz, L. A.; Rorabacher, D. B. *Inorganic chemistry* 1999, *38*, 4233.

(125) Reim, J.; Krebs, B. *J. Chem. Soc., Dalton Trans.* 1997, 3793.

(126) Scarpellini, M.; Neves, A.; Horner, R.; Bortoluzzi, A. J.; Szpoganics, B.; Zucco, C.; Nome, S. R. A.; Drago, V.; Mangrich, A. S.; Ortiz, W. A.; Passos, W. A. C.; de, O. M. C. B.; Terenzi, H. *Inorganic chemistry* 2003, *42*, 8353.

(127) Casella, L.; Carugo, O.; Gullotti, M.; Garofani, S.; Zanello, P. *Inorg. Chem.* 1993, *32*, 2056.

(128) Koval, I. A.; Selmeczi, K.; Belle, C.; Philouze, C.; Saint-Aman, E.; Gautier-Luneau, I.; Schuitema, A. M.; van Vliet, M.; Gamez, P.; Roubeau, O.; Luken, M.; Krebs, B.; Lutz, M.; Spek, A. L.; Pierre, J. L.; Reedijk, J. *Chemistry* 2006, *12*, 6138.

(129) Koval, I. A.; Gamez, P.; Belle, C.; Selmeczi, K.; Reedijk, J. *Chem. Soc. Rev.* 2006, *35*, 814.

(130) Yoon, J.; Solomon, E. I. *Biol. Magn. Reson.* 2009, *28*, 471.

(131) Solomon, E. I.; Chen, P.; Metz, M.; Lee, S.-K.; Palmer, A. E. *Angew. Chem., Int. Ed.* 2001, *40*, 4570.

(132) Decker, H.; Schweikardt, T.; Tuczek, F. *Angew. Chem., Int. Ed.* 2006, *45*, 4546.

(133) Kitajima, N.; Moro-oka, Y. *Chem. Rev. (Washington, D. C.)* 1994, *94*, 737.

(134) Matoba, Y.; Kumagai, T.; Yamamoto, A.; Yoshitsu, H.; Sugiyama, M. *J. Biol. Chem.* 2006, *281*, 8981.

(135) Solomon, E. I.; Sundaram, U. M.; Machonkin, T. E. *Chem. Rev. (Washington, D. C.)* 1996, *96*, 2563.

(136) Inoue, T.; Shiota, Y.; Yoshizawa, K. *J. Am. Chem. Soc.* 2008, *30*, 16890.

(137) Rolff, M.; Schottenheim, J.; Decker, H.; Tuczek, F. *Chemical Society reviews* 2011, *40*, 4077.

(138) Monzani, E.; Battaini, G.; Perotti, A.; Casella, L.; Gullotti, M.; Santagostini, L.; Nardin, G.; Randaccio, L.; Geremia, S.; Zanello, P.; Opromolla, G. *Inorg. Chem.* 1999, *38*, 5359.

(139) Selmeczi, K.; Réglier, M.; Giorgi, M.; Speier, G. *Coordination Chemistry Reviews* 2003, *245*, 191.

(140) Csay, T.; Kripli, B.; Giorgi, M.; Kaizer, J.; Speier, G. *Inorg. Chem. Commun.* 2010, *13*, 227.

(141) Reglier, M.; Jorand, C.; Waegell, B. *J. Chem. Soc., Chem. Commun.* 1990, 1752.

(142) Santagostini, L.; Gullotti, M.; Monzani, E.; Casella, L.; Dillinger, R.; Tuczek, F. *Chem. - Eur. J.* 2000, *6*, 519.

(143) Koval, C. A.; Van der Schilden, K.; Schuitema, A. M.; Gamez, P.; Belle, C.; Pierre, J. L.; Lueken, M.; Krebs, B.; Roubeau, O.; Reedijk, J. *Inorganic chemistry* 2005, *44*, 4372.

(144) Halvagar, M. R.; Solntsev, P. V.; Lim, H.; Hedman, B.; Hodgson, K. O.; Solomon, E. I.; Cramer, C. J.; Tolman, W. B. *J Am Chem Soc* 2014, *136*, 7269.

(145) Hanson, G. R.; Gates, K. E.; Noble, C. J.; Griffin, M.; Mitchell, A.; Benson, S. *Journal of inorganic biochemistry* 2004, *98*, 903.

(146) Hanson, G. R.; Biospin, B., Ed.; Bruker Biospin: Germany, Switzerland, France, United States, 2007.

(147) Vahrenkamp, H. *Dalton transactions* 2007, 4751.

(148) Mancin, F.; Tecilla, P. *New Journal of Chemistry* 2007, *31*, 800.

(149) Parkin, G. *Chem. Rev.* 2004, *104*, 699.

(150) Vahrenkamp, H. *CiuZ* 1988, *22*, 72.

(151) Auld, D. S. In *Encyclopedia of Inorganic Chemistry*; Wiley, Ed. 2007, p 5885.

(152) Brookhaven, Ed. 2007.

(153) Harding, M. M. *Acta Cryst.* 1999, *D55*, 1423.

(154) Harding, M. M. *Acta Cryst.* 2000, *D56*, 857.

(155) Harding, M. M. *Acta Cryst.* 2000, *D57*, 401.

(156) Wilcox, D. E. *Inorganica Chimica Acta* 2008, *361*, 857.

(157) Lipscomb, W. N. *Angew Chem* 1996, *35*, 2024.

(158) Lipscomb, W. N.; Lewis, M.; Rees, D. C. *J. Mol. Biol.* 1983, *186*, 367.

(159) Kimura, E. *JBIC* 2000, *5*, 139.

(160) Kimura, E.; Koike, T.; Shionoya, M. In *From Structure and Bonding* Berlin, 1997.

(161) Angel, N. Z.; Walsh, N.; Forwood, M. R.; Ostrowski, M. C.; Cassady, A. I.; Hume, D. A. *Journal of Bone and Mineral Research* 2000, *15*, 103.

(162) Nuttelman, P. R.; Roberts, R. M. *The Journal of biological chemistry* 1990, *265*, 12192.

(163) Kaija, H.; Alatalo, S. L.; Halleen, J. M.; Lindqvist, Y.; Schneider, G.; Vaananen, H. K.; Vihko, P. *Biochemical and biophysical research communications* 2002, *292*, 128.

(164) Boone, C. D.; Habibzadegan, A.; Tu, C.; Silverman, D. N.; McKenna, R. *Acta Crystallographica Section D Biological Crystallography* 2013, *69*, 1414.

(165) Vahrenkamp, H. *Accounts of Chemical Research* 1999, *32*, 589.

(166) Avvaru, B. S.; Kim, C. U.; Sippel, K. H.; Gruner, S. M.; Agbandje-McKenna, M.; Silverman, D. N.; McKenna, R. *Biochemistry* 2010, *49*, 249.

(167) Carfi, A.; Pares, S.; Duee, E.; Galleni, M.; Duez, C.; Frere, J. M.; Dideber, O. *The EMBO journal* 1995, *14*, 4914.

(168) Millan, J. L. *Purinergic signalling* 2006, *2*, 335.

(169) Liao, R.-Z.; Yu, J.-G.; Himo, F. *Inorganic chemistry* 2010, *49*, 6883.

(170) Lindskog, S.; Coleman, J. E. *Proceedings of the National Academy of Sciences of the United States of America* 1973, *70*, 2505.

(171) Eriksson, E.; Jones, A.; Liljas, A. *Proteins: Structur, Function and Genetics* 1988, *4*, 274.

(172) Domsic, J. F.; Avvaru, B. S.; Kim, C. U.; Gruner, S. M.; Agbandje-McKenna, M.; Silverman, D. N.; McKenna, R. *The Journal of biological chemistry* 2008, *283*, 30766.

(173) Merz, K. M.; Banci, L. *J. Am. Chem. Soc.* 1997, *119*, 863.

(174) Braeuer, M.; Perez-Lustres, L.; Weston, J.; Anders, E. *Inorganic chemistry* 2002, *41*, 1454.

(175) Kimura, E. *Accounts of Chemical Research* 2001, *34*, 171.

(176) Hartmann, M.; Van Eldik, R.; Clark, T. *J. Am. Chem. Soc.* 1997, *119*.

(177) Leitner, W. *Coordination Chemistry Reviews* 1996, *153*, 257.

(178) Kitajima, N.; Hikichi, S.; Tanaka, M.; Moro-oka, Y. *J. Am. Chem. Soc.* 1993, *115*, 5496.

(179) Sola, M.; Lledos, A.; Duran, M.; Bertran, J. *J. Am. Chem. Soc.* 1992, *114*, 869.

(180) Bazzicalupi, C.; Bencini, A.; Bencini, A.; Bianchi, A.; Corana, F.; Fusi, V.; Giorgi, C.; Paoli, P.; Paoletti, P.; Valtancoli, B.; Zanchini, C. *Inorganic chemistry* 1996, *35*, 5540.

(181) Escuer, A.; Mautner, F. A.; Penalba, E.; Vicente, R. *Inorganic chemistry* 1998, *37*, 4190.

(182) Chen, J. M.; Wei, W.; Feng, X. L.; Lu, T. B. *Chemistry, an Asian journal* 2007, *2*, 710.

(183) Klabunde, T.; Sträter, N.; Fröhlich, R.; Witzel, H.; Krebs, B. *J. Mol. Biol.* 1996, *259*, 737.

(184) Mareque Rivas, J. C.; Prabaharan, R.; Parsons, S. *Dalton transactions* 2004, 1648.

(185) Schenk, G.; Elliott, T. W.; Leung, E.; Carrington, L. E.; Mitic, N.; Gahan, L. R.; Guddat, L. W. *BMC structural biology* 2008, *8*, 6.

(186) Mitic, N.; Hadler, K. S.; Gahan, L. R.; Hengge, A. C.; Schenk, G. *J. Am. Chem. Soc.* 2010, *132*, 7049.

(187) Bosch, S., 2015.

(188) Mareque-Rivas, J. C.; Prabaharan, R.; de Rosales, R. T. *Chemical communications* 2004, 76.

(189) Desbouis, D.; Troitsky, I. P.; Belousoff, M. J.; Spiccia, L.; Graham, B. *Coordination Chemistry Reviews* 2012, *256*, 897.

(190) Bertini, I.; Luchinat, C.; Rosi, M.; Sgamellotti, A.; Tarantellilc, F. *Inorganic chemistry* 1990, *29*, 1460.

(191) Kimura, E.; Shiota, T.; Koike, T.; Shiro, M.; Kodama, M. *J. Am. Chem. Soc.* 1990, *112*, 5805.

(192) Woolley, P. *Nature* 1975, *258*, 677.

(193) Woolley, P. *J. Chem. Soc. Perkin Trans 2* 1977, 318.

(194) Zompa, L. J. *Inorganic chemistry* 1978, 2513.

(195) Kodama, M.; Kimura, E. *Dalton transactions* 1977, 2269.

(196) Kimura, E.; Koike, T. *Journal of the American Chemical Society* 1991, *113*, 8935.

(197) Canary, J. W.; Chiu, Y.-H. *Inorganic chemistry* 2003, *42*, 5107.

(198) Ibrahim, M. M.; Shimomura, N.; Ichikawa, K.; Shiro, M. *inorganica Chimica Acta* 2001, *313*, 125.

(199) Ichikawa, K.; Tarnai, M.; Uddin, M. K.; Nakata, K.; Sato, S. *JBIC* 2002, *91*, 437.

(200) Ibrahim, M. M.; Mersal, G. A. *Journal of inorganic biochemistry* 2010, *104*, 1195.

(201) Komiyama, M.; Ishikubo, A.; Yashiro, M. *J. Chem. Soc. Chem. Commun.* 1995, 1793.

(202) Kimura, E. *curr. opin. chem. biol.* 2000, *4*.

(203) Weston, J. *Chem. Rev.* 2005, *105*, 2151.

(204) Mitic, N.; Smith, S. J.; Neves, A.; Guddat, L. W.; Gahan, L. R.; Schenk, G. *Chem. Rev.* 2006, *106*, 3338.

(205) Jarenmark, M.; Csapo, E.; Singh, J.; Wockel, S.; Farkas, E.; Meyer, F.; Haukka, M.; Nordlander, E. *Dalton transactions* 2010, *39*, 8183.

(206) Schenk, G.; Mitić, N.; Hanson, G. R.; Comba, P. *Coordination Chemistry Reviews* 2013, *257*, 473.

(207) Schepers, K.; Bremer, B.; Krebs, B.; Henkel, G.; Althaus, E.; Mosel, B.; Müller-Warmuth, W. *Angew Chem* 1990, *102*, 582.

(208) Gahan, L. R.; Smith, S. J.; Neves, A.; Schenk, G. *European Journal of Inorganic Chemistry* 2009, *2009*, 2745.

(209) Neves, A.; Lanznaster, M.; Bortoluzzi, A. J.; Peralta, R. A.; Casellato, A.; Castellano, E.; Herrald, E.; Riley, M. J.; Schenk, G. *J. Am. Chem. Soc.* 2007, *129*, 7486.

(210) Horn, A.; Vencato, I.; Bortoluzzi, A. J.; Hörner, R.; Silva, R. A. N.; Spoganicz, B.; Drago, V.; Terenzi, H.; de Oliveira, M. C. B.; Werner, R.; Haase, W.; Neves, A. *Inorganica Chimica Acta* 2005, *358*, 339.

(211) Karsten, P.; Neves, A.; Bortoluzzi, A. J.; Lanznaster, M.; Drago, V. *Inorganic chemistry* 2002, *41*, 4624.

(212) Lanznaster, M.; Neves, A.; Bortoluzzi, A. J.; Szoganicz, B.; Schwingel, E. *Inorganic chemistry* 2002, *41*, 5641.

(213) Neves, A.; Aires de Brito, M.; Drago, V.; Griesar, K.; Haase, W. *inorganica Chimica Acta* 1995, 131.

(214) Than, R.; Feldmann, A. A.; Krebs, B. *Coordination Chemistry Reviews* 1999, *182*, 211.

(215) Albedyhl, S.; Averbuch-Pouchot, M.-T.; Belle, C.; Krebs, B.; Pierre, J. L.; Saint-Aman, E.; Torelli, S. *Eur. J. Inorg Chem* 2001, 1457.

(216) Jarenmark, M.; Carlsson, H.; Nordlander, E. *Comptes Rendus Chimie* 2007, *10*, 433.

(217) Belle, C.; Pierre, J.-L. *European Journal of Inorganic Chemistry* 2003, *2003*, 4137.

(218) Bosch, S.; Comba, P.; Gahan, L. R.; Schenk, G. *Inorganic chemistry* 2014, *53*, 9036.

(219) Schroeder, G. K.; Lad, C.; Wyman, P.; Williams, N. H.; Wolfenden, R. *Proceedings of the National Academy of Sciences of the United States of America* 2006, *103*, 4052.

(220) Coleman, J. E. *Annual review of biophysics and biomolecular structure* 1992, *21*, 441.

(221) Kim, E. E.; Wyckoff, H. W. *J. Mol. Biol.* 1991, *218*, 449.

(222) Oddie, G. W.; Schenk, G.; Angel, N. Z.; Walsh, N.; Guddat, L. W.; de Jersey, J.; Cassady, A. I.; Hamillton, S.; Hume, D. A. *Bone* 2000, *27*, 575.

(223) Doi, K.; McCracken, J.; Peisach, J.; Aisen, P. *J. Biol. Chem.* 1988, *263*, 5757.

(224) Yang, Y.-S.; McCormick, J.; Solomon, E. I. *119* 1997, 11832.

(225) Antanaitis, B. C.; Aisen, P.; Lilienthal, H. R. *J. Biol. Chem.* 1983, *258*, 3166.

(226) Valizadeh, M.; Schenk, G.; Nash, K.; Oddie, G. W.; Guddat, L. W.; Hume, D. A.; de Jersey, J.; Burke, T. R., Jr.; Hamilton, S. *Archives of biochemistry and biophysics* 2004, *424*, 154.

(227) Raisanen, S. R.; Alatalo, S. L.; Ylipahkala, H.; Halleen, J. M.; Cassady, A. I.; Hume, D. A.; Vaananen, H. K. *Biochemical and biophysical research communications* 2005, *331*, 120.

(228) Twichett, M. B.; Sykes, A. G. *Eur. J. Inorg Chem* 1999, 2105.

(229) Schenk, G.; Ge, Y.; Carrington, L. E.; Wynne, C. J.; Searle, E. R.; Carroll, B. J.; Hamillton, S.; de Jersey, J. *Archives of biochemistry and biophysics* 1999, *370*, 183.

(230) Schenk, G.; Boutchard, C. L.; Carrington, L. E.; Noble, C. J.; Moubaraki, B.; Murray, K. S.; de Jersey, J.; Hanson, G. R.; Hamilton, S. *The Journal of biological chemistry* 2001, *276*, 19084.

(231) Nakazato, H.; Okamoto, T.; Nishikoori, M.; Washio, K.; Morita, N.; Haraguchi, K.; Thompson, G. S.; Okuyama, H. *Plant. Physiol.* 1988, *118*, 1015.

(232) Durmus, A.; Eicken, C.; Sift, B. H.; Kratel, A.; Kappl, R.; Huttermann, J.; Krebs, B. *Eur. J. Biochem.* 1999, *260*, 709.

(233) Zajaczkowski-Fischer, M., 2010.

(234) Chen, A.; Wadso, I. *J Biochem Biophys Methods* 1982, *6*, 307.

(235) Creagh, A. L.; Tiong, J. W. C.; Tian, M. M.; Haynes, C. A.; Jefferies, W. A. *J. Biol. Chem.* 2005, *280*, 15735.

(236) Spink, C.; Wadso, I. *Methods Biochem. Anal.* 1976, *23*, 1.

(237) Wiseman, T.; Williston, S.; Brandts, J. F.; Lin, L. N. *Anal. Biochem.* 1989, *179*, 131.

(238)

(239) Kano, K.; Kondo, M.; Inoue, H.; Kitagishi, H.; Colasson, B.; Reinaud, O. *Inorganic chemistry* 2011, *50*, 6353.

(240) Kuritani, M.; Tashiro, S.; Shionoya, M. *Inorganic chemistry* 2012, *51*, 1508.

(241) Ohtsu, H.; Shimazaki, Y.; Odani, A.; Yamauchi, O.; Mori, W.; Itoh, S.; Fukuzumi, S. *J. Am. Chem. Soc.* 2000, *122*, 5733.

(242) Shangpung, S.; Kumar, A.; Asthana, M.; Dey, A. K.; Kurbah, S. D.; Basumatary, D.; Lal, R. A. *Inorganic Chemistry Communications* 2015, *58*, 48.

(243) Daumann, L. J.; Schenk, G.; Ollis, D. L.; Gahan, L. R. *Dalton transactions* 2014, *43*, 910.

(244) McLoughlin, S. Y.; Jackson, C.; Liu, J.-W.; Ollis, D. L. *Appl. Environ. Microbiol.* 2004, *70*, 404.

(245) Ghanem, E.; Li, Y.; Xu, C.; Raushel, F. M. *Biochemistry* 2007, *46*, 9032.

(246) Segel, I. H.; Wiley-interscience: New York, 1975.

(247) Kantacha, A.; Buchholz, R.; Smith, S. J.; Schenk, G.; Gahan, L. R. *Journal of biological inorganic chemistry : JBIC : a publication of the Society of Biological Inorganic Chemistry* 2011, *16*, 25.

(248) Baes, C. F.; Mesmer, R. E. *The hydrolysis of cations*; Wiley: New York, 1976.

(249) Richens, D. T. *The chemistry of aqua ions: synthesis, structure and reactivity; a tour through the periodic table of elements*; Wiley: Chichester, 1997.

(250) Daumann, L. J.; Gahan, L. R.; Comba, P.; Schenk, G. *Inorganic chemistry* 2012, *51*, 7669.

(251) Daumann, L. J.; Marty, L.; Schenk, G.; Gahan, L. R. *Dalton transactions* 2013, *42*, 9574.

(252) El-Faham, A.; Albericio, F. *Journal of peptide science : an official publication of the European Peptide Society* 2010, *16*, 6.

(253) Singh, J.; Gordon, T. D.; Earley, W. G.; Morgan, B. A. *tetrahedron Letters* 1993, *34*, 211.

(254) Bunton, C. A.; Farber, S. J. *J. Org. Chem.* 1969, *34*.

10 Appendix

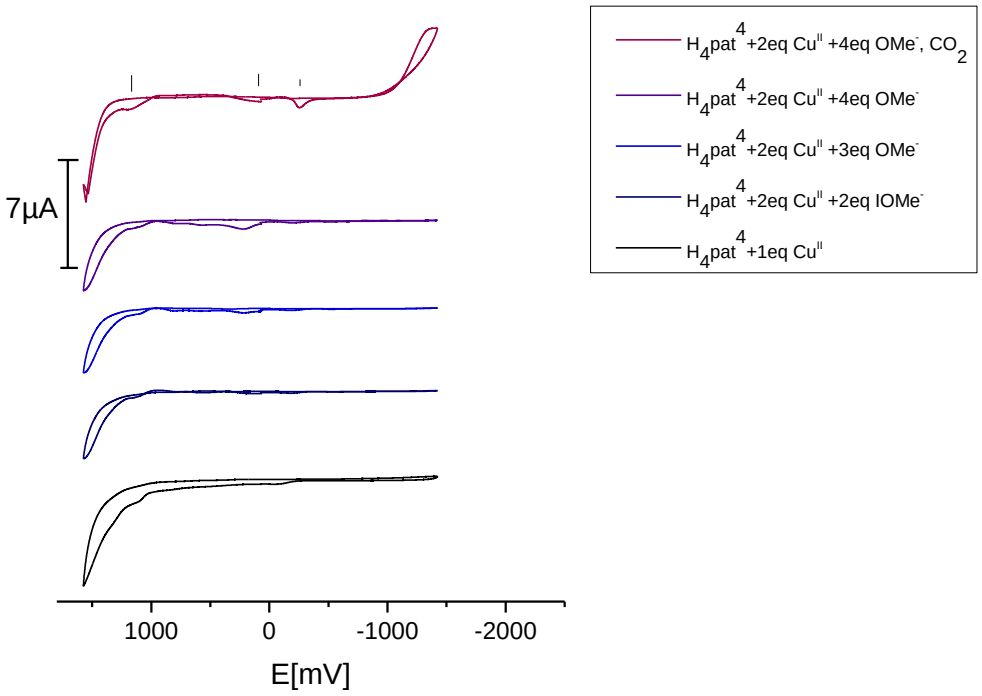

Figure A.1: CV traces for selected copper(II) complexation-steps of H_4pat^4 (0.1mM in methanol with 0.1M (tBu)$_4$NPF$_6$ and vs. Fc/Fc$^+$ at 25°C).

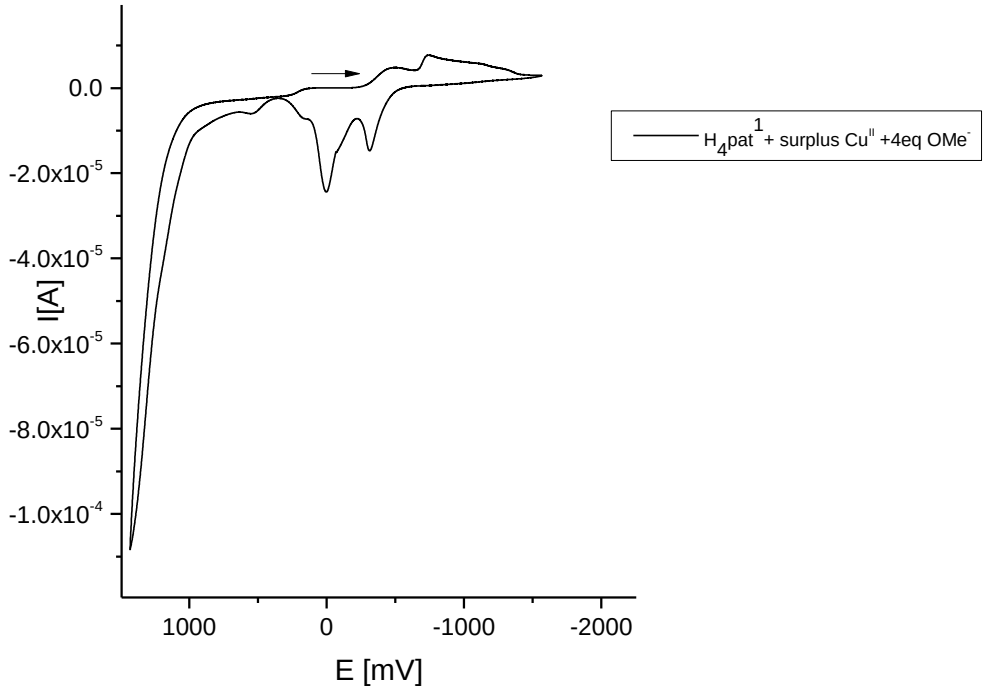

Figure A.2: CV of a selected copper(II) complexation-step of H_4pat^1 (1mM in methanol with 0.1M $(tBu)_4NPF_6$ and vs. Fc/Fc^+, 100 mV/s, $Ag/AgNO_3$ 0.01M,at 25°C).

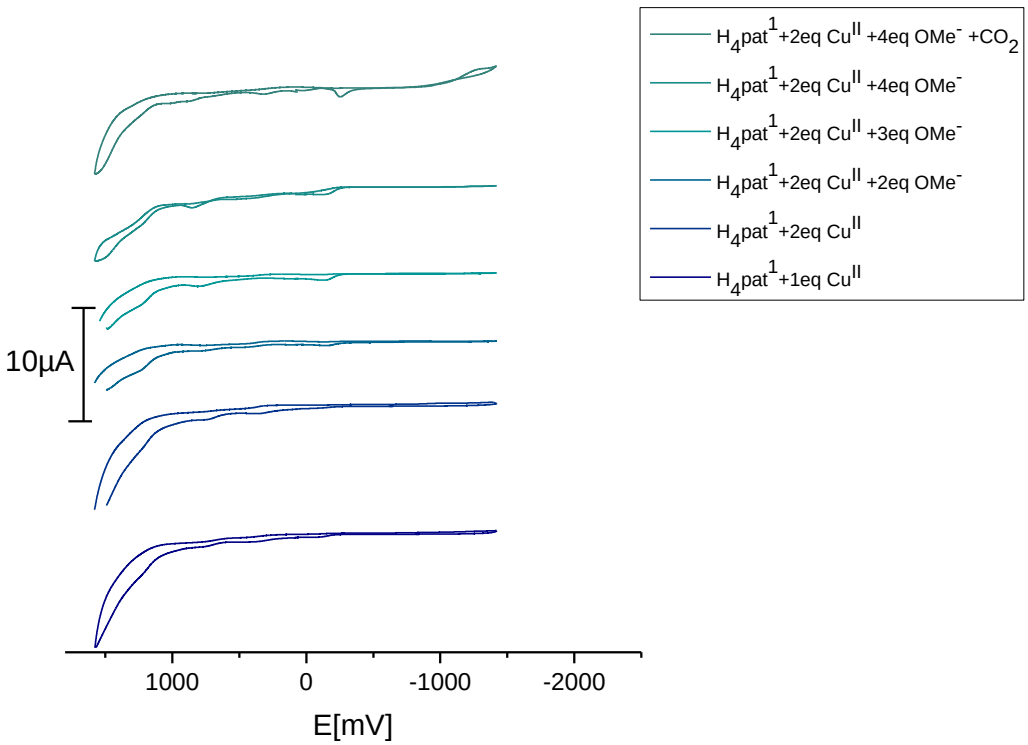

Figure A.3: CV of selected copper(II) complexation-steps of H_4pat^1 (0.1mM in methanol with 0.1M $(tBu)_4NPF_6$ and vs. Fc/Fc^+, 100 mV/s, $Ag/AgNO_3$ 0.01M,at 25°C).

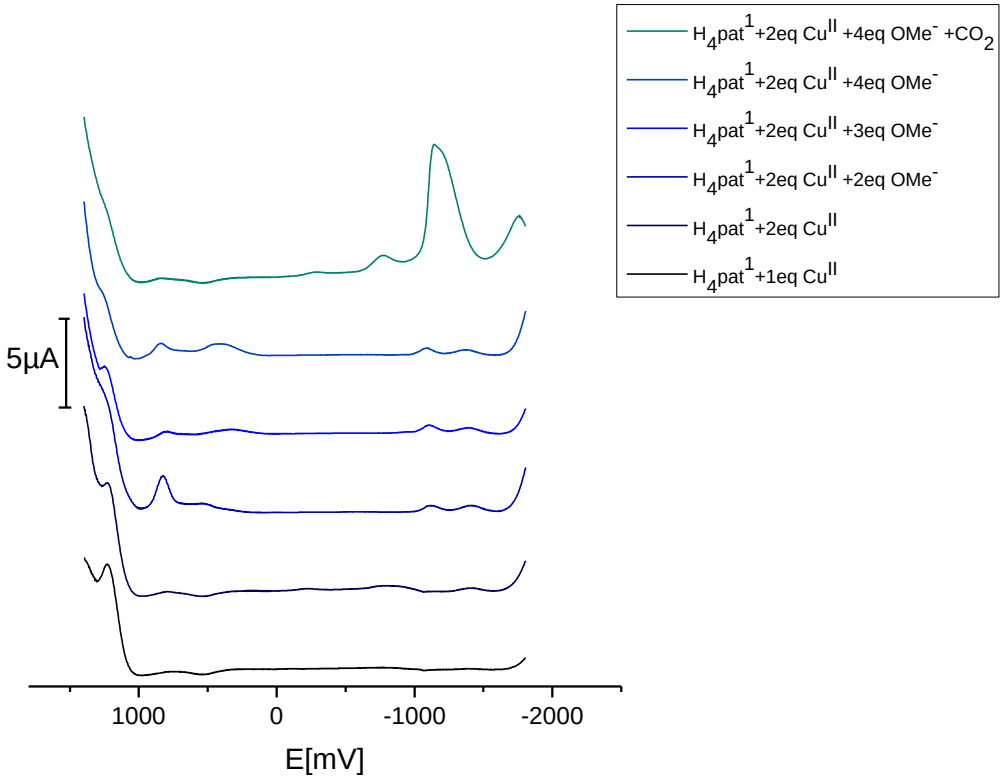

Figure A 4: SQW overlays for selected copper(II) complexation-steps of H_4pat^1 (0.1mM in methanol with 0.1M (tBu)$_4NPF_6$ and vs. Fc/Fc^+, 100 mV/s, $Ag/AgNO_3$ 0.01M,at 25°C).

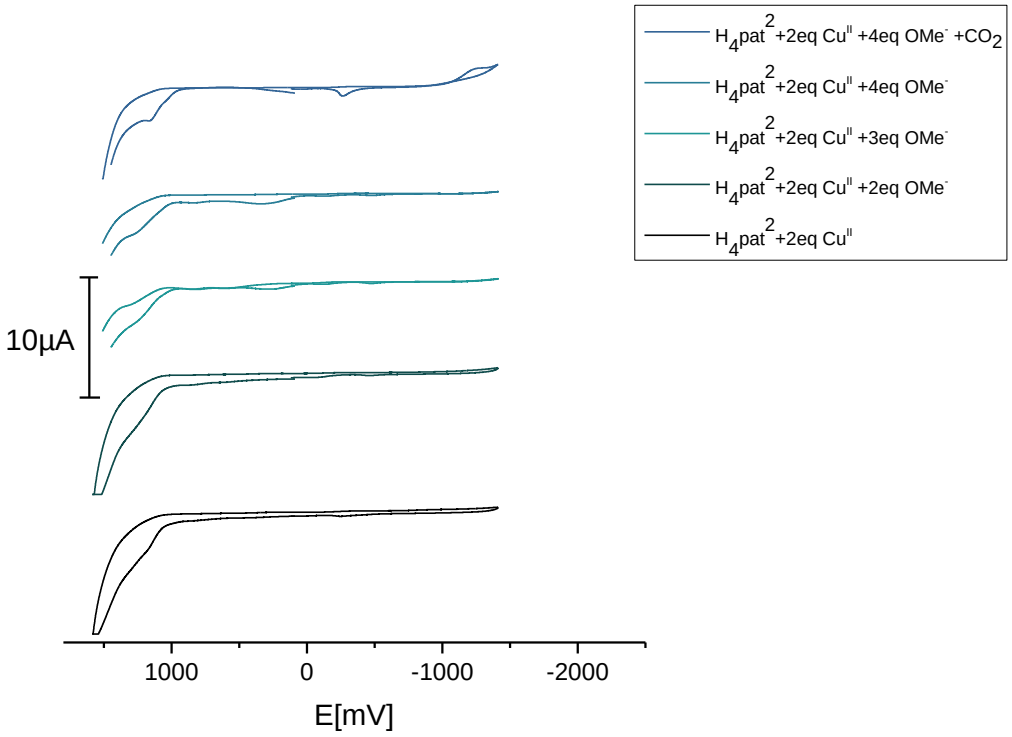

Figure A.5: CV of selected copper(II) complexation-steps of H_4pat^2 (0.1mM in methanol with 0.1M $(t\text{Bu})_4NPF_6$ and vs. Fc/Fc^+, 100 mV/s, $Ag/AgNO_3$ 0.01M,at 25°C).

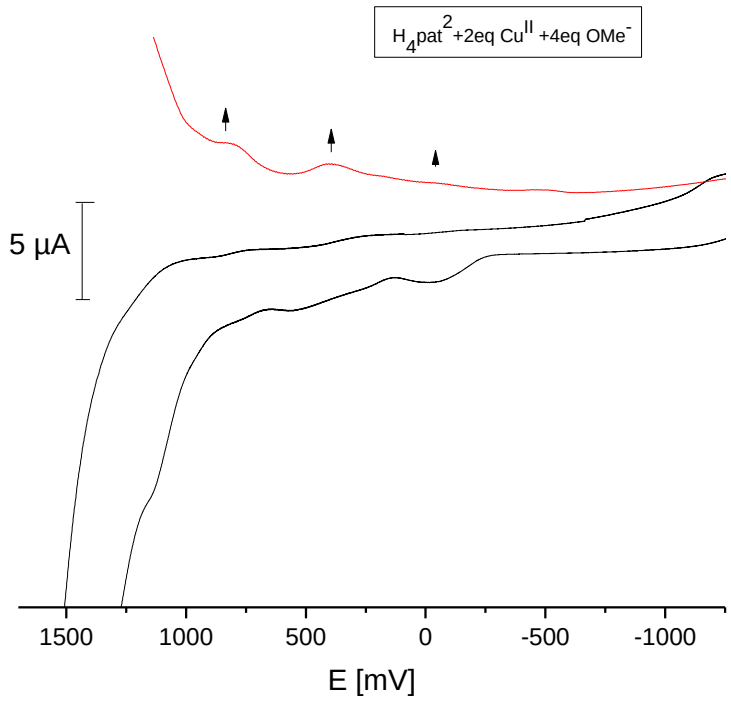

Figure A.6: CV/ SQW overlay of a selected copper(II) complexation-steps of H_4pat^2 (0.1mM in methanol with 0.1M $(t\text{Bu})_4NPF_6$ and vs. Fc/Fc^+, 100 mV/s, $Ag/AgNO_3$ 0.01M,at 25°C).

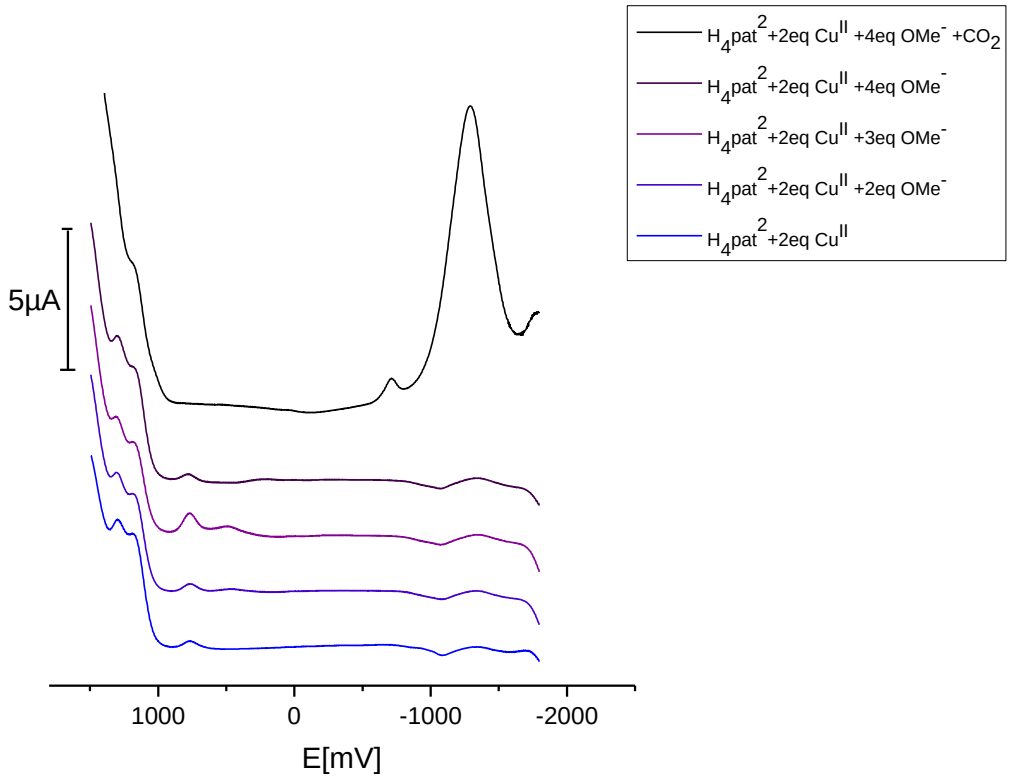

Figure A.7: SQW of selected copper(II) complexation-steps of H_4pat^2 (0.1mM in methanol with 0.1M $(t\text{Bu})_4NPF_6$ and vs. Fc/Fc^+, 100 mV/s, $Ag/AgNO_3$ 0.01M,at 25°C).

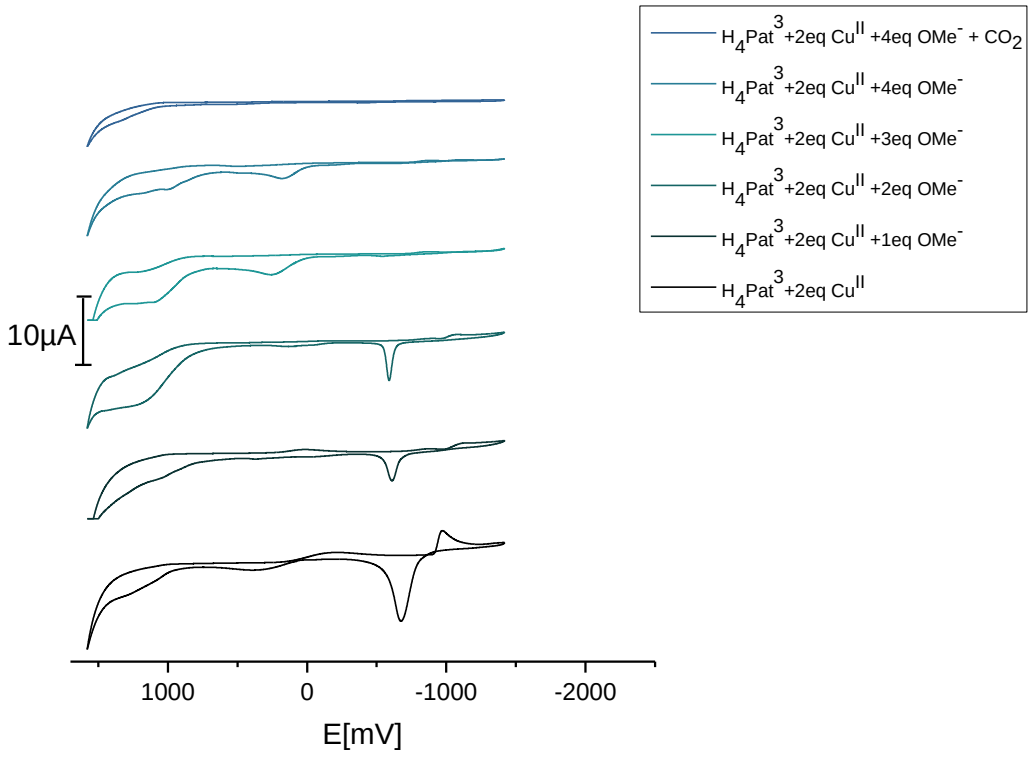

Figure A.8: CV of selected copper(II) complexation-steps of H_4pat^3 (1mM in methanol with 0.1M $(t\text{Bu})_4NPF_6$ and vs. Fc/Fc^+, 100 mV/s, $Ag/AgNO_3$ 0.01M,at 25°C).

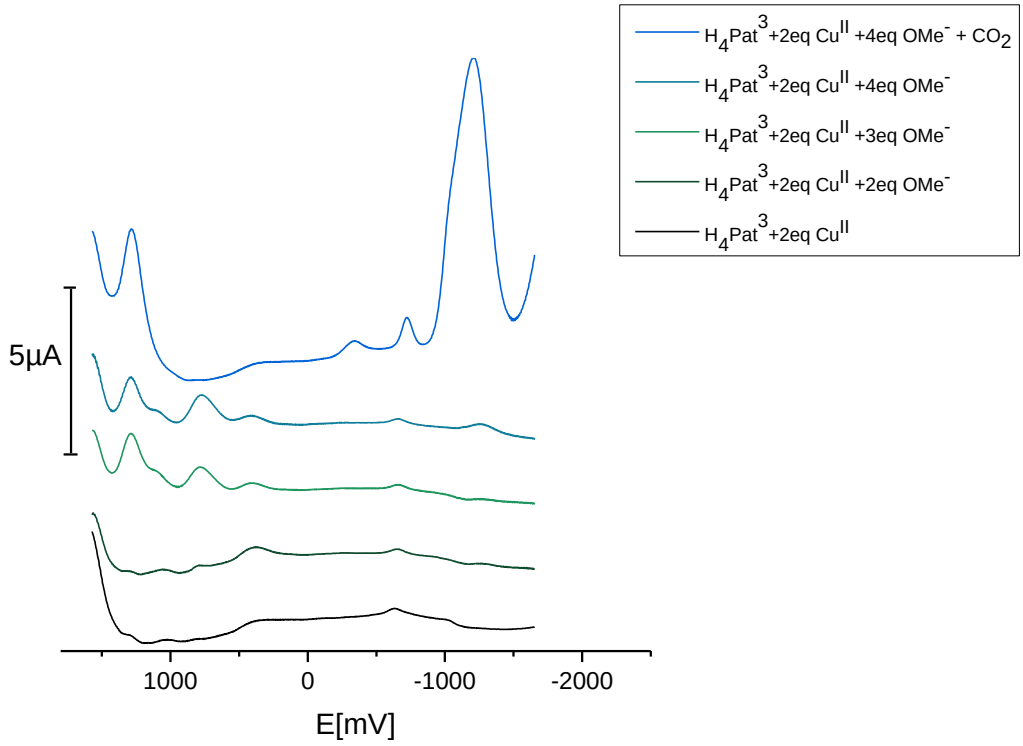

Figure A.9: SQW of selected copper(II) complexation-steps of H_4pat^3 (0.1mM in methanol with 0.1M $(t\text{Bu})_4NPF_6$ and vs. Fc/Fc^+, 100 mV/s, $Ag/AgNO_3$ 0.01M,at 25°C).

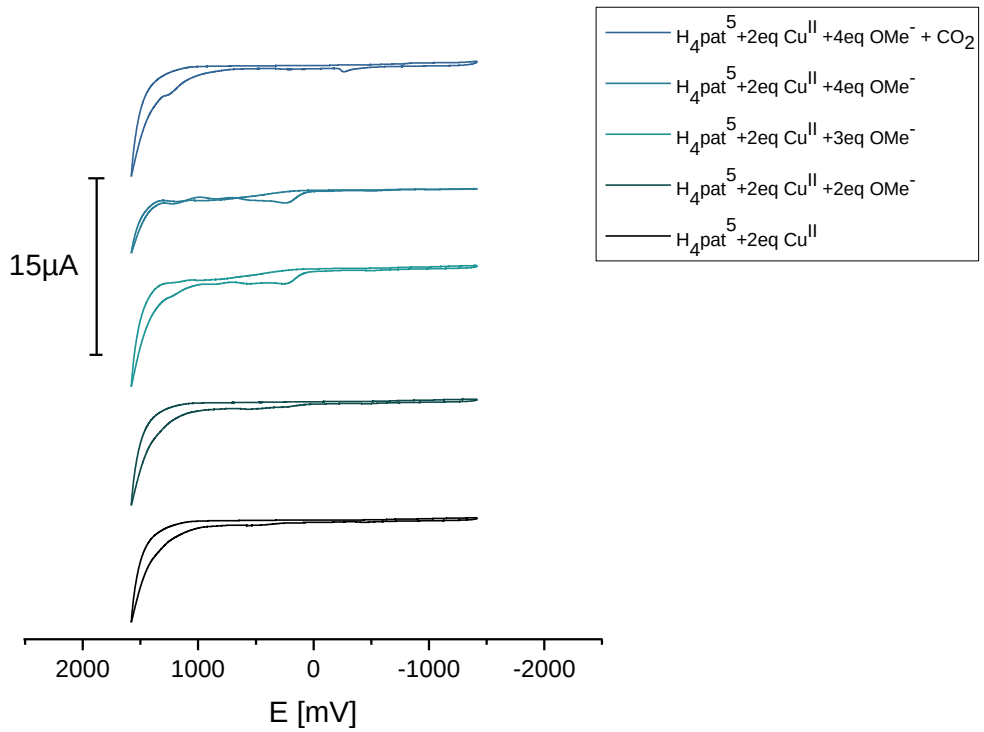

Figure A.10: CV of selected copper(II) complexation-steps of H_4pat^5 (0.1mM in methanol with 0.1M $(t\text{Bu})_4NPF_6$ and vs. Fc/Fc^+, 100 mV/s, $Ag/AgNO_3$ 0.01M,at 25°C).

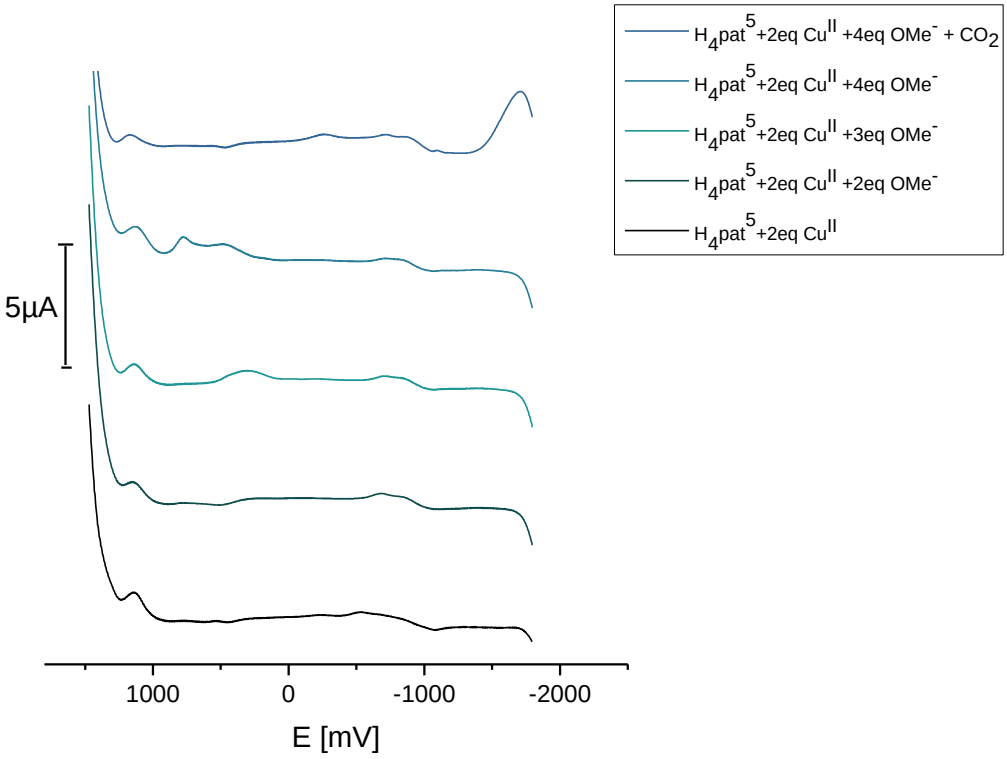

Figure A.11: SQW of selected copper(II) complexation-steps of H_4pat^5 (0.1mM in methanol with 0.1M (tBu)$_4NPF_6$ and vs. Fc/Fc^+, 100 mV/s, $Ag/AgNO_3$ 0.01M,at 25°C).

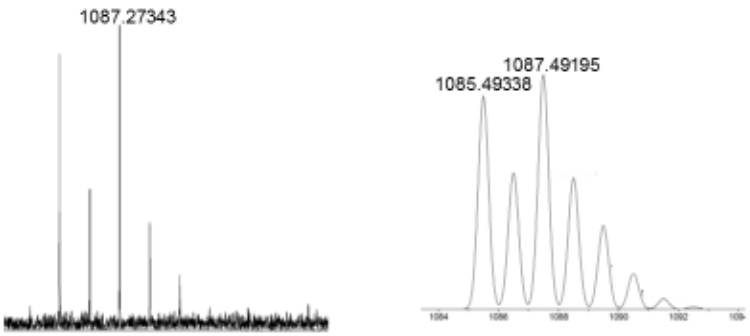

Figure A.12: HR-$^+$ESI MS of oxygenation solution.

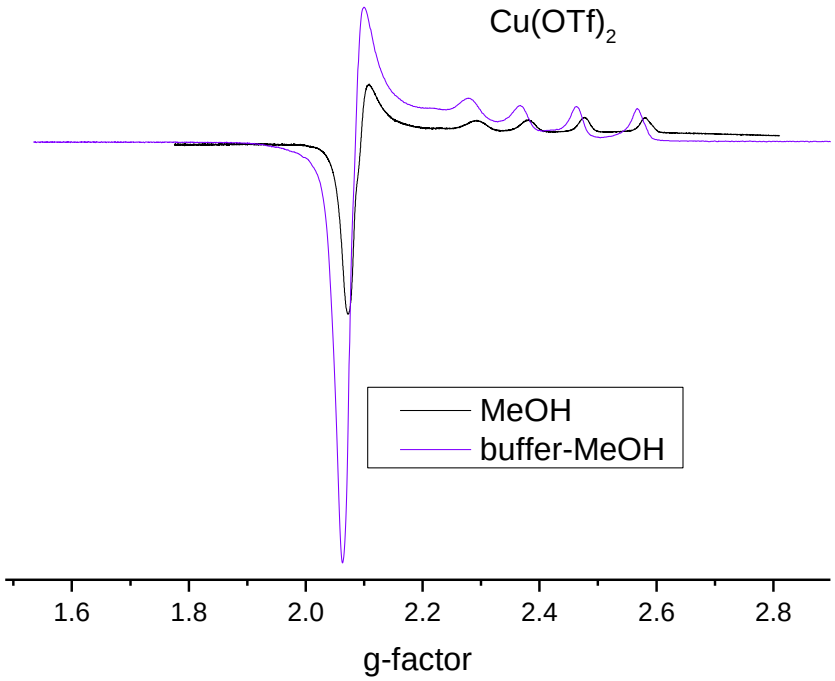

Figure A.13: X-Band EPR spectra of $CuOTf_2$ 1 mM in MeOH (black) and 5 mM in MeOH / Bufffer 3:1 at pH = 6.5, both detected at 140K and 9.44 GHz.

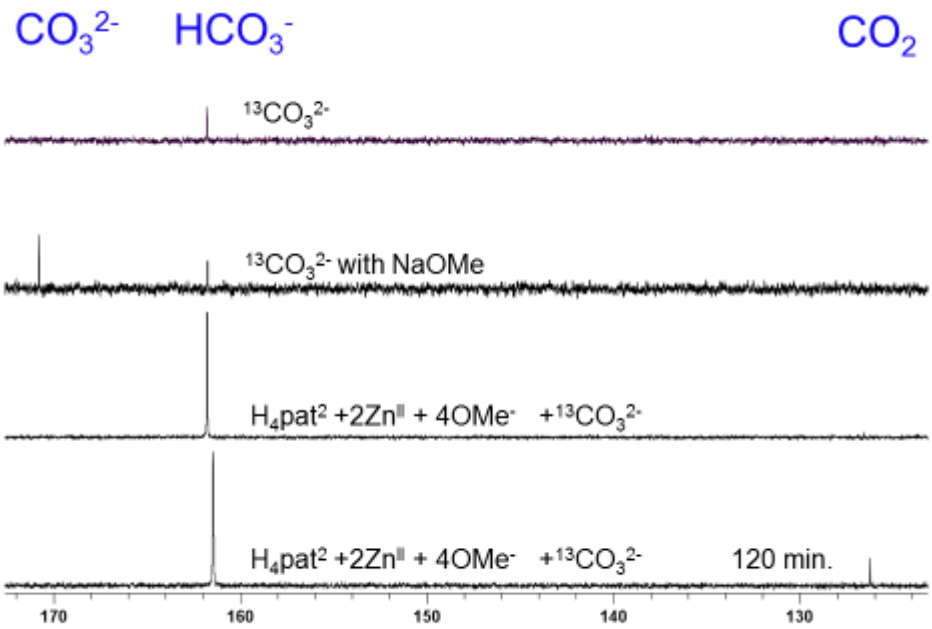

Figure A. 14: Recorded ^{13}C NMR spectra in methanol with and without an *in situ* prepared H_4pat^2 and zinc(II) triflate and sodium methanolate mixture, MeOD 1mM, 25°C, 400 mHz.

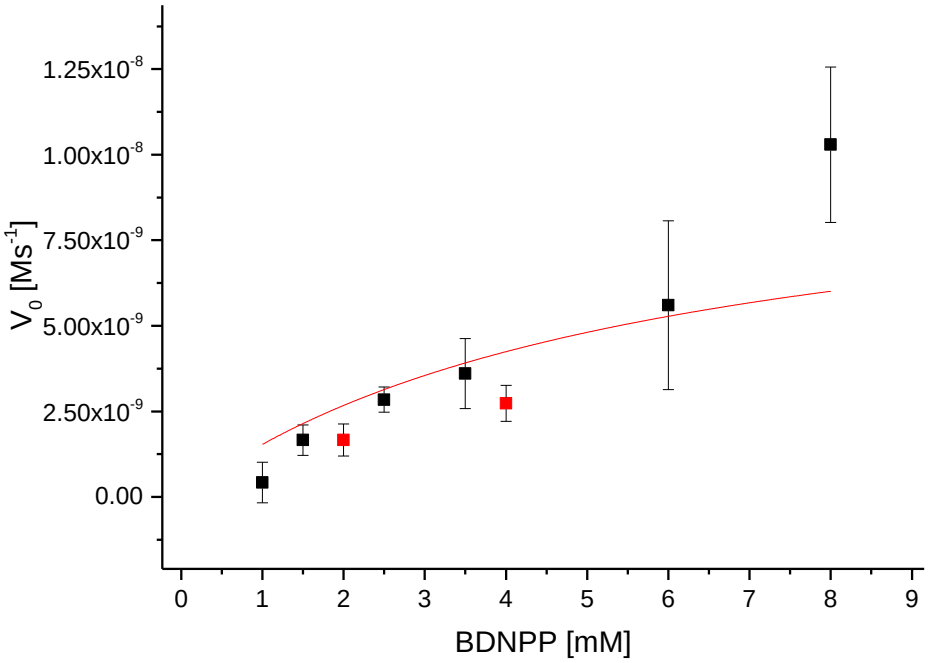

Figure A 15: Michaelis-Menten measurement fitted with equation 6.2; $[CuZn(H_3pat^2)(OH)]^+$ ([cat.] 30µM, 25°C).

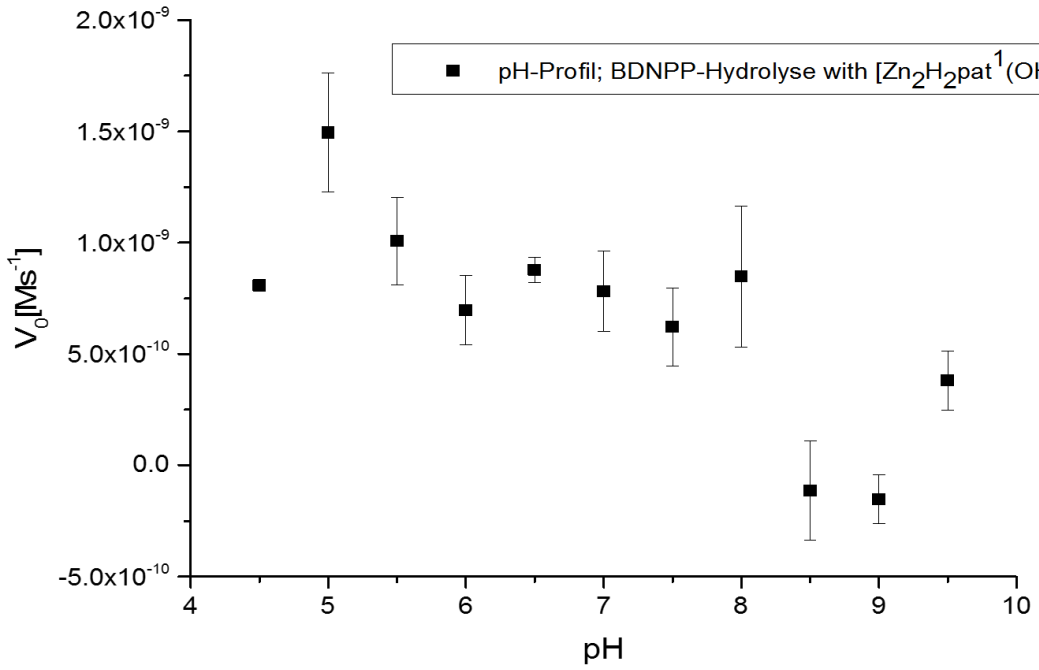

Figure A 16: pH-profiles of the BDNPP hydrolysis with "$[Zn_2(H_2pat^1)(OH)]^+$".

11 Eidesstattliche Erklärung

Eidesstattliche Versicherung gemäß § 8 der Promotionsordnung der Naturwissenschaftlich-Mathematischen Gesamtfakultät der Universität Heidelberg

1. Bei der eingereichten Dissertation zu dem Thema:

´Phosphatase Activity of Homo- and Heterodinuclear Transition Metal Complexes of Patellamide Derivatives`

handelt es sich um meine eigenständig erbrachte Leistung.

2. Ich habe nur die angegebenen Quellen und Hilfsmittel benutzt und mich keiner unzulässigen Hilfe Dritter bedient. Insbesondere habe ich wörtlich oder sinngemäß aus anderen Werken übernommene Inhalte als solche kenntlich gemacht.

3. Die Arbeit oder Teile davon habe ich wie folgt nicht an einer Hochschule des In- oder Auslands als Bestandteil einer Prüfungs- oder Qualifikationsleistung vorgelegt.

4. Die Richtigkeit der vorstehenden Erklärungen bestätige ich.

5. Die Bedeutung der eidesstattlichen Versicherung und die strafrechtlichen Folgen einer unrichtigen oder unvollständigen eidesstattlichen Versicherung sind mir bekannt.
Ich versichere an Eides statt, dass ich nach bestem Wissen die reine Wahrheit erklärt und nichts verschwiegen habe.

_____

Ort und Datum Unterschrift